Use of Large Lysimeters to Monitor Unsaturated Hydraulic Properties of Amended Soils

ASQUITH, JONATHAN,DAVID

Use of Large Lysimeters to Monitor Unsaturated Hydraulic Properties of Amended Soils

Jonathan D. Asquith

Thesis submitted towards the
degree of Doctor of Philosophy

Mechanics Group
School of Engineering and Computing Sciences
Durham University
United Kingdom

March 2015

Use of Large Lysimeters to Monitor Unsaturated Hydraulic Properties of Amended Soils

Jonathan D.Asquith

Abstract

The design and construction of large 1.2 m diameter lysimeters has been implemented to monitor the soil water retention behaviour and permeability characteristics of contaminated soils under remediation. The work was carried out as part of a larger project focussing on the sustainable remediation of low value brownfield land. Three lysimeters have been filled with lead contaminated soil: one control; one with a Water Treatment Residual (WTR) amendment; and one with a WTR and compost amendment. A new software system was built to control the Time Domain Reflectometry (TDR) point water content measurement and irrigation system, which could log data to an online unified data repository; provided an interface for connectivity to any serial port device; deal with templating for simplified setup; and realtime feedback for the end user. High capacity tensiometers were used in conjunction with the TDR point water content measurement system to read volumetric water contents and suctions in the large control lysimeter over a series of wetting and drying cycles, each lasting several months. The results demonstrate that there was a difference between small scale laboratory tests and the data obtained from the lysimeters, particularly in the near surface soil due to cracking. Where cracking was not present, the agreement was stronger, but differences suggested that the drying curves in the lysimeter was predominantly scanning behaviour whereas the element tests were likely more representative of primary drying behaviour.

Declaration

The work in this thesis is based on research carried out in the Mechanics Group, School of Engineering and Computing Sciences, Durham University. No part of this report has been submitted elsewhere for any other degree or qualification and it is all my own work unless referenced to the contrary in the text.

Acknowledgements

This research would not have been possible without generous funding from the UK Engineering and Physical Sciences Research Council (EPSRC).

I would like to thank my supervisors, Professor David Toll and Dr. Karen Johnson for their support, knowledge and friendship. I am particularly grateful for the opportunities provided through the ROBUST project including travel, outreach, demonstrating and working in a great multi-disciplinary environment with fantastic people.

I would also like to thank the other members of ROBUST for their help and friendship. Dr. Stephen Robertson for his sage adviceand upbeat attitude; Dr. Jack Barnard for his friendship and morale; Ms. Nina Finlay for her friendship and expertise on chemistry; Dr. Peter Swift for fun physics presentations; and Dr. Andrew Gallant for his electronics wisdom.

The laboratory work would not have been possible without the assistance of Mr. Stephen Richardson, Mr. Charles McEleavey and Mr. Kevan Longley. Many great ideas and inspiration came from our conversations and the construction of the lysimeters would not have been possible without them. In addition, I would like to thank Mr. Colin Wintrip and his team from the mechanical workshop for consultation and construction of many of the custom components; and Mr. Ian Hutchinson and his team in the electronics workshop for their assistance with the control systems.

In addition, I would like to say thank you to Ms Phillipa Haughton for proofreading; Mr. Adam Poole for helping to fill the lysimeters, proof read and general cheeriness; and Mr Jonathan Smith for his excellent CAD skills.

Finally, a special thank you to Ms. Hitomi Hibino, for supporting me throughout this endeavour.

Jonathan Asquith
Durham, March 2015

Contents

List of Figures

List of Tables

Acronyms

XML	Extensible Markup Language
CRUD	Create Read Update Delete
C#.NET	Visual C# .NET
DOC	Disolved Organic Carbon
DC	Direct Current
DDT	dichloro-diphenyl-trichloroethane
EC	Electrical Conductivity
ERT	Electrical Resistivity Tomography
FDR	Frequency Domain Reflectometry
FIFO	First In First Out
GWC	gravimetric water content
HAEV	High Air Entry Value
IUPAC	International Union of Pure and Applied Chemistry
LVDT	Linear Variable Differential Transformer
MVC	Model-View-Controller
MVP	Model-View-Presenter
MVVM	Model-View-ViewModel
OOP	Object-Oriented Programming
OS	Operating System
PAH	Polyaromatic Hydrocarbon
PCB	Polychlorinated Byphenyl
PTE	Potentially Toxic Element
PTFE	Polytetrafluroethylene
RTD	Resistance Temperature Detector
SWRC	Soil Water Retention Curve
TDR	Time Domain Reflectometry
UI	User Interface
VB6	Visual Basic 6.0

VB.NET	Visual Basic .NET
VOC	Volatile Organic Compound
VWC	Volumetric Water Content
WPF	Windows Presentation Foundation
WTR	Water Treatment Residual
WTW	Water Treatment Works
XAML	Extensible Application Markup Language

Nomenclature

C_k	Coefficient of gradation
C_u	Uniformity coefficient
G	Conductance
K_p	Probe constant
L	Length of TDR Probe
L_a	Apparent length
T	Temperature
V_i	Input voltage
V_o	Output voltage
Z_0	Characteristic impedance of the system
Z_g	Characteristic impedance of empty sample
Z_u	System impedance
c	Speed of light
d	Sample dielectric length
f	Frequency of oscillation
f_e	Effective frequency
f_k	Knee frequency
t	Time
t_r	Rise time
u_a	Pore air pressure
u_w	Pore water pressure
v_p	Propagation velocity
μ_0	Magnetic constant
μ_r	Relative permeability
ω	Angular frequency
π	Osmotic suction
ψ	Total suction
ρ	Corrected reflection coefficient
ρ_∞	Reflection coefficient at infinite time
ρ_b	Bulk density
ρ_c	Closed circuit reflection coefficient
ρ_o	Open circuit reflection coefficient
ρ_s	Specific density
ρ_u	Uncorrected reflection coefficient
σ_a	Soil bulk electrical conductivity
σ_T	Temperature corrected conductivity
σ_u	Uncorrected electrical conductivity
σ_{25}	Conductivity at 25°C
σ_{dc}	Direct current equivalent electrical conductivity
θ_v	Volumetric water content
θ_a	Volume faction of air
θ_s	Volume faction of solid
θ_w	Volume faction of water
ε_r''	Imaginary component of the complex relative permittivity
ε_{relax}''	Permittivity due to relaxation
ε_0	Electric constant
ε_r	Relative permittivity
ε_r'	Real component of the complex relative permittivity
ε_r^*	Apparent relative permittivity
ε_w	Relative permittivity of water
ε_a	Permittivity of air
ε_s	Permittivity of solid
ε_w	Permittivity of water

Chapter 1

Introduction

1.1 Background

In the coming century, the global human population will reach a peak of 11 billion people, all of whom will require clean and sustainable methods of food, energy and goods production. This places a high value upon clean agricultural land, and an emphasis on the clean up of current contamination and prevention of future contamination.

In the last two centuries, many cultures have experienced an unprecedented rapid expansion of industrialised practices. This unfettered growth has had its drawbacks, leaving behind a legacy of blighted landscapes, disused buildings and contaminated land [4]. Unfortunately, the mistakes of the industrialised nations are being repeated in countries undergoing fast economic expansion and current industrialisation. Here, a combination of dirty fuels and low waste disposal standards on a large scale poses a significant risk to current and future generations.

Modern practices, such as those in the U.K., are guided by legislation that attempts to curb some of the unwanted products of industry. Sites often referred to as Brownfield, or previously developed land, are marked for development as a priority over completely undeveloped sites. Active measures monitor and control wastes, filtering off hazardous materials to be dealt with at separate sites. The aim is to limit the proliferation of contaminants through the natural environment.

However, it is not only the prevention of future contamination that is important, but the clean up of old polluted sites. Taking the U.K. as an example, mining has been a significant part of history for the last 2000 years. The cumulative effects of mining compounded with the industrial revolution led to some staggering estimates of up to 0.8%, up to 220,000 hectares, of the U.K. being contaminated [4]. Fortunately, since the 1980s, significant action has been taken to compile registers of contaminated sites and broaden research in the area.

1.2 ROBUST

ROBUST was a project taking a multidisciplinary approach towards the Regeneration of Brownfield Using Sustainable Technologies (ROBUST). The ROBUST projects aims were to address some of the issues with current remediation practices including: costs, effectiveness and the broader impact regeneration has on local communities. This thesis forms part of the works towards these aims, focusing primarily on the geotechnical aspects with strong influences from geochemsitry.

In the terms of the acronym ROBUST, the "R" stood for regeneration, a process that not only included remediation but also the end utilisation of a site and its impact upon the local community, be that of economic or aesthetic value. The Sustainable Technologies aspect focused upon finding new, cheap and replenishable amendments to apply to contaminated sites. The sustainable amendments of interest

coming from what was defined as waste streams, byproducts of industry with no discernable known use. This was to fulfill two important criteria, low cost and sustainable use for the foreseeable future.

1.3 Objectives and Structure

The ROBUST project started out with several broad objectives, including:

- Familiarisation with manganese oxide reactions with organic and inorganic contaminants under wetting and drying cycles;
- Collection of geochemical samples and geotechnical observations at microcosm and 1 m^3 lysimeter trials;
- Understanding of manganese oxide and other potential waste streams (e.g. green compost);
- Understanding of crack and dust generation from soils (and contaminant loading) and what the implications are for human health;
- Public engagement through web pages;
- Public engagement via 1 m^3 lysimeter trials.

These objectives are discussed in detail over the following chapters. Each chapter where relevant, covers a short review of literature and a detailed account of the materials, methods and results obtained.

- This chapter continues to includes a brief introduction to contaminant types, their interaction with materials, and health and safety concerns as background to the following chapters.
- Chapter 2 focuses upon the design and construction methodologies for the 1 m^3 lysimeters. This includes the design of lysimeters and potential instrumentation options, followed by a detailed description of the build process.
- Chapter 3 looks at the use of TDR for monitoring moisture contents and soil conductivity, so as to assess the permeability of large soil columns contained in lysimeters. Commercial systems are reviewed, and the design process for a full TDR system is given including the build process for custom TDR probes. Finally, probe calibrations and performance are assessed to quantify errors and find the most suitable calibration to use for a given soil.
- Chapter 4 reviews the design and manufacture of high capacity tensiometers and their role in measuring suctions in-situ, with particular emphasis upon improving the build success rate of the devices. Comparisons of tensiometers are drawn based upon long term calibration performance, maximum achievable suctions and other observed behaviour.
- Chapter 5 takes a look at a custom software package developed for the control and monitoring of devices connected to serial ports. A discussion of programming languages, architecture and cloud computing is included in a detailed design process that results in software with much improved capabilities over current software practices.
- Chapter 6 focuses on the implementation of the 1 m^3 experiments. An overview of geotechnical properties for soil and amendments is given along with a discussion on the mixes used and fill methods applied to each of the lysimeters.
- Chapter 7 showcases the results obtained in the first 1 m^3 lysimeter and smaller laboratory samples. Permeabilities of the soil are given alongside suctions for a wetting, drying and wetting cycle applied to the soil column. In addition, the soil water retention behaviour is derived for the drying cycle and a comparison drawn between small scale lab testing and large scale lysimeter testing.
- Chapter 8 draws the thesis to a close with conclusions and a discussion of future work.

1.4 Background Literature

1.4.1 Contaminants

An essential part of ROBUST's experimental design is experimenting on contaminated soils. Contaminants may be categorised into two groups, organic and inorganic. Organic contaminants are compounds that contain carbon whereas inorganic contaminants do not.

Inorganic contaminants are predominantly metals or metalloids that may all be found naturally and are often used for agricultural (e.g. fertilisers [5]), residential (e.g. batteries [6]) and industrial purposes. Common examples include Asbestos, Barium, Cyanide, Fluoride, Nitrate, Nitrite, etc. along with the elements listed in Table 1.1.

Table 1.1: Inorganic Contaminants and their Compounds

Contaminant	Natural Sources	Valency	Compounds
Arsenic, As [7–9]	Minerals and Volcanic action	As(III) As(V)	H_3AsO_3 $H_2AsO_4^-$, $HAsO_4^{2-}$
Cadmium, Cd [8, 10]	Zinc Ores and phosphate minerals	Cd (II)	$[Cd(H_2O)_6]^{2+}$ CO_3^{2-}, OH^-, Cl^-, SO_4^{2-}
Chromium, Cr [8, 11]	Minerals and Chromite Ore	Cr (III) Cr (VI)	NH_3, OH^-, Cl^-, F^-, CN^-, SO_4^{2-}, $FeCr_2O_4$ CrO_4^{2-}, $Cr_2O_7^{2-}$
Copper, Cu [8, 12, 13]	Minerals and Copper Ores	Cu (II)	$[Cu(H_2O)_6]^{2+}$, CuS
Lead, Pb [8, 13]	Minerals and Galena Ore	Pb (II) Pb (II,IV)	O^{2-}, SO_3^{2-}, CO_3^{2-}, $(OH^-)_2$, S^{2-} Pb_3O_4
Mercury, Hg [8, 13]	Minerals and Cinnabar Ore	Hg^0 Hg (II)	 S^{2-}
Nickel, Ni [6, 8]	Minerals and Nickel Ores	Ni (II) Ni (III)	$[Ni(H_2O)_6]^{2+}$, $(OH^-)_2$, S^{2-} Ni^{3+}, $HNiO_2$, Ni_3O_4
Zinc, Zn [5, 8]	Minerals	Zn (II)	Cl_2^{2-}, HPO_4^{2-}, SO_4^{2-}, NO_3^{2-} S^{2-}, CO_3^{2-}, O^{2-}, SO_4^{2-}, $Fe_2O_4^{2-}$

Within the grouping of inorganic contaminants is a subset of elements commonly referred to as the Potentially Toxic Elements (PTEs) [14], a group that has no particularly scientific definition, yet contains elements that are of greatest concern in the natural environment when they build up to significant concentrations. A partial list of some PTEs can be seen in Table 1.1. All these elements are commonly found globally, not necessarily in harmful quantities. Most, such as Zinc, are a requirement for the health of living organisms. Indeed Zinc is a good example of an element that in small quantities prevents birth defects yet, in substantially greater quantities may cause an array of symptoms from an unpleasant taste of metal in the mouth through to vomiting [8]. In contrast, Cadmium is one of the big three heavy metals, along with Mercury and Lead, that is used in no known useful biological process yet can have a devastating effect on the normal biological processes in organisms [14].

Background concentrations, functional groups and predominant phase of heavy metals varies by element and global region. Most naturally released heavy metals are produced from the weathering of parent minerals containing trace quantities, often substituted into the crystalline lattice instead of a similarly charged and sized element, or through volcanic actions. Once released, the metals may form a variety of compounds such as sulphates and carbonates, often depending upon the pH and redox conditions. In general, the concentrations of these compounds is rarely toxic and often considered as trace.

Organic compounds are predominantly produced through chemical synthesis and manufactured for

industry, e.g. haloalkanes such as trichloroethene are used as solvents. However, some have applications within the agricultural and residential sectors, for example, as paints, paint strippers, air fresheners, pesticides and disinfectants. Early synthesised compounds were few in number and date back to the early 17th century, and include substances such as chloroform and carbon tetrachloride [15]. Since then, the number of different compounds we can synthesise has grown. Some, such as dichloro-diphenyl-trichloroethane (DDT), have been taken out of production due to serious environmental concerns that were not initially apparent, whilst many have been in use for many years. Organic compounds can be categorised into two subsets: aliphatic compounds that contain no benzene ring in their structure and aromatic compounds that contain at least one benzene ring [16].

Aliphatic compounds may be straight chain, branched chain or cyclical of varying lengths and functional group, denoted by their name as defined by the International Union of Pure and Applied Chemistry (IUPAC). One series of increasing length straight chain alkanes, the simplest of the aliphatic compounds, is demonstrated as an incomplete list in Table 1.2 along with the names and compositions of each compound mentioned. The properties e.g. boiling point, of these chains may vary greatly as the length increases, with some chains being substantially longer than others. For instance, Hexacontane, a solid at room temperature, is composed of 60 carbon atoms and 122 hydrogen atoms. Other common examples of a series i.e. varying lengths of a chain with the same functional group, are demonstrated in Table 1.3. Again this is an incomplete list. Like the compounds shown in Table 1.2, these too may vary in length with changing properties as the chain is lengthened or shortened. Chain length is very important in assessing hazards associated with organic substances; compounds with the lower chain lengths will have a lower vapour pressure and may be deemed a Volatile Organic Compound (VOC). Although international definitions differ on how to determine what is and is not a VOC, the general consensus is that the compound may become air born at room temperature and standard atmospheric pressure. What is shown here are but a few of the large range of possible compounds that can be formed and come under the umbrella term “aliphatic compounds”.

Table 1.2: The Alkanes

No. of Carbon Atoms	Prefix	Alkane	Composition
1	meth-	Methane	CH_4
2	eth-	Ethane	CH_3CH_3
3	prop-	Propane	$CH_3CH_2CH_3$
4	but-	Butane	$CH_3CH_2CH_2CH_3$
5	pent-	Pentane	$CH_3CH_2CH_2CH_2CH_3$
6	hex-	Hexane	$CH_3CH_2CH_2CH_2CH_2CH_3$

As for aromatic compounds, benzene consists of a ring of six carbon atoms. Round the outside, bonded to each carbon, is a hydrogen atom that can be substituted for different functional groups or entire molecules. The notation for benzene is shown in Figure 1.1a. The ease of substituting these hydrogen atoms for other groups greatly depends upon the current functional groups bound around the ring.

A subset of these aromatic compounds is the Polyaromatic Hydrocarbon (PAH). PAHs are formed from two benzene rings linked by either a single bond in the case of byphenyls, as seen in Figure 1.1b, or in the case of naphthalene shown in Figure 1.1c, when the rings share two carbon atoms and are hence fused together [16]. PAHs are characterised by a high degree of hydrophobicity and a high resistance to degradation, hence they will persist in the environment for extended periods. A common PAH contaminant is the Polychlorinated Byphenyl (PCB), a material used in the construction of electronic components such

Table 1.3: Aliphatic Compounds

Series	Suffix	Functional Group	Example	
Alkene	-ene	C=C	Propene	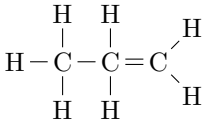
Alcohol	-ol	−OH	Ethanol	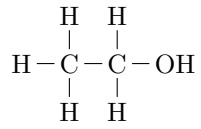
Aldehyde	-anal	−CH=O	Propanal	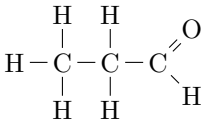
Ketone	-anone	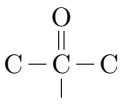	Butanone	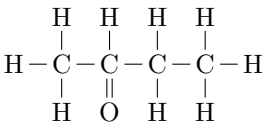
Ester	-yl-anoate	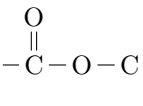	Ethyl Ethanoate	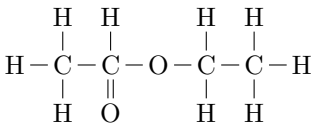

as capacitors and transformers. Another common source of PAHs is as a byproduct of the production of coke known as coal tar, a raw material used in the creation of a large range of organic compounds.

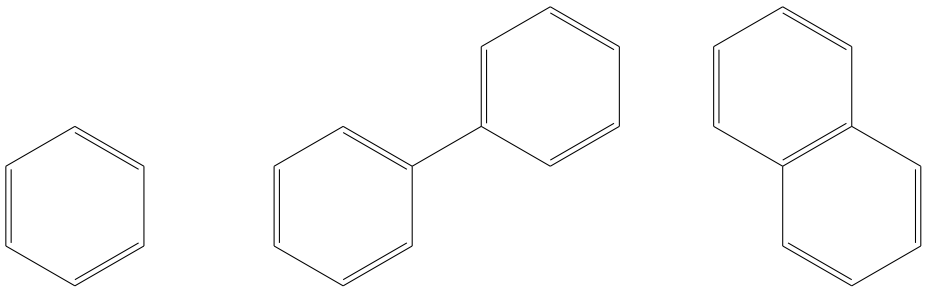

(a) Benzene (b) Byphenyl (c) Napthalene

Figure 1.1: Aromatic Functional Groups

1.4.2 Contaminated Land

For land to become contaminated there needs to be a source containing the said contaminant. Common inorganic sources found in rural locations are fertilisers, pesticides and manures used within the farming sector. Fertilisers contain the common nutrients required for plant growth however, may also include trace amounts of the heavy metals that have no known physiological activity [8]. Upon repeated amendment of the soil, these trace amounts may build up to more toxic levels over time. Pesticides and manures similarly build up heavy metal concentrations in soils, particularly as pesticides contain toxic components

to many of the pests they target, and the manure collected from livestock fed a supplemented diet will contain excessive amounts of required trace elements. Less common in rural areas is metal mining and in industrial areas, the milling process and industrial wastes, all of which contribute to excessive quantities of their respective heavy metals being released into the environment through waste water, mine tailings, dust, airborne emissions etc.

Organic contaminants have serious health and environmental implications because of their carcinogenic, mutagenic and teratogenic properties [17]. With these chemicals being produced industrially, it is unsurprising that organic compounds can be found on industrial land, in nearby water sources such as rivers or indeed upon agricultural land sprayed with organic pesticides. Modern day identification and characterisation of organic compounds found in the environment is still an ongoing process with many new substances, or substances previously ignored, having been identified [15] for future monitoring efforts.

Worldwide, public information as to the extent of contamination is generally lacking, although much can be inferred from the practices of agriculture, mining and industry. Within Europe and North America, countries generally have stable populations and are in a post industrialisation era, with contamination associated with industrial processes. In contrast, countries such as China and India, which are undergoing massive economic expansion, will undoubtedly require remediation technologies in the foreseeable future. Africa is well known for its substantial deposits of minerals mined on both the small scale, such as gold panners who use mercury as an extraction agent, and on the larger scales with large pits and mines. Africa is not the only place that mining takes place; sites across the world are being exploited for minerals with often inadequate environmental protections to prevent toxic build ups of contaminants in nearby environments. With the worldwide population still growing towards eleven billion or so, the agricultural needs, especially in regions with increasing population such as Asia and Africa, continue to increase. Of concern here should be the level of fertilizers and pesticides used to sustain growth, since in the long run, sustained use of these chemicals may prove to be detrimental both to crops and human health.

Within the U.K., the Environment Agency has produced detailed reports to estimate the quantity of contaminated land [18]. With the heavy industrialised history of the country it is not surprising that estimates in 1993 put the quantity of contaminated land at between 100,000 and 220,000 hectares [4]. Further estimates made in 2005 of land within England and Wales, only put the upper limit at 300,000 hectares or approximately two percent of the land coverage [18].

Within England and Wales remediation of contaminated sites is predominantly funded through use of the planning system [18], where those that benefit from the development of land pay to clean it up. The sites funded through planning, and those cleaned up voluntarily, account for approximately ninety percent of all land remediated in England and Wales. The responsibility of remediating the other ten percent falls on local councils with, in the case of England, a small sum of government money totalling $£1m$ (Phil Hartley, personal correspondence). Out of the sites deemed contaminated in England and Wales under the jurisdiction of local councils, numbering 781 as of March 2007, almost ninety percent contained metals and metaloids with around 57 percent containing organic compounds [18].

1.4.3 Remediation Methods

Remediation of contaminated sites revolves around breaking a simple source, pathway, receptor relationship, which is known as a pollutant linkage [4]. By removing any one of these three elements, a site is effectively remediated i.e. the significant risk of significant harm is negated or reduced to acceptable levels.

A source is a loose term that refers to the origin of contamination. A source may be soil, soil water, debris, the atmosphere or other more direct sources such as leaks in storage facilities and mine tailings.

In any case, removing the source of the contamination removes the potential for it to cause harm, hence the site becomes remediated.

The second and third terms, pathways and receptors, are directly interlinked. A pathway refers to the route a contaminant takes to get in contact with a receptor, with a receptor being anything that may potentially be harmed, be that flora or fauna. Pathways include dermal e.g. the touching of contaminated material, inhalation such as breathing of contaminated dust or VOCs, and the ingestion of contaminated material, be that soil particles or plants that have taken up contaminants. By blocking pathways or removing receptors, the probability of significant harm is thereby reduced and the site may be considered remediated, be that for the long or short term.

What can complicate matters is a single plot of contaminated land may have multiple receptors, each of which may be susceptible to multiple pathways. Coupled with the possibility of a range of contaminants being available on any one site, the problems of remediating land can be far from straightforward. The simplest means of remediating land in these cases is to remove the source, however, this may be easier said than done effectively and with the long term benefits in mind.

Remediation strategies broadly fall into two categories, the engineering based approaches and the process based approaches. Within the U.K., the two most widely used methods of land remediation by county councils are the engineering based approaches, those of excavation with off-site disposal and containment [18].

Excavation involves the removal of material deemed to be contaminated and its deposit in a special landfill along with other contaminated materials. This in effect moves the contamination from an openly accessible site to one where precautions have been taken to limit exposure through pathways. Containment aims to limit or prevent migration of contaminants and, therefore, blocks any exposure pathways that may be present for receptors [19]. Options here include hydraulic measures to prevent groundwater movement; capping with an impermeable membrane, concrete or other material; applying a break layer to effectively bury the contaminated soil under a permeable membrane and a thick layer of soil [20]; and finally a low permeability barrier such as that given by a clay. Neither of these engineering based approaches effectively removes or breaks down the contaminants which is where process based approaches come in.

Process based approaches may be split further down into physical, biological, chemical, stabilisation and thermal processes and other extensive technologies [19]. These treat a soil so as to remove, break down or alter compounds considered to be harmful. All, except for the extensive technologies, are energy intensive and costly, and each type of process has its own advantages and disadvantages for different contaminant types. Indeed, it may be the best solution to use a combination of different approaches.

Physical processes attempt to remove contaminants from the soil matrix resulting in residues containing high levels of concentrated contamination [4]. This residue may be disposed of safely as it is or treated with subsequent methods including biological, chemical and thermal processes. The biological methods depend upon the natural physiological behaviour of micro organisms such as bacteria and fungi. These micro organisms interact with compounds, either fixing, mobilising, transforming or destroying [4]. Some microbes will be better at treating certain contaminants than others and, once again, a combination of microbes, or indeed methods, may be appropriate depending upon the range of contaminants available on site. Similar to the biological processes, chemical methods aim to destroy, fix or neutralise compounds, although the outcomes are achieved through the application of chemical compounds. Thermal methods, as the name suggests, involves heating a contaminated media until the compounds break down. Stabilisation methods solidify a contaminated media into an insoluble matrix. The final category of process based methods is that of extensive technologies. Extensive remediation uses methods that

are less focused on intensive short term remediation, but provide a slower, cheaper, low energy and low management solution. For example, multiple remediation techniques may be used over a number of years and each technique may be applied as a reaction to the current status of the site [21].

In summary, remediation strategies are predominantly costly and energy intensive, with process based approaches possibly requiring multiple treatments and engineering based approaches not solving the problem in the long run. All, bar the extensive technologies, are only applicable to sites that have a ready supply of funds available leaving low value sites with a significantly lower chance of being cleaned up. The methods explored on this project aim to change this.

Chapter 2

Construction

2.1 Introduction

In this chapter, the design and construction of 1 m^3 lysimeters is discussed in the context of ROBUST and its objectives. To this end, an overview of contaminants, contaminated land and related studies is given as context for the design requirements of lysimeters dealing with contaminated soil. A detailed discussion of previous lysimeter studies is provided in relation to design, construction and implementation issues, summarising the advantages and disadvantages of different approaches.

The design process is then discussed in detail. Covering the suitability of construction materials, compaction methods, design of the walls, base, instrumentation ports and irrigation system. Details of the construction of each of these aspects is then provided.

2.2 Background

Lysimeter studies are comprised predominantly of three areas of research. The first area is geotechnically focused studies, which have a strong emphasis on a soils physical properties, where experiments are designed for monitoring the permeability, water retention behaviour and strengths of a soil. The second area of research is that of contaminant transport studies. These consider permeabilities and water contents as before, however the emphasis is more towards contaminants, the phase they are in within the soil structure, their mobility, bioaccessibility and leachate i.e. water leaving the soil containing contamination. The third is that of crop studies, that tend to involve experiments that focus on the density and quality of crops through segregating sections of a field with large in-situ containers. The three areas typically provide different information but through combining good experiment design from all three, an ideal experimental design and procedure can be created.

2.2.1 Lysimeters

Studies involving soil columns on the research topics of contaminant transportation and crop growth often refer to the containers as lysimeters. These may be of any size or geometry, with the predominant features of a side wall, a free surface at the top and a drain at the base, either directly into the ground in some in-situ designs or funneled into a collection point for sampling the soil water (otherwise referred to as leachate) as shown in Figure 2.1.

A lysimeter is used to segregate soil from its surroundings, and allows input and output to be quantified whilst retaining, to some extent, the natural environment that the soil sits in. Size and geometry may vary but in general it can be said that experiments involving lysimeters lie somewhere between field monitoring and small scale lab experiments.

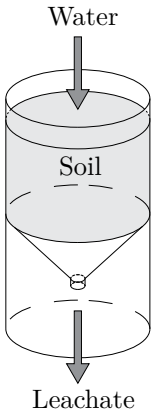

Figure 2.1: Lysimeter Layout

Location, as in whether the soil column is in-situ or ex-situ and off site or on site, varies depending upon the needs of a particular study. Often factors such as the disturbed or undisturbed state of a soil will direct the sampling methods applied, its in-situ/ex-situ status and overall geometry.

Table 2.1: Soil Column Excavation Methods

Study	**Sampling Method**	**Column Geometry**
Corwin and LeMert[22]	Loose	Cylindrical
Derby et al. [23]	Loose	Cuboid
Derby et al.[23]	Hammered	Cylindrical
Brown et al.[24]	Excavated	Cuboid
Bowman et al.[25]	Excavated	Cuboid
Strock and Cassel[26]	Excavated	Cuboid
Brown et al.[27]	Pressed	Cylindrical
Vink et al.[28]	Pressed	Cylindrical
Tackett et al.[29]	Loaded	Cylindrical
Moyer et al.[30]	Loaded	Cylindrical
Schneider et al. [31]	Loaded	Cuboid

Table 2.1 demonstrates the variance in methods used to create a soil column. The first lysimeter sampling technique noted is the collection of loose soil, followed by compaction into a lysimeter, either through tamping or through the combination of applying thin soil layers, time and irrigating heavily [22]. The chief advantage of loose sampling is the degree of control achievable, through refining the sample and removing anomalies that do not represent the site as a whole. This comes with a significant disadvantage too: much of the soil fabric is disturbed, with the soil converted into a more homogeneous medium. However, in the case of contaminant transport studies where this method is predominantly used, the advantages appear to outweigh the disadvantages.

Excavation sampling is a method by which a soil column is cut from its surroundings. The geometry of a cuboid helps in this case, simplifying the work of diggers as four flat faces are cut. Once the monolith is free standing, the lysimeter walls can be built round the soil column to strengthen its integrity before forcefully inserting a base plate underneath the structure and finally removing the soil column from its in-situ position [24–26]. In the cases of Bowman et al. [25] and Strock et al. [26] the soil columns were relatively small at approximately 0.10 m^3 and this is where excavation is most suitable, requiring small quantities of soil to be excavated and not necessitating heavy machinery.

The third method includes hammered, pressed and loaded techniques, all of which involve applying some measure of force on a lysimeter wall with a sharpened edge at the base. Predominantly cylinders are used, as when compared to their cuboid counterparts, they form a more rigid structure which is particularly important with this technique as the forces exerted on the body may be considerable. The three techniques refer to the methods by which the forces are applied, and hammered refers to applying an impulse of force at intervals either manually or through a machine. Pressed and loaded are somewhat similar with pressed referring to the use of a machine to drive the body into the ground in one continuous stroke whilst loaded is a simpler and somewhat cheaper method that involves applying a heavy mass on top of the lysimeter and waiting. These methods may be combined with excavation for removal off site yet are predominantly used in in-situ studies looking at crop yields by segregating small sections of field.

Each of these sampling methods has implications for the design requirements of the lysimeter. Loose sampling provides the most flexibility, design wise, and the most control over the sample, yet may be time consuming and will not represent the site strata as well as the other two methods. Excavation requires a multi-part lysimeter design that seals properly against water and remains rigid if moved. Sampling using this method may be moderately quick yet care needs to be taken; too much sample may result in breaking the soil integrity during encasing yet too little may lead to gaps between the wall and column creating problems in other areas. The methods using forces applied to the lysimeter wall may be the simplest and quickest, yet careful design is required to limit compaction of the sample as the cutting edge passes. A neat sample is produced with a tight fit to the wall, in the soil's current state, but the design requires a very much stronger body, possibly increasing costs and limiting material choices. Thus, each sampling method has its own inherent advantages and disadvantages which must be weighed with other project specific needs.

Location is an important consideration for lysimeter experiments. The major choice faced is whether to situate the lysimeter inside or out in the elements. For some scenarios the choice is obvious. For instance, crop yield studies where the advantages of being outside and in-situ makes for a more relevant study and comparison than the alternatives.

The two predominant factors to be regarded with the internal vs. external argument, come down to two needs. One is to monitor the lysimeter environment and the other to control the lysimeter environment. For monitoring internally, there are more systems available and it is far cheaper to organise equipment suitable for indoor use as as opposed to external use, where appropriate weather proofing, power requirements, temperature dependance and other site specific problems need to be addressed. Additionally, prototyping and testing equipment undercover in like for like conditions improves development speeds and aids in the iterative approach. That said, the data retrieved from external experiments is more interesting and more relevant to other real world problems.

As for control, noting that some degree of monitoring of the controlled variables is required, this is very project specific. The three most important properties to assess are:

- Precipitation;
- Temperature;
- Humidity.

The most pertinent property to control is rainfall, as this will likely have the greatest impact upon experimental results. Rainfall may be controlled both internally using an irrigation system and externally using a combination of a permanent cover and irrigation system, or through a temporary cover system combined with natural rainfall supplemented with irrigation.

In terms of temperature, ex-situ soil columns are easier to control as heating may be applied to the surface area of the lysimeter exposed or the lysimeter set up in a controlled laboratory environment. Care however must be taken that this is done appropriately either to site specific conditions or project needs, due to the natural non-uniform nature of heating and cooling for in-situ soils. More specifically for humidity, control requires either a sealed environment around an individual lysimeter or a humidity controlled laboratory.

In general, ex-situ samples housed inside a laboratory provide the most controllable environment, followed by ex-situ outside and finally in-situ lysimeters. Unsurprisingly this order is reversed for the most realistic to least realistic conditions.

Table 2.2: Soil Column Geometry

Study	**Geometry**	**Dimensions**	**Volume (m^3)**
Brown [27]	Cylindrical	0.85m h, 0.57m d	0.22 m^3
Vink [28]	Cylindrical	0.80m h, 0.3m d	0.06 m^3
Tackett [29]	Cylindrical	2.70m h, 0.40m d	0.34 m^3
Tackett [29]	Cylindrical	2.70m h, 0.95m d	1.91 m^3
Moyer [30]	Cylindrical	0.75m h, 0.76m d	0.34 m^3
Moyer [30]	Cylindrical	1.15m h, 0.76m d	0.52 m^3
Corwin [22]	Cylindrical	1.83m h, 0.60m d	0.52 m^3
Derby [23]	Cylindrical	1.68m h, 0.61m d	0.48 m^3
Derby [23]	Cuboid	1.20m x 1.20m x 1.50m h	2.16 m^3
Brown [24]	Cuboid	3.00m x 3.00m x 1.50m h	13.5 m^3
Bowman [25]	Cuboid	0.46m x 0.46m x 0.46m h	0.10 m^3
Strock [26]	Cuboid	0.38m x 0.38m x 0.65m h	0.09 m^3
Schneider [31]	Cuboid	2.00m x 4.00m x 1.68m h	13.44 m^3

Preference in geometry in a range of different studies over the years is shown in Table 2.2. There is no particular preference for small volume sample geometry; predominantly the choice comes down to sampling method. However, for the larger soil columns it can be seen that the preference lies with that of cuboids, likely due to manufacturing techniques for building such large containers.

Leachate collection techniques vary dependent upon the resolution required for a project, from the simplest design with one drainage point [28, 30] through to more complex multi-drainage designs with points correlating with locations of interest within the sample [25, 26]. Regardless of the complexity, the typical leachate collection point includes a method of preventing soil passing through with the leachate. The two main methods employed as a filter are either a well graded block of granular material, increasing in particle size with depth [22], or the use of a synthesized composite such as a combination of geo-textiles and geo-meshes. Leachate is commonly allowed to freely flow as in a gravity drain, yet in some cases it has been noted that either a water table was required or a suction was imposed as in the work of Corwin et al.[22].

2.2.2 Instrumentation

Not all lysimeter studies require instrumentation, indeed the focus may be limited to leachate generation and collection for the purposes of chemical or flow rate studies as in the work of Moyer et al. [30] and Vink et al. [28]. That said, when the geotechnical behaviour of a soil is of interest a range of sensors are available. These are commonly employed to gather data such as moisture contents [23], suctions [25] and temperatures [22], where relevant.

Suctions, which may be monitored using a multitude of methodologies in the laboratory, have predominantly one method of measurement within larger sample specimens, as with lysimeters. The instrument,

a tensiometer, is a device which has undergone some radical changes over the last two decades and is detailed more fully within chapter 4. In brief, tensiometers in previous studies have had a hard upper limit of detecting suctions of up to 100 kPa [22, 25] but, with more modern redesigns and methods, it is possible to far exceed this cap.

Moisture contents, on the other hand, have been readily readable in their full range for a much longer period of time. Within soil columns and other field monitoring experiments two methods stand out as being more commonly used than others: reflectometry based and resistivity based approaches. The most popular with lysimeters is the reflectometry approach [22, 25, 32, 33], a method that was originally developed by Smith-Rose [34] in the frequency domain and later expanded upon into the time domain by Topp et al. [35], hence the common acronym Time Domain Reflectometry (TDR). This approach is discussed in more detail in Chapter 3. The resistivity method, commonly referred to as Electrical Resistivity Tomography (ERT), has been used in numerous studies [36], more predominantly in field conditions where it provides valuable in-situ data and requires minimal disturbance of the soil structure.

Temperature and humidity sensors are commonly available technologies suitable for a range of industrial and research based situations. There are three common types of temperature sensor, thermistors, resistance thermometers and thermocouples; each of which comes in a range of designs suitable for different temperature ranges and resolutions [37]. Properties such as response times, precision, material and geometry may affect the choices made; for example, resistance thermometers, otherwise known as Resistance Temperature Detectors (RTDs), may be generalised as operating over a smaller temperature range and with a slower response time, when compared with thermocouples, yet have a significantly higher degree of precision. Thermistors, on the other hand, are predominantly constructed from ceramics or polymers (unlike both RTDs and thermocouples) so in some situations this may be deemed advantageous. In terms of lysimeter applications, temperature sensors are moderately common and there is no general preference for type or manufacturer. Humidity sensors are not commonly used except in the rare case where the entirety of the surface is enclosed.

2.2.3 Materials

Material choice for lysimeter construction is influenced by a number of factors including:

- Scale, geometry and availability;
- Cost;
- Physical and Chemical Properties.

Scale, geometry and availability are interlinked, with some materials only being purchasable in common shapes and sizes. These limitations may increase the complexity of designs; for example the inclusion of joints requires suitable bonding agents or manufacturing techniques. For custom designs it is often worth trying to re-purpose existing products to fit a task and only if that fails resorting to a design built from the ground up.

Cost varies on a per material basis, where each material may be prized for certain physical or chemical properties. Some may have a superior strength or better machinability, likely costing a premium, and each bringing their own manufacturing and technical challenges. It is a case of finding the right balance to create an overall superior design.

Where soil water chemistry is not of concern there is the greatest freedom in material choice. Lysimeter designs in the literature are predominantly built from metals, commonly steel, when samples are taken in-situ using techniques that exert significant forces upon the lysimeter body. These are typically fully custom built when the design is cuboid, and often a modified section of steel pipe when cylindrical.

Alternative materials such as plastics have been used in ex-situ designs where fill methods exert lesser stresses on the lysimeter body. Here, the higher degree of machinability and quicker manufacturing techniques applied to plastics can be taken advantage of, such as with the work of Corwin and LeMert [22].

Where soil chemistry is a concern, ideal materials are those that are chemically inert, or at least with the lowest reactivity with the elements or compounds of interest. The greatest wealth of information with this respect is found within literature upon soil water samplers, otherwise referred to as suction cups [38].

Soil water samplers are buried devices constructed from a permeable intake, a connection pipe and a reservoir for collection of effluent, with some mechanism for applying a suction to aid in removal of the soil water. Due to the nature of soils and the extremely low rates that soil water can be expected to be extracted, low quantities of soil water are drawn out and the effect of material choice on aqueous concentrations is significant. Three mechanisms affect the chemistry of the stored sample: sorption, precipitation and leaching [39]. Sorption is the ability of the body material to interact and bond with chemicals in the solution, precipitation is the formation of solid material, and leaching is the addition of chemicals into the soil water during extraction and storage.

Materials vary based upon the chemistry of interest; since organic chemistry is composed of carbon based molecules, it is better to avoid plastics and instead focus on metals such as stainless steel. Conversely, with the metal containing compounds of inorganic chemistry, the focus should be on avoiding metals such as steel and instead use plastics. Common materials to consider for these roles include [38]:

- Aluminium Oxide
- Glass sinter
- Ceramic
- Stainless steel
- Plastic 'Organic' polymers
  - PVC
  - PP
  - PVDF
  - PTFE

Each material will behave differently depending upon the ions and compounds exposed. Materials such as ceramic and Polytetrafluroethylene (PTFE) are often regarded as being particularly resistant to such interactions yet even PTFE shows some level of adsorption of metal ions [40]. More interestingly is the order in which adsorption takes place, wherein some ions are adsorbed in preference to others available in solution. In the case of PTFE in a solution containing Zinc, Cobalt, Chromium and Cadmium ions; trace metals are adsorbed in the order Zn>>Co>Cr>Cd [40].

As for precipitation and leaching, precipitation is highly dependent upon the species present in a soil water sample and the interaction with the materials used in extraction and storage. Leaching introduces new chemical species into the soil water solution, for example additional Disolved Organic Carbon (DOC) [41], which may come from bonding agents used in the construction of samplers.

The solution to overcoming the interference of materials lies in scale; larger samplers have been noted to have a far greater reliability, and more importantly, give results closer to actual soil water values due to the ratio of surface area to volume decreasing. This skews the equilibrium adsorption towards the

solution retaining a more representative proportion of the chemical species concentration found in the original soil water. The other concern is in reducing the likelihood of leachate being produced by the materials themselves, ideally joins are limited and, where they are needed, physical locks and fittings are used in preference over bonding agents.

2.3 Lysimeter Design

The design of the lysimeters took into account the inherent advantages and disadvantages of material choice, instrumentation requirements, remediation scheme and size. Detailed here are some of the ideas, rationales and improvements made as a design was finalised and some comments on the construction process.

2.3.1 Site Selection

Working towards maintaining ROBUST's sustainability objective, sites as a source of contaminated soil were viewed with regards to distance from the geotechnical laboratory, based in Durham, and distance to possible locations for providing the amendment, discussed in more detail in Chapter 6. Given the North-East of England's strong industrial history, it is unsurprising that two heavily contaminated sites were found nearby in Newcastle Upon Tyne. Both sites lie directly on the river Tyne, adjacent to one another, yet each had a completely different set of contaminants.

The first plot of land housed a tar works until 1983, when the works were closed and demolished, leaving behind a hard asphalt surface and debris. Since then, tar has continued to leach into the tidal river, leaving a visible sheen on the surface. The tar itself contains low levels of benzene and napthalene with skin contact causing irritation. Longer periods of exposure, however, lead to an increased probability of greater health problems.

The second site is a 19th century lead works. Closed, then demolished in the first half of the 20th century, the area was landscaped, covered in a layer of top soil and converted into a public park. At the beginning of the ROBUST project, this site had yet to be remediated, with metal contamination having spread into the top layer of soil, the site was a worry to the local council. Upon a full investigation by Newcastle City Council, high levels of lead and arsenic containing compounds were found throughout the soil layers.

With the advantages of laboratory based lysimeters, to be discussed shortly, seeming to outweigh those of field based lysimeters, a choice had to be made with regards to soil selection. Following the route of organic contaminants as with the tar works site, would mean constructing a lysimeter predominantly out of metal based materials, likely involving a steel body, access ports and base plate. Conversely the lead works soil, being contaminated with metal containing compounds, would lead to plastic based lysimeter being built. Producing a plastic lysimeter was both cheaper than a metal based design and more importantly, safer from a health and safety perspective based on the contaminants involved. The risks involved with soil contaminated with tar in such an extreme case were too high, primarily due to the vapours given off. The other advantage of plastics was production speed, both from a machinability perspective and the wide range of available pre-made plastic parts such as glands and piping. In summary, the bias from a materials perspective definitely lay towards selecting soil containing a metal based contaminant.

The hazardous nature of the soils was of primary concern. With the lysimeters to be placed within a laboratory for long term testing the health implications for researchers and visitors had to be addressed. The lead works soil, although heavily contaminated, showed to be the most promising of the two. Minimal safety requirements were needed to block pathways for the contaminants to come into contact with receptors, and included dermal protection through gloves and other appropriate clothing; inhalation by using dampened soil and face masks; and ingestion through self restraint. The tar works soil proved to

have more serious issues with regards to minimising the risk of contamination. Primarily, the volatility of hazardous compounds inside an enclosed environment was of concern. This meant the lead works soil was, at least from a safety standpoint, far more attractive.

In conclusion, it was seen that for a large lysimeter study, the lead works was a superiour choice. Construction was quicker and cheaper, the health concerns were minimisable in a laboratory environment and, with metal contamination being found on the majority of sites within England and Wales, the experimental outcome from a geochemical perspective was seen as highly relevant and applicable to other contaminated sites.

2.3.2 Experimental Procedure

Wetting and drying of the soil matrix was of geotechnical interest and monitoring changes over prolonged periods of time. This required control of precipitation at the soil surface and a means to insert instrumentation into the soil matrix for the measurement of soil water retention behaviour and flow related properties. Geochemically, a means of collecting soil leachate during the cycling was required and methods of monitoring in-situ parameters such as pH were of interest.

The known flaws in lysimeter experiments had to be addressed, at least to some extent. Two points of interest that were deliberated over were the shrink swell behaviour of the soil under wetting and drying conditions and the stress states imposed upon the soil matrix in a confined environment.

Firstly, the shrink swell behaviour leads to problems in experimental design when a fixed boundary is being used. In the case of confined experiments, this often means that the soil is exposed to unrealistic wetting conditions dependent upon the extent of soil desiccation and hence the influence of these air gaps. As discussed earlier, with regards to lysimeters, this is referred to commonly as side wall flow.

Another problem with confined soil columns is the effect of the very same confinement on stress states within the soil matrix. For small experiments this is often negligible, yet in the case of 1 m^3 samples it is worth some due consideration for lysimeter wall, port and instrumentation design.

2.3.3 Location

Four options were available initially with regards to a location for housing the lysimeters. On-site, both in-situ and ex-situ, off-site inside a laboratory or off-site and maintained outside.

Firstly, on-site in Newcastle Upon Tyne was considered. A map of the nine acre plot being shown in Figure 2.2. As can be seen, the park was made up of a series of terraces on a hill, each subsequent plateau being higher than the last as distance from the river, shown to the south, increased. Between each plateau, were relatively steep slopes covered in dense foliage, primarily consisting of non-coniferous trees and bushes making them generally impassable. Footpaths interlinked the open grassy plateaus through shallower inclines and there were no buildings within the confines of the park.

In-situ conditions were not considered feasible because of the layering encountered on site. As shown in Figure 2.2, the lead works was a dominant feature across the site until it was demolished in the mid twentieth century. This left the site with considerable quantities of debris which was landscaped and finally covered in a thin layering of top soil. While the near surface soil appeared usable at the start of this project, since it contained high levels of contamination, digging below this layer revealed much rubble and debris. Compounding this, one location on site could not be said to be representative of the site as a whole.

Ex-situ conditions on site were not considered to be much more advantageous. Maintenance and security would be an issue, particularly as this site was liable for having cables stolen for valuable metals. Apart from the security concerns, the site itself was due for remediation in the immediate future.

The alternatives were housing the lysimeters in, or outside of, the main civil engineering laboratory

at Durham University. This would mean collection and transportation of soil from a suitable location on site back to the laboratory. Inside housing of the lysimeters was more advantageous that external housing. Firstly, the laboratory would offer a far steadier temperature, that only varied with the seasons by a few degrees between the peak temperature of summer and the minimum temperature winter. This was deemed more appropriate than the daily variance that would have been experienced by the soil column outside. Secondly, precipitation could be controlled better with an indoor irrigation system guaranteeing that no natural rainwater would find its way in. Thirdly, costs could be reduced by not requiring waterproof housing for many of the data logging systems.

In summary, the advantages of an indoor, well controlled lysimeter experiment outweighed the advantages of on-site or outdoor scenarios which were beset with large unknowns and little repeatability, stability and control over influencing conditions.

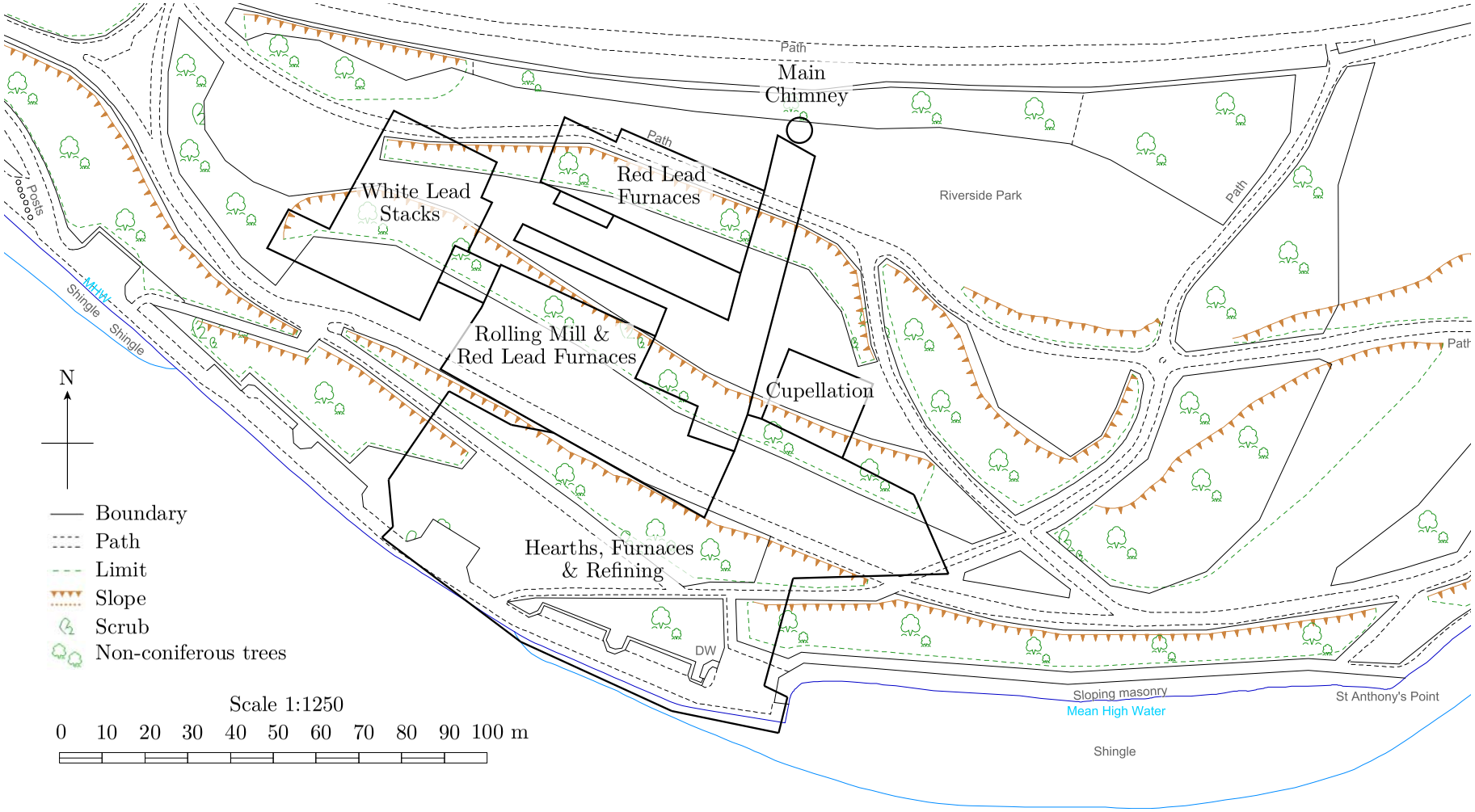

Figure 2.2: Map of St Anthony's 19th Century Lead Works Foundations

2.3.4 Geometry

Originally, the lysimeters were envisaged as 1 m^3 perspex boxes. These were to be mobile with transparent walls for public engagement events, yet fully functional for science experiments. Quickly it was realised that this design was unrealistic; with the expected mass of the lysimeters approaching well over two tonnes they would be impossible for the average person to move. Additionally, a movable chassis to hold these boxes would have had to have been custom built and safety tested and all of the data logging equipment made mobile, with duplicates being required for lysimeters left in the laboratory. In addition, there were safety concerns associated with bringing contaminated soils to schools, science fairs and other events. It was decided that the optimal approach was to separate the concerns of public engagement and thorough scientific study, into two more focused constructs. Public engagement activities had their own smaller, clear plastic versions of lysimeters whilst the scientific lysimeters were focused on their core role without unnecessary complexity.

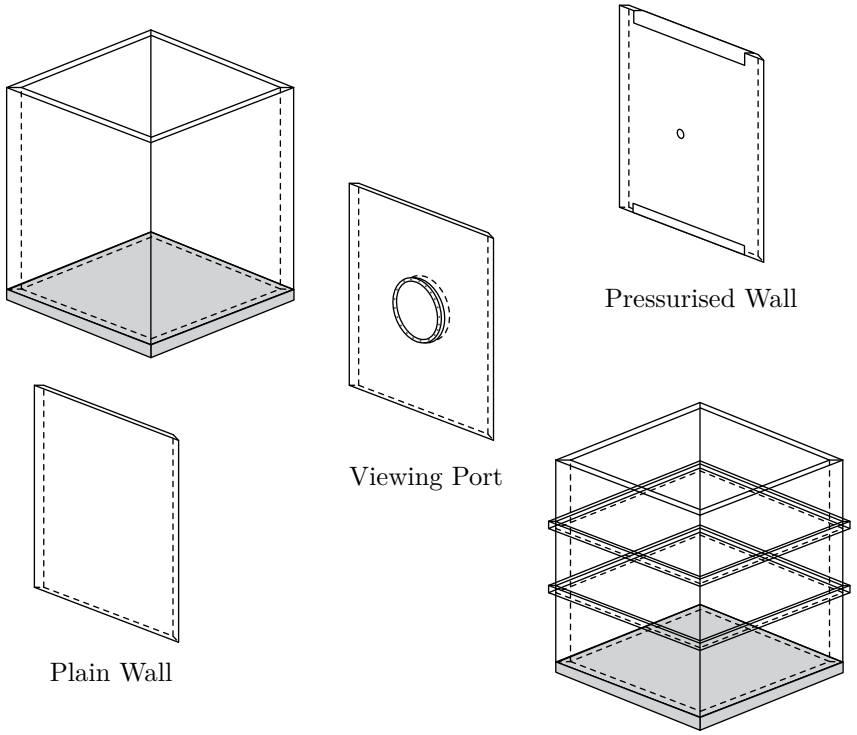

Figure 2.3: Cuboid Lysimeter Concepts

Initial ideas were very similar to those first sketches, cuboid shapes constructed in house made from perspex. Some of the original sketches are shown in Figure 2.3. Other ideas originated along the lines of repurposing industrial refrigeration units, storage cells from warehouses or chemical containment units.

Similarly, cylindrical designs were deliberated upon. Size wise, it was maintained that the volume of soil should be kept at around 1 m^3 by choosing a container of a suitable diameter and height. This volume was seen as a critical advantage over smaller lysimeters, closer representing field conditions and potentially overcoming some of the pit-falls of smaller volumes such as side wall flow significantly affecting the entire sample. Large diameter piping was evaluated for its expected strength, cost, ease of construction and overall suitability for integration with other components. Again, both metal and plastic designs were considered until the site selection was confirmed with some of the sketches shown in Figure 2.4.

Between cuboid and cylindrical designs, the cylinder had several, although slight, advantages. Firstly,

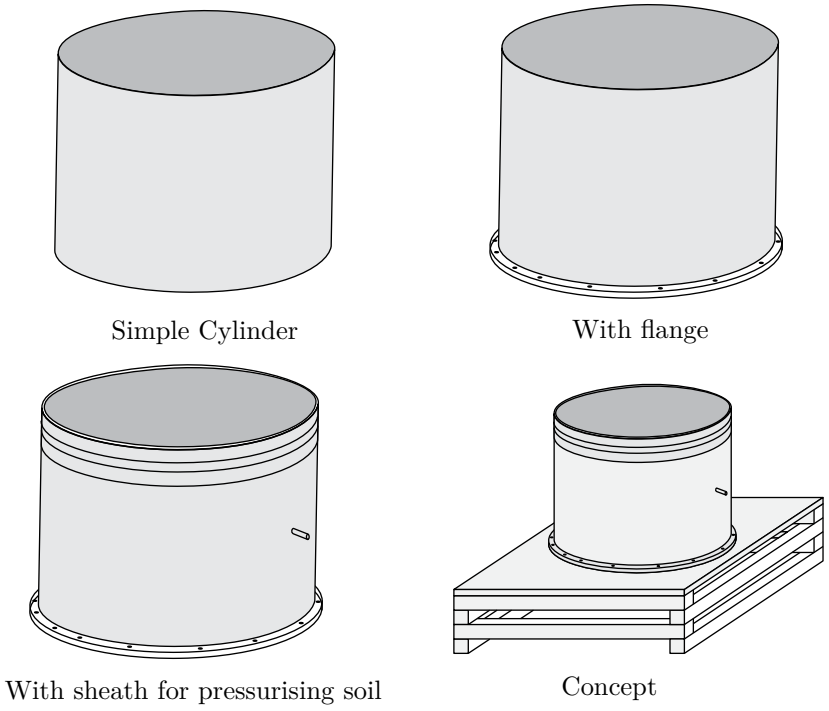

Figure 2.4: Cylindrical Lysimeter Concepts

an overall more uniform and symmetrical compaction could be achieved with a circular compaction surface, removing the need to deal with varying shear forces resisting compactive efforts at the side walls, nor fitting compactive tools into tight corners. Another advantage was the minimisation of lysimeter boundary walls affecting one set of instrumentation in preference over another due to proximity. Making the assumption that adjacent instrumentation was inserted to the same depth in a cylindrical design would make conditions almost, if not exactly, the same, which would result in two sets of data that could be more reliably correlated with one another. Finally, the ease to which irrigation systems can be integrated with a circular geometry was far better; they avoided complex corners and gave a more uniform level of precipitation.

Preference erred towards cylindrical designs with large pipe diameters available at fixed intervals over a range of 400 mm in diameter up to diameters of 3500 mm. The most sensible maximum size was one limited by standard geometries of materials to be procured for use as a base plate. Plastics for this base plate were limited to being any size smaller than 1.22 m x 2.44 m, meaning a maximum internal diameter of 1.2 m could be fitted on any one sheet. In terms of strength, the pipes were constructed out of a high density poly-ethylene produced through a continuous spiral winding process, forming a 50 mm thick rigid wall containing air voids as shown in Figure 2.5, suitable for burial at depths of up to 6 m. In terms of material, high density polyethylene had two major advantages. Firstly, it is regarded to be in the same class as PTFE in terms of its low adsorptive capability; secondly, the surface is of very low friction meaning a minimisation of shear stresses applied to the soil column during shrink swell cycles. In terms of the final size, 1.2 m diameter pipe was the most favourable. With a depth of 1 m of soil, the overall volume to be monitored lied in the region of 1.13 m^3, well above the minimum quantity intended initially. Also, with the largest of the suitable lysimeter diameters, the curvature of the surface around port joints would be limited, giving a cleaner and better fit with fewer leaks expected. The optimum length of pipe was also debatable. One extreme was a 1 meter length, meaning the pipe would end flush

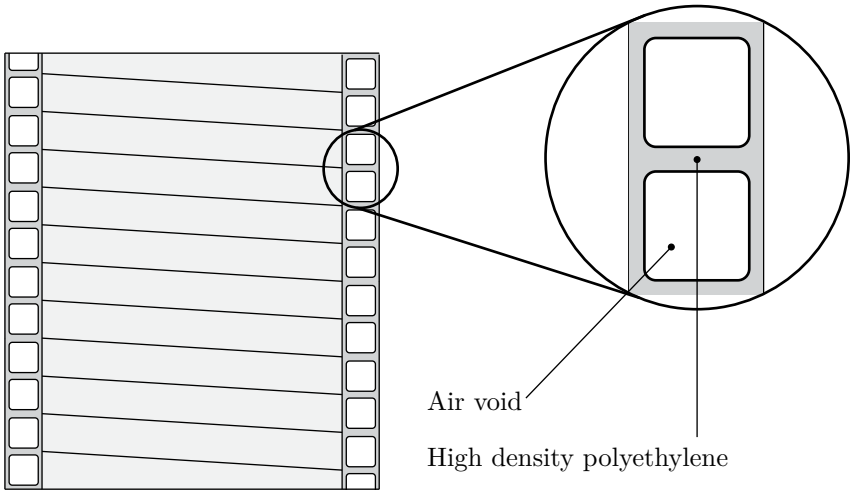

Figure 2.5: Pipe Geometry

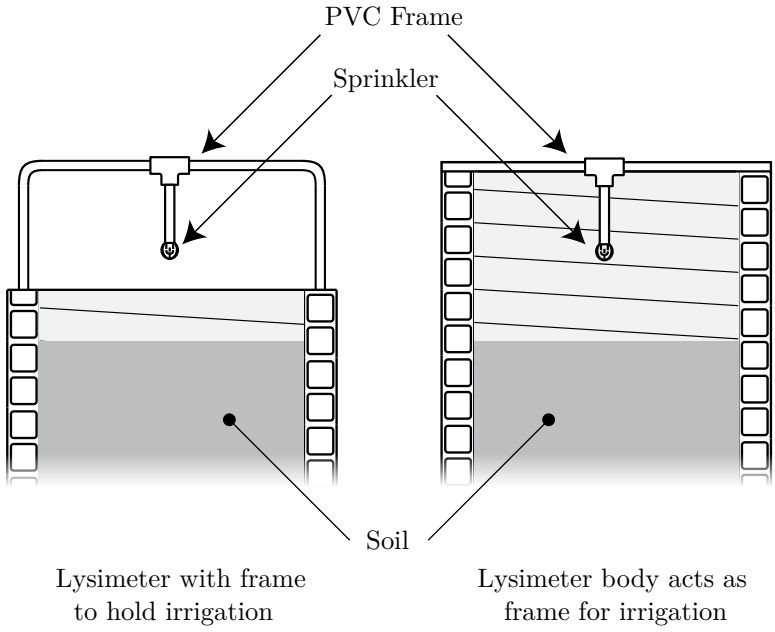

Figure 2.6: Comparison of Irrigation Designs

with the soil surface. This was disregarded due to problems that could be foreseen with the irrigation system and guaranteeing the water applied reached the soil surface and had the opportunity to infiltrate along with air flow over the surface. Two alternatives were seen as shown in Figure 2.6, the first being a low lip to keep precipitation within the confines of the lysimeter combined with a frame for the irrigation to sit on. The other involved using a longer section of pipe for the lysimeter that could act as a frame itself, fulfilling multiple purposes and acting as a mounting point for any further instrumentation added and could function as part of a full enclosure should that be required at a later date. With the longer pipe being preferential, the final section size was determined as 1.2 m internal diameter, 1.3 m external diameter and with a length of 1.5 m.

2.3.5 Irrigation

Two primary methods of applying water to the soil surface were considered. The first was an agricultural sprinkler for use in greenhouses which, with a circular spray pattern, coupled easily with the piping design. There were two concerns, however. The first being the height to which the sprinkler needed to be set above the soil surface to avoid much of the water hitting the side walls and flowing down between soil column and wall in the gap that would appear over the course of wetting and drying cycles. The second concern was with the uniformity of the spray pattern, the more uniform the better, but with limited data available from suppliers this had to be acquired through laboratory testing. A diagram of the sprinkler head is shown in Figure 2.7. The head piece consists of tubing funnelled into a revolvable rotor, turned by the forces exerted as water is ejected under pressure. To keep the rotor in place, the body's head piece loops underneath blocking the spray of water for a few degrees at two poles.

The radial distribution for the sprinkler head was assessed using the planned setup in an empty lysimeter. Water was pumped over the correct head and collected from the sprinkler over a period of one minute. This resulted in the distribution shown in Figure 2.8 where it can be seen there was a preferential distribution over the mid point of the lysimeter's radius.

The alternative to the sprinkler system was a drip system, consisting of a tray the same size as the soil surface. Holes were drilled through, allowing water droplets to form (the size being dependent on hole diameter) and drip onto the soil surface. Although sound in principle, and much more realistic in intention, controlling such a system was more complex than a sprinkler approach. Issues with monitoring the quantity and rate of water application, along with ensuring an even distribution, were foreseen in such an approach over a large surface area, where a perfectly flat surface and method of quickly applying water evenly throughout the tray were required.

The design of the water supply firstly required a suitable water source. Rainwater, as opposed to distilled or de-ionised alternative, was decided on for similarity to field conditions. With this as a given, a system was required for collecting, storing and transmitting water to the lysimeters in the correct quantities. The first task was already completed in part with rainwater being collected off the roof of the building, housing the civil engineering laboratory, into a large 4 m^3 vessel.

With rainwater collection happening externally, a method was required for transportation inside. Due to limitations imposed by pump drawing distances along with health and safety, this process was split into two parts. Firstly, a smaller storage tank of volume approximating 50 l was placed internally, adjacent to the lysimeters, reducing the length of piping required for the primary irrigation system. This smaller tank was to be filled through a submersible pump as and when required, instead of something more permanent. This was made feasible due to the limited quantities of water required per day to act as a standard quantity of rain. Secondly, a pumping system was required to take the water from ground level, raise it by approximately 1.5 m and send it jetting out through a sprinkler.

Importantly, with regards to regulating the applied irrigation, flow rate is dependant on the pumping

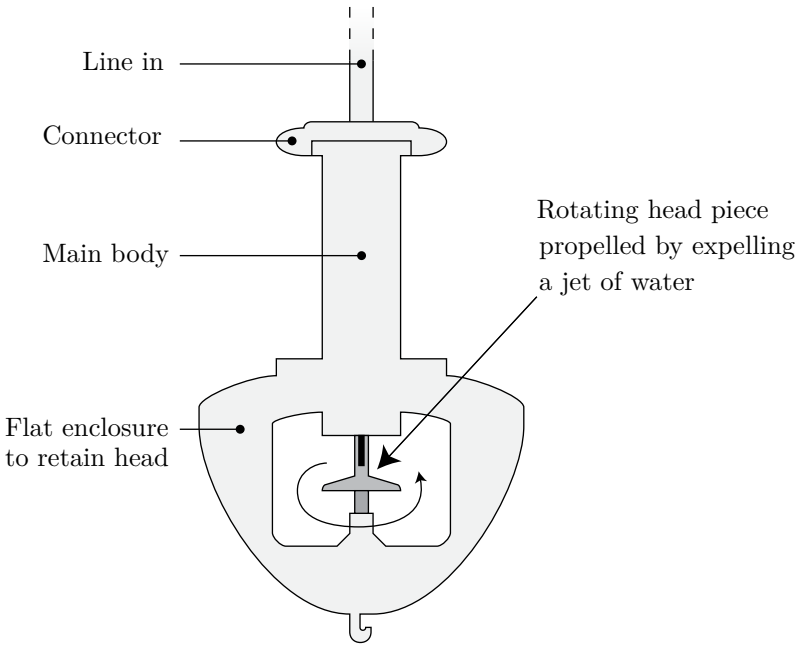

Figure 2.7: Sketch of Sprinkler Head

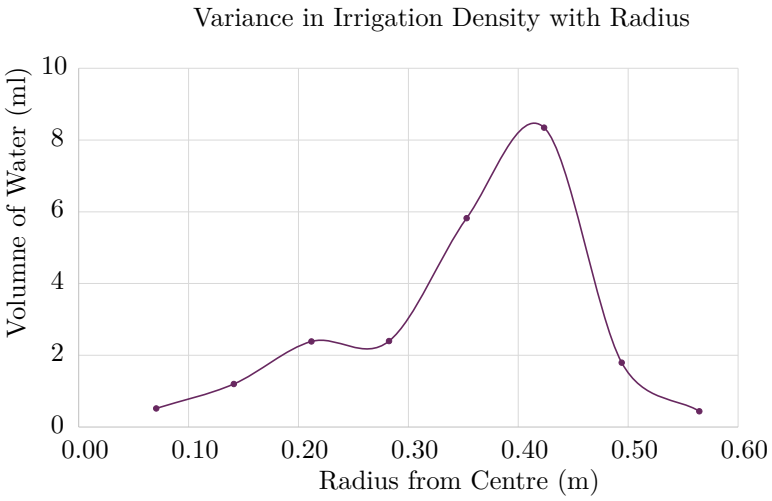

Figure 2.8: Graph Depicting Spacial Variance in Sprinkler Irrigation

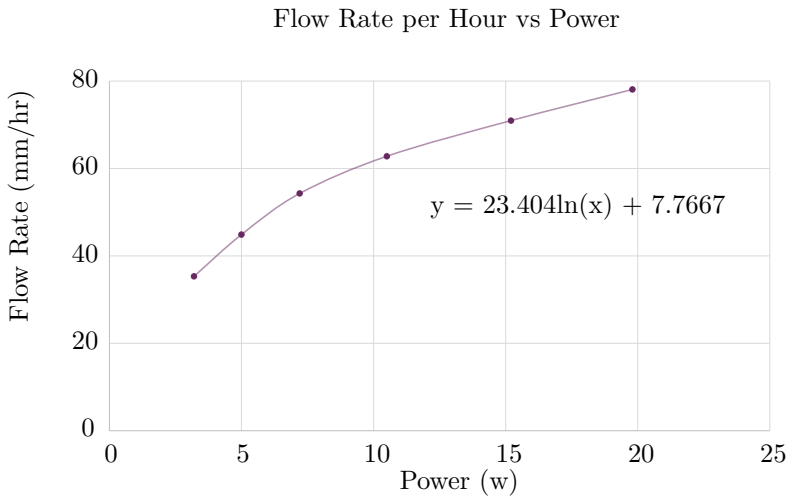

Figure 2.9: Diagram of Power vs Irrigation Rate for the Irrigation System

head, piping diameter and power supplied to the system. The exact head of water to pump depended upon several factors, namely the head of the water in the storage tank, the height above the lysimeter surface required of the sprinkler for full coverage, the height of the lysimeter base and the given fact that the soil was to be filled to a depth of 1 m. A pump capable of delivering suitable quantities of water at pressure, with room to maneuver, was sought out and a small unit decided upon, capable of delivering pressures up to 2.4 bar and volumes of water up to 3.8 litres per minute. This was tested to gauge coverage area, in similar conditions to those expected in the final design which gave an approximate height above the soil surface that the sprinkler head should sit. Combined with the height of the base, to be discussed shortly, and the height of the soil, this gave an absolute head for the pump to work under. Powering the pump at this head at various rates and monitoring the flow rates yielded the curve showed in Figure 2.9. As can be seen, flow rates varied between 0.67 litres per minute and 1.47 litres per minute with power rates below this range being unable to operate the pump sufficiently and higher power rates becoming unstable. Translating the flow rates into millimeters per hour applied to the lysimeter surface puts the range between 35 and 78 mm/hr.

The base the lysimeters were to sit on had to fulfill several objectives to fit in with the rest of the design, these were:

- Strong enough to hold in excess of three tonnes off the floor;
- Provide room for collection of leachate;
- Only plastics in contact with soil;
- Reasonable price;
- Cope with the effects of side wall flow.

The latter point was put as an objective here due to design flaws in measures that prevented side wall flow. Several alternatives were considered, such as Corwin's annular rings [22], disregarded due to applying stresses over wetting and drying cycles; and a floating side wall, where a pressurised latex

sheath would maintain contact with the soil at all times. This last option was interesting as it would have prevented significant sidewall flow, although the difficulties inserting instrumentation would have been significant. A potential solution was for a central core to be bored from the lysimeter and used as a method of entry for inserting probes, but again this would have reintroduced issues with flow between fixed walls and the more dynamic soil fabric, hence this was disregarded. The best alternative was to differentiate the run-off from the surface, going down the gap between soil and lysimeter wall, and the water passing through the soil column itself. It was this idea that led to using a geocomposite base layer separated into sections.

Two sections were decided upon, an outer ring taking away the excess water and an inner circle covering the majority of the soil column, where the influence of boundary conditions could be minimised. More sectioning could have been used, but considering the size of the column and the nature of the soil the expected flow rate through the sample was low. This was especially important considering the required volumes for a suite of chemical tests for the geochemical aspects of ROBUST. To at least guarantee 50 ml sample sizes, an approximation of the volumes required for testing with repeats, at regular intervals the best course of action appeared to be using the minimal number of sections.

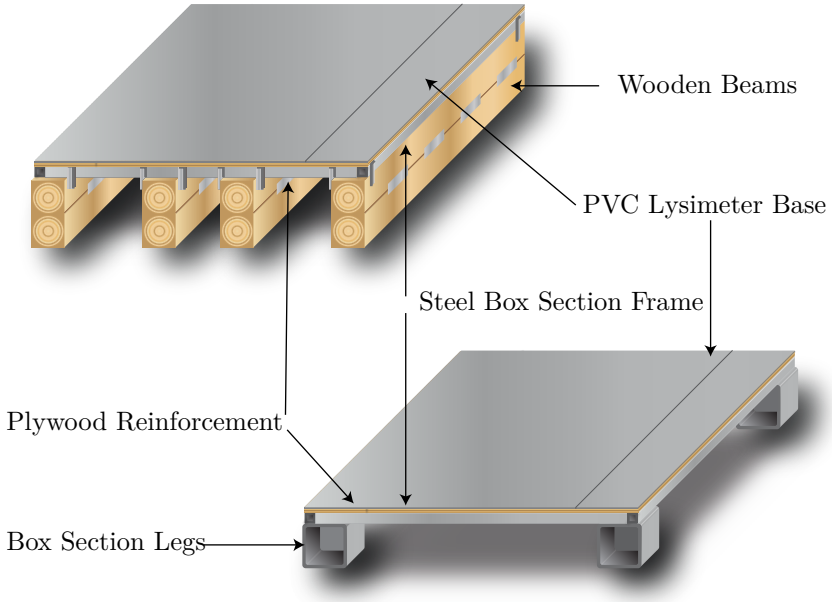

Figure 2.10: Diagrams of some initial base design ideas

2.3.6 Base

For the base, several designs were made as shown in Figure 2.10. These consisted of a plastic or a reinforced plastic base plate supported by beams or feet constructed from a variety of alternative materials. Wooden sections were moderately cheap, steel sections stronger and more expensive, yet the optimal, and by far the best tried and tested design was that of industrial plastic pallets. These were superior for several reasons. Firstly low cost; no labour or construction time was required increasing the build speed and reducing costs compared to other alternatives. Secondly, load capacity was well documented, commonly in the region of 6000 kg of static load capacity, making the choice of pallet relatively easy and removing

a lot of design work that alternatives required. Finally, the pallets would support the above lysimeter base evenly across its full area, meaning the base plate thickness would predominantly be limited by construction requirements and not its ability to resist bending moments over larger spans.

The final design consisted of a double layer of pallets, one on top of the other, allowing enough clearance for pipe fittings beneath the base plate. On top, a 10 mm thick PVC base was sufficient for supporting the lysimeter above it.

2.3.7 Instrumentation

The consensus was that TDR probes, resistivity probes and tensiometers were to be used, or likely to be used in the future. The TDR probes were to provide point volumetric water contents throughout the lysimeter, as discussed in detail in Chapter 3. Given enough probes, wetting fronts could be tracked through the soil column. Tensiometers (discussed in Chapter 4) were to provide data on suctions allowing for the soil water retention behaviour of the soils to be characterised. Figure 2.11 shows sketches of a TDR probe and tensiometer indicating probe sizes.

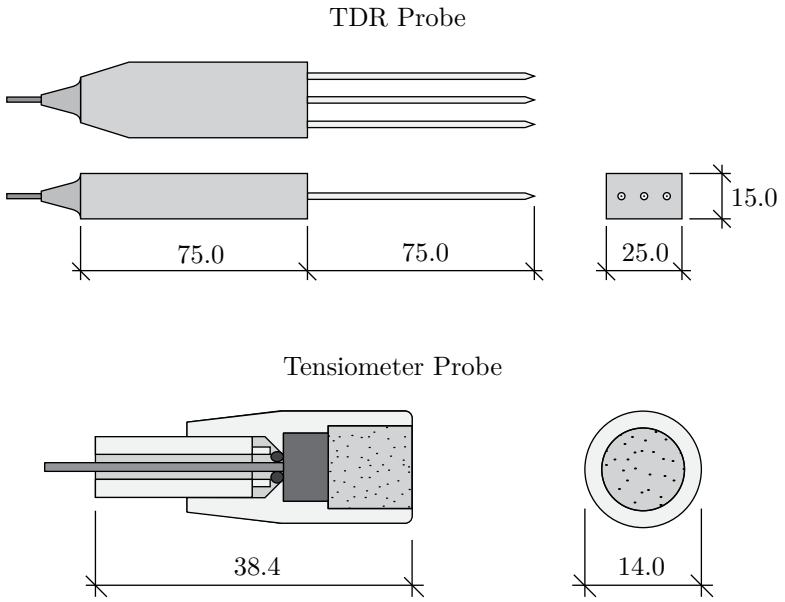

Figure 2.11: Dimensions of Probes

Firstly, with the combination of TDR probes and tensiometers allowing for the characterisation of soil water retention behaviour, it was required that the probes could be placed directly adjacent to each other, so as to be able to read suctions and water contents within the same region and correlate them accordingly. This meant the ports had to be reasonably sized so they could be situated close to one another, yet the probes had to be far enough apart to prevent significant influence on the others readings. A second point was the need to minimise the effects of the lysimeter boundary wall's influence on the probe readings. For this it was decided to place the probes so as they were taking measurements on an inner column of soil, that aligned with the leachate drain at the base, as opposed to being placed directly in contact with the surface of the soil at the lysimeter wall.

Combining the above needs with the requirements of tensiometers yielded the design as shown in

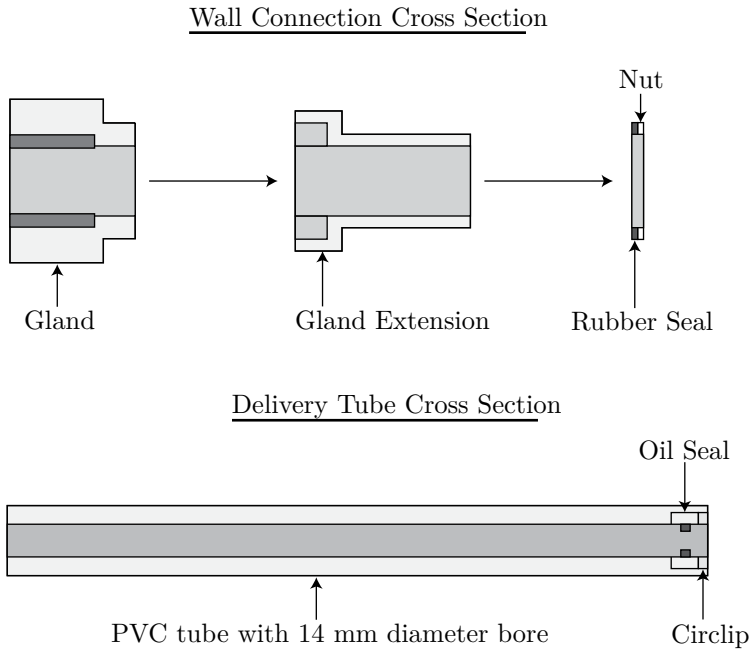

Figure 2.12: Diagram of Tensiometer Port Cross Section

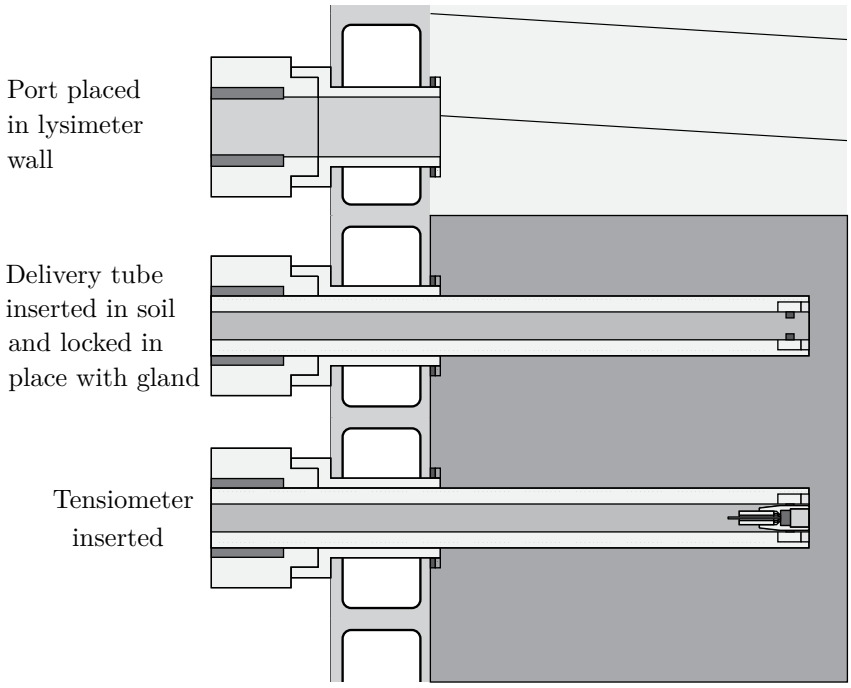

Figure 2.13: Tensiometer Port Inserted through Lysimeter Wall

Figures 2.12 and 2.13. The predominant aspect of this design was the ability to remove tensiometers for maintenance, including resaturation and calibration. The port consists of a 30 mm diameter PVC tube with a 10.5 mm bore, allowing delivery of a tensiometer to wherever the tube is inserted. At the tip placed into the soil is an oil seal. When either a tensiometer or a blank, a rod of 10 mm diameter used for sealing an inactive port, is inserted, they are held firmly in place by the oil seal. This maintains a water tight environment within the soil column, both limiting evaporation and leakage under saturated conditions. At the lysimeter wall, an M40 cable gland with extension was required. The extension was 55 mm in length to pass through the 50 mm thick lysimeter wall, allowing enough room for a nut and rubber seal on the lysimeter's inside face. The rubber seal for the nut to press against was needed to seal against the curvature of the inside wall and the threaded extension meant the full gland could sit on the outside of the lysimeter. This avoided having to inset it into the 50 mm thick wall itself, which would have weakened the structure giving it a rough finish. Inserting the PVC tube through the gland and closing the gland round the rod completes the water tight environment for the tensiometer ports.

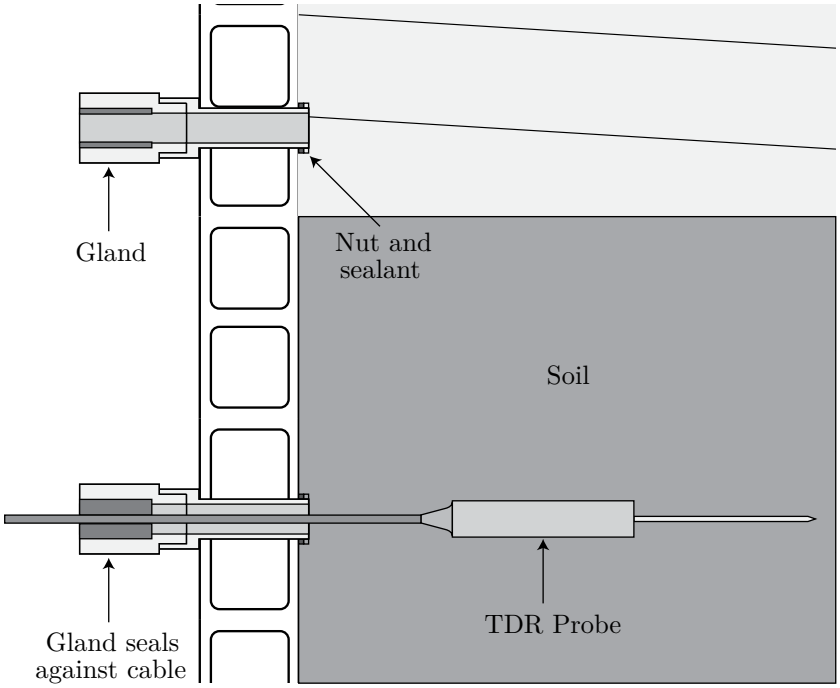

Figure 2.14: TDR Port Inserted through Lysimeter Wall

The TDR probes required a somewhat slightly different approach, as shown in Figure 2.14. As the probes were to be buried permanently within the soil as it was compacted, there was no need for their removal for maintenance. So long as the probes were checked upon insertion for an expected response, there was unlikely to be any major problems with this approach. The alternative, designing ports to allow removal, was deemed more complicated and held many disadvantages. Firstly, the port's delivery system would have to be substantial in size to contain a TDR probe and considering the planned close proximity to the tensiometer port, which is already substantial in size, the cumulative effects on the soil would be much greater. Another concern was the port at the lysimeter wall; given the size of the delivery system, this would require a large diameter assembly limiting the ability of placing the port adjacent to other ports. The third point is the effect of reinsertion of TDR probes on their effective readings. Inserting the frontal prongs on the probe into holes made previously changes the resultant readings and can particularly

affect the measurement of conductivity, which relies so heavily upon good contact with the soil. In all, it was decided to use a very simple cable gland, again with an extension to allow full passage through the thick lysimeter walls. The advantages were significant: fully flexible placement within the soil column, minimal disturbance and influence upon the surroundings and a simple watertight environment without multiple fail points. This also had the effect of permanently tying the TDR probes to the ports, with the BNC connector at one end and the probe at the other, making full removal of the probe hard.

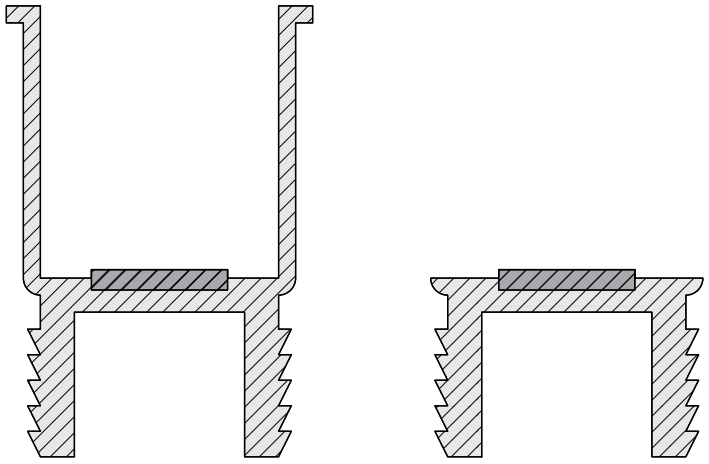

Figure 2.15: Diagram of ERT Port Cross Section

For future proofing the design with Durham University's new resistivity system that was under development during the design process, it was decided to investigate the possibility of ports for the insertion of resistivity electrodes into the soil surface. A simple method was developed for this purpose using self healing, hermetically sealing rubber septums as shown in Figure 2.15. One was inserted on the outside wall and a second was trimmed to a flat finish before insertion on the inside wall as shown in Figure 2.16. A resistivity probe could be inserted through both into the soil itself. With the self healing nature of the rubber, upon removal of a probe the rubber would heal and maintain the watertight environment.

The layout and quantity of the ports was of great importance to the level of detail achievable, both variance within a layer and variance with depth. It was decided to go with four equidistant TDR ports and four tensiometer ports in each layer as shown in Figure 2.17. This gave a measure of variance within a layer and a degree of redundancy in the case of probe failure or other unforseen circumstances. For the resistivity ports, sixteen per layer gave a reasonable spacing of 255 mm circumferential distance between ports on the outside wall corresponding to 236 mm circumferential spacings at the inside wall. Vertical spacings were chosen to be variable as shown in Figure 2.18. As near surface changes were to be more prominent, quicker and of more general interest, probe placement was biased towards this region whilst still maintaining good overall coverage throughout the height of the soil column. To this end, six layers were chosen with the near surface probes being just 50 mm below the soil surface and then at spacings of 150 mm, extending to 200 mm spacings further down.

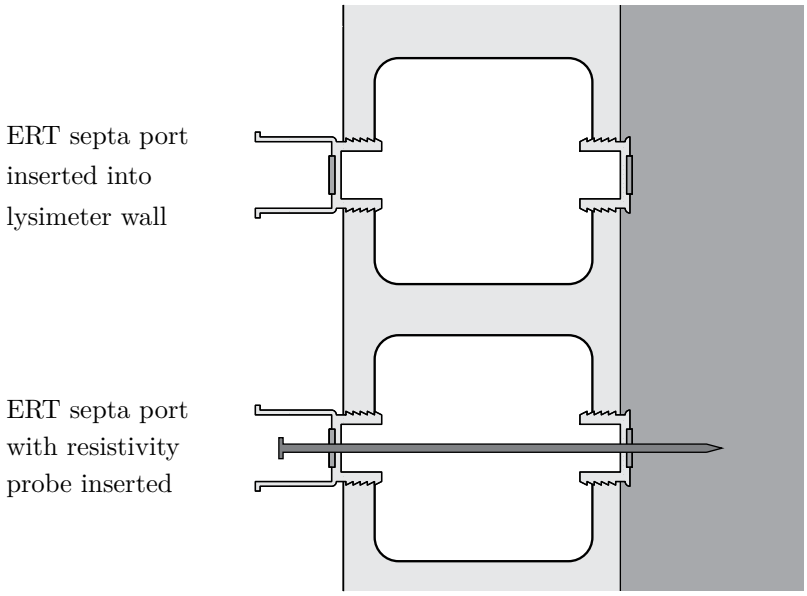

Figure 2.16: ERT Port Inserted through Lysimeter Wall

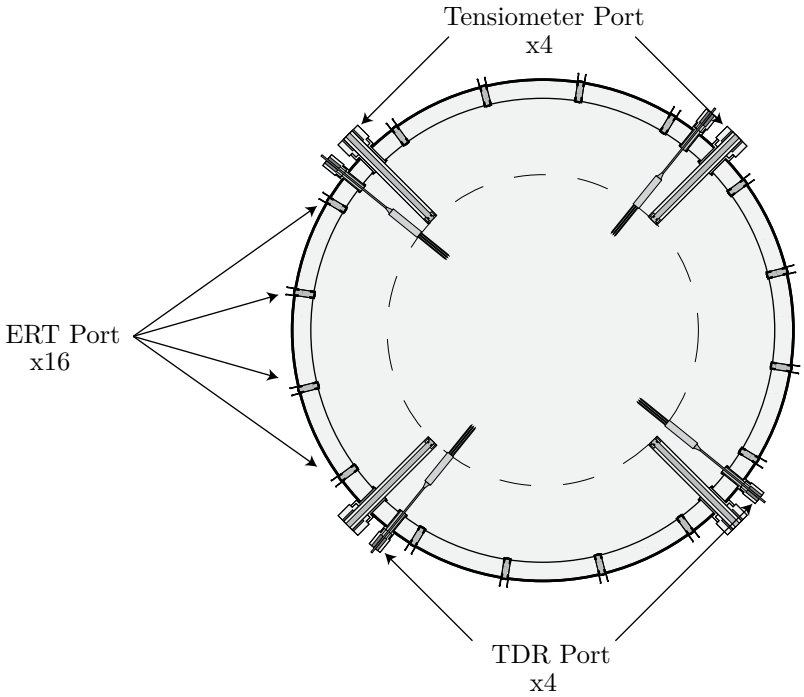

Figure 2.17: Diagram of Horizontal Port Positioning

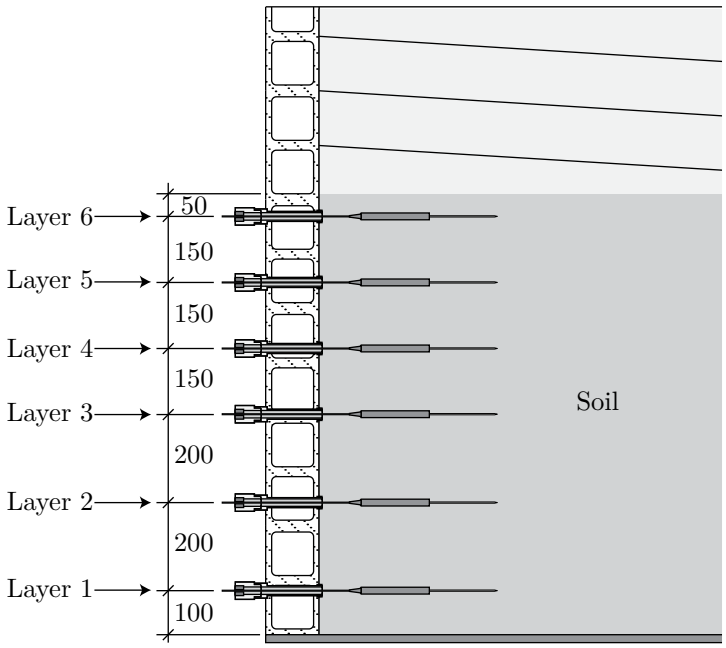

Figure 2.18: Diagram of Vertical Port Positioning

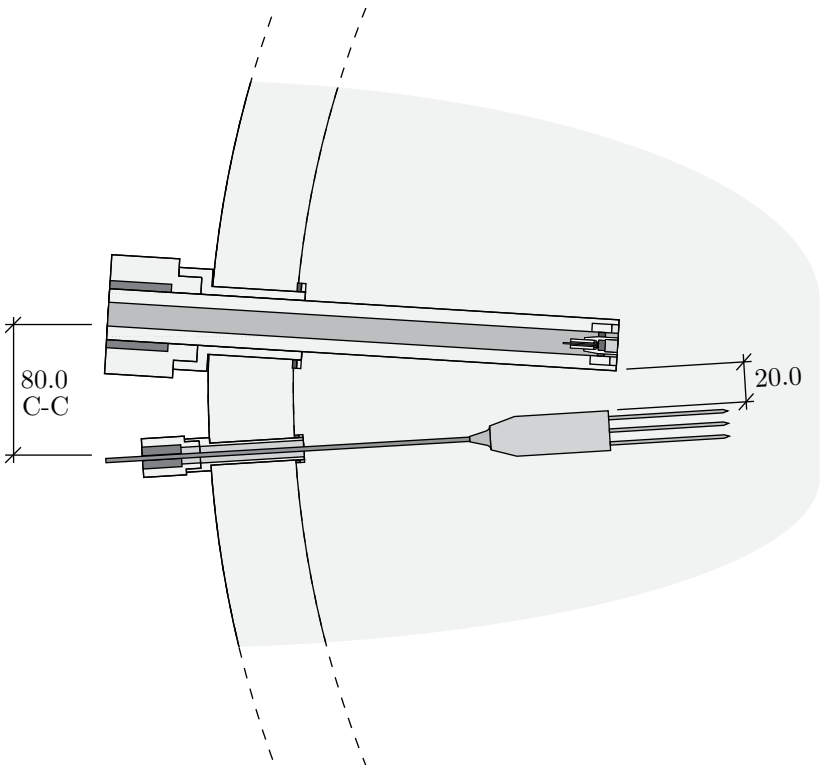

Figure 2.19: Diagram of Detailed Horizontal Port Positioning

Locally, the TDR ports and tensiometer ports were placed adjacent to each other for readings within the same zone. Figure 2.19 shows the relative spacial arrangement of the ports. This kept the TDR probe far enough away from the tensiometer port that the TDR readings were not influenced by the presence of the tensiometer and tensiometer port to any significant degree. Considering the volume of soil the TDR probe sampled, an absolute distance of around 20 mm between the two would be more than adequate whilst still maintaining a high degree of relevance. This distance also included some degree of flexibility due to the variable nature of drilling soil for the insertion of the port, post filling. The relative positioning of the ports on the outside wall were then calculated ready for construction.

2.4 Construction

Construction of the lysimeters followed a logical process and included some aspects not influenced directly by the needs of the design, such as storage for instrumentation, leachate and general organisation of the structures. Below the process is outlined including some of the finer details, materials and methods used in the process along with some of the problems encountered and their solutions.

2.4.1 Lysimeter

The lysimeter base was constructed out of a series of heavy duty pallets, each capable of holding six tonnes of static load, yet each was not quite large enough in size by themselves to hold an entire lysimeter even if they were sufficient in load capacity with a lysimeter weighing under 3 tonnes. The solution was to arrange them with all the lysimeters sharing the same run of pallets. Twelve were required in total, a run six long by one wide, stacked two deep as can be seen in Figure 2.20. The pallets were then linked with a long location baton screwed into place to maintain rigidity so they would not move during subsequent build phases.

Figure 2.20: Photo of Lysmeter Base Design Post Construction

The PVC base plate was ordered in custom cut sizes to fit the six meter run exactly. Before placement, a circular groove was cut with a router for each of the lysimeter walls, as shown in Figure 2.21. This

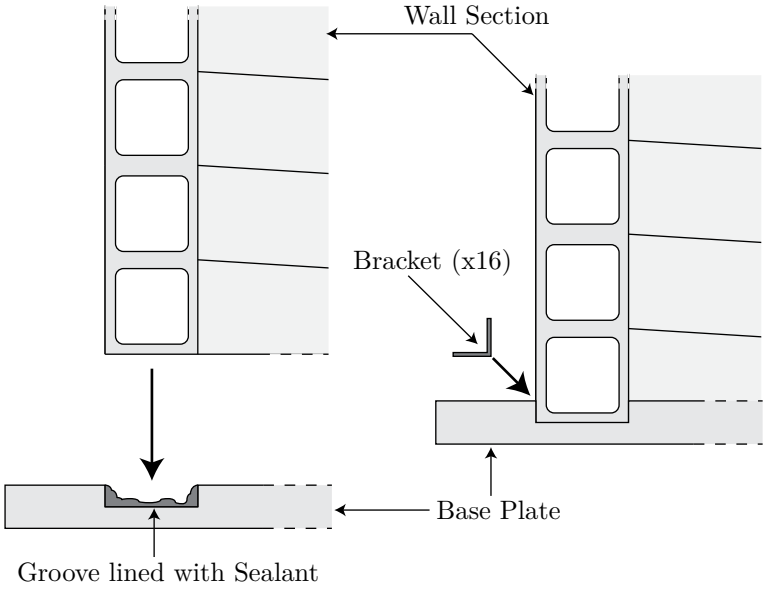

Figure 2.21: Construction Diagram of Joint between Base and Wall

aided in locating and sealing around the base to make the whole design water-tight. Once routed, the ends of the PVC sheets were painted in a PVC glue and were pressed together in place on the pallets whilst being screwed down and left to set in place. Once completed, two leachate drainage holes were drilled and tapped for each lysimeter for connecting piping to take away the leachate for collection then storage. The first leachate drain was for the central soil column, having an off centre location due to the central support provided by the pallets being directly under the centre. This was for collecting the leachate that had passed through the soil. The second leachate drain was at a radius of 0.525 metres, to collect leachate from the outer 0.15 m of the soil column and to also collect any water passing down the lysimeter walls. Finally bracketing was applied to keep cables tidy around the base.

Next, the large diameter pipes used to construct the lysimeters were cleaned and degreased at one end before placement in the awaiting grooves which had been prepared with a bedding of sealant. As soon as the pipes were in place, sixteen 50 mm brackets were screwed in using four screws each, around each lysimeter's outer wall, applying pressure to the sealant and holding the pipes in place during curing. Once finished, a secondary layer of sealant was applied to both the inside and outside walls around the base to reaffirm this watertight seal. With this stage complete the general structure of the lysimeters was ready for populating with ports, irrigation and instrumentation.

2.4.2 Ports

To allow installation of the ports, holes were bored in the lysimeter bodies. The 0.30 m tensiometer ports were cut from 2 m lengths of PVC rod, using a circlip and sealant to hold the oil seal in place at the end of the bore due for insertion into the soil column. Threaded extensions were made of PVC for the large diameter cable glands, allowing them pass through the thick lysimeter wall. These were then inserted into the lysimeter walls and screwed into place on a rubberised gasket for sealing. The delivery system containing a blank tensiometer body was inserted next and left flush against the inside face of

the lysimeter wall ready for the filling process, as shown in Figure 2.22.

Figure 2.22: Photo of Lysimeter Port inserted with the Face Flush to the inside of the Lysimeter Wall with the Blank Tensiometer seen below

The TDR ports underwent a similar process, with gland extensions made of PVC passing through the lysimeter wall, set into a sealant on the inside wall. Once the probes were made, the cables were passed through and the gland locked for the filling process.

Resistivity ports involved drilling holes through the lysimeter body at the appropriate locations measured out using plum lines and lasers forming a grid on the surface of the lysimeter. The self healing septums had the flange cut off half of them for insertion on the inside wall, which was a simple matter of cleaning the bore, deburring and applying enough pressure for the bung to go in just short of flush to the surface, relying on a small remaining lip left on. The remaining half were plugged into the outside holes after they were also cleaned out and deburred.

2.4.3 Irrigation

The irrigation system was fitted as shown in Figure 2.23 with a T section of structural piping crossing the width of the lysimeter. Originally attached at the top of the lysimeter, it was modified so as to be mounted slightly below the lip inside the lysimeter wall, allowing for placement of a lid over the whole construct. This meant the lysimeter could effectively be sealed. At the base of the T section, the irrigation sprinkler was inserted and with water supply piping passing through and out of the structural T section via a hole drilled in the lysimeter wall as seen in Figure 2.24, down to the computer controlled pumping system installed outside the lysimeter on its base. The water tank containing a fresh rainwater was kept directly adjacent to the base as a supply to the pumping system.

2.4.4 Instrumentation

Although the majority of instrumentation could be housed conveniently nearby, the TDR array required steps to minimise the lengths of cable used. Part of this process was setting up the multiplexer array

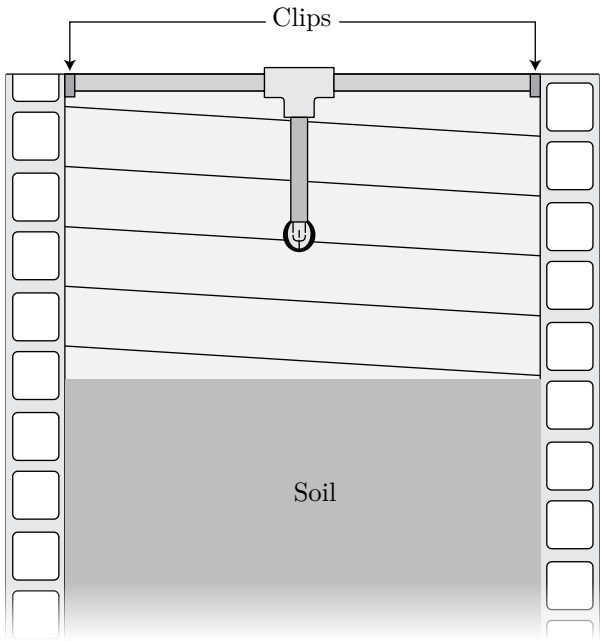

Figure 2.23: Diagram of Final Irrigation Implementation

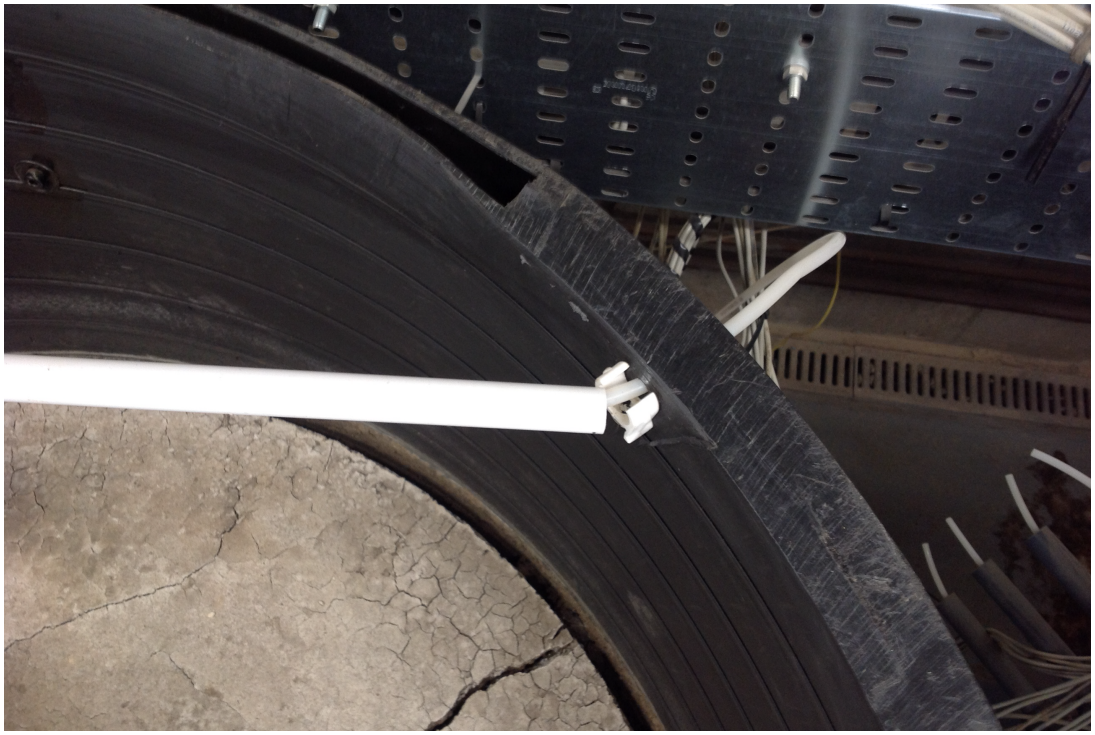

Figure 2.24: Lysimeter Irrigation Connection and Pressurised Water Line

directly on the back of the lysimeters, with the associated equipment for each lysimeter located next to it.

Figure 2.25: Photo of the finished lysimeters

For this purpose, a cable tray was mounted vertically, as oppose to its normal use horizontally, on spacers near the top of the lysimeters as can be seen running along at the back of Figure 2.25, separating the TDR cabling from the tensiometer and irrigation control system that ran along the base of the lysimeter. The cable tray worked well, with much of the TDR equipment being able to be screwed to the holes already present in the cable tray and much of the wiring cable tied on. This arrangement also aided in the reduction in cable length used for communication purposes, meaning a cheaper and more reliable set up with less chance for data loss.

2.5 Conclusion

In summary, a series of three large novel lysimeters have been designed and built for monitoring soil containing metal contamination. The material choices have been made to minimise the effects on the geochemistry and the geometry and scale of the design has been chosen to minimise the influence of unrealistic boundary conditions upon results. This has been achieved whilst retaining the capability to monitor soil properties insitu and in great detail over the course of the experiments. The following chapters will expand upon the instrumentation; its reliability, precision and accuracy before the results are discussed in detail in the final chapter.

Chapter 3

Time Domain Reflectometry

3.1 Introduction

Time Domain Reflectometry is a method employed across multiple disciplines for obtaining information on the response a medium gives to an electromagnetic wave passing through it. Within geotechnics, this response is often tied to the volume of water present in the voids within a soil. Due to the small nature of the probes and their relatively high degree of precision, Time Domain Reflectometry (TDR) is a well respected means of obtaining point water content measurements within a bulk soil in-situ with minimal disturbance to the natural state of the soil.

This chapter will first cover a brief history of the methods developed up to and including TDR, its uses in the world of geotechnics, and the array of modern systems available today commercially. Secondly, a detailed description of the background theory is discussed, from derivation to application, and the precision of the results given. Finally, the system design is discussed from device selection through to the construction of probes and then their performance.

3.2 Background

The history of TDR starts with another similar technology, Frequency Domain Reflectometry (FDR). Both technologies are based upon observing the electromagnetic responses of materials, with FDR looking at the response under varying frequencies, and TDR, the time response of a broadband signal composed of many frequencies [2]. Both techniques output a single number representing the interference nearby materials have on the propagation of a wave passing through wave guides within the material. Depending on the material, this number may be correlated to a physical property of interest. To do this, an understanding of electromagnetic waves and material interactions is required.

3.2.1 Electromagnetic Waves

Electromagnetic waves travelling through free space have a propagation velocity equal to the speed of light, approximately $3 \times 10^8\ ms^{-1}$. This velocity may be related to two components, an electric and magnetic component (expressed in equation 3.1).

$$c = \frac{1}{\sqrt{\varepsilon_0 \times \mu_0}} \tag{3.1}$$

Where c is the speed of light in ms^{-1}, ε_0 is the electric constant equal to $8.854 \times 10^{-12} Fm^{-1}$ and μ_0 is the magnetic constant equal to $4\pi \times 10^{-7} Hm^{-1}$. The propagation of a wave through a wave guide surrounded by materials is, however, hindered by the electrical and magnetic properties of the material.

This is represented in equation 3.2 through the introduction of two new parameters: relative permittivity, ε_r, a factor representing the influence of the material on the electrical component of a wave, and relative permeability, μ_r, likewise except with the magnetic component of a wave. Here the speed of light has been exchanged for a new measurement, propagation velocity v_p, representing the slower propagation of waves through a medium.

$$v_p = \frac{1}{\sqrt{\varepsilon_r \varepsilon_0 \mu_r \mu_0}} \tag{3.2}$$

Setting both ε_r and μ_r to a value of 1 yields the previous equation 3.1 once more and indeed equation 3.1 can be substituted for the electric and magnetic constants to give a relationship between propagation velocity and the speed of light, relative permittivity and relative permeability, as shown below in equation 3.3.

$$v = \frac{c}{\sqrt{\varepsilon_r \mu_r}} \tag{3.3}$$

This equation is the basis for both time and frequency domain reflectometry methods.

3.2.2 Material Interactions

In a vacuum, both relative permittivity and relative permeability defer to a value of 1. Yet when a wave passes through the vicinity of a material, these values increase dependent upon the type and state of the material, hence reducing the propagation velocity of the wave below that of the speed of light. To explain this reduction a description at a molecular level is required, which will in turn lead to an explanation of losses due to these interactions.

During the early 20th Century determining the electrical and geometrical structures of molecules was of prime interest. One experiment that produced relevant results was the application of a field to gaseous molecules. The molecules would respond with a shift in position of the electrons relative to the nuclei, yet it was observed that not all molecules responded as expected. For instance, an inert gas such as neon, with a full stable outer electron shell, would exhibit a much smaller response than say a molecule of water or ammonia, which were noted to have responses some forty times greater [32].

This notable difference was attributed to two summating effects: firstly a displacement, as could be seen with neon, that was assumed to always be present whenever a field was applied to any molecule; secondly, a rotational movement of the molecule as it orientated itself under the influence of a field, due to the permanent moment created by the nonuniform distribution of electrons. In terms of relative significance, orientation could account for the majority of the displacement observed in molecules with a permanent dipole. With the example of ammonia, 90% of the observed displacement was due to the orientation of the permanent dipole and only 10% due to deformation of the electron cloud. These interactions account for the various permittivities of different materials, where neon has a low relative permittivity of 1.000148 [42] and ammonia a much higher permittivity nearer to 20 (although this number varies considerably with temperature).

With regards to losses, two primary effects were of concern. The first was due to a second observation that was made experimentally, once again focusing on the gaseous state, whereby increasing the frequency of incident radiation resulted in the rotation of molecules dissipating until all that remained was the effect of displacement. This was attributed to the finite time required for a molecule to reorient itself in line with a field, referred to as a relaxation time and was readily observable as a sudden change in behaviour with gaseous molecules. Liquids on the other hand, had more influencing factors. The intermingling of molecules hindered their response due to inter molecular interactions that varied considerably based on

molecular dimensions, viscosity of the bulk liquid and temperature. This resulted in both lowering and blurring the upper limit of frequencies away from the sudden changes observable in gases.

This effectively meant that there was an upper limit on frequencies that could be applied if a response in terms rotation, associated with energy storage, was to be expected. Beyond this limit, the losses in the system would artificially increase measured permittivity from the true value associated with that medium and simultaneously make measuring responses in the wave more difficult to read.

The second dominant effect causing losses in the system is that of conductivity. This was first explored in the work of Smith-Rose [34] who worked on the systematic characterisation of soil using FDR. With all prior work either being on gaseous or non-conducting liquids, Smith-Rose was the first to study the effects of conductivity in this context. The study found that as frequency decreased, conductivity losses in the system increased exponentially. This again had the effect of inflating the measured permittivity of a medium beyond its true value.

Considering the above, relative permittivity can be expressed as a complex equation including real quantities associated with energy storage and imaginary components associated with energy losses. Given that the component associated with energy storage is typically of interest and considering the true permittivity of a medium, the resulting permittivity given by the combination of all components is commonly referred to as the apparent relative permittivity as given by equation 3.4.

$$\varepsilon_r^* = \varepsilon_r' - j\left(\varepsilon_{relax}'' + \frac{\sigma_{dc}}{2\pi f \varepsilon_0}\right) \tag{3.4}$$

The real component is denoted by (ε_r') and the imaginary component, typically denoted by (ε_r''), consists of all losses within the system. As discussed above, equation 3.4 includes losses due to relaxation (ε_{relax}'') and losses due to conductivity ($\sigma_{dc}/2\pi f\varepsilon_0$), where σ_{dc} is the equivalent direct current conductivity and f is the frequency of oscillation.

This relationship is useful to acknowledge when the real permittivity of a material, or indeed a combination of materials, is leveraged to gain an insight into other properties associated with that medium, as with both time and frequency domain reflectometry.

3.2.3 Time Domain Reflectometry

In 1969 switching from the frequency to the time domain was first seriously considered for experimental work [43]. The inherent advantage of working in the time domain was that all frequencies of interest could be provided simultaneously [43] as opposed to the lengthy measurements of FDR whereby each individual frequency was applied and response observed separately. In addition, the equipment required for this task was already in operation commercially, being used as cable testers as early as the 1930s [44], finding the position of faults in long lengths of coaxial cable. This was achieved through applying a step input voltage to the core conductor and observing the amount of time taken for a partial reflection of the signal, due to a change in impedance, to occur. The time taken for a response could then be used to find the physical fault in the cable.

The idea for materials testing was to monitor the resident time of a propagating wave through a wave guide of known length, in a material of interest. This in turn would allow calculation of a velocity which could be directly related to the apparent relative permittivity of the medium, assuming a relative permeability of 1. A typical TDR system is shown in Figure 3.1.

The system consists of a unit capable of creating short rise time step inputs associated with a range of frequencies below that of relaxation yet above that of significant conductivity losses e.g. for water the lower limit is approximately at 1 MHz and the upper limit at 1.5 GHz. The system also makes use of a precise timing circuit for coordinating measurements with the sampling unit monitoring the voltage on

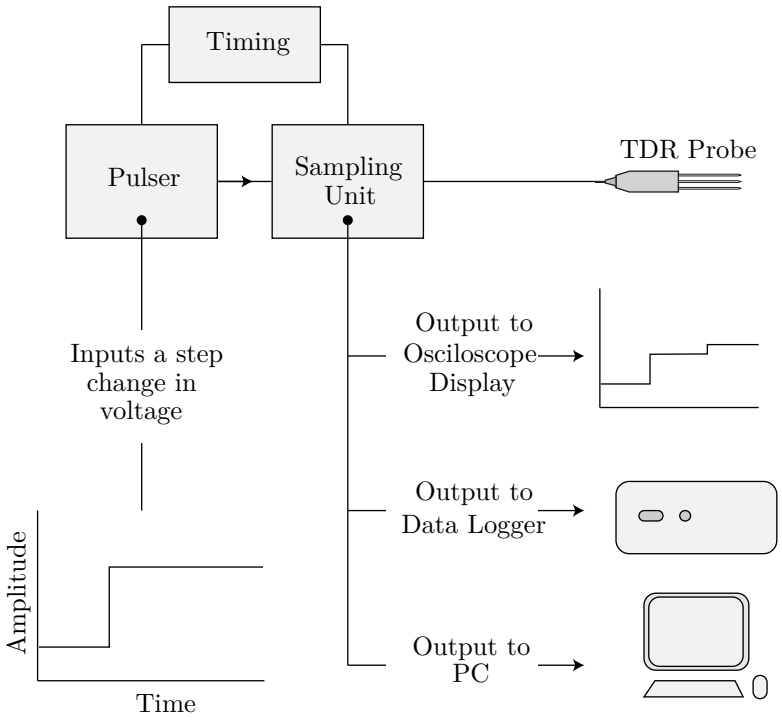

Figure 3.1: TDR System

the coaxial core. Outputs vary by commercial system, with the main two options being a visual display on the device in the form of an oscilloscope or communicating data to a data storage device such as a logger box or PC. The TDR probe head is connected to the system via coaxial cabling and essentially acts as an open ended extension of the cable immersed in the medium of interest.

The probe head ingeniously uses the fact that a change in impedance causes a partial reflection of the applied signal (as with damaged coaxial cables). This can be used as a marker in the form of a change in material within the probe head, to define the start of the signal entering the wave guides. When the input signal reaches the open end of the wave guides, a full reflection occurs then once again the signal passes the change in impedance, this time indicating the majority of the signal exiting the probe head.

In terms of expected voltage response, a system consisting of a signal generator and oscilloscope connected to an open ended coaxial cable, given an initial step voltage, would return a full reflection of the signal. Similarly with a closed system no reflection is expected. The common way to express this is through the use of a reflection coefficient, assuming a reference voltage of zero, this is shown in equation 3.5.

$$\rho_u = \frac{V_i - V_o}{V_o} \tag{3.5}$$

This equation returns a value for the reflection coefficient, ρ_u, between -1 and +1 for any system so long as the output voltage from the device, V_o, is known and the reflected or input voltage, V_i, is monitored. A value of 1 denotes a doubling in the measured voltage whereas a value of -1 indicates that the voltage is zero.

Observing changes in the reflection coefficient through the probe head allows calculation of the residence time within the wave guides (which are of a known length); hence the propagation velocity associated with a material can be determined. Rewriting equation 3.3 in terms of length and time, and

assuming a relative permeability (μ_r) of 1 yields equation 3.6.

$$\frac{2L}{\triangle t} = \frac{c}{\sqrt{\varepsilon_r^*}} \tag{3.6}$$

Where L is the physical length of the waveguide used and $\triangle t$ is the time taken for the signal to travel both ways through the probe head. The relative permeability (μ_r) is assumed to be 1 predominantly as materials with a value greater than this are uncommon in soils. This equation can be simplified to be written in terms of a ratio between apparent probe length and actual probe length giving equation 3.7

$$\sqrt{\varepsilon_r^*} = \frac{L_a}{L} \tag{3.7}$$

Where L_a is an apparent length equivalent to $c\triangle t/2$ and works as an alternative for time as the X-axis, as demonstrated in Figure 3.2. The figure shows a waveform given by a probe immersed in water. As the signal propagates, a partial reflection occurs on entry into the probe head, which is denoted by the first peak in reflection coefficient. The signal continues and fully reflects at the probe tip before exiting the probe head at the second significant increase in reflection coefficient. Both the entry and exit points are denoted on the figure by dashed lines.

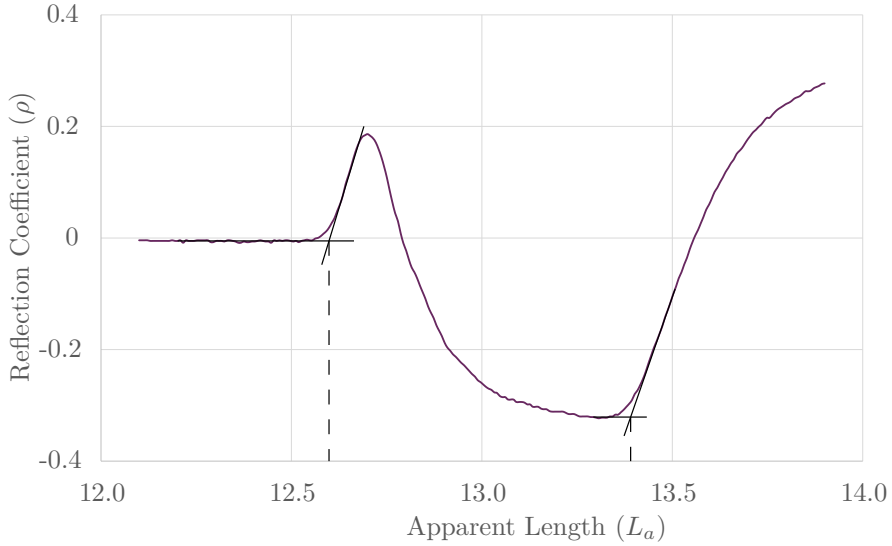

Figure 3.2: TDR Waveform for Water

Entry to the probe head is calculated through the intersection of two tangent lines at the base of the first rise in reflection coefficient. This is the most stable point to take measurements around because the peak moves slightly dependant upon the permittivity of the material the wave guides are immersed in. Similarly, tangents are drawn for the exit point calculation around the base of the second significant rise.

In general, TDR has proven to be a successful method for measuring the apparent relative permittivity of materials, being both accurate and quick.

3.2.4 Volumetric Water Content of Soils

In 1980 the work of Topp et al. [45] noted that the significant difference between the permittivities of soils and water could be exploited, so that TDR could be used for the determination of water contents. Table 3.1 demonstrates the approximate relative permittivities of various materials found within soils.

It can be seen that, while minerals may vary in terms of relative permittivity, most dry soils have

Table 3.1: Permittivities of Soil Materials [1]

Material	**Relative Permittivity**
Basalt	12.0
Granite	7.0 to 9.0
Sandstone	9.0 to 11.0
Dry Loam	3.5
Dry Sand	2.5
Air	1.0
Water	80 at 20°

a value of around 3 [45]. Importantly, the permittivity of water is significantly higher than that of any common mineral.

Through experimentation, Topp et al. were able to derive empirical equations relating the apparent relative permittivity for a material analysed using the broadband TDR technique, to the volumetric water content present within the soil matrix. For mineral based soils equation 3.8 was derived and similarly for soils with large quantities of bound water, such as those containing high quantities of organic matter, equation 3.9 was derived [45].

$$\theta_v = -5.3 \times 10^{-2} + 2.92 \times 10^{-2}\varepsilon_r^* - 5.5 \times 10^{-4}\varepsilon_r^{*2} + 4.3 \times 10^{-6}\varepsilon_r^{*3} \tag{3.8}$$

$$\theta_v = -2.52 \times 10^{-2} + 4.15 \times 10^{-2}\varepsilon_r^* - 14.4 \times 10^{-4}\varepsilon_r^{*2} + 22.0 \times 10^{-6}\varepsilon_r^{*3} \tag{3.9}$$

Other similar expressions were later developed by Ledieu et al. [46] in 1986, given in equation 3.10 and that of Malicki et al. in 1996 [47] which incorporated the bulk density as an additional factor as shown in equation 3.11.

$$\theta_v = 0.1138\sqrt{\varepsilon_r^*} - 0.1758 \tag{3.10}$$

$$\theta_v = \frac{\sqrt{\varepsilon_r^*} - 0.819 - 0.168\rho_b - 0.159\rho_b^2}{7.17 + 1.18\rho_b} \tag{3.11}$$

All the equations above work for a typical range of water contents associated with soils, between that of around 5% and 45% θ_v. At lower water contents, the permittivity of the soil increasingly influences the interpretation with the decrease in propagation velocity still being entirely attributed to water. Water contents above 45% are typically unrealistic of soils and hence are not included in the design of these equations.

A second method for determination of volumetric water content are volumetric models. These require knowledge of the volume factions for each constituent material, and their associated permittivities, to reliably give accurate interpretations. A common volume model applied to soils is that of the power law approximation [48–50]. This assumes a soil is constructed out of nearly spherical oblate spheroid inclusions, meaning an exponent of value of 0.5 is applied to each factions permittivity as in equation 3.12.

$$\varepsilon_r^* = \theta_w\varepsilon_w^{0.5} + \theta_s\varepsilon_s^{0.5} + \theta_a\varepsilon_a^{0.5} \tag{3.12}$$

Where the volume factions of solid, water and air are denoted by θ and permittivity by ε, with subscripts s, w and a respectively. An alternative is that proposed by Whalley [49] which represents the

soil as three homogeneous layers perpendicular to the propagation of the TDR signal, as given in equation 3.13.

$$\theta_v = \frac{(\sqrt{\varepsilon_r^*} - 1) - \frac{\rho_b}{\rho_s}\left(\sqrt{\varepsilon_s} - 1\right)}{\sqrt{\varepsilon_w} - 1} \tag{3.13}$$

Where the bulk density is given by ρ_b and the specific density of the solid material by ρ_s. Neither of these models capture the microstructure of soil as a porous medium, which is still the case with some of the more complex models, though with continued work a more comprehensive physically based model suitable for use on soils could be developed. In comparison to the empirical formulae of Topp and Ledieu, a higher degree of accuracy is expected with the volumetric models. This, however, comes with the cost of requiring more information on a soil in the first instance, something that cannot be guaranteed both in terms of ease of gaining the information nor consistent reliability.

3.2.5 Electrical Conductivities of Soils

The Electrical Conductivity (EC) of soils is of interest due to two main factors. Firstly, the apparent correlation that exists between the electrical and hydraulic conductivities [51–53] and secondly, the correction of apparent permittivities to real permittivities associated with volumetric water content calculations [2, 54, 55]. With regards to time domain reflectometry, the bulk EC σ_a of a soil can be correlated to attenuation of the signal, resulting in a lower steady state reflection coefficient [56]. To illustrate, given a system with no losses, an open circuit response would correspond to a steady state reflection coefficient of +1. Conversely, a perfect closed circuit response would tend to a reflection coefficient of -1. Anywhere in between these two states could therefore be associated with a conductivity somewhere between that of a pure conductor and pure resistor.

The basic derivation of a relationship between reflection coefficient and electrical conductivity assumes a system with no losses apart from those experienced by the probe head. Also assumed is that as time tended towards infinity the associated frequencies tended towards zero and the probe acted as an imperfect capacitor. This results in equation 3.14 [57].

$$\sigma_a = \frac{1}{Z_0} \times \frac{Z_g c \varepsilon_0}{d} \times \frac{1 - \rho_\infty}{1 + \rho_\infty} \tag{3.14}$$

Where σ_a is the bulk electrical conductivity; Z_0 is the characteristic impedance of the system, typically around 50Ω; Z_g is the characteristic impedance of the empty sample at $\varepsilon_r* = 1$; d is the sample dielectric length and ρ_∞ is the measured reflection coefficient at infinite time. This can be simplified somewhat by equating the second set of terms to an experimentally measurable value termed the probe constant as per equation 3.26 with the remaining terms forming the sample conductance as per equation 3.25

$$K_p = \frac{Z_g c \varepsilon_0}{d} \tag{3.15}$$

$$G = \frac{1}{Z_0} \times \frac{1 - \rho_\infty}{1 + \rho_\infty} \tag{3.16}$$

Considering that the relationship between electrical conductivity and conductance is linear and passes through zero, determining the probe constant experimentally is a simple affair. What can complicate matters, however, is the inclusion of losses in the system as a whole. Since the relationship given in equation 3.14 assumes no losses, something must change to take account of the waveform sampling occurring near the point the step input is generated. Anything between this point and the probe head will influence the measured steady state reflection coefficient.

One method to account for attenuation in the cables themselves is the use of a frequency dependant attenuation constant, yet this has issues with systems that include discontinuities such as multiplexers for switching the signal to different probes, as these are much harder to include in the analysis. A broader and better solution was presented by Castiglione and Shouse [57] who investigated scaling the measured reflection coefficient in different ways so as to ensure a linear trend between conductivity and conductance. With losses in a system, the open circuit value would diminish to less than 1 whilst the close circuit value would likewise tend upwards. The magnitude of these changes depends greatly upon the system, particularly cable length prior to the probe head. The method concluded to be the best by Castiglione and Shouse was to scale, relative to both open and closed circuit conditions as per equation 3.17:

$$\rho = 2\left(\frac{\rho_u - \rho_o}{\rho_o - \rho_c}\right) + 1 \tag{3.17}$$

In the above equation ρ is the corrected reflection coefficient for use in equation 3.14, ρ_u is the as-measured uncorrected reflection coefficient, ρ_o is the open circuit response in air and ρ_c is the closed circuit response formed by shorting the wave guides. This method also takes account of discrepancies between the change in magnitude of open and closed responses, caused by discontinuities. Replacing ρ_∞ in equation 3.14 with $\rho_{corrected}$ calculated in equation 3.17, yields a corrected value of soil bulk conductivity σ_a that resembles much more closely the true value associated with a soil system.

In terms of using the soil bulk electrical conductivity to account for the imaginary component (ε_r'') of the apparent permittivity (ε_r^*) as given in equation 3.4, some theoretical [2], modelling [55] and practical work has been done [54], yet there is room for improvement. Assuming the apparent permittivity can be described as a sinusoidal plane wave as according to Von Hippel [58], it can be calculated according to equation 3.18:

$$\varepsilon_r^* = \frac{\varepsilon_r'}{2}\left[1 + \sqrt{1 + \left[\left(\varepsilon_r''(\omega) + \frac{\sigma_{dc}}{\omega\varepsilon_0}\right) / \left(\varepsilon_r'(\omega)\right)\right]^2}\right] \tag{3.18}$$

The work of Bittelli took this a step further by following the suggestions of Topp et al [59]. Losses due to relaxation were ignored and it was assumed that the bulk electrical conductivity was equivalent to the Direct Current (DC) current electrical conductivity given above in equation 3.18. These assumptions meant all the unknowns were essentially accounted for, allowing equation 3.18 to be rearranged to give real permittivity yielding:

$$\varepsilon_r'' = \varepsilon_r^* - \frac{{\sigma_a}^2}{4\varepsilon_r^*{\varepsilon_0}^2\omega^2} \tag{3.19}$$

In the above equation, ε_r^* and σ_a are known values measured by a TDR system and ε_0 is a constant. The only unknown being the angular frequency ω equal to $2\pi f$ where f is the frequency in Hertz. This is where there is some disagreement in the literature as to the frequency that best represents a broad band technique. The work of Or and Rasmussen (1999) [60] compared the response of a TDR system to that of FDR to characterise the associated frequency with the broadband technique yielding an empirical equation for that particular system. In the work of Robinson et al. (2003) [2] this was referred to as the maximum frequency when contrasted to another interpretation named the effective frequency given below in equation 3.20:

$$f_e = \frac{\ln(0.9/0.1)}{2\pi t_r} = \frac{0.35}{t_r} \tag{3.20}$$

Topp et al. (2000) [59] argued that f_{eff}, the effective frequency, should represent the frequency where the majority of the energy is contained and t_r is the rise time. An alternative to equation 3.20 was used by Bittelli et al. (2008) [54] based on the work of Johnson and Graham [61], given below in equation 3.21

$$f_k = \frac{0.5}{t_r} \tag{3.21}$$

Here the calculated frequency, named the knee frequency (f_k), equates to a frequency below which most energy is concentrated. To give a rough estimate of magnitude based on the work of Or and Rasmussen, f_k is around $0.64 f_{max}$ and f_e is approximately $0.45 f_{max}$. Further complicating which frequency to use when assessing the magnitude of complex permittivity is the method used when determining the rise time, t_r. The most popular method is to calculate the time difference between 10% and 90% of the second inflections change in magnitude, described in several texts and given in Appendix C of the Tektronix TDR system. For the work based upon f_{knee} a different approach was used: t_r was calculated as the difference in time between the base of the second inflection to the intercept of two tangents, one drawn as a tangent to the rise in reflection coefficient and one drawn tangent to the steady state reflection coefficient [54]. This is contrary to the original source referenced for this relationship, which suggests the use of the 10% through 90% method [61] and would likely result in a reduction in calculated rise time.

There is still some work required to improve corrections of apparent relative permittivity to real relative permittivity, yet for now the capability of assessing an approximate magnitude for these losses is at least available.

3.3 System Design and Construction

An implementation of a TDR system, as shown earlier in Figure 3.1, was required for monitoring the volumetric water contents at various layers and spacings within the large lysimeters. The system had the following requirements:

- Computer controllable;
- Generic probe compatibility;
- Expandable for multiple probes;
- Capability for custom calibrations;
- Ability to measure conductivity;
- Good accuracy;
- Reasonable costing.

3.3.1 TDR System Selection

A summary of available commercial TDR systems is given in Table 3.2. In terms of controlling the systems, all were to some degree capable of being driven by a computer, yet not all had the capability for automated logging. Indeed, some such as the Campbell Scientific TDR100 could only be controlled manually with supplied software, although data loggers could be purchased to perform this function at additional cost. Other systems had several pieces of software capable of analysing TDR waveforms, such as the Tektronix 1502, a well proven piece of equipment for automation [62] with its three freely available options of software choices. Another of the alternatives were hand held devices e.g. Easy Test FOM/mts,

Table 3.2: Comparison of TDR Devices and Features (Expanded from Robinson et al. [2].)

Feature	**Tektronix DSA8200**	**Tektronix 1502(B,C)**	**Easy Test FOM/mts**	**Soil Moisture Mini Trase 6050X3**	**Environmental Sensors Inc MP-917**	**Campbell Scientific TDR100**	**Soil Moisture Trase System I 650X1**	**Mesa Systems Trime FM2**
Transmitted Signal Rise Time (ps)	12	200	200	125-155	>200	170	125-155	300
Output Pulse Magnitude (V)	0.25	0.30	2.00	1.60	0.30	0.25	1.60	
Weight (kg)	21	6.5	3.8	3.4	5	0.7	12	0.9
Size (cm)	46x42x34	44x32x13	26x18x13	23x20x13	27x25x17	21x11x6	28x42x23	18x8x6
Minimal Cost to Use [a]	$25,000	$11,695	$4,707	$6,895	$5,350	$4,600	$9,550	$4,370
Probe Compatibility	Generic	Generic	Propriety	Generic	Propriety or Generic	Generic	Generic	Propriety
Display Options	LCD, PC	LCD, PC	LCD, PC	PDA, PC	LCD, PC	Data Logger, PC	LCD, PC	LCD, PC
ε, θ Calibration	None	None	Fixed	User Defined	Fixed	User Defined	User Defined	User Defined
Device Output [b]	WF	WF	EC, θ, T	WF, ε, θ	WF, θ	WF, EC, ε, θ	WF, ε, θ	θ
Waveform Size (pixels)	480	251		1200	255	100-2048	1200	
Storage Options	HD, CD, DL, PC	PC, DL	PC	PC, DL, PDA, IS	PC, DL, IS	PC, DL	PC, DL	PC
Electrical Conductivity	Manual	Manual	Yes	No	No	Yes	No	No
Cable Connection Type	SMA	BNC	BNC	BNC	BNC	BNC	BNC	Proprietry
Reported Accuracy (%)		±1	±2	±2	±1	±1	±2	±1
Power Supply	AC	AC, Battery	AC, Battery	AC, Battery	AC, Battery	Battery	Battery	Battery
Analysis Software	IConnect	TDRANA, WINTDR, TACQ	Propriety	WinTrase, TraseTerm	View Point	PCTDR, WINTDR	WinTrase	Imp232 Micronet

[a] All US$ prices are accurate for 2003 and are shown for comparative purposes.
[b] WF = Waveform, EC = Electrical Conductivity, θ = Volumetric Water Content, T = Temperature, ε = Apparent Relative Permittivity

yet these had proprietary hand held computers with fixed settings and no real scope for adapting to a lysimeter monitoring system.

In terms of probe compatibility, the majority of systems allow for generic probe designs, with the only limitations being imposed by hand held devices requiring proprietary probes to work with the system e.g. Mesa Systems TRIME FM2, Delta-T Devices Theta Probe ML2x, and Easy Test FOM/mts. Other table top systems all use standard available BNC connectors which work with a range of available probe designs, both from manufacturers or custom built alternatives.

An easily expandable system is inferred by the need for monitoring multiple probes using a single system to generate and sample TDR signals. As before, hand held devices do not meet these requirements, yet the majority of desk top systems can be connected to a series of multiplexers. The Tektronix 1502 systems are capable of being connected up to both the Dynamax TR-200 16 channel multiplexer and the Campbell Scientific SDMX50 multiplexer which can be controlled by the TACQ software. Similarly Campbell Scientific's own TDR100 system works with the SDMX50 multiplexer although the PCTDR software lacks automated readings. The Soil Moisture Mini Trase 6050X3 has its own compatible multiplexer system for expanding to read multiple probes, although this system only stores data to a robust field ready data logger with limited capacity unlike its larger brother, the Soil Moisture Trase System 6050X1. In general, all these systems have more than adequate capacity to read the 72 probes required for the lysimeters.

Custom calibrations are easily applicable to all the desktop systems, with each having the capability of providing waveforms as direct output. With the Tektronix 1502 system, this is the only way to obtain a volumetric water content, the other desk top systems are, however, simultaneously capable of interpreting the waveforms, outputting permittivities and water contents.

An additional parameter of interest, especially considering the nature of the amendments added to the soil (discussed in chapter 6), was conductivity. It was very apparent here that some systems were incapable of measuring this property; the two remaining systems that could were the Campbell Scientific TDR100 and the Tektronix 1502. As with the measure of permittivities and volumetric water contents with the tektronix device, conductivity readings were a fully user based interpretation, as opposed to the TDR100 device, which offered in built capability for determining the conductivity of a medium.

Another important point to discus is the accuracy of these systems. The hand held devices lose out again here due to limited customisation and a greater focus on a smaller product for quick readings of water contents. The larger desktop alternatives can provide a greater degree of accuracy, partially through repeat readings and partially through being better equipment.

In terms of costs, equipment varies wildly from manufacturer to manufacturer. The costs shown in Table 3.2 are approximate for a basic working system around 2003, yet since then the tektronix 1502 device has gone out of production and is only available second hand. The other devices have remained relatively steady in cost, with the Campbell Scientific system being the cheapest to get up and running. Others include additional costs presumably to cover the inclusion of enclosures, their portability and other accessories, such as the Soil Moisture Trase systems.

Each system has its own unique niche and some had features that were unnecessary for the needs of the project. The Tektronix 1502 device was one of the more powerful and readily usable devices, capable of meeting all the requirements discussed above apart from costing and availability. The system was the most expensive system and also was out of production put it at a disadvantage. The hand held devices were unsuitable for monitoring large lysimeters, although the acquisition of a small hand held device has proven useful for other needs. The Soil Moisture Trase systems, both the 6050X3 and 6050X1 were worth considering, although the designs were more in line for field monitoring of a site and the inability to

measure conductivities was a disadvantage. The Environmental Sensors Inc. MP-917 also had the same disadvantages. The final system was the Campbell Scientific TDR100 system, fulfilling all of the above requirements bar being controllable by a PC for which a full software development kit was available.

Between the two most favourable systems, the TDR100 and 1502, it was decided to go with the TDR100 which was the most flexible system available direct from a manufacturer. It was capable of being expanded to monitor 512 probes in series, it had in built functionality for interpreting waveforms and conductivities and had good accuracy of reading, which meant the system would all round perform well and did not come with unnecessary additions such as weather proof housing etc. that may be more desirable on other projects.

3.3.2 TDR Probe Design

Campbell Scientific, the company producing the TDR100 system chosen, also produced TDR probes. The probes came in three main sizes, 0.075 m, 0.15 m and 0.30 m length rods, each with the own benefits depending upon the user requirements. Yet it was decided fairly early on that building and designing probes in the laboratory would have several benefits over buying in the probes from Campbell. Firstly, the probes could be customised for the lysimeters; secondly, the ability to design and build probes for any application would be advantageous for any future experimental work were non-standard sized probes required and thirdly, costs could be reduced allowing for a greater number of probes to be embedded within the lysimeters meaning more replicates of data and a greater clarity of events could be achieved within the soil columns. The main desirable characteristic of the TDR probes was precise measurement of point water contents with the design coming down to four main wave guide properties:

- Number;
- Length;
- Spacing;
- Diameter.

The number of wave guides is known to greatly affect the sampling cross sectional area, and hence sampling volume, of TDR probes. Two prongs, one being attached to the central core of the coaxial cable and the other the metallic shielding, have the most dispersive effect and hence the greatest cross sectional area. Using three prongs and up, with one central prong being connected to the core and the remainder attached to the shield, reduces this cross sectional area significantly. Considering that the objective was to measure soil water retention behaviour at points within the soil columns, three pronged designs had the most appeal. The more concise sampling area would allow for placing the TDR probe closer to other probes and would also provide a more accurate portrayal of the point water content. Any more than three prongs would have complicated the construction process for no real benefit.

Regarding probe length, as short as was reasonably possible would give a better representation of point water contents, with sample volume increasing linearly with wave guide length. The longer the wave guides the more precise the waveform interpretation, however at extreme lengths or in highly saline conditions conductivity losses have a negative impact by reducing power and resulting in a smoothing of the resultant waveform. Longer probes are most susceptible to this, which can lead to inaccuracies in interpretation. In comparison, shorter probes fare well, limiting the time the wave is susceptible to such losses. Conversely, if the wave guide is too short, inflections of the step input within the probe begin to overlap and blur the waveform beyond recognition. The wave guide length opted for was that of 75 mm. Experience dictated that if the length was much shorter than this, the waveform would

become unintelligible whilst at 75 mm, however, reasonable accuracy could be maintained. The short length allowed for easier insertion; the prongs were considerably stiffer, resisting horizontal and vertical movements upon entry; and conductivity losses minimised, a concern due to the highly conductive nature of the amendments applied to the soils, as discussed in chapter 6.

In terms of spacing and diameter of wave guides, most designs sold commercially and described in the literature have a ratio of outer spacing to diameter somewhere between 5 and 15. Considering a fixed diameter set of wave guides, as the spacing increases the energy distribution varies such that there is a greater bias towards the surface of the prongs [63]. This fact is particularly important with regards to soils, as upon insertion of a probe there is inevitable some compaction occurring, predominantly near the surfaces of the wave guides. With large spacings some bias in readings is expected leading to figures that neither represent the bulk soil water content nor point water content. With small spacings usability emerges as a problem. Although the energy distribution is more uniform, the ability to insert the probe head into the soil at any point becomes more of a concern as the bulk material may have a significant quantity of particles that exceed in diameter the spacing available between wave guides. Regarding diameter, smaller diameters are preferred due to limiting the compaction of soils upon insertion, yet a limit exists such that the prongs are stiff and hence remain parallel during insertion. Considering the nature of the soil, as discussed in chapter 6, which has no particle diameters greater than 10 mm, it was therefore decided to opt for 1.6 mm diameter prong with an outer spacing of 15 mm, giving a three pronged probe with 7.5 mm spacings between prongs as shown in Figure 3.3.

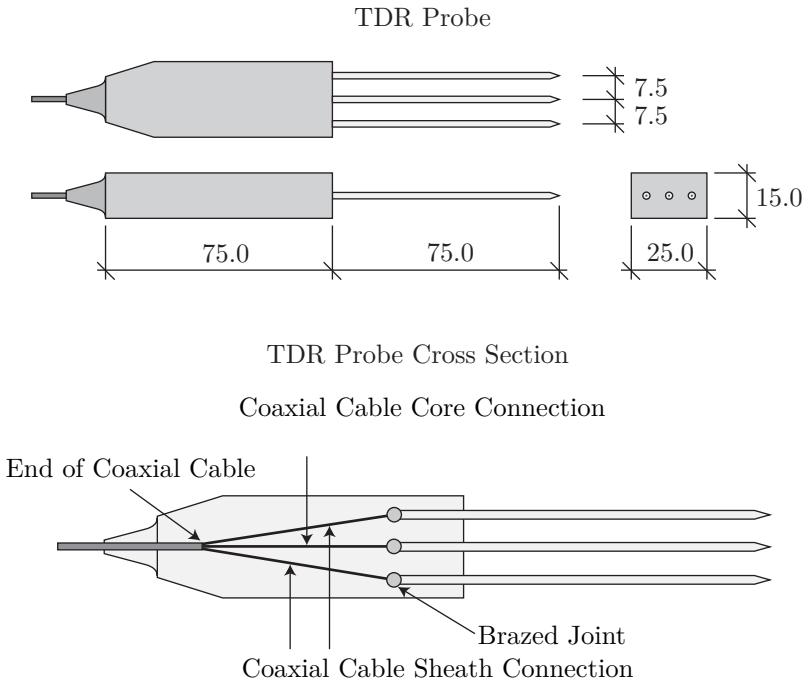

Figure 3.3: TDR Probe Design

In terms of the probe body, encapsulation of both a section of coaxial cable and wave guide was required in addition to room for making the connection between both. Some 20 mm of wave guide was set aside for inclusion inside the probe body to keep the prongs held rigidly, making the final wave guide length 95 mm. At the rear of the encapsulation, where the coaxial cable entered, the body was tapered onto the cable. This was to prevent excessive bending from causing a tear between cable and body,

allowing water entry to the internals of the probe and altering readings. The length of the join between the two was very much a restriction applied due to construction techniques. With the cable and wave guide being brazed together at temperatures in the region of 800 $^{\circ}C$ it was necessary for some distance between the join and coaxial cable to limit damage. This was conservatively put at around 45 mm hence the length of the probe body used to accommodate this.

3.3.3 TDR Probe Construction

In terms of materials choice, the design follows closely that suggested by Robinson et al. [2]. In their paper they suggested the use of stainless steel welding rods of type 316L for the probe wave guides and connecting by use of silver solder in a brazing process. Coaxial cable choice followed that of commercial probes sold by Campbell, using Belkin 50 ω coaxial cable and matching 50 ω BNC connectors to match the TDR100 system. The encapsulation material was decided upon after some trial runs with different epoxy resins through the use of a basic three part open top mould and a fake set of TDR wave guides and coaxial cable. The material chosen was called Flexane 80, an opaque black two part resin chosen for its ability to set into a very hard wearing, water impervious solid; it was stiff enough to hold the wave guides in a fixed position under repeated insertions and removals and also flexible in a thin covering, allowing a good tapered fit onto the coaxial cabling.

Creating repeated consistent probes was assisted through the design of moulds into which the epoxy resin could be poured. The moulds were designed in Solidworks, a CAD package which could export the drawings to a 3D printer for fabrication. The moulds were created through the subtraction of the desired probe design from a block of material. This material was then split into two and excess unwanted material removed. A two part mould was decided upon, the base consisting of the majority of the features. At one end, there was a butt for the prongs to push against ensuring an even 75 mm prong length, with a clamp consisting of a rubberised spacer and metal cross brace which was screwed down into position to hold the prongs. The other end of the base had a similar clamping system for holding the coaxial cable in place. Round the central area were four locating pins for matching to the top half of the mould, and through the center of each was a hole for threading a screw through to ensure a tight fit between top and bottom.

Two designs for injecting the resin were trialed. The first used two holes on the top of the mould, one for epoxy and the other for escaping air. This particular design was found to be sub par on several accounts, firstly the injection process took considerable time, all the while the epoxy was setting and becoming less manageable. Secondly, pressures could build up on the inside attempting to force the mould apart as air was squeezed out. As a result, epoxy could escape through the small gap between the top and bottom halves of the mould. The third problem was that of air pockets which were noted to be considerable in number with this design. The second design attempted to rectify some of these problems by turning the mould on its side and replaced the injection holes with a slit, nearly the full length of the side wall of the probe, allowing the resin to be poured in. This greatly sped up the pouring process, especially when pouring a heated and therefore less viscous mixture, into the mould. Heating the epoxy also had the effect of removing bubbles introduced through the mixing process and ensuring the resultant epoxy mixture was homogeneous. Although a significant improvement, the method could still be improved, with some small air pockets clearly visible on the upper corners of the design. However, these were the only visible blemishes on the final product.

The step by step method used for construction of the probes is listed below:

1. A suitable length of coaxial cable was cut. Long lengths produce a rounded waveform decreasing achievable accuracy. For all probes constructed 5 metre lengths were used.

2. A length of plastic jacket was stripped back and removed so that the metallic shield was visible. The length chosen here was 50 mm to leave some room to protect the coaxial cable during brazing and for trimming. The shielding was unwoven and split into two equal sets of wire strands and twisted back together. The dielectric insulator was removed and the central core twisted followed by trimming the wire sets to 45 mm in length.

3. Three 95 mm long prongs were cut from type 316L steel solder. One end was refined to a point to aid insertion into soil using an industrial sander.

4. The prongs were brazed to the three wires prepared earlier using silver solder.

5. The mould was prepared with a fine layer of silicon grease to aid removal. The method involved applying a good quantity of grease with a brush to ensure the face and top of both halves of the mould were well covered before removal of any excess using soft paper towel. As a side note, the recommended release agent for the epoxy resin was found to be insufficient due to the nature of the mould, constructed out of a semi permeable material the release agent appeared to seep in and provide reduced functionality.

6. The probe head assembly was placed in the lower half of the mould. First, the wave guides were clamped in position, followed by the coaxial cable, whilst simultaneously trying to keep the wiring relatively taught. Ensuring the wires did not touch was achieved through delicately running the tip of pliers down towards the junction at the head of the coaxial cable so that a gap was clearly visible. The top half of the mould was then placed over the locating pins and clamped into place with a series of screws and rotated on its side ready for pouring the epoxy resin.

7. The two part epoxy was mixed as individual batches per probe in order to avoid the resultant liquid becoming too viscous. About thirty grams of the mix was required per probe and this was prepared in the bottom half of a cleaned out container. To ensure a homogeneous mix, heat was applied by using a hair dryer to the side of the container whilst the epoxy was rapidly mixed, then left to cool and settle for a few seconds before pouring into the mould. Originally, when heat was found to improve the manageability of the mix, a warmed mould was used, however, this tended to force the epoxy to separate as it cooled, leaving unset tacky probes.

8. After 24 hours the probes were ready to be removed and left to continue curing outside the mould as new probes were being built. With the epoxy not wholly set, yet still solid, the flash round the edges was quite easily removed with a sharp blade.

9. After a period of a couple of weeks the probes were ready to be attached to a BNC connector for calibration and use.

3.4 Probe Performance

Probe calibration was required for both measuring apparent relative permittivities and electrical conductivities. The first requirement was that the system was set up as it was to be used, as this meant that any errors introduced by the system as a whole were reduced. A diagram of the final system is given in Figure 3.4.

The diagram shows the system spread across four levels, with level 0 being the TDR100 device itself. Across other layers, computer controlled multiplexers were used to switch the signal between different multiplexers and probes further down the tree, with eight outputs each. Level 1 was used as a node for connecting subsequent levels of multiplexer to and had no TDR probes itself. Level 2 consisted of

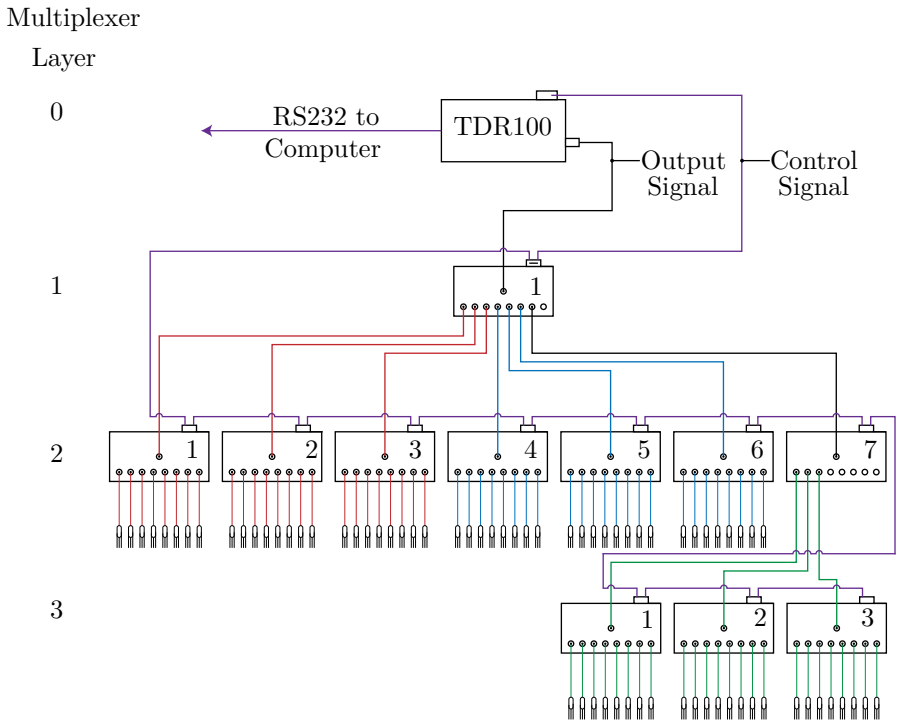

Figure 3.4: TDR100 and Multiplexer Layout

seven multiplexers, six of which were devoted to TDR probes and the final one for controlling the level 3 multiplexers, of which there were three. The multiplexers were referred to with two numbers, the first indicating level and the second position on that level. Each lysimeter required a total of twenty four probes, conveniently three multiplexers worth, hence multiplexers 2-1, 2-2 and 2-3 were designated for lysimeter 1; 2-4, 2-5 and 2-6 designated for lysimeter 2 and 3-1, 3-2 and 3-3 set aside for lysimeter 3. The remaining connections were left available for further expansion.

3.4.1 Calibration Procedure

Calibrations proceeded once the TDR probes had been set up as shown in Figure 3.4. The calibrations for calculating apparent relative permittivity were required, as with any TDR probe, due to the short length of wave guide held within the body of the probe. An offset was required to be calculated so that the true value of apparent relative permittivity, ε_r^*, for any sample material could be calculated. The process involved placing the probe in a solution of known relative permittivity and calculating the offset required for the correct reading, as detailed below:

1. The TDR probe was clamped and the wave guides immersed in de-ionised water, making sure to keep away from the side walls and base of the container. A minimum distance of 50 mm was ensured for all calibrations.

2. The start of the apparent window length, the apparent length at which the TDR100 device starts reading data points, was set appropriately to be approximately 0.5 m before the peak denoting the signal entering the wave guides. The start point varied depending on the distance that the signal had to travel in the system, before entering the probe. A standardised reading consisted of 251 data points, with each point averaged four times over a window of apparent length 1.8 m. The resultant waveform allowed the start point and end point of the wave guides to be calculated and hence the

total apparent length associated with the wave guides was calculable.

3. The contribution to the measured apparent length due to the permittivity of water was calculated based on the known length of the probe immersed in water, 0.075 m, and the permittivity of water, calculated from the empirical relationship given in equation 3.22 using the measured temperature in degrees Celsius. The calculation used is given in equation 3.23.

$$\varepsilon_w = 78.54 \times [1 - 4.5791 \times 10^{-3}(T-25) + 1.19 \times 10^{-5}(T-25)^2 - 2.8 \times 10^{-8}(T-25)^3] \quad (3.22)$$

$$L_a = L \times \sqrt{\varepsilon_w} \quad (3.23)$$

4. From this information, to take account of probe entrance time, the offset could be acquired by subtracting the apparent length due to water from the apparent length of the waveguide, corresponding to the wave guide embedded within the encapsulation material.

In practice, this procedure was repeated multiple times per probe ensuring a higher degree of accuracy when determining apparent relative permittivities. Electrical conductivity calibrations were carried out on a probe by probe basis as detailed below:

1. The steady state reflection coefficient was measured at an apparent length of 200 meters, by setting the start of the apparent window length, approximating conditions for time approaching infinity, for both open and closed states. The open state was measured with the probe held in air yielding ρ_o and the closed state by short circuiting the three wave guides giving ρ_c.

2. The probe was immersed in a standard solution of electrical conductivity, 84 μScm^{-1}, modified for temperature effects using equation 3.24, where σ_{25} is the conductivity at $25°C$ and T is the temperature in degrees Celsius. The steady state response at 200 m was then measured for the solution, returning an associated value of reflection coefficient ρ_u.

$$\sigma_T = \sigma_{25} \times (1 + 0.02 \times (T-25)) \quad (3.24)$$

3. A corrected value for the solutions steady state reflection coefficient was then calculated using equation 3.17, essentially scaling the response between -1 and +1.

4. The corrected reflection coefficient was then used to calculate the conductance, G, through equation 3.25 where Z_u was the system impedance for the TDR100 device equalling 50 Ω.

$$G = \left(\frac{1}{Z_u}\right)\left(\frac{1-\rho}{1+\rho}\right) \quad (3.25)$$

5. Given the probe constant, K_p, is the slope of the graph of electrical conductivity versus electrical conductance, this could be calculated using equation 3.26.

$$K_p = \frac{\sigma_T}{G} \quad (3.26)$$

6. Considering the TDR100 system returns a value of conductance based on the uncorrected reflection coefficient, an improvement in accuracy could be obtained for each probe reading by back calculating the uncorrected coefficient, correcting it and recalculating the electrical conductivity all using equation 3.27.

$$\sigma = -K_p \times \frac{\sigma_u \times Z_u - K_p + \rho_o \times \sigma_u \times Z_u + \rho_o \times K_p}{Z_u(\rho_c \times \sigma_u \times Z_u + \rho_c \times K_p + \sigma_u \times Z_u - K_p)} \tag{3.27}$$

Again, the electrical conductivity calibrations were repeated a number of times to ensure that it was possible to achieve a high degree of accuracy.

3.4.2 Probe Calibration Performance

Calibrations were conducted in three batches of twenty four probes, each associated with one of the three lysimeters. The procedures carried out on each probe were identical to those described above, although the number of repeats varied between batches to aid in assessing the true precision of the TDR system. For each probe four numbers were required: the probes offset in apparent length, for calculating apparent permittivities, as given in Table 3.3; and the open circuit response, closed circuit response and probe constant for calculation of a sample electrical conductivity, given in Table 3.4.

With regards to probe offsets, each probe had a mean value associated with it. Probes 1 through 24 had the mean calculated from five repeats, as was recommended in the Campbell Scientific manual. The remaining probes, 25 through 72, had their mean offsets calculated from a much increased one thousand repeat readings, collected through automation implemented in custom software instead of manually using Campbell Scientific's PCTDR software. Along with each offset is given a standard deviation, denoted S.D. and a 95% confidence interval denoted 95% C.I..

It can be seen that for Probes 1 to 24 there is comparatively substantial variability in standard deviations, ranging from 0.0008 to 0.0039, when compared to probes 25 through 72 ranging from 0.0022 to 0.0029. This variability was due different sample sizes, yet on average for the data set, the numbers aligned well with the remaining probes calibrated with an increased number of repeats. The standard deviations given actually represent the variability in determining the period, in apparent length, a wave is propagating through a probe waveguide, given a constant is removed for calculating the probe offset. Considering 98% of all readings for a normal distribution, for which the data achieved a high probability plot correlation coefficient, occur within two standard deviations this yields a variability in apparent length approximating $\pm 0.005m$. In the case where the probe is submersed in water an expected apparent length is in the region of $0.78m$, so it can be concluded that the imprecision of the system is not insignificant at $\pm 0.64\%$ of the apparent length.

The variability when determining the probe offset can be clearly seen affecting Probes 1 to 24, where a large confidence interval bordering on a value of one standard deviation suggests that we can be 95% sure that the true probe offset is within the margins given either side of the calculated mean offset. This can lead to over or under estimation of the offset, essentially introducing a bias in the determination of apparent permittivity and hence water contents. The magnitude of the bias cannot be seen or calculated directly, however, the confidence interval can be converted from apparent length to a more tangible approximate volumetric water content by applying Ledieu's relationship, which yields a 95% certainty that the bias introduced is less than 0.42% Volumetric Water Content (VWC). Better approximations may be achieved through custom calibrations and will be discussed later, but for comparative purposes this is sufficient.

As for Probes 25 to 72, with one thousand repeat readings each, the 95% confidence interval can be seen to be significantly reduced by a factor roughly 17. This leads to a much tighter approximation of

Table 3.3: TDR Calibrations: Probe Offset for Probes 1 through 72

Probe	**Mean Offset** (m)	**S.D.** (m)	**95% C.I.** (m)	**Probe**	**Mean Offset** (m)	**S.D.** (m)	**95% C.I.** (m)	**Probe**	**Mean Offset** (m)	**S.D.** (m)	**95% C.I.** (m)
Probe 1	0.1106	±0.0017	±0.00217	Probe 25	0.1121	±0.0021	±0.00014	Probe 49	0.1285	±0.0027	±0.00017
Probe 2	0.1089	±0.0028	±0.00347	Probe 26	0.1189	±0.0025	±0.00016	Probe 50	0.1335	±0.0025	±0.00016
Probe 3	0.1183	±0.0039	±0.00490	Probe 27	0.1069	±0.0024	±0.00015	Probe 51	0.1329	±0.0025	±0.00016
Probe 4	0.1030	±0.0017	±0.00213	Probe 28	0.1127	±0.0025	±0.00016	Probe 52	0.1339	±0.0026	±0.00017
Probe 5	0.1159	±0.0027	±0.00338	Probe 29	0.1100	±0.0025	±0.00016	Probe 53	0.1300	±0.0026	±0.00017
Probe 6	0.1178	±0.0014	±0.00168	Probe 30	0.1132	±0.0023	±0.00015	Probe 54	0.1321	±0.0026	±0.00017
Probe 7	0.1142	±0.0038	±0.00470	Probe 31	0.1069	±0.0022	±0.00014	Probe 55	0.1290	±0.0027	±0.00017
Probe 8	0.1204	±0.0015	±0.00191	Probe 32	0.1042	±0.0025	±0.00016	Probe 56	0.1304	±0.0027	±0.00017
Probe 9	0.1065	±0.0008	±0.00102	Probe 33	0.1081	±0.0028	±0.00018	Probe 57	0.1329	±0.0024	±0.00015
Probe 10	0.1114	±0.0012	±0.00148	Probe 34	0.1099	±0.0023	±0.00015	Probe 58	0.1276	±0.0028	±0.00018
Probe 11	0.1114	±0.0013	±0.00163	Probe 35	0.1128	±0.0026	±0.00017	Probe 59	0.1342	±0.0026	±0.00017
Probe 12	0.1166	±0.0032	±0.00397	Probe 36	0.1104	±0.0025	±0.00016	Probe 60	0.1357	±0.0028	±0.00021
Probe 13	0.1108	±0.0028	±0.00353	Probe 37	0.1123	±0.0026	±0.00016	Probe 61	0.1232	±0.0028	±0.00018
Probe 14	0.1117	±0.0019	±0.00240	Probe 38	0.1094	±0.0023	±0.00015	Probe 62	0.1214	±0.0031	±0.00020
Probe 15	0.0991	±0.0024	±0.00303	Probe 39	0.1113	±0.0025	±0.00016	Probe 63	0.1252	±0.0027	±0.00017
Probe 16	0.1122	±0.0026	±0.00317	Probe 40	0.1115	±0.0026	±0.00017	Probe 64	0.1233	±0.0026	±0.00016
Probe 17	0.1017	±0.0034	±0.00418	Probe 41	0.1103	±0.0026	±0.00017	Probe 65	0.1261	±0.0026	±0.00017
Probe 18	0.1126	±0.0005	±0.00065	Probe 42	0.1078	±0.0024	±0.00015	Probe 66	0.1163	±0.0026	±0.00018
Probe 19	0.1106	±0.0016	±0.00202	Probe 43	0.1106	±0.0027	±0.00017	Probe 67	0.1247	±0.0025	±0.00016
Probe 20	0.1085	±0.0039	±0.00488	Probe 44	0.1092	±0.0026	±0.00016	Probe 68	0.1296	±0.0025	±0.00016
Probe 21	0.1125	±0.0028	±0.00349	Probe 45	0.1078	±0.0024	±0.00015	Probe 69	0.1225	±0.0025	±0.00016
Probe 22	0.1136	±0.0021	±0.00259	Probe 46	0.1116	±0.0027	±0.00017	Probe 70	0.1292	±0.0025	±0.00016
Probe 23	0.1224	±0.0018	±0.00223	Probe 47	0.1069	±0.0025	±0.00016	Probe 71	0.1207	±0.0026	±0.00018
Probe 24	0.1111	±0.0020	±0.00245	Probe 48	0.1130	±0.0029	±0.00018	Probe 72	0.1233	±0.0026	±0.00017
Average	0.1117	±0.0023	±0.00279	Average	0.1103	±0.0025	±0.00016	Average	0.1278	±0.0026	±0.00017

Table 3.4: TDR Calibrations: Probe Constant for Probes 1 through 72

Probe	ρ_{open}	ρ_{closed}	K_p	**Probe**	ρ_{open}	ρ_{closed}	K_p	**Probe**	ρ_{open}	ρ_{closed}	K_p
Probe 1	0.9760	-0.9650	6.20362	Probe 25	0.9757	-0.9662	6.19230	Probe 49	0.9757	-0.9615	6.12639
Probe 2	0.9760	-0.9650	6.14042	Probe 26	0.9761	-0.9682	6.09002	Probe 50	0.9755	-0.9624	6.11919
Probe 3	0.9760	-0.9680	5.98351	Probe 27	0.9755	-0.9679	6.12226	Probe 51	0.9767	-0.9605	6.04391
Probe 4	0.9740	-0.9670	6.10257	Probe 28	0.9752	-0.9684	6.25146	Probe 52	0.9745	-0.9607	5.96154
Probe 5	0.9730	-0.9660	6.03052	Probe 29	0.9759	-0.9670	6.06458	Probe 53	0.9747	-0.9621	5.94075
Probe 6	0.9720	-0.9660	6.06738	Probe 30	0.9757	-0.9668	6.15886	Probe 54	0.9761	-0.9626	6.13642
Probe 7	0.9730	-0.9660	6.13801	Probe 31	0.9754	-0.9690	6.08869	Probe 55	0.9748	-0.9611	5.97334
Probe 8	0.9740	-0.9670	6.03427	Probe 32	0.9756	-0.9686	6.16366	Probe 56	0.9750	-0.9626	6.24685
Probe 9	0.9760	-0.9670	5.95590	Probe 33	0.9752	-0.9663	6.20927	Probe 57	0.9750	-0.9529	6.18598
Probe 10	0.9770	-0.9670	6.05118	Probe 34	0.9749	-0.9670	6.08553	Probe 58	0.9746	-0.9620	5.92071
Probe 11	0.9740	-0.9670	5.88886	Probe 35	0.9744	-0.9668	6.07574	Probe 59	0.9763	-0.9601	6.04093
Probe 12	0.9730	-0.9670	5.95641	Probe 36	0.9745	-0.9654	6.19379	Probe 60	0.9759	-0.9619	6.13404
Probe 13	0.9730	-0.9650	6.11933	Probe 37	0.9747	-0.9645	6.10382	Probe 61	0.9757	-0.9621	6.04171
Probe 14	0.9760	-0.9650	6.17368	Probe 38	0.9738	-0.9681	6.10545	Probe 62	0.9755	-0.9625	6.23541
Probe 15	0.9760	-0.9650	5.99852	Probe 39	0.9758	-0.9673	6.09543	Probe 63	0.9767	-0.9621	6.08136
Probe 16	0.9760	-0.9650	6.06015	Probe 40	0.9754	-0.9674	6.09747	Probe 64	0.9759	-0.9623	6.08145
Probe 17	0.9740	-0.9640	6.11049	Probe 41	0.9755	-0.9668	6.03668	Probe 65	0.9751	-0.9619	6.01848
Probe 18	0.9740	-0.9630	5.94207	Probe 42	0.9752	-0.9661	6.02143	Probe 66	0.9751	-0.9623	6.20439
Probe 19	0.9740	-0.9670	5.96000	Probe 43	0.9754	-0.9663	6.03243	Probe 67	0.9754	-0.9628	6.13241
Probe 20	0.9730	-0.9670	6.07769	Probe 44	0.9753	-0.9663	6.05853	Probe 68	0.9742	-0.9556	6.06380
Probe 21	0.9740	-0.9670	6.09481	Probe 45	0.9752	-0.9670	5.90432	Probe 69	0.9770	-0.9627	6.02392
Probe 22	0.9750	-0.9680	6.14600	Probe 46	0.9752	-0.9683	6.08072	Probe 70	0.9757	-0.9633	6.12710
Probe 23	0.9730	-0.9680	5.97434	Probe 47	0.9756	-0.9666	6.09325	Probe 71	0.9759	-0.9631	5.98462
Probe 24	0.9740	-0.9690	6.06838	Probe 48	0.9742	-0.9669	6.00965	Probe 72	0.9764	-0.9634	6.07840
Average	0.9744	-0.9663	6.05325	Average	0.9752	-0.9670	6.09731	Average	0.9756	-0.9614	6.07930

the true probe offset and reduces bias introduced to the system for determinations of volumetric water contents. Calculating the confidence interval in terms of volumetric water content, as before with Ledieu's relationship, yields an approximate value of 0.025% VWC, a significant improvement to say the least.

With regards to the magnitude of probe offsets calculated, a trend can be seen between probes associated with shorter cable length having a decreased probe offset when compared to probes with a longer cable length. As per Figure 3.4, probes 1 through 48 all have approximately the same cable length between the probe head and the TDR100 signal generator, yet probes 49 through 72 all exist on the next multiplexer layer down, essentially adding another 1.5 m or so of cable length. Table 3.3 shows this clearly as probes 49 through 72 have an offset approximating $0.1278m$ and probes 25 through 48 have an offset around $0.1103m$. Similarly, with a Campbell Scientific CS640 probe, similar in dimensions and waveguide length, a stated offset of 0.035 was given as calculated with a very short cable length, yet when calibrated on multiplexer layer two of this system, an offset of $0.0552m$ was reached which firmly makes the case for calibrating TDR systems as they are to be used.

With regards to Table 3.4 and the measurement of electrical conductivity, as with probes offsets, the length of the cable prior to the probe head has an impact upon the calibration. This can be seen in the open and closed circuit responses ($\rho_o pen, \rho_c losed$) being attenuated away from perfect reflections of +1 and -1 due to attenuation of the signal in the cable. The longer the cable, the greater the attenuation in the signal caused by the system reducing the open circuit reflection coefficient below 1. Yet this is not the only effect occurring. As Castiglione and Shouse [57] point out, systems that include multiplexers, connectors or other discontinuities incur an asymmetry in magnitude between the two responses. This is most apparent for probes 49 through 72 on the lowest tier of multiplexer i.e. the probes with the greatest number of discontinuities, whereby the average open circuit response approximates 0.9756 and the average closed circuit response -0.9614. To summarise, this method of calibration takes account of both attenuation caused by the system's cable length and the discontinuities involved.

As for the probe constant, denoted K_p, there is a significant variability observable between probes, for example, Probes 49 to 72 have a standard deviation of ± 0.0876. Given the final electrical conductivity reading over a short range is approximately scaled linearly, these variations can have a significant impact upon the final results.

Part of the variability may be due to uncertainty in the open circuit, closed circuit and uncorrected responses used in the calculation of the probe constant. Indeed the probe constant was particularly sensitive in calculation to the open circuit and uncorrected responses. Both featured relatively large standard deviations in the region of ± 0.001 when compared to the closed circuit response of ± 0.0005. If a change of one standard deviation with either open or uncorrected response was propagated through to the calculation of probe constant, a change in K_p of 0.070 could be observed, as opposed to a much more conservative change of 0.002 for the closed circuit response. That said, considering the small confidence intervals, large deviations in probe constant seemed somewhat unlikely. The confidence intervals for the open and uncorrected response expressed in terms of K_p approximate to ± 0.007 hence, another source of error was expected to contribute.

Aside from the assumed value of $50\Omega \pm 1\%$ internal impedance, the next source for error was the experimental method or more precisely the process of inserting the probes into a solution of know conductivity to retrieve a value for the uncorrected response. Probes 1 through 24 were each inserted into several different solutions of known conductivity and the resultant probe constants are plotted out in Figure 3.6. First of interest, the $84\mu Scm^{-1}$ solution was the initial attempt at calculating each probes' associated probe constant. This was done after trialing the probes in soils and the probe heads had been insufficiently cleaned with distilled water and paper towel. Two standard batches of the solutions were

used, as can be clearly seen in the figure, and as the solutions became more contaminated with additional ions increasing conductivity, the resultant probe constants decreased. Obviously these values are not the same as those used for determining K_p in Table 3.4 but they do provide a useful context for comparison of the other calibrations.

The other solutions presented in Figure 3.6 offer better repeatability after having cleaned the probe heads thoroughly before calibration. Two standard solutions other than the $84\mu Scm^{-1}$ were chosen, typically used in the laboratory for calibration of more traditional electrical conductivity meters, these were $147\mu Scm^{-1}$ and $1409\mu Scm^{-1}$ solutions. As can be seen in the figure, there is a clearly defined difference between the two different solutions on both repeats. Interestingly, and quite contrary to the trend seen in the contaminated $84\mu Scm^{-1}$ solutions, the higher conductivity $1409\mu Scm^{-1}$ solution tended to present a higher probe constant than the $147\mu Scm^{-1}$ solution. As to an explanation for this, inconsistencies in temperature correction for the conductivity of the solutions, with temperatures varying between $20.7°C$ and $22.4°C$, and small air pockets remaining at the waveguide-probe body interface are possible. Temperature variation seems more likely for consistent changes but more work is required to prove it, whilst air pockets could certainly cause some of the more inconsistent variation observed.

A general probe constant could be derived by plotting the known solution conductivities against conductance as measured by the probe. An example of this can be seen in Figure 3.5 where the gradient is the probe constant derived from all solutions and the intercept is theoretically zero.

As for the solution used to calibrate for the lysimeters, an $147\mu Scm^{-1}$ solution was chosen. As with calibrating traditional electrical conductivity meters, it was felt using a solution most representative of the medium to be monitored was the best course of action, given some uncertainty between the different solutions. With the help of some trial runs, $147\mu Scm^{-1}$ was confirmed as the closest to the electrical conductivities expected across the different lysimeter soils.

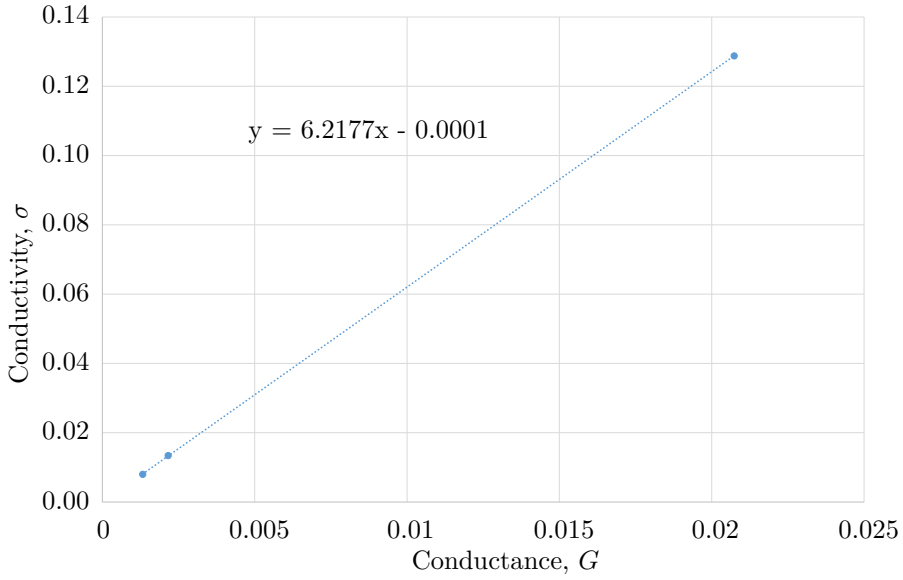

Figure 3.5: Graph Showing Plot of Conductivity against Conductance for Different Conductivity Solutions

With regards to the total expected error in electrical conductivity measurement, there are uncertainties involved. Zegelin et al. [64] estimated the uncertainty produced by TDR probes using the same base method, but prior to the correction of the reflection coefficients suggested by Castiglione and Shouse [57], as in the region of ±10%. This error was calculated by comparing the TDR measurements to the electrical

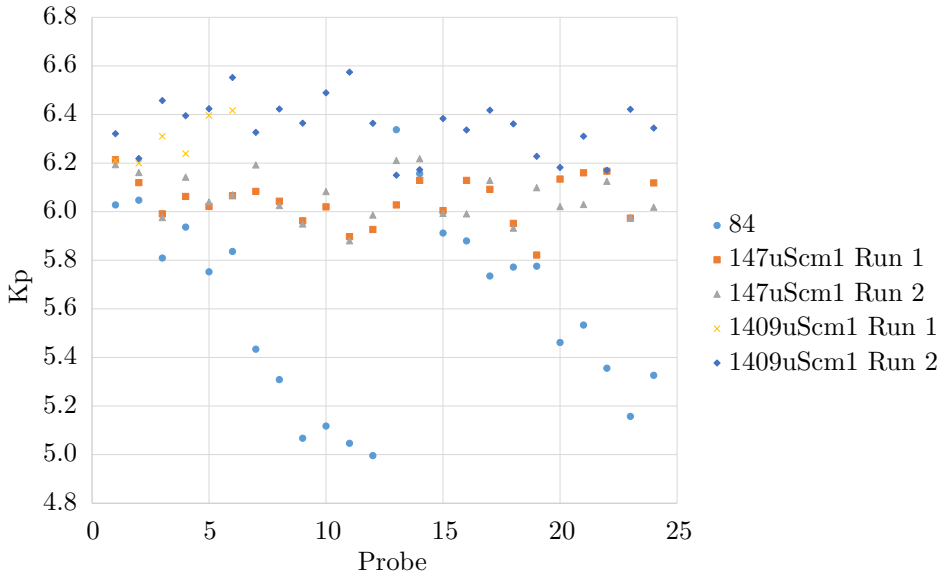

Figure 3.6: Graph Comparing Probe Constants for Different Calibration Solutions

conductivities measured through different techniques. As a worst case scenario, this seems reasonable. For a single probe the greatest difference between two reliable calibrations as shown in Figure 3.6 is associated with probe 11, at around 0.7 (5.9 to 6.6) which, when take as a percentage change in probe constant approximating 6.0, is ±11.7%.

In summary, seventy two probes have been calibrated both for measuring apparent permittivities and electrical conductivities. All probes have an offset standard deviation approximating $\pm 0.0025m$, yielding the expectation that the probes read within ±0.76% VWC. Probes 1 through 24 have a potential significant bias due to uncertainty in the offset calculated. This offset has the potential to approach ±0.42% VWC. For the remaining probes this was improved upon by an increased number of readings to ±0.025% VWC. Calibration for measurement of electrical conductivity took sufficient readings to guarantee that the data acquisition process minimised errors, yet this could not fully explain variability in probe constants observed between repeat methods. Therefore, a conservative error of ±10% was deemed suitable.

3.4.3 Volumetric Water Content Calibration

With the probes calibrated to a reasonable degree of accuracy, allowing for accurate determination of apparent permittivities, the next step was choosing the most suitable method to convert to volumetric water content. The three main methods, as briefed in the literature, considered for this purpose were firstly, empirical relationships such as Topp and Ledieu, based on the average response of a large range of soils; Secondly, volumetric models which require a more intimate knowledge of fraction volumes and permittivities, in addition to the TDR response; and finally there are custom relationships that can be built through trialling the probes in the soils of interest and calibrating the response to true determined water content.

To test the different approaches the probes were first trialled over a range of water contents, in builders sand with and without the amendments to be added to the lysimeters. This allowed three pieces of information to be obtained:

- The expected accuracy of each approach to calculating volumetric water content;
- The effect of adding amendments on the calibrations;

- Any problem areas or significant sources of error;

The unamended builders sand samples were made up in intervals of 2.5% gravimetric water content (GWC) between 0% and 17.5% GWC, the latter water content being approximately saturation. Each sample was hand tamped into a screw top plastic container measuring $83mm$ in diameter and on average $99mm$ in depth, there being a small punt at the base. The tamping was aimed at the removal of the larger air voids which could significantly alter the TDR response. The fill method approximated five layers with twenty tamps per layer using a $47mm$ diameter cylindrical tamper, typically requiring an additional thin layer to top off before skimming the surface. The containers of soil were wrapped in cling film to minimise evaporation during calibration and kept lidded when not in use. As for the samples with amendments, these were made up with the same method yet, as discussed in chapter 6, the amendments contained a significant proportion of water, hence the true water contents were increased above the nominal values.

Testing involved placing each of the twenty four probes (Probes 49 to 72) in every sample and taking twenty repeat measurements of apparent permittivity, and in addition a measurement of electrical conductivity. For each sample, the average apparent permittivity and electrical conductivity was then assessed, meaning any potential bias from anomalies could be effectively eliminated. From here, the assessment of each calibration to calculate volumetric water content could begin. The effects of holes created through the insertion of the probes was taken account of by inserting the probes at a unique point within each sample and plotting the results out in time order to observe trends as more holes were created. It was found for each sample that there was no significant deviation in results as more holes were generated, primarily due to the small sample size of these probes.

The empirical relationships as given by Topp (eq. 3.8), Ledieu (eq. 3.10) and Malicki (eq. 3.11) were applied and the results are displayed in Figure 3.7. Topp's equation for organic soils is excluded because the results are irrelevant for the builders sand, essentially being the mineral relationship but offset upwards by several percent. With the remaining relationships there are several points of interest. Firstly with the actual data, the latter points at high water contents deviate significantly from a straight line fit, essentially reading a much higher response from the TDR probes for a given water content than would otherwise be expected. This sudden change can be seen quite visually by using the power law volume model given in equation 3.12 to back calculate the permittivity of the soil, the result is given in Figure 3.8. Small variations in permittivity were expected but the sudden change occurring in the final three water contents had to be attributed to some physical change in the sample. This physical change was attributed to the insertion of the TDR probe causing a shift in volume fractions in the most sensitive area of the probe, that near the wave guide surface [63]. Essentially the TDR probes were detecting a greater volume of water than was representative of the bulk sample. This is supported by the conductivities as given in Figure 3.9 where a non-linear increase is observed, particularly in the upper region of the graph. Removing the misleading values from the data set produced Figure 3.10, allowing for a much clearer comparison of the techniques.

Indeed, this procedure was adopted for each sample set the probes were tested in with good success. To generalise the result, regardless of the amendment, each sample that produced a well representative reading when judged against its peers, seemed to do so as the dry densities increased with water content. When the dry densities peaked and then dipped, the insertion of the probes affected the readings significantly leading to the tentative conclusion that samples wet of optimum were more likely to be a problem area when generating a custom calibration for a soil.

With regards to the ability of the generic empirical equations to estimate water contents on these soils, Figure 3.10 with the reduced data set sheds some light. The data can be observed to have a close linear relationship between apparent permittivity and volumetric water content, which is to be expected for

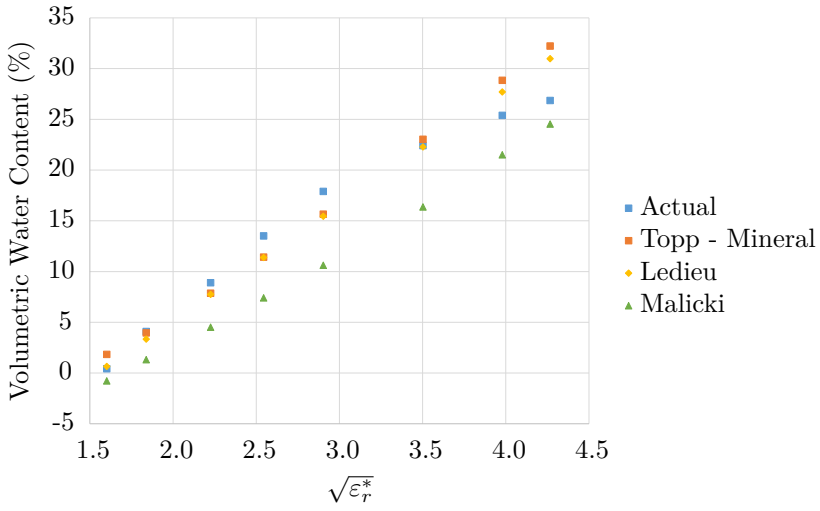

Figure 3.7: Graph Comparing Empirical Relationships for Builders Sand

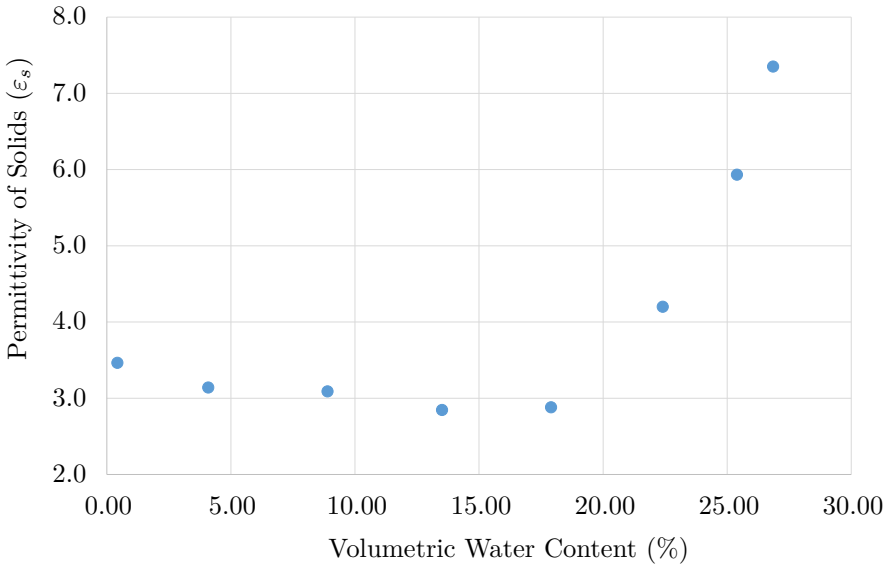

Figure 3.8: Graph Depicting the Permittivity of the Solids as Back Calculated Using a Power Law Volume Model

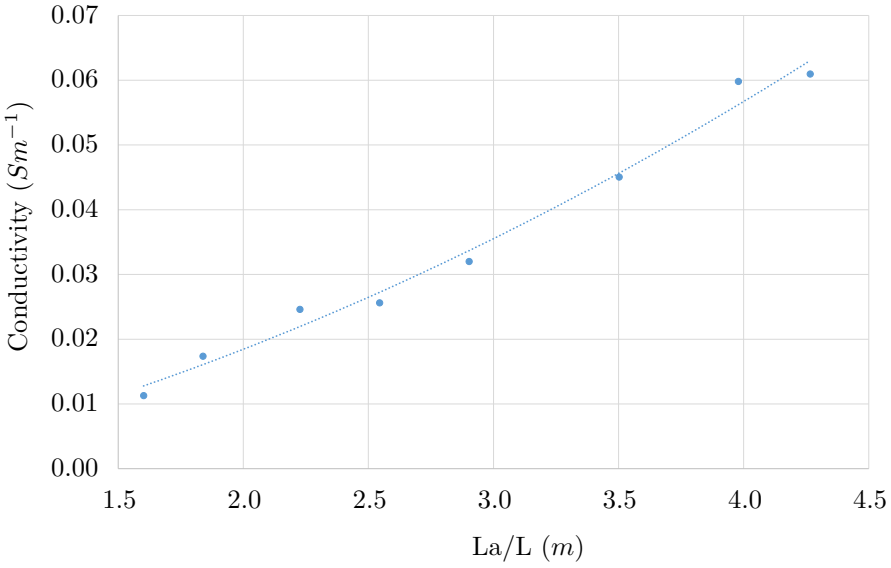

Figure 3.9: Graph Depicting Changes in Conductivity for Builders Sand

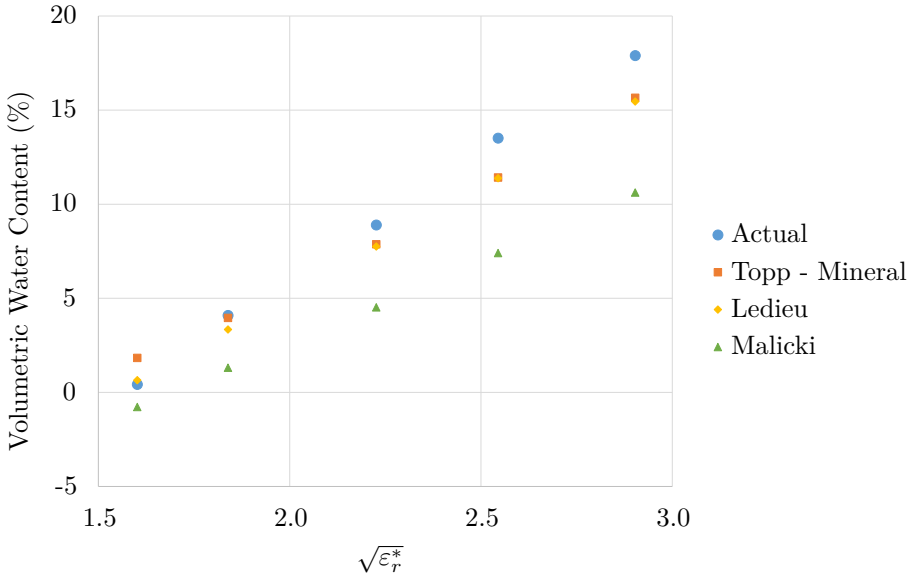

Figure 3.10: Graph Comparing Empirical Relationships for Builders Sand

the typical usage range of TDR probes is 5% to 45% VWC, yet appears to continue to be true here below the 5% mark. All three equations shown have some significant differences displayed, which unfortunately continue over the remaining data range for Malicki. Topp's mineral equation and Ledieu's equation provide a better estimation, agreeing well over the majority of the data range, yet underestimating the water content by up to 2.5% VWC at the higher permittivities. This can be explained in some part by the relatively low permittivity of the sand compared to some of the other components in a normal soil, which would tend to increase the overall permittivity for a given water content bringing the result more in line. In any case, the best estimation can be gauged from the mean difference and the sum of the difference squared for each equation as given in Table 3.5. It can be seen that both Topp's mineral and Ledieu's equations perform similarly in either metric which serves as a good comparison for the other methods to be discussed.

Table 3.5: Errors in Empirical Determination of Volumetric Water Contents in Builders Sand

Property	**Topp - Mineral**	**Topp - Organic**	**Ledieu**	**Malicki**
Mean Difference	1.38	5.91	1.34	4.35
$\sum difference^2$	12.47	175.93	12.46	118.68

The volume fraction relationships are shown in Figure 3.11 with error metrics in Table 3.6. These methods appear to give a consistently better estimation of volumetric water contents, particularly with the simple volume model, when compared to empirical methods. The mean difference was reduced to less than 0.6% as compared to 1.4% previously, although the trend for larger errors with high permittivities appears to remain true. The main downside of this method is the need for knowledge of volume fractions, which will change considerably over the course of wetting and drying.

Custom calibrations further improve upon this estimation of volumetric water content by relating the known volumetric water contents empirically to the permittivity of the samples. In some cases the water contents were related to both the permittivity and a density value. In Figure 3.12 both a linear fit and one taking into account the variability in dry density are near indistinguishable from the real data. Bulk density however shows a drop off with the higher permittivities, generally underestimating the volumetric water content. In terms of metrics as given in Table 3.10, the best fit is that of a linear fit including dry density as a parameter, being a mere 0.17% VWC off on average over the full range. Compared to the empirical and even the volumetric methods, this is a significant improvement, one that can be increased marginally through change to a polynomial fit.

With a method and base line established for comparison, creating a custom calibration for the lysimeter soil was feasible. Firstly however, it must be noted that difficulties in penetrating samples of low water content with the TDR wave guides were encountered. It was for this reason that that the range of water contents was reduced to that of between 15% and 25% GWC, and hence why with the custom calibrations only linear fits were considered, with polynomials being unpredictable outside the calibration range.

Table 3.6: Errors in Empirical Determination of Volumetric Water Contents in Builders Sand

Property	**Volume (0.5)**	**Whalley**
Mean Difference	0.55	0.95
$\sum difference^2$	1.85	5.87

The general trend in Figure 3.13 appeared to be non-linear, with higher permittivities leading to much increased estimations of volumetric water content, however it will be shown that this is not the

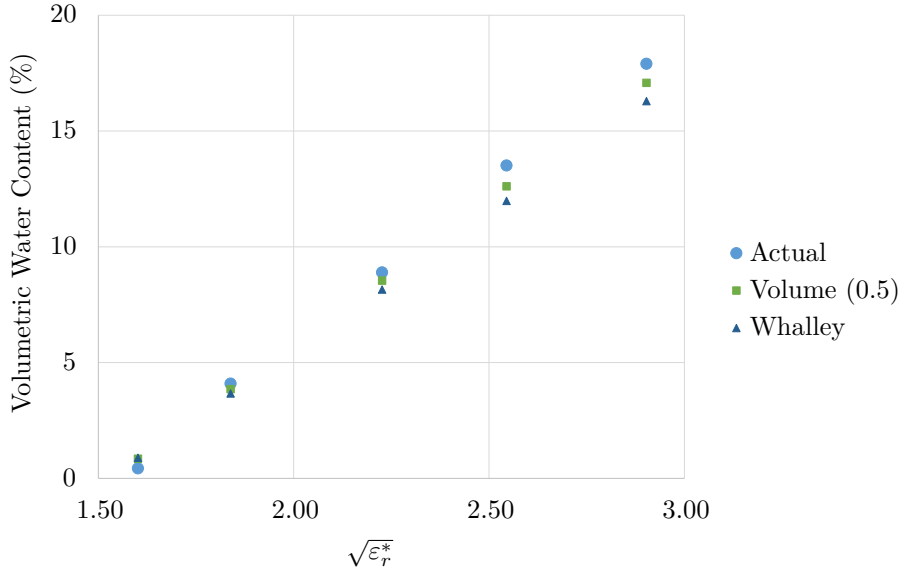

Figure 3.11: Graph Comparing Volumetric Relationships for Builders Sand

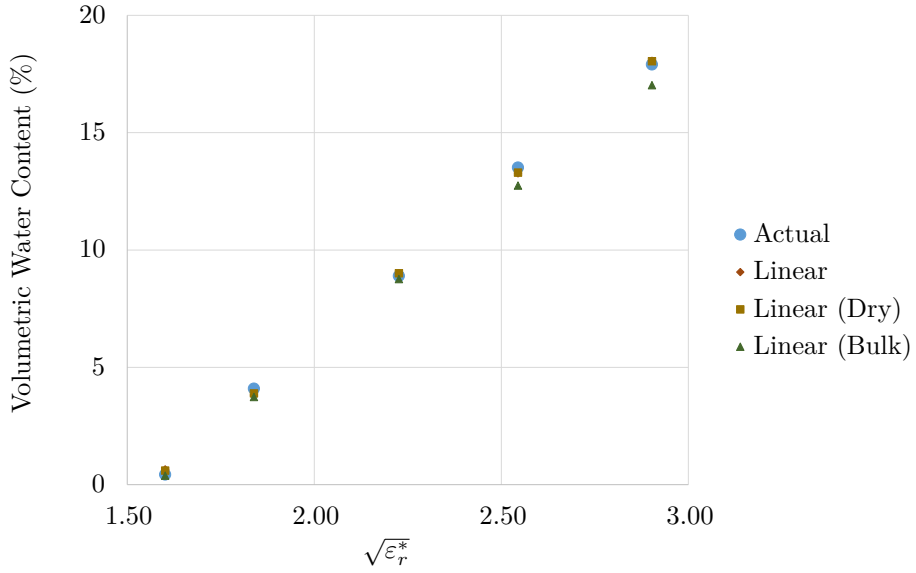

Figure 3.12: Graph Comparing Custom Calibrations for Builders Sand

Table 3.7: Errors in Custom Determination of Volumetric Water Contents in Builders Sand

Property	Linear	Linear (dry)	Linear (Bulk)
Mean Difference	0.20	0.17	0.43
$\sum difference^2$	0.22	0.15	1.51

case. Close inspection of the back calculated soil permittivities did yield two areas of interest, as shown in Figure 3.14. When compared to the builders sand in Figure 3.8, no longer is there a fairly consistent permittivity calculated but there is a trend for increasing permittivity with water contents. In contrast to that trend, one sample of particularly low density for its water content, has a permittivity of 3.1 for a volumetric water content approaching 24%. What is more inexplicable is the two data points at the higher water contents which have a sudden deviation from established trend from the permittivities. Closer inspection of the electrical conductivities also yields a similar result, as can be seen in Figure 3.15 and offers a possible explanation. As with the TDR probes altering the fabric of the sand, something similar appears to be happening here upon probe insertion, possibly attributed to a smearing effect such as a clay layer coating the probes, reducing the conductivity of the sample and reading an abnormally high volume attributed to soil minerals. Ignoring the justifiable spurious readings gives Figure 3.16, for which there is a much clearer linear fit.

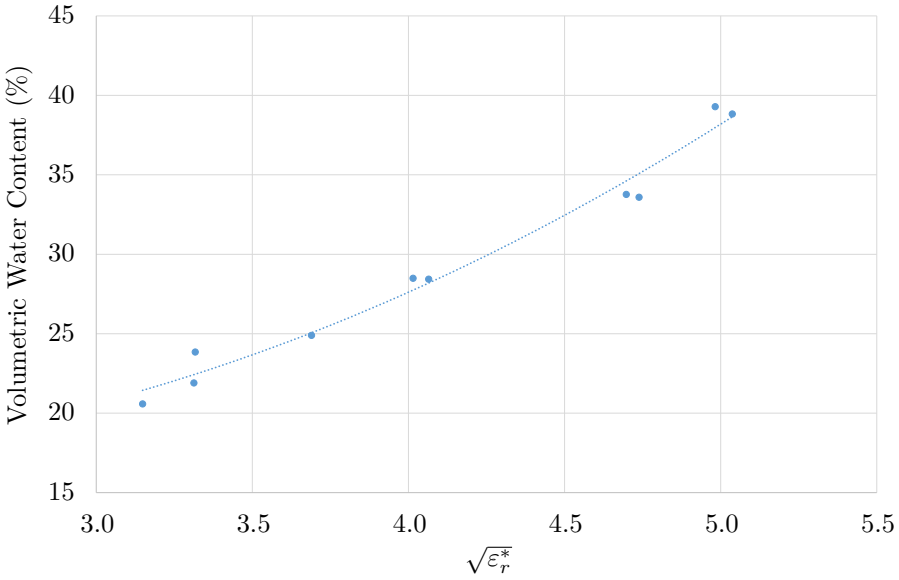

Figure 3.13: Graph of Volumetric Water Contents for Lysimeter Soil

As for how the calibrations between permittivity and volumetric water content perform, the empirical relationships are shown in Figure 3.17. Here it can be seen once again that Malicki's equation falls short, under-estimating the volumetric water content consistently whereas Topp and Ledieu are somewhat closer. Indeed, rather than a consistent underestimation, as with the builders sand, Topp and Ledieu demonstrate an under-estimation as with Malicki at the lower water contents, yet a significant over estimation at the higher water contents. This is explained to some extent by an observed trend with clayey soils, as is the case here, where generic empirical equations tend to under-estimate at lower water contents and over estimate at higher water contents [65]. Calculating some metrics yields Table 3.8, wherein Ledieu has a smallest average difference between calculated and real, at 1.86% VWC. Interestingly, Malicki's equation

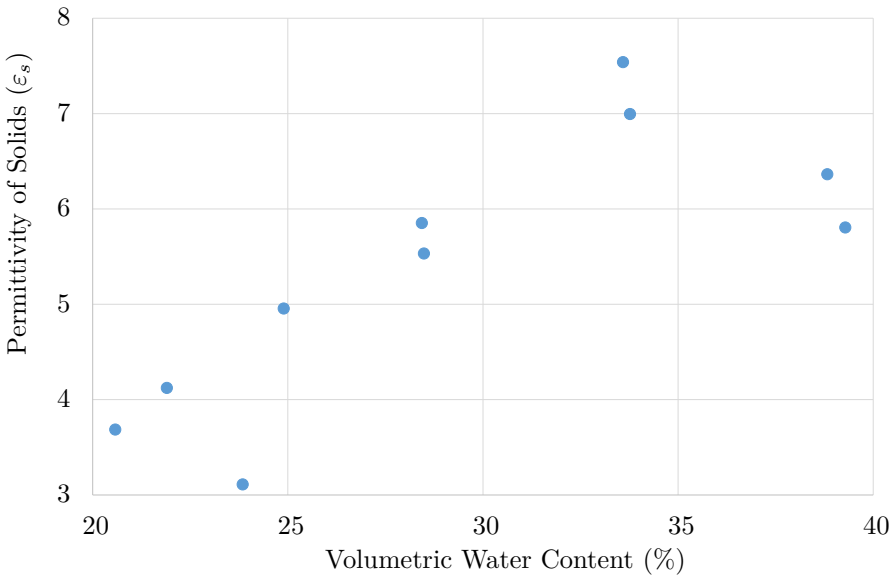

Figure 3.14: Graph of Permittivities for Lysimeter Soil

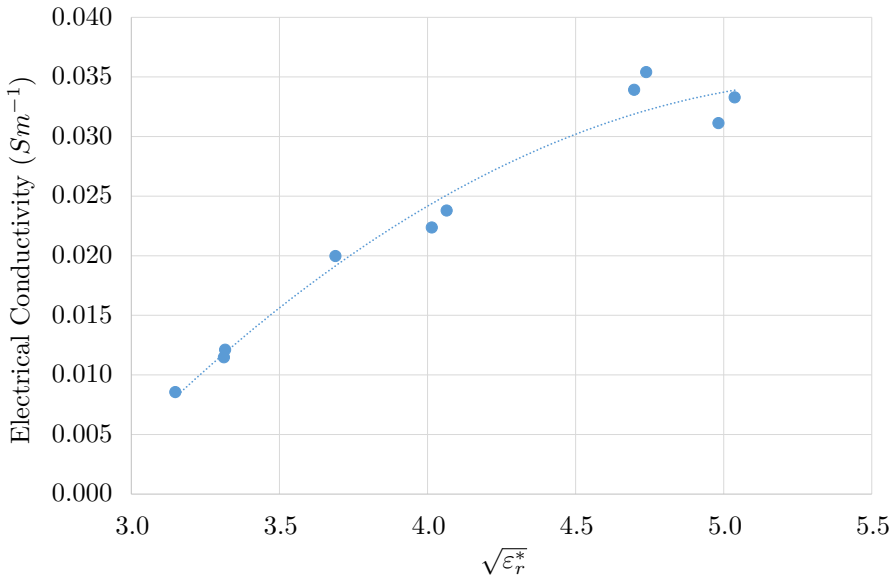

Figure 3.15: Graph of Electrical Conductivities for Lysimeter Soil

improves upon Topp's in terms of average offset and also consistency, matching the gradient yet always falling short. Indeed, whereas the other equations have worse metrics between the builders sand and lysimeter soil, Malicki's equation is the only one to have improved.

The volumetric relationships also deteriorate somewhat as demonstrated in Figure 3.18. Both volume models predict a steeper slope with the volumetric model only just beating Ledieu in terms of average difference from the true water content, as can be seen in Table 3.9. This is in stark contrast to how well the predictions turned out for the builders sand, suggesting such a simple three phase model is not suitable for this particular soil.

As for the custom calibrations, they again perform better but not quite as well as with the sand, due to the greater possible variability of the material. Relative to the other interpretations for the lysimeter soil, the custom calibrations were particularly accurate, which can be seen in Figure 3.19 and Table 3.10. The simple linear fit appears to be the best fit of all, with a mean difference of 0.50% and the other empirical fits taking densities into account close behind at 0.62% and 0.65% VWC. As for polynomial fits, considering the large range of water contents unaccounted for in this data set, it was thought best to avoid these due to the uncertainties they introduce outside of a data range and considering the mean offsets were very similar to those of the linear fits. In practice with the lysimeters, the straight linear fit was preferential over those involving density terms, as these would add another degree of uncertainty over large shrink and swell cycles.

Table 3.8: Errors in Empirical Determination of Volumetric Water Contents in Lysimeter Soil

Property	**Topp - Mineral**	**Topp - Organic**	**Ledieu**	**Malicki**
Mean Difference	2.25	7.44	1.86	2.01
$\sum difference^2$	52.15	468.14	43.54	52.30

Table 3.9: Errors in Volumetric Determination of Volumetric Water Contents in Lysimeter Soil

Property	**Volume (0.5)**	**Whalley**
Mean Difference	1.79	2.39
$\sum difference^2$	35.39	65.71

Table 3.10: Errors in Custom Determination of Volumetric Water Contents in Lysimeter Soil

Property	**Linear**	**Linear (dry)**	**Linear (Bulk)**
Mean Difference	0.50	0.62	0.65
$\sum difference^2$	3.08	4.90	5.33

Retracing back to calculating the potential accuracy of the TDR system, it is possible to recalculate the errors in terms of this new relationship as given in equation 3.28. With Probes 1 to 24 this works out as 95% confidence that the bias is less than ±0.30% VWC and probes 25 through 72 as ±0.02% VWC, purely from uncertainty of the offset. As for the standard deviation, this approximates as ±0.27% VWC or a 98% chance the reading is within ±0.54% VWC. Finally, the certainty of this calibration as taken from Figure 3.19 and Table 3.10 suggests the average difference between the calibration and the true value is around 0.50% VWC so there is the potential for some error but this is significantly reduced from using the recommended 5 data point calibration described in the TDR100 manual combined with using

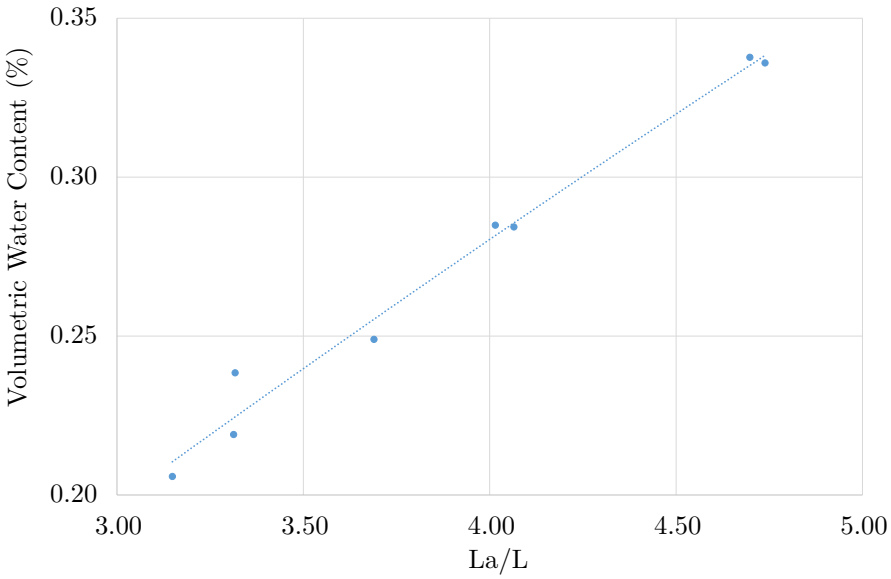

Figure 3.16: Corrected Graph of Volumetric Water Contents for Lysimeter Soil

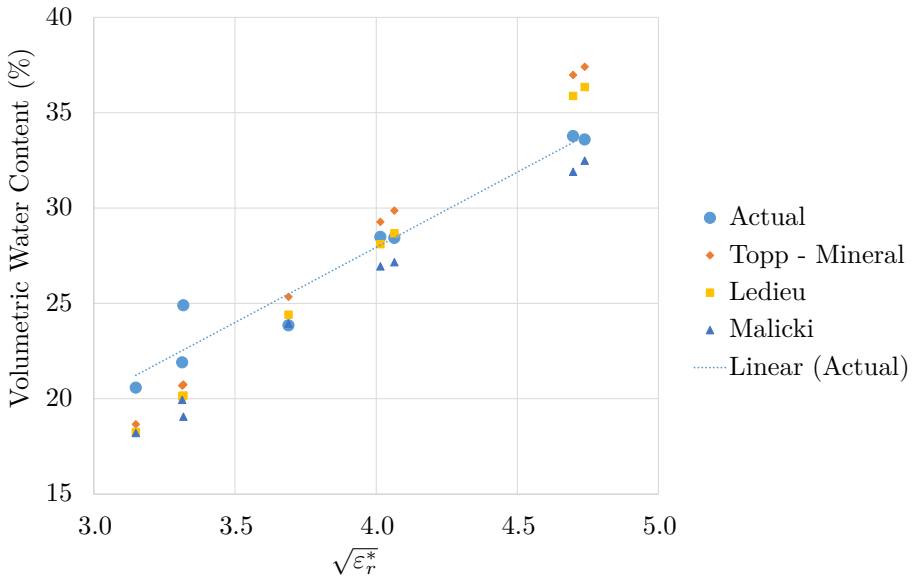

Figure 3.17: Graph Comparing Empirical Relationships for Lysimeter Soil

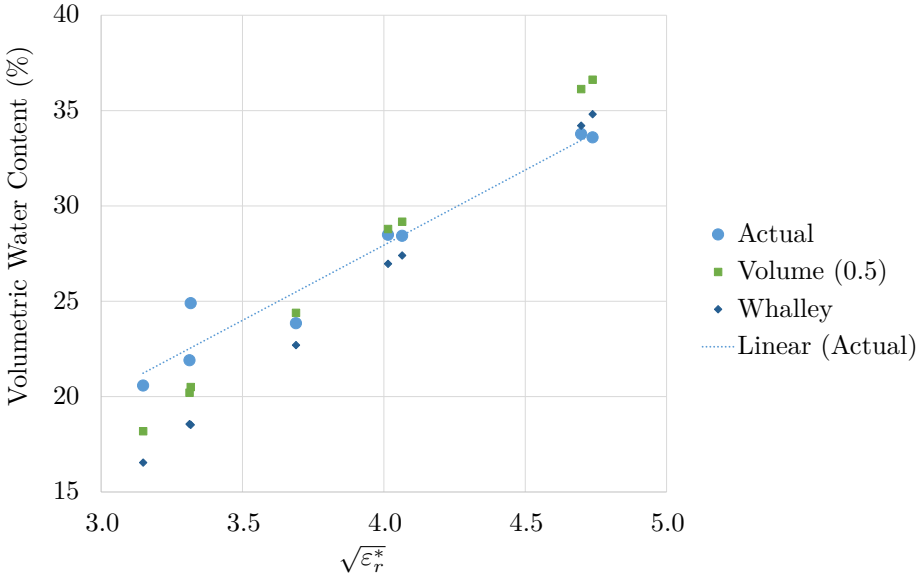

Figure 3.18: Graph Comparing Volumetric Relationships for Lysimeter Soil

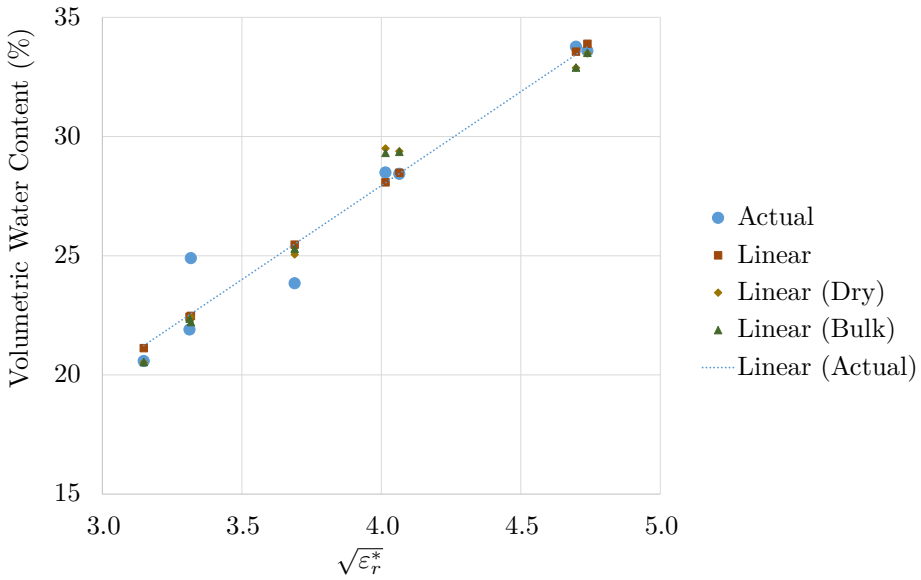

Figure 3.19: Graph Comparing Custom Relationships for Lysimeter Soil

a generic empirical calibration such as that of Topp.

$$\theta_v = 0.0803\sqrt{\varepsilon_r^*} - 0.0416 \tag{3.28}$$

.

The main methods to minimise these errors included a greater number of readings for calculating probe offset, as implemented for probes 25 through 72, and with the lysimeters taking frequent readings and applying a moving average to essentially negate the ±0.54% VWC noise. Taking a closer look at the samples with the more extreme offsets from the chosen calibration reveals they have certain properties that do not represent the final lysimeter samples as much as the majority of the other data points, for instance much lower or higher densities. The data suggests accurate determination of volumetric water content is achievable with this system.

Regarding the correction of apparent permittivity to real permittivity before applying conversions to volumetric water content, some conversions were attempted by hand, with no convenient way of automating the process as of yet. In particular, there is some disagreement on the best way to calculate a frequency for this use. The potential for these corrections is certainly positive, as when trialled with a sand-compost mix, the corrected permittivities fell more in line as with what was expected from a simple volume model, falling from an average difference of 0.62% VWC to 0.26% VWC. As for use with the lysimeters, further work was required hence the correction was ignored.

3.5 Conclusion

In conclusion, a commercial TDR system was selected and custom TDR probes designed and built. The probes were rigorously tested to assess their accuracy when determining water contents in both a sand and the soil of interest. The probes performed well in both, with the sand custom calibrations and volumetric models giving, in comparison to the empirical calculations of Topp and Ledieu, significant improvement. With the soil placed in the lysimeters however, the simple volumetric models could no longer accurately predict water contents and the recommended solution was to use a custom calibration, a linear fit between the square root of apparent permittivity and volumetric water content. This combined with the recommendation to use frequent readings and a moving average, suggests volumetric readings are very likely to be within 0.5% VWC. As for correcting readings of apparent permittivity for any losses due to conductivity, so as to reach a real value of permittivity, the recommendation is that more work is required before it can be trusted and automated to a useful extent.

Chapter 4

Tensiometers

4.1 Introduction

Tensiometers are instruments for measuring pore water pressures in materials such as soils, where the pore water pressure represents the soil's affinity for free water [66]. In particular, it is the measurement of negative pore water pressures (suctions) in the unsaturated (vadose) zone of soils that is of interest and these are capable of being measured by these devices. Here, hydro-mechanical behaviour of a soil involves both wetting and drying processes and the shrink and swell behaviour of soil.

An understanding of the relationship between water contents and suctions, under wetting and drying scenarios, is important for a number of issues. Particularly the extremes of high water contents and swelling; low water contents and shrinkage; and switching between these two states. From an engineering perspective, cycling between these states can be detrimental to infrastructure; affecting soil stability and infiltration rates of water.

In this chapter, Durham University's high capacity tensiometer are discussed, with particular emphasis on the building of these devices. With the core components being assembled off site at the start of the project and high resultant failure rates, it was decided to bring the assembly to Durham to diagnose and improve upon the build quality.

4.2 Background

4.2.1 Suction Measurement

Tensiometers fill a niche amongst other techniques for the measurement of pore water pressures. They are a direct measurement technique, that reads the matric suction, the component of pore water pressure attributed to capillary forces [67]. Total suction is comprised of both the matric suction and osmotic suction, osmotic suction being caused by imbalances of salt concentrations within pore waters [67]. Written as an expression, these different suctions give Equation 4.1

$$\Psi = (u_a - u_w) + \pi \tag{4.1}$$

where ψ is the total suction; $u_a - u_w$ represents the matric suction caused by surface tensions at air-water interfaces, where u_a is the pore air pressure and u_w is the pore water pressure; and π is the osmotic suction.

A range of devices and methods are available for assessing pore water pressures, with some being listed in Table 4.1. The methods are split between those that measure the total potential and those

that measure only the matric component. For each, an estimate of the typical suction range the device or method covers is given, alongside approximate times taken to reach equilibration, a point where the technique first represents the true pore water pressure of a sample.

Table 4.1: Methods for obtaining pore water pressure measurements

Component	Methodology	Range (kPa)	Equilibration Time
Total Potential	Thermocouple Psychrometer	300-7,000	1 hour
	Transistor Psychrometer	100-18,000	1 hour
	Non-contact Filter Paper	400-30,000	5-14 days
	Vapour Equilibrium	500-1,000,000	1-2 months
Matric Potential	Contact Filter Paper	30-30,000	5-14 days
	Suction Plate	0-100	days
	Pressure Plate	0-1,500	2+ days
	Conventional Tensiometer	0-100	hours
	High Capacity Tensiometer	0-1,500	hours
	Osmotic Control	0-10,000	3+ weeks

Measuring a broad spectrum of suctions can require multiple instruments or techniques, each with their own advantages and disadvantages. Tensiometers stand out amongst all the others mentioned in Table 4.1 as the only method with the potential for measuring pore water pressures in-situ. All the other techniques require samples of soils to be taken. Most methods require multiple samples and only provide discrete readings e.g. the filter paper test. Pressure plates however use the same sample of soil for multiple readings, yet they employ a method for preventing the cavitation of the pore water (where a cavity of vapour or air forms within a liquid), entitled axis translation. Axis translation elevates the pore water pressures and air pressures unnaturally to impose suctions that may not reflect natural conditions.

4.2.2 Tensiometers

Traditional tensiometers measure matric potential down to $-100\ kPa$, whilst their high capacity counterparts, first proposed by Ridley and Burland (1993) [68], typically measure potentials down to $-1500\ kPa$ or lower [3]. Although the range is limited when compared to other techniques, the flexibility of the devices is far superior, offering point continuous measurements of natural matric potentials with very short equilibration times. A typical high capacity tensiometer has three requirements:

1. A pressure transducer of sufficient range capable of monitoring negative pressures;
2. A water reservoir of sufficient depth to allow for the flexing of the pressure transducers face, but of minimal volume to prevent cavitation;
3. A High Air Entry Value (HAEV) porous stone capable of remaining saturated to high pressure differences.

Some examples of tensiometers and their properties are given in Table 4.2. A wide variety of devices have been built in different studies, with pressure transducers ranging in maximum measurable pressures from as little as 700 kPa through to $15,000\ kPa$, each exceeding their rated HAEV stone air entry value. Interestingly, the air entry value of the HAEV porous stones does not necessarily correspond with the maximum noted potentials measured with these devices, for example Lourenço et al. (2008) [69] measured potentials down to 2.1 MPa whilst using a tensiometer with a stone of air entry value 1.5 MPa and transducer rated to 2.0 MPa. As for water reservoir volumes, they vary but for the higher capacity devices, tend to be in the order of magnitude of a few cubic millimeter.

Table 4.2: Characteristics of tensiometers (modified from Toll et al. 2013 [3])

Study	Stone Air Entry Value (kPa)	Pressure Transducer Range (kPa)	Water Resevoir Volume (mm^3)
Ridley and Burland (1993) [68]	1500	3500	-
Guan and Fredlund (1997) [70]	1500	15000	20
Sjoblom (2000) [71]	-	1380	-
Tarantino and Mongiovi (2003) [72]	1500	-	<4.5
Mantho (2005)[73]	1500	-	-
Lourenço et al. (2006) [74]	1500	2000	5
Meilani et al. (2002) [75]	500	1500	-
Ridley et al. (2003) [76]	1500	8000	3
Take and Bolton (2003) [77]	300	700	-
Poirier et al. (2005) [78]	500	1380	-
Mahler and Diene (2007) [79]	500 & 1500	-	5-112
Jotisankasa et al. (2007) [80]	1500	-	60

Tensiometers are prepared for use by removing all air and saturating the water reservoir and HAEV stone with de-aired water under pressure. This helps to prevent cavitation within the stone or reservoir whilst under negative pore water pressures. Three different responses of a tensiometer as it is opened to air are displayed in Figure 4.1.

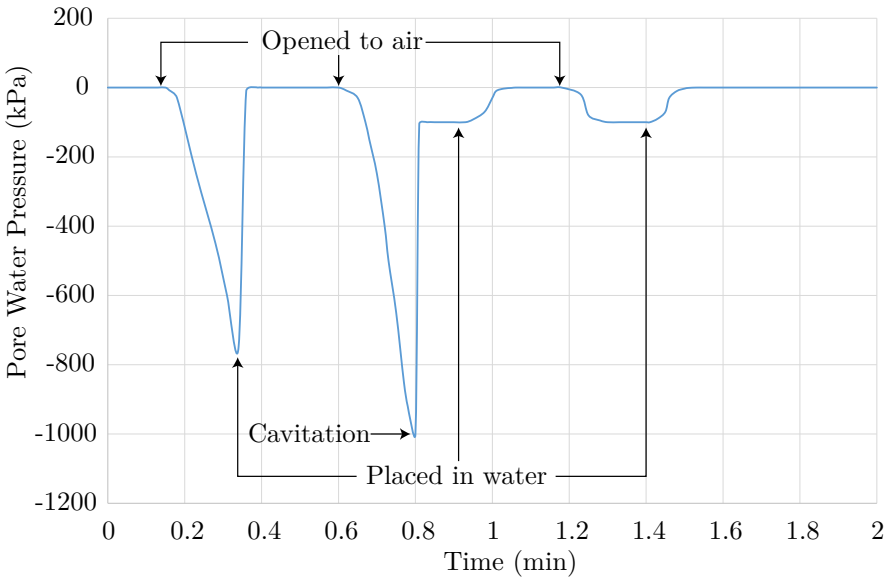

Figure 4.1: Tensiometer Response Behaviour

The first response demonstrates the behaviour when opened to drying in air and immersed in water, but before cavitation occurs. Initially, the tensiometer starts to read negative pore water pressures slowly as water evaporates off the surface of the HAEV stone. As evaporation starts to draw water from within the HAEV stone, the tensiometer rapidly measures higher suctions until prevented by immersion of the face in water, in this case at $-770\ kPa$, at which point the device returns to a reading of $0\ kPa$.

The second response takes the tensiometer to a lower pore water pressure, just as before, but at this lower pore water pressure cavitation has occurred. The device immediately relaxes back to a measured value of $-100\ kPa$. After cavitation, the tensiometer can theoretically only measure pore water pressures down to a maximum of $-100\ kPa$, as with traditional tensiometers, demonstrated by the third response.

Returning the tensiometer to normal functionality is achieved by resaturating in a pressure vessel, to once again remove air entrapped within the device.

In summary, tensiometers are excellent devices for monitoring of matric potentials in soils down to 1.5 MPa or greater. The ability to measure discreet or continuous readings and the capability to monitor soils in-situ or ex-situ provides great flexibility for experimental design and suits long term continuous measurement of soil columns well.

4.2.3 Soil Water Retention Behaviour

With regards to the context of the pore water pressure measurements, it is useful to present the results alongside water content measurements. For comparison between different soils, the water contents should take into account the volume changes for the sample, hence water states for soil water retention behaviour are best expressed as either volumetric water contents or degrees of saturation. The chart plotting water content against suction on a log scale, is commonly referred to as a Soil Water Retention Curve (SWRC). An example of a SWRC is shown in Figure 4.2.

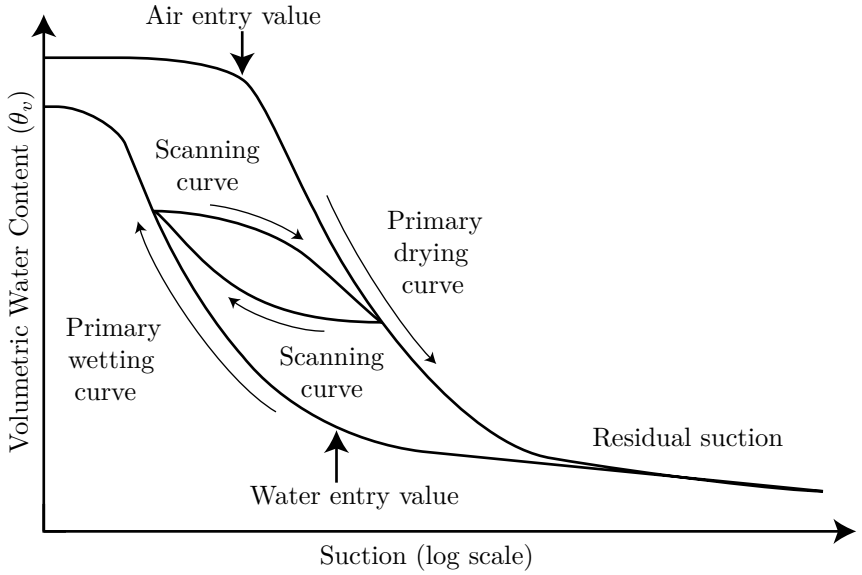

Figure 4.2: Hysteretic Soil Water Retention Curve

The curve in the figure demonstrates the hysteretic behaviour of a soil. Starting with a saturated sample under drying conditions, air enters the soil as it begins to follow the primary drying curve down to residual suctions at low water contents. Initially, large voids desaturate leading to small increases in suction. As water contents decrease, more numerous smaller voids desaturate causing suctions to increase more rapidly. At low water contents, the curve flattens off to a residual state.

Wetting from the residual state increases the water content and decreases suctions, following the primary wetting curve until the sample is saturated, essentially reversing the wetting process and saturating ever larger voids. In the case of Figure 4.2, the discrepancy between the start and end volumetric water contents at saturation are caused by either the overall shrinkage of the sample, reducing the volume of voids yielding a lower volumetric water content at saturation, or air bubbles being entrapped within the sample.

In practice however, soils do not exclusively switch between saturated states with no suction and desaturated states with very low water contents and levels of suction approaching residual. Instead, soils may follow scanning curves, bridging between the extremes of the primary wetting and primary drying

curves.

4.3 Tensiometer Components

The Durham University tensiometer design is shown in Figure 4.3. It consists of two steel components that form the casing, a main body to house the transducer assembly and a threaded insert for sealing the cabling against water ingress at the rear using an O-ring. The transducer assembly consists of a HAEV stone, a steel spacer and a ceramic transducer. The transducer assembly is itself connected to a suitable length of four core cabling which protrudes out of the back of the casing and is attached to a 5-pin DIN connector for direct connection to logger boxes.

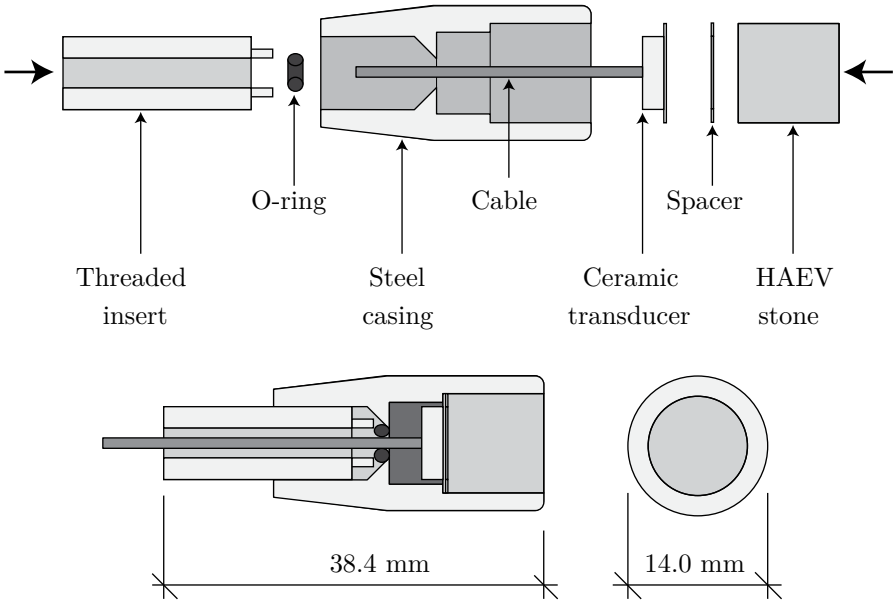

Figure 4.3: Tensiometer components and assembly

4.3.1 Transducer

The ceramic transducers were built by an external firm and consisted of a diaphragm placed on a structural ring with circuit board on the underneath. The circuit diagram for the layout is shown in Figure 4.4. The large circle represents the transducers diaphragm, with four resistors laid out as a Wheatstone bridge on the reverse side. Connected to this are a series of resistors to act as current limiters and filters, so when powered by a 5 V D.C. supply the output is stable. The inputs and outputs protrude from the base of the transducer in the form of four small wires, as can be seen in Figure 4.5, which are connected to four core cable for use in the tensiometers.

The transducers are capable of measuring both positive and negative pressures. The negative pressures only so long as there is space for the diaphragm to flex into. Within tensiometers, this space is created by using a spacer between the transducer face and the flat face of the ceramic stone.

4.3.2 HAEV Stone

The HAEV porous stones are used to prevent air entering the tensiometer body, hence stones are selected based upon their air entry value, the pressure difference at which air penetrates the medium. The air entry value of a material is primarily controlled by the size of the largest pore within its structure, with smaller maximum pore sizes yielding higher air entry values.

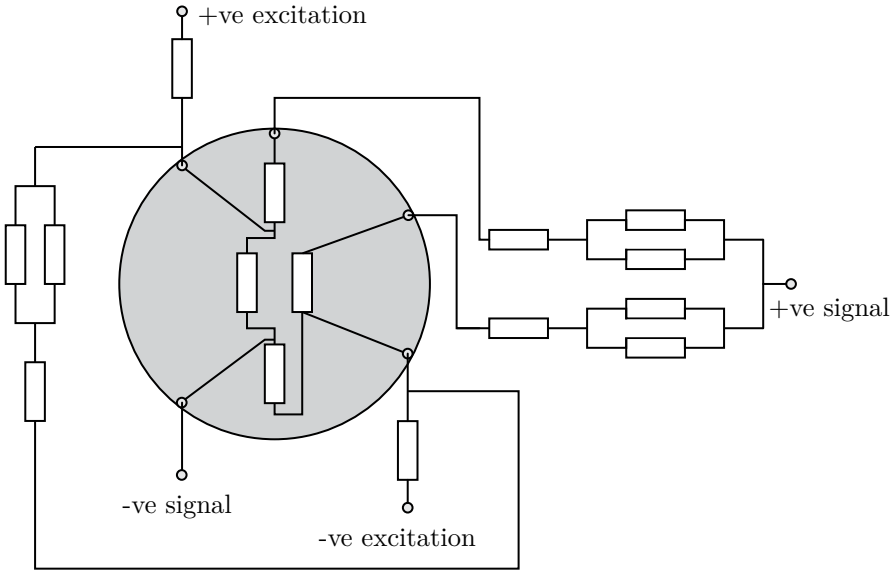

Figure 4.4: Ceramic Transducer Circuit Diagram

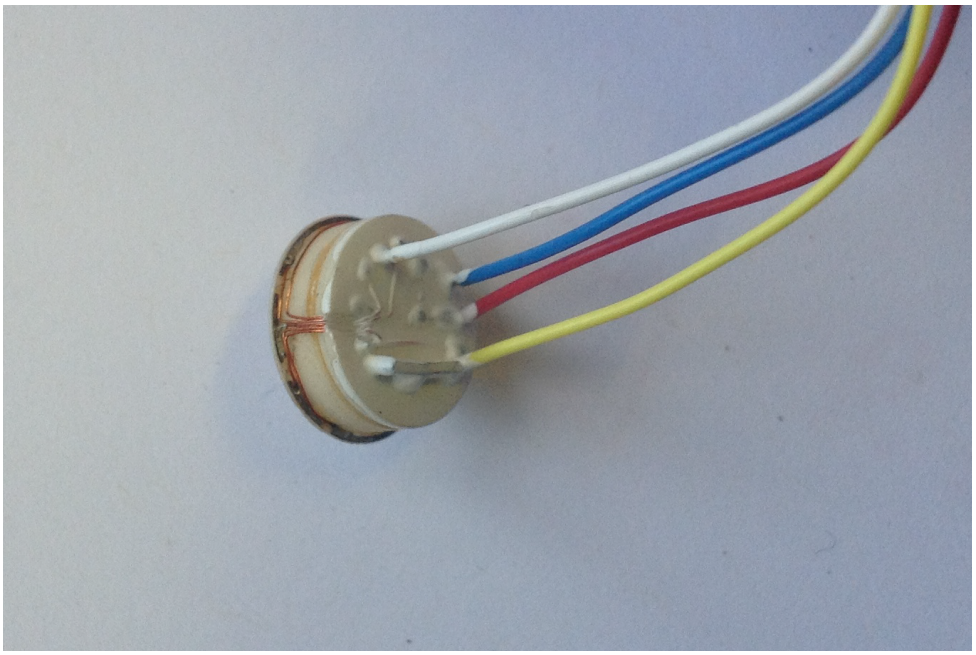

Figure 4.5: Image of Ceramic Transducer

Unfortunately, the first porous stones used in the construction of tensiometers for this project proved to be defective. The defective 'type1' porous stones were trialed in a custom built testing rig as shown in Figures 4.7 and 4.6 to ascertain their true air entry value.

The rig consisted of a base plate with a central hole, the size of the HAEV stones, approximately 10 mm in diameter with a chamfered edge. The top plate matched the chamfered edge and hole, and was attached by means of four screws. When joined together, a v-shape was formed by the meeting of the two chamfered edges, inside which an O-ring resided. When testing, the O-ring would surround the HAEV stone and be clamped between the two surfaces of the base plate and top plate, forming an air and water-tight seal.

Figure 4.6: Image of HAEV test rig - open

The stone was then saturated inside a pressure vessel, with the reverse of the stone attached to a volume change apparatus. Applying a constant back pressure, the cells air pressure was increased in steps as is shown in Figure 4.8 until a change was registered in the volume change, indicating air had entered the stone.

With the 'type1' stones, this consistently occurred at pressures far below the quoted 1.5 MPa, for Figure 4.8 the matric potential was in the region of 336 kPa. Testing a second source of stones, denoted herein as 'type2', none of the stones hit their air entry value within the pressure vessel. In the case of Figure 4.9, the stone depicted had still not hit its air entry value at the limits of the pressure vessel, with the volume change registering constant over a range of imposed pressures, finishing at a matric potential of 1490 kPa. These were the stones then used to construct all further tensiometers.

4.3.3 Spacers

The spacers used in the construction of the tensiometers were custom cut from sheet steel to the required size. These were predominantly 0.1 mm thick, although some were 0.2 mm and 0.3 mm thick, with an internal diameter of 8 mm and external diameter of 10 mm, matching the outer dimension of the ceramic transducer.

The inner diameter of the spacer was made as large as possible but was limited due to the potential for the spacer to spring and curl up if the wall thickness became too small. Heights varied when testing out

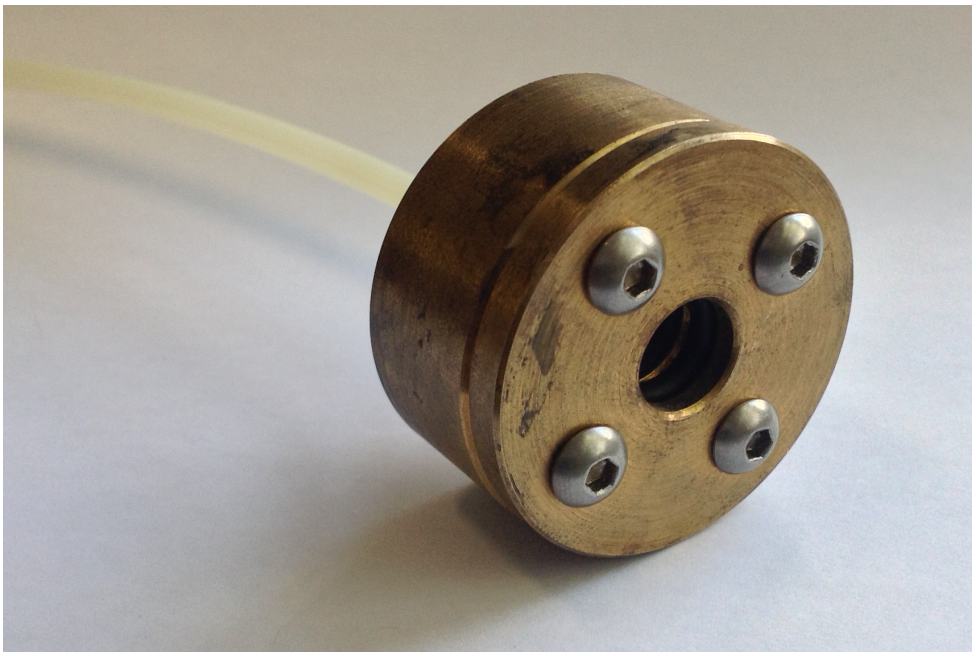

Figure 4.7: Image of HAEV test rig - closed

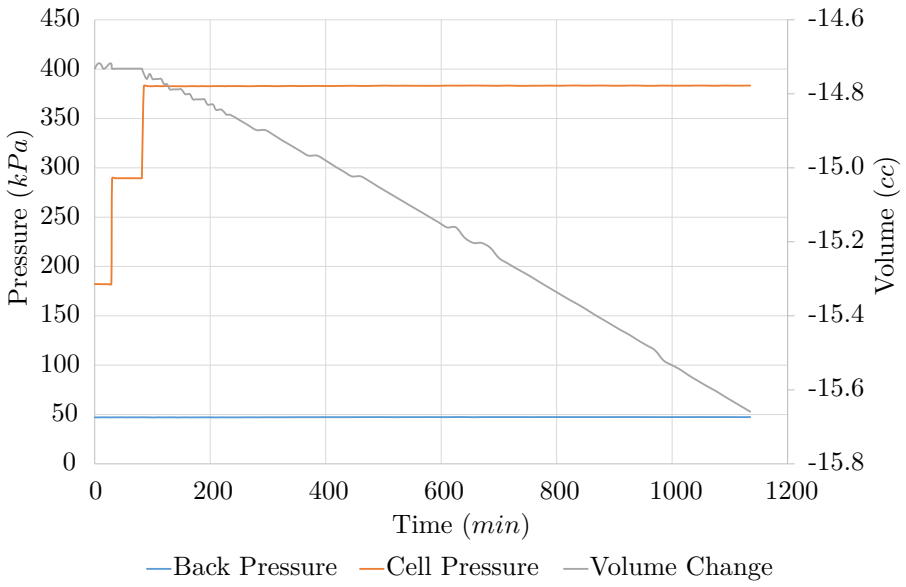

Figure 4.8: Type 1 HAEV stone tested under high pressures

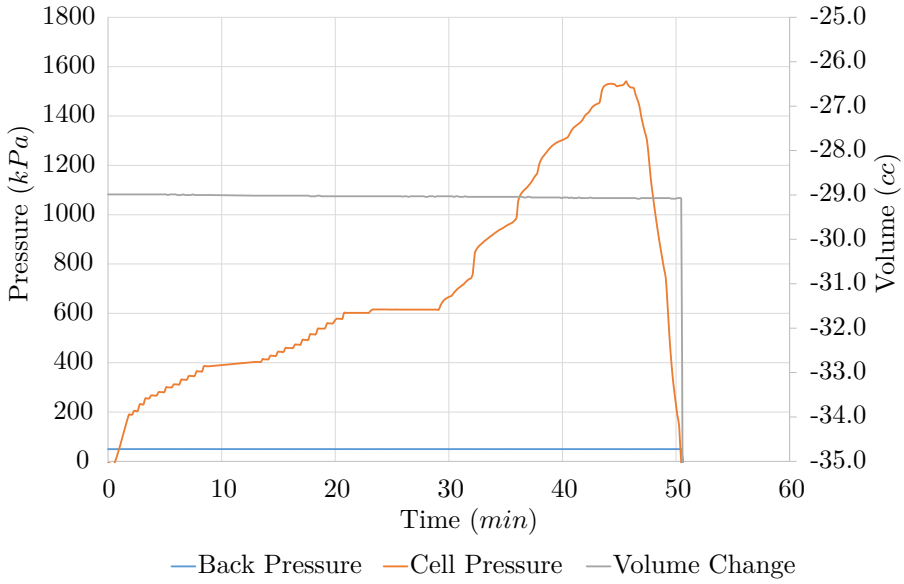

Figure 4.9: Type 2 HAEV stone tested under high pressures

potential problems during production, however the major issue encountered was corrosion of the spacer material, as demonstrated in Figure 4.10.

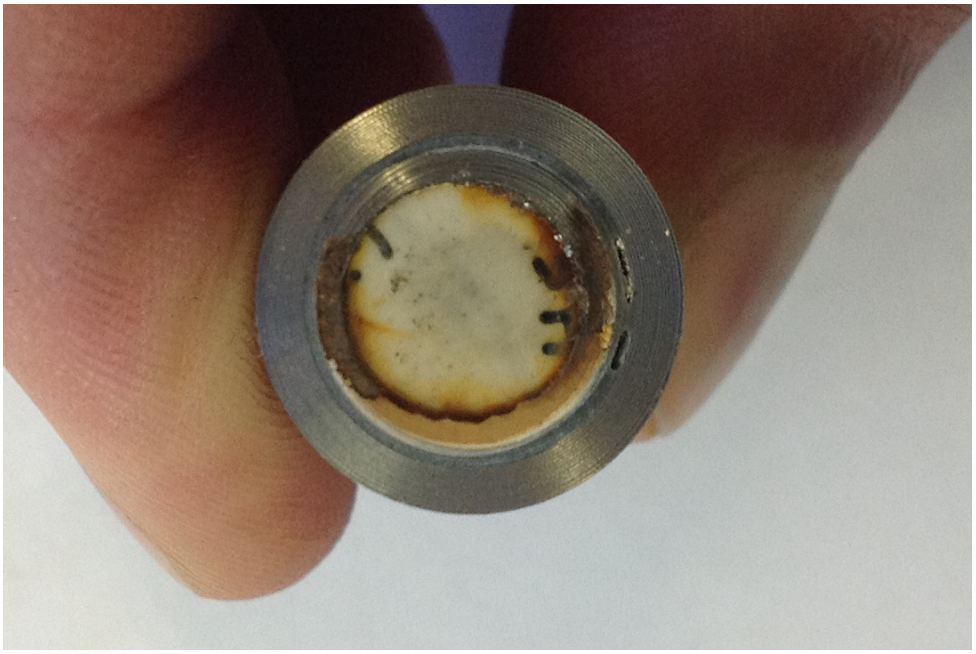

Figure 4.10: Tensiometer spacer showing signs of corrosion

The corrosion was due to the material being mild steel, which is susceptible to rusting, with inadequate protection against its environment. This was solved by upgrading further builds to using stainless steel spacers at some additional expense.

4.3.4 Casing

The casings were all custom made in the mechanical workshop at Durham University. They were constructed from stainless steel to prevent corrosion and to remain rigid whilst clamped in the saturation

vessel under high pressures.

4.3.5 Coatings

A range of coatings were trialled and used for the construction of tensiometers. The original builds simply used one for all purposes, this being Araldite® type 2014-1. Araldite® type 2014-1, was a high strength two part adhesive with low shrinkage and high resistance to temperature changes and water, making it a potentially ideal material for constructing tensiometers. There were concerns however, particularly with consistency across builds and the difficulty of managing small quantities.

It was found the Araldite® was not suitable for protecting the wired circuitry at the back of the ceramic transducer, due to both its hardness when cured and high viscosity limiting liberal use. Ideally, both the reverse of the ceramic transducer and the attached wires were to be sealed, with some of the early tensiometers shorting either against the casing or other cables. In addition, some flexibility was required in the coating material. Final assembly involved potting the internal assembly in the casing with the cable connections having to fit into a very small space behind the ceramic transducer.

Instead a more flexible acrylic was employed. The acrylic coated the entire back of the transducer, sealing against water ingress and preventing short circuits from forming on the transducer wiring. The acrylic also was applied up to and beyond the connections to the four core cable, in addition to shrink wrap. The acrylic was flexible enough to withstand the cables being coiled during potting and sealed against another potential point for short circuits to form.

4.3.6 Adhesives

Another issue with the Araldite® was its high viscosity allowing voids to permanently form in the cured product. Voids could be seen in the Araldite® when slicing cross sections from old tensiometers, as seen in Figure 4.10 on the right of the image. In general, this was not seen as much of a problem during potting but could be indicative of issues during coating and sealing of the internal assembly.

Two alternatives were trialled separately for coating the internal assembly, both with incredibly low viscosities. M-bond 610 was a two component solvent thinned epoxy-phenolic adhesive designed for bonding high performance transducers. Glue lines could be created as thin as 0.005 mm, which created an extremely hard and importantly void free barrier. Application was easy, forming uniform layers of adhesive and aided by the low viscosity, though there was some concern over ingress into the HAEV porous stone. The second adhesive was M-bond 600, which had similar properties to its counterpart but required lower curing temperatures and as a result had a much reduced shelf life, approximating 2 weeks as opposed to 6 weeks for M-bond 610.

The final result for the later tensiometers was three different bonding agents/coatings being used per tensiometer. An acrylic for sealing the reverse of the transducer against potential water ingress and short circuits, an epoxy-phenolic adhesive for bonding and coating the internal assembly of transducer, spacer and HAEV stone, and finally Araldite® 2014-1 for potting the assembly in the tensiometer casing.

4.4 Construction, Saturation and Calibration

Due to concerns over high failure rates (up to 50 %), assembly of these tensiometers was all done in house. This was opposite to prior tensiometers where the entire transducer, spacer and HAEV stone were bought as an assembled unit ready for potting into a casing. This meant a higher degree of control could be had over the construction process and issues encountered through use could be associated with problems in the construction procedure more directly.

A total of thirty two tensiometers were built over the course of the project, with their general construction properties listed in Table 4.3. All tensiometers used the exact same casing design but differed

in their other construction materials and build techniques.

Table 4.3: Tensiometer Construction Properties

Identifier	Transducer Range (MPa)	Spacer Thickness (mm)	Spacer Material	HAEV Stone	Bonding Agent
V1	1	0.1	Mild Steel	Type 1	Aryldite
V2	1	0.1	Stainless Steel	Type 2	M-bond 610
V3	1	0.1	Stainless Steel	Type 2	M-bond 600
V4	1	0.1	Mild Steel	Type 1	Aryldite
V5	1	0.1	Mild Steel	Type 1	Aryldite
V6	1	0.1	Mild Steel	Type 1	Aryldite
V7	1	0.1	Stainless Steel	Type 2	M-bond 610
V8	1	0.1	Stainless Steel	Type 2	M-bond 600
V9	1	0.1	Stainless Steel	Type 2	M-bond 610
V10	1	0.1	Stainless Steel	Type 2	M-bond 610
V11	1	0.1	Mild Steel	Type 1	Aryldite
V12	1	0.1	Stainless Steel	Type 2	M-bond 610
V13	1	0.1	Stainless Steel	Type 2	M-bond 610
V14	1	0.1	Mild Steel	Type 1	Aryldite
V15	1	0.1	Mild Steel	Type 1	Aryldite
V16	1	0.1	Mild Steel	Type 1	Aryldite
V17	1	0.1	Mild Steel	Type 1	Aryldite
V18	1	0.1	Stainless Steel	Type 2	M-bond 610
V19	1	0.1	Mild Steel	Type 1	Aryldite
V20	1	0.1	Mild Steel	Type 1	Aryldite
V21	1	0.1	Stainless Steel	Type 2	M-bond 610
V22	1	0.1	Mild Steel	Type 1	Aryldite
V23	1	0.1	Stainless Steel	Type 2	M-bond 610
V24	1	0.2	Mild Steel	Type 1	Aryldite
V25	1	0.1	Mild Steel	Type 1	Aryldite
V26	1	0.1	Mild Steel	Type 1	Aryldite
V27	1	0.2	Mild Steel	Type 1	Aryldite
V28	1	0.1	Stainless Steel	Type 2	M-bond 610
V29	1	0.3	Mild Steel	Type 1	Aryldite
V30	1	0.3	Mild Steel	Type 1	Aryldite
VI1	2	0.1	Stainless Steel	Type 2	M-bond 600
VI2	2	0.1	Stainless Steel	Type 2	M-bond 600

4.4.1 Construction

The construction process differed between batches of tensiometers with experience and modifications, but in general the following procedure was adhered to:

1. Each transducer had the base of the small wires protruding from the rear coated in a hard acrylic;
2. The small wires on the transducer rear were then trimmed to an appropriate length and soldered onto four core cable;
3. The connections between transducer wire and four core were coated in shrink wrap, coiled into a neat position for fitting inside the steel casing, and sealed with acrylic;
4. For each transducer, a steel spacer was cleaned and degreased for an ideal application of bonding agent;

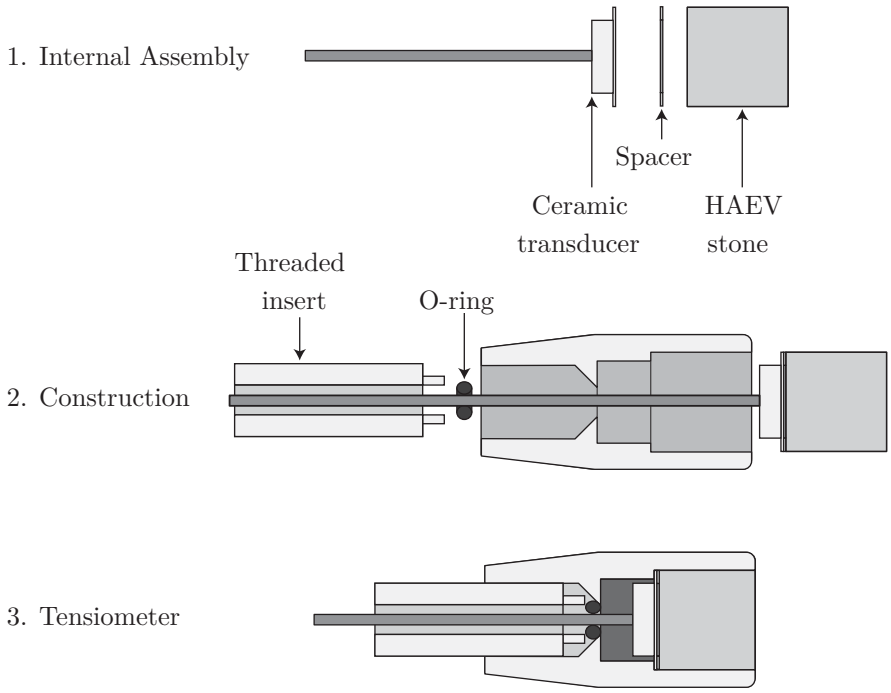

Figure 4.11: Tensiometer Construction Steps

5. The HAEV stones were cored from larger HAEV porous plates using a diamond tipped 10 *mm* diameter corer;

6. The three components were assembled, as in Figure 4.11 step 1, in a custom built jig for application of a bonding agent (Araldite® 2014-1, M-bond 600 or M-bond 610) through either:

   (a) Application of the bonding agent exclusively to the exterior of the assembly, including the outside of the transducer, spacer and side walls of the HAEV stone;

   (b) Application of the bonding agent to both the spacer faces and the exterior of the assembly, including the outside of the transducer, spacer and side walls of the HAEV stone;

7. The bonding agent was left to cure until either:

   (a) If more layers were to be applied, tacky, at which point another layer would be applied;

   (b) If no more layers were required, hard;

8. The casing was then prepped for the internal assembly by degreasing;

9. The four core cable was threaded through the casing, the O-ring and the the stainless steel rear insert, as in Figure 4.11 step 2;

10. The two part Araldite® 2014-1 adhesive was mixed for each tensiometer and inserted carefully, to prevent formation of air bubbles, in copious quantities inside the casing;

11. For each tensiometer the internal assembly was eased into the casing, displacing the epoxy resin, with excess cleaned off;

12. At the rear of the casings, the threaded insert was screwed tightly onto the O-ring to form a seal;

13. The tensiometers were then left in the custom jigs to hold the unit steady as the adhesive cured;
14. Once cured, the protruding HAEV stone from the front face of the steel casings was ground back for a flush finish, also removing any excess adhesive that may have touched the face;
15. Once a tensiometer was finished, a 5 pin DIN connector was attached to each and the process of saturating could begin.

The variations in build were primarily due to material changes as shown in Table 4.3 but there was some variation in method. The coating on the reverse of the ceramic transducer was fairly consistent yet the bonding of the internal assembly varied considerably, finally resulting on the use of the M-bond series of adhesives.

Each of the two adhesives had different recommended curing temperatures and times and it remains to be seen whether one was superior over the other. For both, the curing temperature used was below that recommended for the product, primarily to prevent damage to the assembly through melting insulators etc.. with temperatures maximising at 60 $^{\circ}C$. This meant much longer curing times were required but also left a longer window of opportunity open for application of additional layers whilst the previous layer was still tacky to the touch, improving bonding. This process was repeated several times until the outside of the assembly had taken on a distinct yellow hue associated with the cured adhesive and could potentially run over a period of two weeks with the slower to cure M-bond 610.

As for application of the bonding agent to the faces of the spacer, no discernable difference was observed between those that were sealed from the outside only and those sealed on the outside and on the faces.

In general, so long as the materials were up to the task, there was some leeway in constructing the tensiometers and as yet there can be no conclusion drawn on whether some of these minor changes affected the functionality of the tensiometers significantly, or if at all.

4.4.2 Saturation

A good saturation procedure was important for the tensiometers to function correctly, preventing cavitation at high magnitudes of negative pore water pressure. Cavitation occurs when undissolved gas expands from nucleation sites, such as cracks in a wall or ceramic, within a body of water under increasing tension. As water in a tensiometer is exposed to ever increasing values of tension; cavities form, expand and finally release, cavitating the device [77, 81, 82].

Saturation is a process which aims to remove significant quantities of air from within the porous HAEV stone and water reservoir prior to filling with de-aired water. Pressurisation of this water further helps to prevent cavitation.

The saturation process used the equipment shown in Figure 4.12. Distilled water was de-aired using a vacuum line, to provide a fresh supply of gravity fed de-aired water to the system.

Two brass manifolds were attached to the de-aired water line, capable of holding ten tensiometers, each tensiometer held vertically in the manifold using an O-ring compressed into the surround using a brass clip and three screws, forming a water tight seal. On one of the manifolds, a vacuum line was attached for removing air before saturation and a pressure transducer for monitoring the positive pressures during saturation. The other manifold had a release valve, used for removing residual pressures and flushing the system through.

Pressures were applied using two pumps connected to a pressurised air line. The air line could provide pressures up to 0.7 MPa but was used only up to 0.5 MPa which was fed directly into the pressure multiplier pistons. The pressures in the lower pump were stepped up by a factor of four using the upper

pump which in turn pressurised the de-aired water connected to the manifolds. The saturation procedure being as follows:

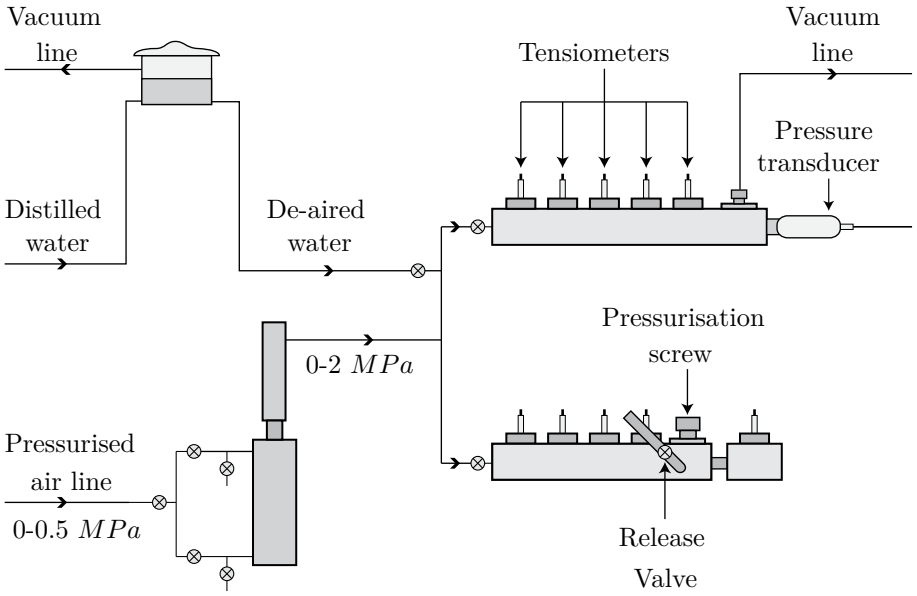

Figure 4.12: Tensiometer Saturation Schematic

1. The distilled water in the feed to the saturation system was de-aired;
2. The pump was flushed and filled with de-aired water;
3. The manifolds were drained of water and the tensiometers inserted into the vessel;
4. A vacuum was applied to the manifolds to remove any air from the saturation system;
5. While under vacuum, the de-aired water line was opened to allow the manifolds to fill, then the vacuum was stopped and the de-aired water feed cut off;
6. The manifolds were then pressurised to 1 MPa or 2 MPa, the same rating as the transducers. A saturation period of 2+ weeks was used for new tensiometers undergoing their first saturation and tensiometers that were dry or had long since cavitated. Shorter saturation periods were used for resaturating freshly cavitated transducers.

4.4.3 Calibration

The tensiometer calibrations were performed in the positive range, as per Lourenço et al. (2008) [69], using the saturation manifolds in a temperature controlled room. This involved stepping down the pressures in the manifolds, between the saturation pressure and atmospheric pressure, and noting the pressure and voltage response to obtain a linear fit for each tensiometer. Reapplying the pressure was then used to check the tensiometers for hysteresis.

This method, in addition to providing calibrations, also gave an indication as to the state of the tensiometers. Figures 4.13 through 4.17 display two calibrations for each of five different tensiometers. In each case, the first calibration displays evidence that the tensiometer is not fully saturated, showing a distinct divergence from the initial trend set when decreasing from high pressures, each initial reading taken within a couple of days of placement in the saturation vessel. The second calibration for each

tensiometer shows the calibration after each was fully saturated, displaying a typical linear correlation between pressure and voltage response.

The first two graphs, in Figures 4.13 and 4.14, show the result for two 'old' tensiometers, built before this project and with no designation hence referred to as 'unknown batch (UB)' followed by a number. These two tensiometers appeared to behave well, with voltage responses at atmospheric pressure within a few thousand microvolts of zero. When saturated, the step to vacuum the manifolds was skipped and instead only de-aired water was run through the vessels.

This had the impact of increasing the pressure that the sudden deviation in calibration was observed at, potentially due to an air cavity forming in the water reservoir thus preventing the transducers diaphragm from fully relaxing. Another interesting point being both tensiometers underwent the same exact procedure for the same period of time, yet produced a significantly different responses to partial saturation. In Figure 4.13 tensiometer UB14 produces the deflection at 650 kPa, whereas in Figure 4.14 the deflection occurs at 450 kPa, a difference of 200 kPa. Assuming the same exact dimensions, this would suggest a larger cavity in tensiometer UB15.

The final three tensiometers in Figures 4.15 through 4.17 are for tensiometers built during the project and simultaneously saturated with a vacuum stage in the manifold. Again, some significant deviation is observed in Figures 4.15 and 4.16, with a slight hint at the final point of Figure 4.17 at atmospheric pressure of some deviation. For all, this perhaps suggested the vacuum stage was not long enough or a leak existed in the vacuum line.

Like the previous two tensiometers, all three showed different points at which the calibrations deviated. All were constructed in the same manner, using the exact same materials, bar tensiometer VI1 which had a transducer to a higher rating of 2 MPa over the 1 MPa rating of the others. Two potential sources for these differences come to mind here, the first being subtle differences in the tensiometers and the second being the order in which the tensiometers were flooded, perhaps concentrating what air remained into tensiometers further along the manifold.

If indeed the deviation in calibrations is due to air cavities, it seems likely that a linear calibration may be read whilst the tensiometer is not yet fully saturated to the point that there are no cavities within the water reservoir, meaning looking for deviations is no guarantee that the tensiometer is to function as expected. It is however a useful indicator that there may be problems with the way saturation is applied, be this with the equipment or method.

4.5 Performance

The need to build more reliable and consistent tensiometers was the major driving force in assessing performance. Much of the work went into why the tensiometers behaved in an ideal manner or not, particularly the differences between the broken or unreliable ones and those considered 'good'. Three generalised attributes were considered for each tensiometer:

- Calibrations;
- Cavitation;
- Other observed behaviour.

The calibrations for each tensiometer were kept for comparison over the period of study. This allowed for the observation of long term trends that occurred with the tensiometers. Cavitation pressures were useful to assess both how well a saturation procedure had gone and also how well a particular tensiometer

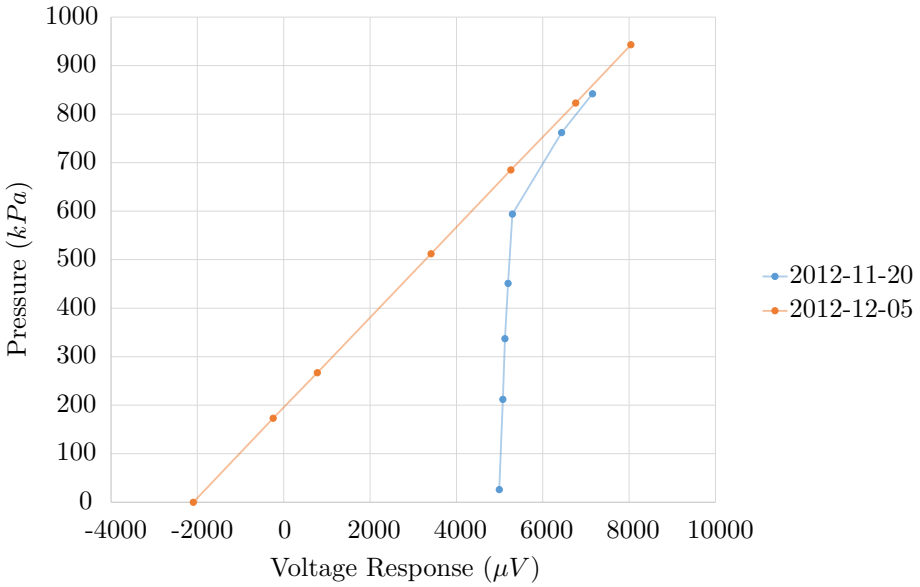

Figure 4.13: Tensiometer UB14 before and after full saturation

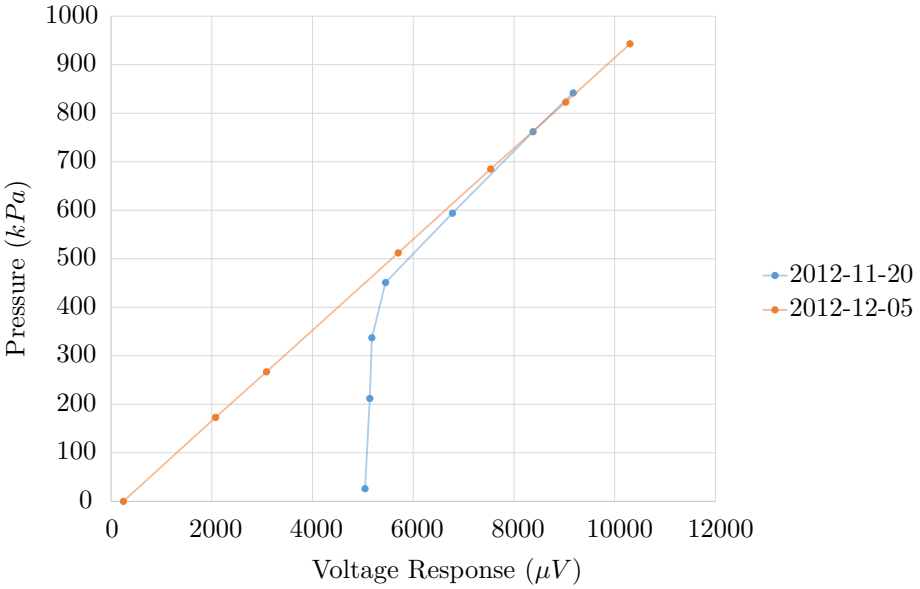

Figure 4.14: Tensiometer UB15 before and after full saturation

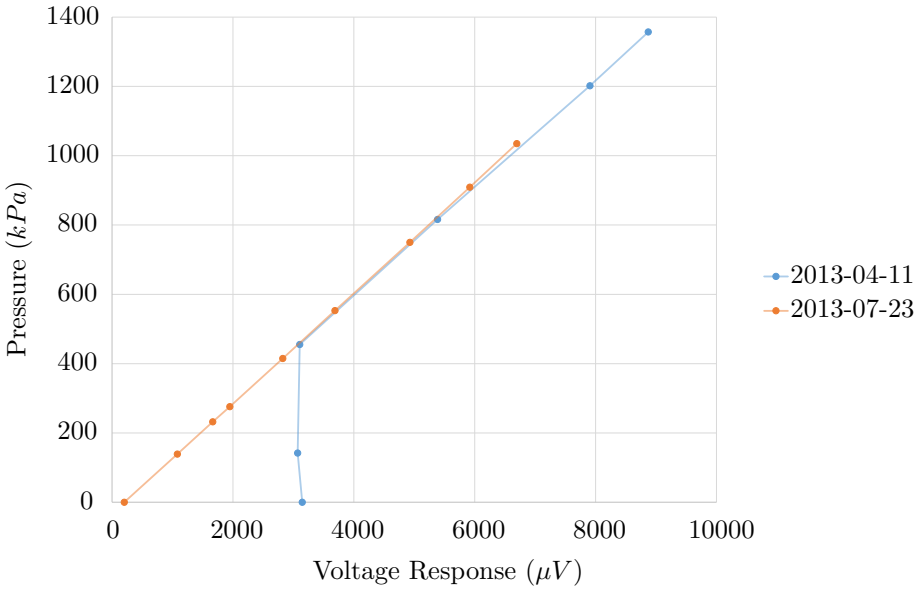

Figure 4.15: Tensiometer VI1 before and after full saturation

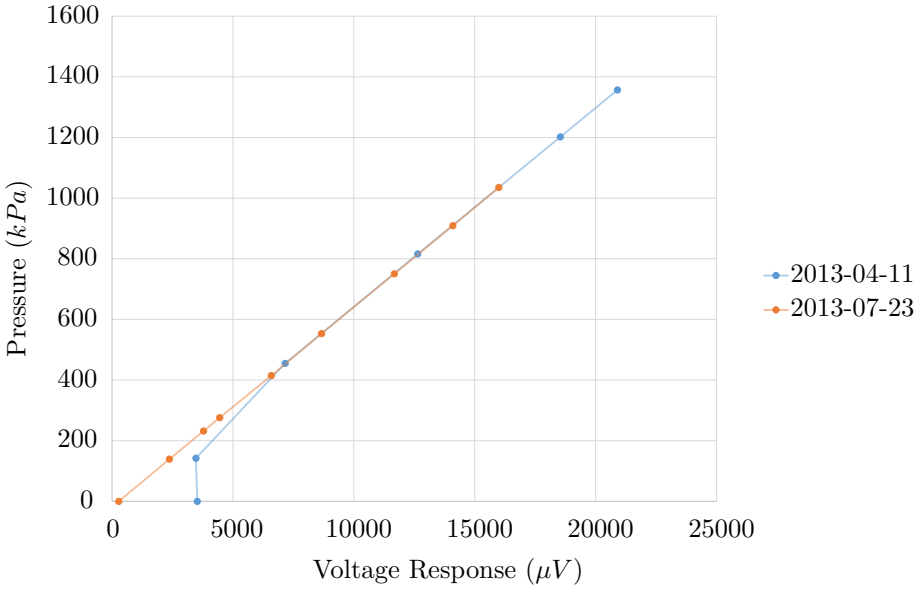

Figure 4.16: Tensiometer V8 before and after full saturation

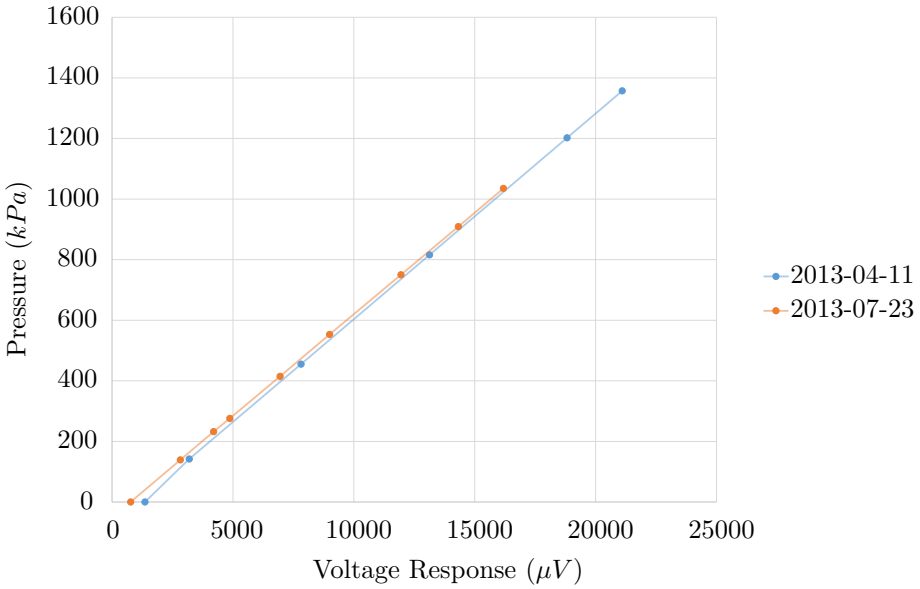

Figure 4.17: Tensiometer V3 before and after full saturation

design performed. As for the other observed behaviour, this was for small defects in each of the tensiometers. Such defects included short circuits, open circuits, slowness of response, hysteresis and non-linearity, amongst others.

Herein, to aid in discussion the tensiometers have been split into three generations. The first was a grouping of tensiometers which were built prior to the ROBUST project. These were all common, in that the internal assembly of ceramic transducer, spacer and HAEV stone were assembled off site and potted inside the casing inside the laboratory. Included were tensiometers constructed over many years with several different casing designs, but which had a poor build success rate.

The second generation of tensiometers discussed were those built on site using the 'type 1' HAEV stone, mild steel spacer and only Araldite® as an adhesive. These can be characterised as working poorly, showing an interesting array of strange symptoms and leading onto many improvements.

The third and final generation of tensiometers addressed a significant number of the defects in the second generation. Changing the 'type 1' HAEV stones for the 'type 2' stones, a corrosion resistant stainless steel spacer and using a range of adhesives to aid both in construction and performance. Although not as well tested as prior generations, signs are positive that build success rates are up and performance is both reliable and consistent.

4.5.1 First Generation Tensiometers

The first generation tensiometers were all built and used prior to the commencement of the ROBUST project and during the course of this work were saturated and calibrated repeatedly. A total of eighteen tensiometers were available initially, entitled UB1 through UB16 (for the unknown batches) and III4 and III6 from prior works [83, 84], however many of these were not functional at the offset, leaving only ten potentially working.

The tensiometers, in their air dried state, were tested in a small manifold connected to the air line to gauge functionality in the positive pressure range between 0 and 700 kPa. Those that were broken displayed problems ranging from high voltage responses that did not correlate with applied pressures through to a reasonable voltage responses that did not vary with pressure at all. Some displayed significant hysteresis returning to non zero values for atmospheric pressure, or indeed only registering changes over

certain pressure ranges.

In most cases however, the impedance values across the inputs and outputs were within normal limits of 10 $k\Omega$. Occasionally the values were outside the normal range, dropping to zero suggesting a short circuit was forming, or many Mega-ohms suggesting circuits were broken on the device. In those cases where the impedances were normal, it was difficult to assess why the transducers were behaving in a particular manner. Some behaviour was potentially caused by plastic deformation and perforated diaphragms, the most likely cause of hysteresis and zero responses respectively, but this was difficult to prove.

As for the tensiometers which were responding linearly, these were saturated and used with mixed results. One tensiometer, UB12, was known to work very well with almost ideal behaviour, having achieved potentials down to 2.1 MPa suction. Several calibrations for tensiometer UB12 are given in Figure 4.18.

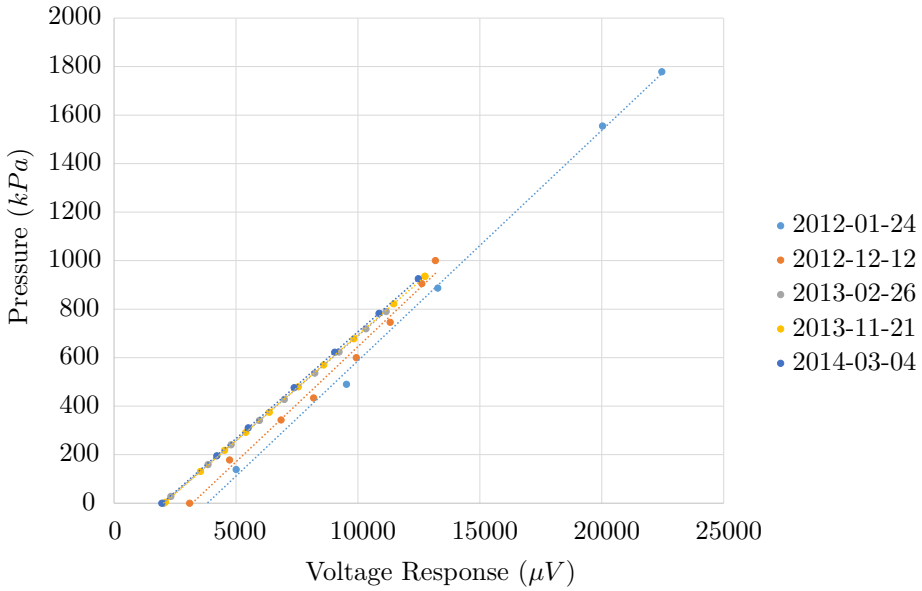

Figure 4.18: Tensiometer UB12 Calibrations over 2 Years

Firstly, the tensiometer demonstrated corresponding atmospheric pressure readings to voltage responses within a few thousand micro-volts of zero. This correlated well with ceramic transducers prior to being used in the construction of a tensiometer, showing values within $\pm 3000\mu V$, although more commonly $\pm 500\mu V$. Tensiometers that had much higher voltage responses at atmospheric pressure fell into two categories. Those within approximately $30,000\mu V$, in which case the trend was for the tensiometers to stop functioning in the near future, or those with very high nonsensical readings, essentially broken.

Secondly of note, tensiometer UB12 appeared to show convergence of straight line fits towards a repeatable result with continued use, each fit offering the same approximate gradient or rate of change of pressure with voltage response. There are two applicable explanations for this behaviour in this particular case.

The first explanation assumes all five calibrations are reliable, in which case some process is causing the continuous shift to the left combined with a convergence of the calibrations. This convergence would therefore be explained by an effect caused by cycling of pressures, the most likely candidate being a bedding in process for the strain gauge adhesive on the reverse of the diaphragm. However, with tensiometer UB12 being relatively old and having had high usage, this would not necessarily make sense. The adhesive should have been cycled sufficiently by this point, unless there was an additional aging effect of the strain gauge adhesive or some alternative explanation to the same end. Regardless, a similar

trend can be seen in the newer third generation tensiometers discussed later.

The alternative explanation placed doubts on the reliability of the first two calibrations and their marginally below unity r^2 values, essentially ignoring them. This was somewhat unacceptable as neither showed any signs that the tensiometer was behaving out of the ordinary above a slight scattering of the data points which could have been introduced by not allowing enough time for the tensiometer to stabilise at each pressure decrement during calibration. If anything, this explanation appears worse than the previous.

In total, of the ten tensiometers four proved to be unreliable and six worked as expected over the longer term. Those that worked typically displayed concise repeat calibrations without large shifts, as with tensiometer UB12, and could potentially reach suctions down to 1 MPa when saturated at that same pressure. On the other hand, those that broke on occasion demonstrated discrepancies, such as tensiometer UB5 with the calibration gradients increasing over time suggesting sensitivity was being altered; tensiometers UB11 and UB14 showing large shifts in calibrations before giving a wandering response and finally large scatters; and the odd one out, tensiometer UB6, which demonstrated concise calibrations but whose results wandered significantly.

4.5.2 Second Generation Tensiometers

The second generation tensiometers worked poorly due to large flaws in the build materials and issues during manufacturing. Eighteen tensiometers were built using similar materials in total. Out of the eighteen:

- Two did not make it to calibration;
- Four had significant scatter and high voltage responses after saturation;
- Four got calibrated with a single good linear fit calibration before subsequently breaking;
- Eight made two or more successful calibrations.

The two tensiometers that broke before calibration short circuited, either between the cable and casing or between the various inputs and outputs on the device, subsequent efforts were therefore made to reduce the likelihood of these occurrences. The four tensiometers showing a high degree of scatter after saturation appeared to have faults with the transducer, either being saturated at too high a pressure, there being a leak allowing water behind the ceramic face, or the transducer was not fit for purpose. As for the probes which had single good linear fits, the fact that these broke so early on suggested there were flaws with the build process.

Initially, two tensiometers were built with 0.1 mm spacers. They were saturated for a period of two weeks before testing in open air by drying the surface and observing the response. Unlike the tensiometers from the first generation, the responses differed when reaching higher suctions and cavitated at around 250 kPa. Upon a subsequent saturation and tests, the tensiometers cavitated at 350 kPa as demonstrated in Figure 4.19, a result that was repeatable for both tensiometers.

Four tensiometers were built with thicker spacers. Two were built with 0.2 mm and two with 0.3 mm thick spacers to confirm whether the low cavitation suctions were due to over confinement of the transducer faces, or whether this was an occurrence of a different nature, i.e. the HAEV stone. This concluded with similar results, suctions maximising at 350 kPa at which point the tensiometers cavitated.

The twelve remaining tensiometers were built using 0.1 mm spacers with additional changes to the build methods. These introduced coatings to elements, including the wiring and the transducer, spacer and HAEV stone assembly, and additional shrink wrap applied around connections on the reverse of the

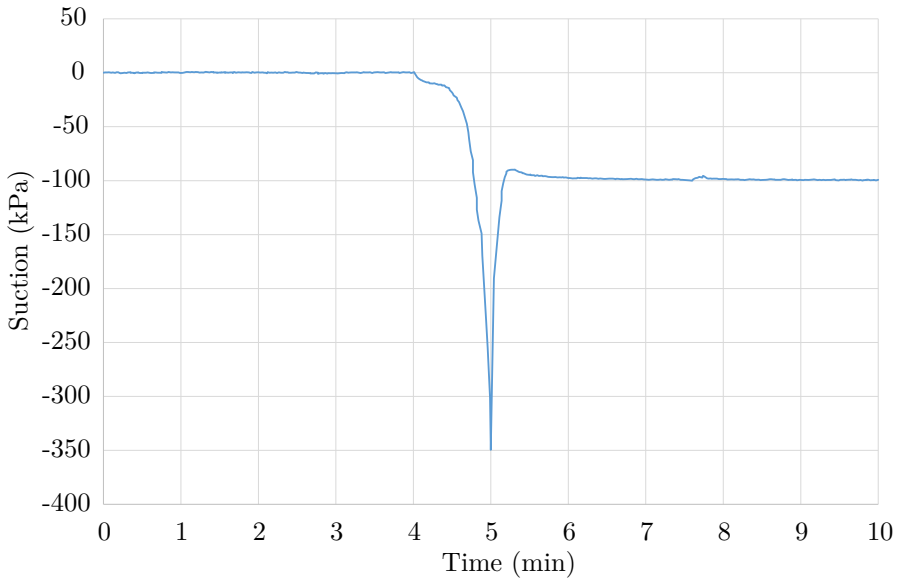

Figure 4.19: Cavitation of second generation tensiometer

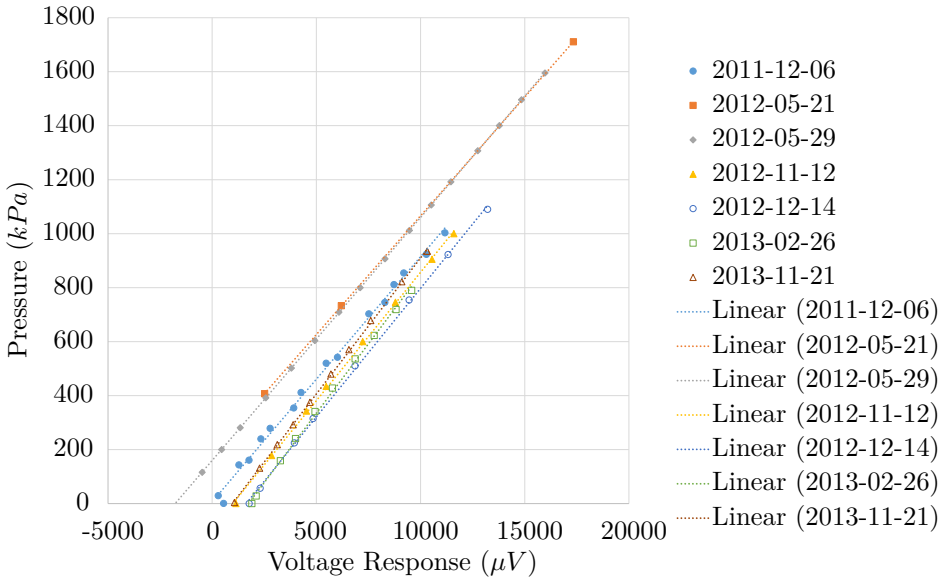

Figure 4.20: Calibrations for Tensiometer V30

ceramic transducer. The addition of these coatings decreased the number of probes produced that suffered from short circuits although, as with the other tensiometers in this generation, maximum cavitation pressures were in the region of $-350\ kPa$. This maximum suction was finally attributed to the limits posed by the 'type 1' HAEV stones which were under-performing significantly.

In the long term, the variability in the second generation probe calibrations was of concern. Figure 4.20 displays the individual calibrations for tensiometer V30 over many saturations and calibrations. Whereas the previous generation of tensiometers displayed convergence towards a repeatable result, as in Figure 4.18, these probes behaved erratically. The calibrations shifted, both left and right, after each successive saturation without any particular trend. This was attributed to the degradation of the spacer, expanding as corrosion occurred and eroding into the water reservoir.

4.5.3 Third Generation Tensiometers

The third generation of tensiometers used improved materials for the HAEV stone and spacer, addressing the issues of the second generation devices. In addition, two new bonding agents were trialled, the M-bond 600 and M-bond 610 series of two part glues, used for assembly of the internal components. A total of 14 tensiometers were built using these methods and of them three failed to work.

The first failure was due to a short circuit connection within the transducer between two of the four connection wires. The second and third tensiometers failed during saturation, both having steady readings in an air dry state. When placed in contact with water and subsequently pressurised, the readings started to show a large amount of scatter and high voltage outputs that no longer corresponded to changes in water pressure.

The eleven that were saturated at 1 MPa and calibrated successfully, were tested to find highest suction values achievable by exposing the face of the tensiometers to air and allowing drying until the tensiometer cavitated. Figure 4.21 shows the cavitation of tensiometer V3, which reached a maximum suction of $-944\ kPa$. Cavitation took around 40 seconds, after which the tensiometer immediately rebounded to an expected response of around $-97\ kPa$. The remainder of the working third generation tensiometers behaved similarly, with all cavitating in excess of $-900\ kPa$.

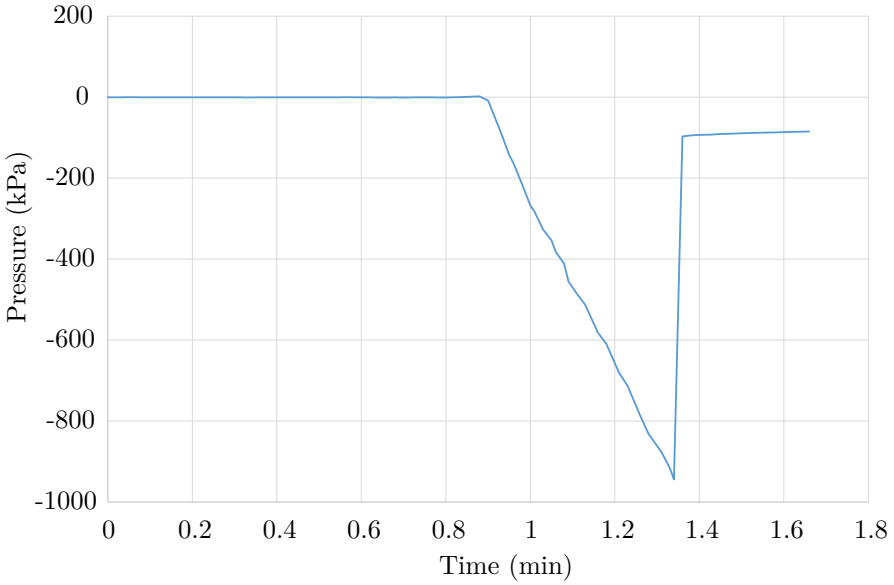

Figure 4.21: Cavitation of Tensiometer V3 by drying in air

In terms of long term behaviour, four calibrations for tensiometer V3 are shown in Figure 4.22. The

calibrations display good agreement, and similarly to Figure 4.18, there is convergence as successive calibrations shift to the left, most significantly between the first and second calibrations. Several of the other probes from this generation have also proven to show similar trends, with the tensiometers built later lacking sufficient data to be certain.

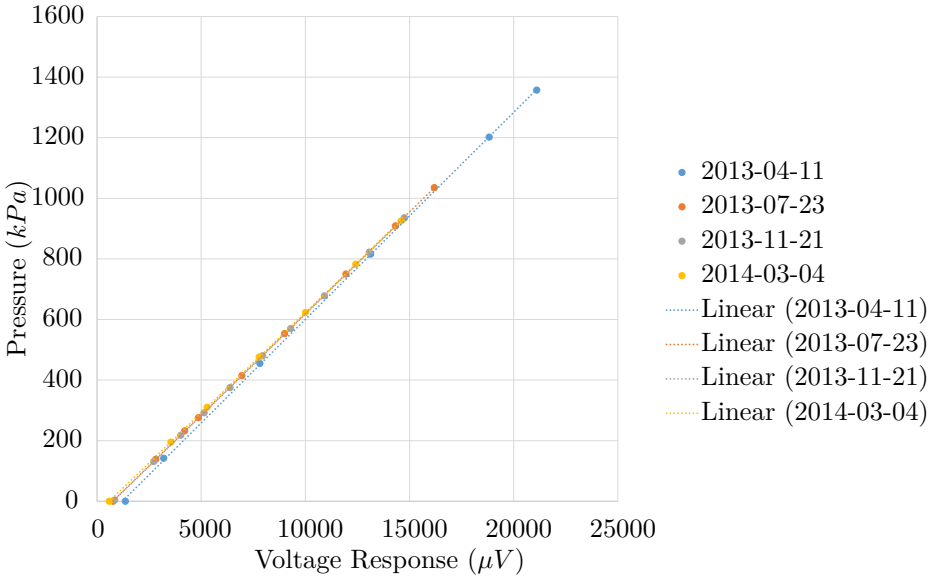

Figure 4.22: Calibrations for Tensiometer V3

In summary, the improvements made to the build process have led to the third generation tensiometers outperforming the second generation tensiometers significantly. Their performance is comparable to the better first generation tensiometers and with approximately 80 % of tensiometers working first time, this is a large improvement over the estimated 50 % success rates from externally sourced internal assemblies.

4.5.4 Temperature Sensitivity

To investigate the cause of variability in suction measurements, several tensiometers were tested for temperature sensitivity. The ceramic transducer information sheet stated the sensitivity was 10 $\mu V/°C$. When applied to a typical range of several thousand micro-volts, it did not lead to a significant offset that accounted for the variability in suctions. Tensiometers were not however just dependent on the transducer's sensitivity. Being made from a range of materials meant each tensiometer behaved more as a composite device, where the expansion and contraction of the materials as a unit affected the temperature sensitivity.

Several tensiometers were therefore saturated and placed in warm water at approximately 40 $°C$ before allowing to cool to gauge any trends. The results for cooling tensiometers are shown in Figure 4.23. Each calibration was approximately linear, with some considerable variation between different tensiometers. In the worst case presented, for every increment in temperature of 1 degree, the pore water pressure reading would decrease by 4.5 kPa.

There are two potential causes for this. Firstly, expansion and contraction of the tensiometer as a composite device affecting the transducer diaphragm and hence readings. Secondly, the expansion and contraction of fluids within the tensiometer reservoir and porous stone. This includes both water and air, which in the case of poor saturation can lead to excessive variation in behaviour and temperature sensitivity.

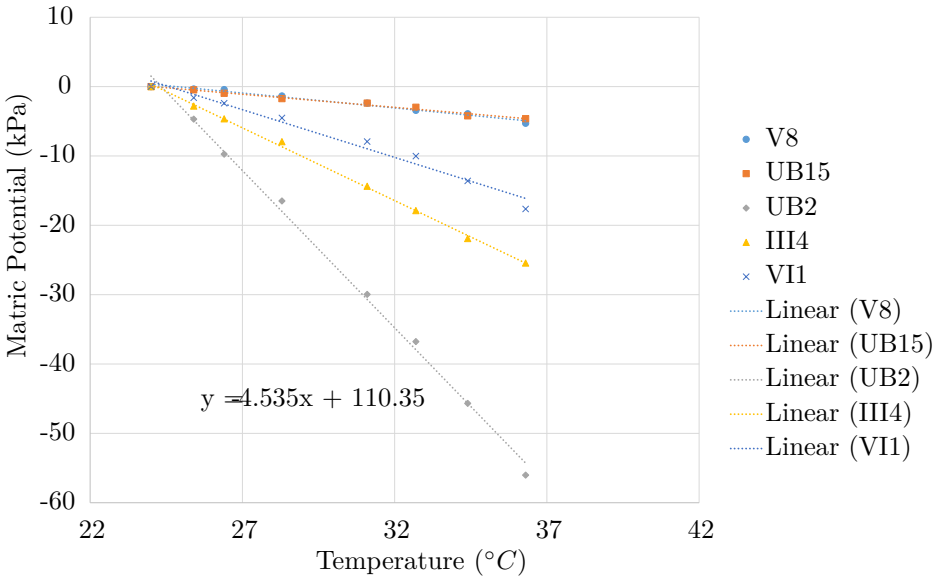

Figure 4.23: Calibrations for Pore Water Pressure against Temperature

4.6 Conclusion

The assembly of the internal components for the Durham University high capacity tensiometers was brought in-house to alleviate build quality concerns brought about by high failure rates. A total of eighteen tensiometers were built by varying build methods to address issues with water ingress and short circuits, however some issues were found with the material the spacers were constructed from corroding and the HAEV stone was found to have a low air entry value of approximately 350 kPa. The spacers were altered to be built from stainless steel and the supplier for HAEV stone was changed. Both issues were then confirmed to have been addressed by checking for corrosion and testing that the air entry value was greater than the 1500 kPA using a pressure cell. A further 14 tensiometers were built using the new materials combined with higher quality adhesives for gluing the internal units together.

All tensiometers were tested by checking calibration history and maximum cavitation pressures. It was found the most reliable first generation tensiometers, those built before the project began, all exhibited the same behaviour, a convergence of calibrations with successive saturations towards a repeatable result. The maximum cavitation suctions associated with these tensiometers was 2.1 MPa but experience dictated they would more commonly cavitate at 1200-1500 kPa. The second generation tensiometers, built with poor quality materials, exhibited erratic successive calibrations which are explained as being due to corrosion of the mild steel spacer and unimpressive cavitations of 350 kPa suction, attributed to the air entry value of the HAEV stone. The third generation tensiometers showed similar behaviour to the original first generation tensiometers, with successive calibrations converging and cavitation occurring in excess of 900 kPa suction.

Chapter 5

Software

5.1 Introduction

Devices are used everywhere in the field of geotechnics, from the laboratory to the field environment for measuring properties of interest. Properties such as water content, suction, temperature etc. and for each there is a multitude of different devices capable of monitoring and storing data. Unfortunately, with such a choice of different devices comes an array of different methods for storing the data, from data loggers through to direct recording of data to a computer hard drive, with each offering different syntax and formats. Small projects or experiments such as those focusing upon a single measurand will find the implications of this insignificant. Larger projects on the other hand, may focus upon multiple measurands and/or devices, and as such the overheads associated with gathering, cleaning and formatting the data for analysis may be significant. The large lysimeters built suffered from just such a problem, with multiple devices for monitoring water contents using Time Domain Reflectometry (TDR); suctions with tensiometers; and temperature and humidity [85].

The solution to this disparity between data stores and devices was twofold. Firstly to store the data in a single repository. Secondly to provide a framework so as all the devices could be connected to the repository through a single piece of software acting as an interface. The devices used with the large lysimeters interfaced via one of the common industry standard ports called the serial port, which can be controlled to open, send commands and close. Automatic data collection is therefore a simple case of programming this process, from opening a port, sending the commands in the correct order and logging the response to a data repository. The proviso is that for a single program to be able to control a multitude of different devices, it has to be flexible enough to successfully describe any physical set up the user can create, including those with multiplexers or devices with multiple channels.

This chapter covers the design and implementation of a new data acquisition software package, programmed from the ground up for modern computing. The software has numerous features: it leverages the power of The Cloud as an online unified data repository; provides an interface for connectivity to any serial port device; offers templating for simplified setup and offers realtime feedback for the end user.

5.2 Design Goals

The design goals for the software were to cover areas from three distinct perspectives; that of the programmer, the end user focused on the functionality of instrumentation and finally the end user interested in data analysis. The broad design goals that encompassed all three perspectives were:

1. Modern software for a modern computer;

2. Simple to use whilst maintaining power and flexibility;
3. Communicate and automate any device on a serial port;
4. Offer real time feedback of user input and device output;
5. Capable of logging to a single modern data store;
6. Enforce data retention.

Modern software refers to both current and future climes as its context. It is the requirement that the software runs well not only on machines and operating systems today, but also on the machines and operating systems of the future. Primarily this deals with the back end components of the software, bringing quality of life improvements for the programmer to provide maximum flexibility, extensibility and code maintenance, ultimately influencing design choices as to programming language and design patterns employed. Secondary influences were the need for a modern, clean and responsive user interface for the end user, to give a great overall experience.

'Simple to use whilst retaining power and flexibility, refers to the quality of life provided to the end users. It influences the design of the interface, to maintain a clean look and provide only the controls and feedback that are necessary at any one time. This also refers to the power of communicating to any serial port device and how templating was implemented to simplify the process of adding and controlling a new device.

Communication to and automatic control of any serial port device was core to the programs functionality. Communication with any device on a serial port had its own list of goals, so the software could control serial ports; comprehend devices and their layouts and act accordingly; and group and send commands based upon the structure of the attached systems and timers. Logging also had its own aims; to aid the user interested in instrument functionality by providing interconnectivity between devices, calibrations and data; to disassociate devices from individual computers, meaning two devices did not necessarily have to be attached to the same computer; and to provide a searchable, exportable and backup friendly data repository.

Preventing loss of data due to user deletion was the main aim of enforcing data retention and covers not only results, but calibrations and device listings. This meant a full list of devices for a given environment could be maintained and for each device the history of its behaviour could be analysed through the preservation of its calibration history.

5.3 Design and Implementation

The design and implementation process took the design goals and prioritised elements that were core to base functionality of the program, so as it could begin monitoring the large lysimeters early in the project.

5.3.1 Program Architecture

At the start of the process it was important to select the most suitable programming language and design philosophy. The combined features had to align with the goals of the project by simplifying the code base and being maintainable, testable and expandable.

The platform of choice was the Microsoft® Windows® Operating System (OS). This was primarily due to the majority of laboratory based machines running a version of this OS, making it convenient to program for this system. Another influencing factor was the move to modern OSs, with Windows® XP becoming obsolete during the course of the project and the newer OSs becoming more prominent, it was

important to adopt newer conventions. This was helped somewhat by all post XP operating systems, from Vista through to 8.1, supporting the same language frameworks.

The programming language was limited by what was supported by Microsoft® in its current generation of compilers and what suited based on personal experience. The two languages considered were Visual Basic .NET (VB.NET) and Visual C# .NET (C#.NET), which both make use of the .NET framework making them Object-Oriented Programming (OOP) languages. This is opposed to the previous iteration of languages through and up to Visual Basic 6.0 (VB6) which only partly implemented some OOP functionality. OOP languages offered the following benefits:

1. Full abstraction of complex problems as a set of objects;
2. Encapsulation of methods hiding the internal implementation;
3. Polymorphism, meaning multiple implementations of the same method could provide different outcomes;
4. Inheritance, allowing for the reuse of classes.

This allows for the programming code to be broken down into logical objects representing groups of functionality within a project. Encapsulation can expose private members on these objects in a robust and dynamic manner such as public properties exposing private members. Whilst polymorphism allows for members to be overridden, e.g. in such a case as inheritance is used, whereby a class is used as a base class, with its caller inheriting all its functionality, part of that functionality can be overridden and repurposed. All these tools help to make a robust yet adaptable program that promotes code reuse.

Returning to the language choice, there are minor differences between the C#.NET and VB.NET compilers but not so great as to make one necessarily better than the other for this application [86]. Personal preference leant towards C#.NET due to experience programming in C and the active community associated with this language was from experience larger, hence C#.NET was adopted.

Another base layer to the architecture was the implementation of a framework, a set of code that can provide generic functionality as a basis for any project. A framework provides the following benefits [87]:

1. Encourages consistent coding and minimises the likelihood of bugs;
2. Allows for more flexible applications regardless of complexity;
3. Allows an application to be easily extended.

Framework implementation meant the use of consistent code to provide the core functionality that was used throughout the project, and also prescribes where certain data or function types should preside within the code. This made for consistent reading, without a lot of the additional code for internal functionality. In addition the framework made it simple to expand functionality and scale through the reuse of base classes.

Three types of framework were considered for the project, each imparting the same high level benefits described above. However each implementation had its own suitability for their own niche settings, for example web based applications and stand-alone applications found on personal computers. The most popular framework for programming a stand-alone application for use in the Windows® environment is the Model-View-ViewModel (MVVM) framework, as will become apparent. The MVVM framework splits an application into three distinct logical blocks that are loosely coupled as per Figure 5.1 [88].

The Model contains data in its original format and presents this publicly through the use of properties to the class that instantiated the Model. The Model itself has no knowledge of the ViewModel or the

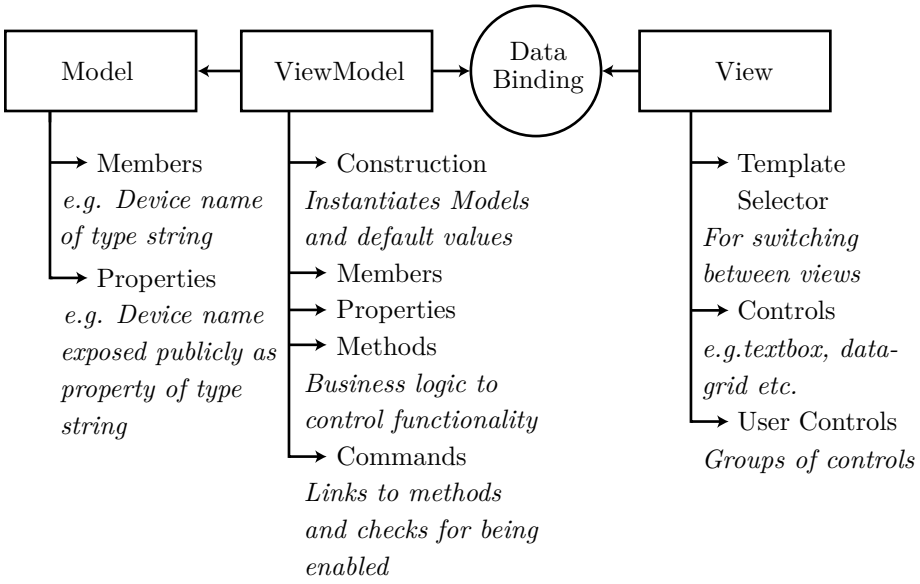

Figure 5.1: Model-View-ViewModel Framework

View and simply acts as a local data store. The ViewModel contains all the business logic (functionality) of an application, including methods and commands, and is also where the Models and potentially other ViewModels are instantiated. The ViewModel exposes properties on the Model to the User Interface (UI) through databinding, a method by which the View and ViewModel are loosely coupled together. For databinding to function correctly, the ViewModel exposes properties stored on the Model through another public property. The ViewModel then sends an event trigger to refresh the view when and only when the value of that property has been changed.

The View is the interface for the user, displaying data and commands through a range of controls such as data grids, plots, text blocks, text boxes and buttons. Each control can be data bound to any property exposed publicly on any ViewModel, meaning the scheme is very loosely coupled. When a property updates, databinding automatically updates all relevant information displayed to the user on any control the property is bound to. Databinding also allows for two way communication; for example, with textboxes, typing causes the property to update as the user types. If a block of text is data-bound to the same property this will reflect the same text that the user is typing in the text box, in real time.

In contrast, Model-View-Presenter (MVP), an alternative framework, has a tightly coupled view and presenter representing the data held in the model. This is used by Windows Forms, a subsystem for rendering interfaces for Windows based applications [89]. This leads to issues of non-reusable code, and changes in the view require changes in code and similarly vice versa. Data-binding gets around this because of the loose coupling it provides and is in-built with Microsoft's replacement for Windows Forms, Windows Presentation Foundation (WPF) which is a newer subsystem for rendering interfaces.

Model-View-Controller (MVC) is most suitable to situations where the view does not have constant access to the remainder of the application i.e. the view is passive as opposed to MVVMs active, realtime view. A common example of this frameworks use is in web browser delivered interfaces, where the user requests data from a database and a snapshot of the data is delivered.

In general, MVVM is the framework with the greatest flexibility and suitability for a stand-alone application such as this. As for the implementation of the MVVM framework, several versions are available 'out of the box' and for free. Using an 'out of the box' pre made framework meant a fully tested piece of

code could be used immediately, minimising the bugs which was one of the main advantages of using a framework.

The MVVM framework implementation chosen was one entitled MVVM Foundation, created by Smith [90]. This was the most lightweight implementation found, providing a base class to inherit from for all ViewModels, and simplifying the implementation of databinding. In addition, the MVVM Foundation framework offered an internal messaging system for communication between ViewModels. The messaging system was of significance because normally, a ViewModel can only access child elements instantiated below it in the hierarchical data structure, but with the messaging system of a MVVM framework, communication can occur with parent ViewModels or ViewModels on a different branches of the program structure. This becomes particularly effective when combined with the separation of the Model and ViewModel, meaning not only can a message contain a text string but a ViewModel can send entire objects, including Models, containing data within a message.

Alternatives considered were MVVM Lite which offered more advanced features such as subscribing and unsubscribing to messages [91], Caliburn Micro which offered more features such as automated association of data-context for Views, through convention over direct association, and Microsoft's® Prism which was a very feature rich and powerful yet complex framework. Although many of the features simplify some core tasks in the long run, much of the additional code these provided was felt to be over complicated.

In summary, the programming language chosen was Visual C#.NET for its familiarity and object oriented features. This was chosen to be used in conjunction with the MVVM framework entitled MVVM Foundation and the MVVM databinding compatible modern UI, WPF [92]. Combined, a substantial part of the programs core features and layout were provided for, meaning much of the coding was focused upon the core tasks required of it.

5.3.2 The Models

The Models represent a single object, with each ViewModel having one to store its local properties, e.g. device name or channel number. In the Model, each property is first declared as a private local member of correct data type, e.g. a device name would be stored as a string, a baud rate stored as an integer etc.. Each private member is only accessible within the Model class that created it and so for the ViewModel that instantiated the Model to be able to access the value of that member, the members are exposed as a public property of the same type. When written verbosely, this yields Algorithm 5.1 for a string containing the name of a device.

Algorithm 5.1 Model member and property declaration

```
1  private string _deviceName;
2
3  public string DeviceName
4  {
5      get{ return _deviceName;}
6      set{ _deviceName = value;}
7  }
```

The property includes the *get* and *set* commands on lines 5 and 6, returning the value stored in the private member and setting the value of the private member respectively. Although all the business logic should be maintained in the ViewModel when following a MVVM framework strictly, validation can benefit from splitting input checks into two stages [93], one stage in the Model class and the other in the ViewModel class. With this approach, each property exposed to the user can have its own personalised multi-stage validation, providing meaningful feedback.

The first stage of meaningful validation is placed in the ViewModel, checking that the input value can be converted to the correct data type of the member in the Model. If this check fails, the user can be informed of the issue with a relevant comment. If the input passes this check, the second layer of validation can check whether the input is within the correct range, and this is the logic that can be applied to the *set* part of a property in the Model. For example, if the member is an integer, the first checks will confirm that the input can be converted to an integer, if not a relevant prompt message can appear for the user suggesting an integer be entered. The second validation would be to check that the integer is, for example, not negative. If the second check fails, a different prompt message appears to the user informing them that the input is out of range.

Validation is not necessary for every member, particularly for the internal members that are never exposed to the user, yet this particular implementation is powerful for user input checks for an application such as this, where users are defining new devices and how they operate. In such a circumstance, the built in properties can greatly benefit from meaningful validation.

5.3.3 Overview of the ViewModels

The ViewModels are classes that represent logical blocks of the program and include all the business logic relating to that block. This includes methods, the first layer of validation, command definitions for databinding to the UI and internal message subscriptions. Each ViewModel in this particular application has its own associated Model for storing local data and most instantiate child ViewModels or collections of ViewModels. These are arranged as per Figure 5.2.

As can be seen at the top of Figure 5.2, there is a Main ViewModel which acts as a parent for all other child ViewModels. As with all the other ViewModels, it inherits functionality from the MVVM Foundation framework class entitled *ObservableObject*, thus allowing the ViewModel to support databinding. The MainViewModel itself includes the scheduler factory for creating and removing schedules on demand, as discussed later, and also many of the application wide commands, including commands to open and close all serial ports and to start and stop all timers. Another prominent feature is a local log of actions the application has run recently. The log provides feedback on where in the application hierarchy a command or method was run from, a relevant message describing what occurred or what error was raised, the state of success and date-time. Each message has its own ViewModel which is stored in an observable collection and exposed to the View via an ICollectionView interface. Combined with a simple search-text property, exposing through an ICollectionView interface allows for real time search as the user types across any of the properties held on the message ViewModels in the observable collection. The UI for the log is shown in Figure 5.3. In the centre of the screen is a grid showing the actions the application has performed and in the top right is the search box for refining the view.

The main ViewModel instantiates a single MySQL ViewModel, written and dedicated for connecting to a MySQL database. The MySQL ViewModel contains the connection information entered by the user, a connection object included from the MySQL connector dynamic link library provided with all MySQL distributions and a First In First Out (FIFO) queue running on a background worker thread. These work together for effective communication to the database. Nominally, all processing in an application runs on the UI thread, a thread being a series of instructions executed by a computer's processor. Most applications are single threaded, but in scenarios where a large amount of data processing is required, this can lead to an unresponsive UI as no more new instructions can be processed until the instructions analysing the data are complete. A background worker thread is effectively a second series of computer instructions that are run in parallel. Running the queue and connection object for the program on a background worker thread therefore ensured all commands passed to the MySQL connection remained orderly, and for instances where a large number of commands are run in quick succession, the background

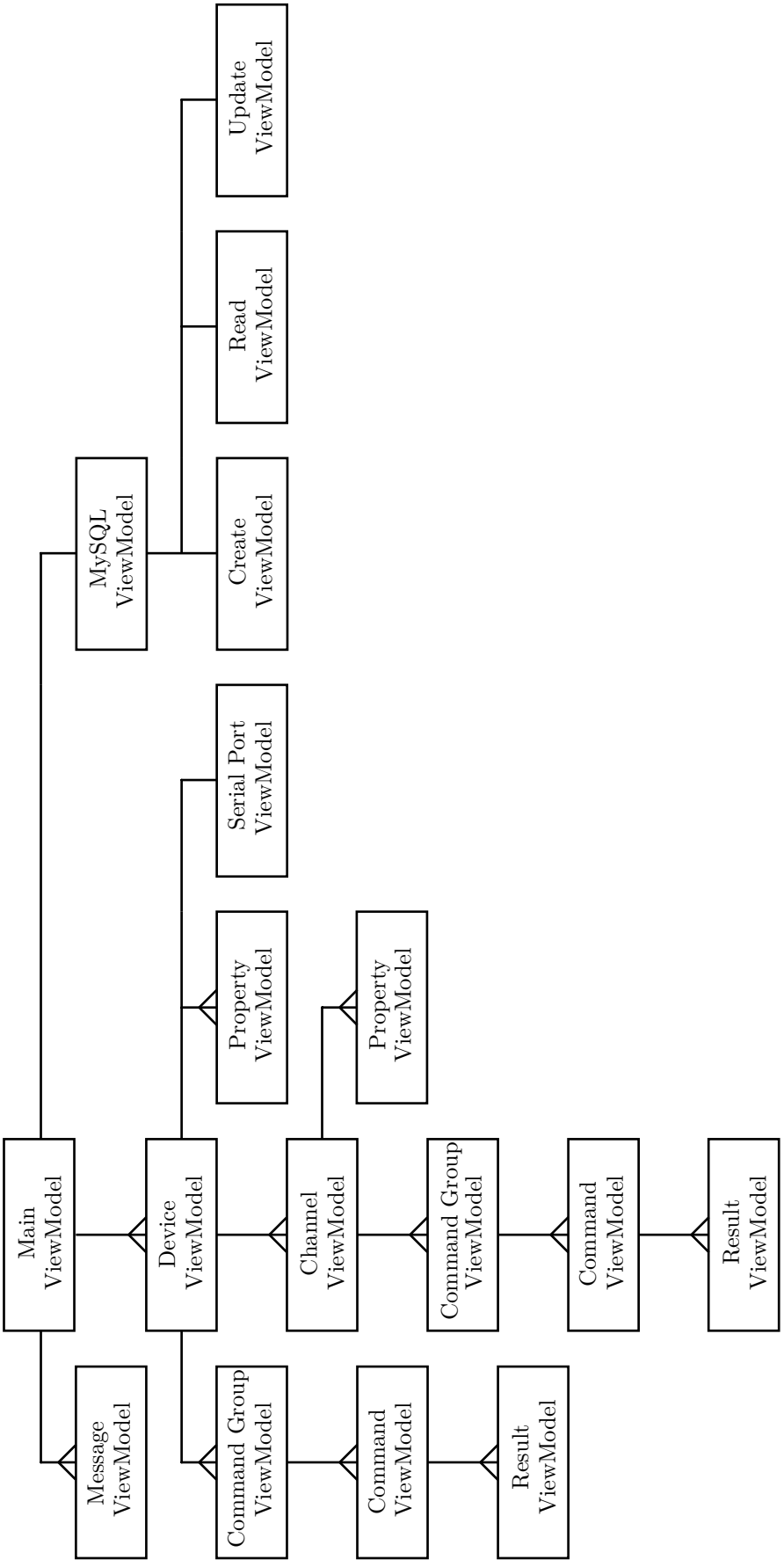

Figure 5.2: ViewModel Parent-Child Relationship

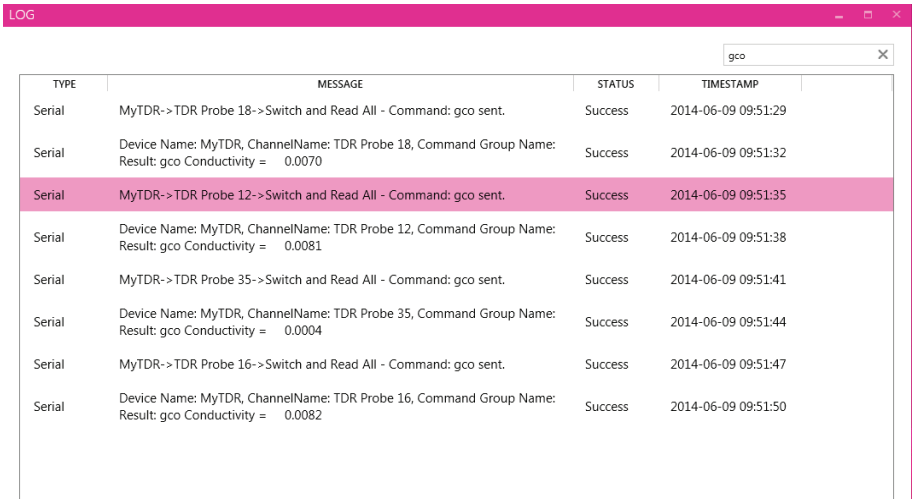

Figure 5.3: Screenshot of the Log Window

thread keeps any heavy processing away from the UI thread thus preventing it from locking up and becoming unresponsive.

Beneath the MySQL ViewModel are a series of single ViewModels, each dedicated to compiling one of the Create Read Update Delete (CRUD) command types to be sent to the database. The create ViewModel for instance, can compile MySQL commands for adding new content to the database and also contains the command series for constructing a fresh database. The read ViewModel contains the commands for reading back the devices associated with the computer, and the update ViewModel can compile commands for updating instances of devices on the database. The ability to delete selections on the database has been disabled in line with the goal to retain all data, as it may prove useful for a number of reasons as described earlier.

The core of the program is communication with serial port devices and as such, the main ViewModel contains an observable collection for device ViewModels. Using a collection object means any number of devices may be attached to the computer, limited only by the number of serial ports physically available. Each device ViewModel in the collection contains properties pertaining to a devices description, including its name, type, serial number etc., which enable both the user to identify the device e.g. by its name, and the computer to identify the device by its unique ID. The device ViewModels are populated normally when the MySQL database is read, at which time the MySQL ViewModel reads each device and checks for ownership. If the device is owned, the MySQL ViewModel stores the information in a device Model and uses the internal messaging system to send this model to the main ViewModel. Upon receipt, the main ViewModel uses the information to create a new device ViewModel and adds it to the observable collection.

A device ViewModel is also parent to three collections of ViewModels and another ViewModel, the serial port ViewModel. The serial port ViewModel functions similarly to the MySQL ViewModel. It has a FIFO queue for dealing with the commands sent, which also runs on a background worker thread to ensure a responsive UI. Instead of a MySQL connection object, there is a serial port connection object distributed with the .NET framework as a dynamic link library, that enables all of the serial port functionality. One point of interest is the different requirements of varying devices for controlling the serial ports. With the TDR device, it was necessary to group commands into logical blocks, primarily for coping with the multiplexers. Instead of sending a command to read a single channel, e.g. read channel 2, the switching commands for the multiplexers were separate to the read commands so it was vital that

the switching commands preceded the read commands else unexpected behaviour would occur. The same behaviour, linking commands together, was also leveraged for controlling the irrigation system. Both the on and off commands were given simultaneously in a single command group and another attached property was used to prescribe a wait time between the commands. The wait time puts the thread to sleep, making it inactive, for a specified amount of time for which the device remains unavailable before the next command in the queue is sent.

The first device ViewModel child collection contains property ViewModels. Each property ViewModel contains information on a custom user set property associated with that device, which includes the property name and an associated value. The same feature is available for another of the device ViewModels child collections, the channel ViewModel. The device and channel ViewModels therefore, both allow for the description of some more complex physical devices in a simpler manner as will become apparent shortly.

A second commonality between the channel and device ViewModels is the use of a child collection containing command group ViewModels. A command group ViewModel is simply a user named parent to another child collection of command ViewModels. A command ViewModel houses the definition of a command including its name, a description and the command itself, alongside an execution order number. When a timer or user triggers a particular command group to be fired, the command group ViewModel recompiles the list of commands into a message, ensuring the commands are in the correct order for queueing. This is then sent using the internal messaging system and dealt with by the associated serial port connection for that device.

Combining the functionality of the command group ViewModels and property ViewModels allows for some more complex behaviour. The property ViewModel permits for custom descriptors for a device or channel to be set, and more interestingly, for commands to utilise these properties. Instead of a series of commands explicitly stating that, for example, a multiplexer switch to channel 1, channel 2 or channel 3, a shorter generic command can be used in conjunction with a pointer to a property type, in this case the command could be entitled ‘switch’ and the property could be entitled ‘multiplexer channel’ with values of 1, 2 and 3 to the same effect. This results in the user defining fewer commands and makes the resulting format generic, meaning a new command grouping will not have to be defined for every new instrument attached. Instead, the associated property values need only be changed.

Finally, each command ViewModel has its own child collection of result ViewModels. Each result containing the raw value returned as a response from the serial port. For example, a TDR device response for a command to retrieve the moisture content of a soil could be *“gmo measured/actual = 5.54”*. Plotting the return value had two factors that hindered it, the first being the inclusion of the initial text string and the second being the raw value returned is an interpretation but not the final result, an additional calibration function was required.

Removing the unwanted text or indeed to be able to filter out any numbers from a string, required the use of a regular expression. A regular expression tests to see if any part of a string matches a specified pattern. These patterns can be loosely defined or very specifically defined, an example in this case being “[-+]?[0-9]*\.[0-9]+” which picks out the first floating point number in any string, with or without sign and with any quantity of leading or trailing digits. Secondly, once the text string had been trimmed to give the resultant number, it was desirable to convert this into what was initially sought, a moisture content. This was done by defining a calibration for the application to apply.

5.3.4 Data Storage

Storage was required for two primary elements, device settings and data. Ideally both were to be stored in the same location so as to keep the data linked with the device settings and vice versa. Each response

logged could then be correlated to its device and used to analyse the core program, how an instrument was performing or to simply keep track of all readings associated with a particular piece of equipment.

As to the best location, first hand experience dictates device settings are typically stored with the files of a data logging program. Similarly, data is normally stored locally on the hard drive in a user specified folder as per requirement. This method is simple to implement and familiar to use, however maintaining the link between devices, calibrations and data can be hard. In general, this system is not very flexible. When switching equipment between machines, finding the set up file or creating it from scratch can be time consuming and if a computer experiences a breakdown, it can lead to data loss.

An alternative was to use a database technology to store all the settings and data in one location, as with cloud storage. Although more work was required to implement such a system and it potentially required the use of a constant server connection for data logging, the advantages were immediately apparent. Storage of device settings and data could be centralised, acting as a list of all devices and calibrations for each device over its history, useful for performance analysis. If a user were to switch which machine a device was connected to, it became a case of removing the tag associating the device with the computer, unplugging the device, connecting it to a new computer and tagging it in the software. This transferred across all settings for the device, maintaining the channel listings, command groups and timings etc., meaning the device would be ready to run immediately. Another advantage was that all devices could have their data stored in the one central location, regardless of what computer the device was attached to. Combined with powerful queries, the resultant data could be selectively downloaded in a flexible manner, e.g. a specific selection of probes over a set period of time could be selected. This avoids storing data across many separate files, maintains a raw copy of the data in the database and allows for custom interpretations in, for example, spreadsheet applications. Finally, instead of many computers to back up, all data can be backed up from one single location on a schedule minimising the potential for significant data loss.

The implementation of the cloud storage solution used a common database technology entitled MySQL, a well tried and tested platform used the world over that acts as the back end for websites and other database applications. The implementation of the database tables took an approach to simplify user set up times by allowing for the use of templates. The database was split into two loosely coupled parts, one representing definitions or templates and the other representing data or customisations, as shown in Figure 5.4.

On the left hand side of Figure 5.4 are the tables that represent templates for devices. These contain data that represents a device regardless of where it is or what the user wishes to do with a particular device e.g. the same series of basic commands will always be the same. On the right hand side of the figure are the user customisations of this data e.g. what serial port the device is attached to, the frequency commands are sent at etc. and these can vary with devices, channels and commands.

At the top of the database hierarchy is the device definition table which has two properties, an ID and a device type, in the case of the TDR system this was set as a TDR100. All other tables either refer to this table directly, or indirectly via other intermediary tables. Directly associated with this are two other tables, one for storing communication attributes and hence has properties such as baud rates, parity, data-bits etc., and the other being device properties. The device properties table includes a property name and any units if applicable. At the same level on the right of the figure, the device and property tables fill out the missing data including customisable properties such as the device name and serial port for the device, and property values associated with the device property table.

The next tier down focuses on the channels. Each device may have any number of different channel types designed for it, hence the many to one relationship e.g. with a logger box there may be tensiometers

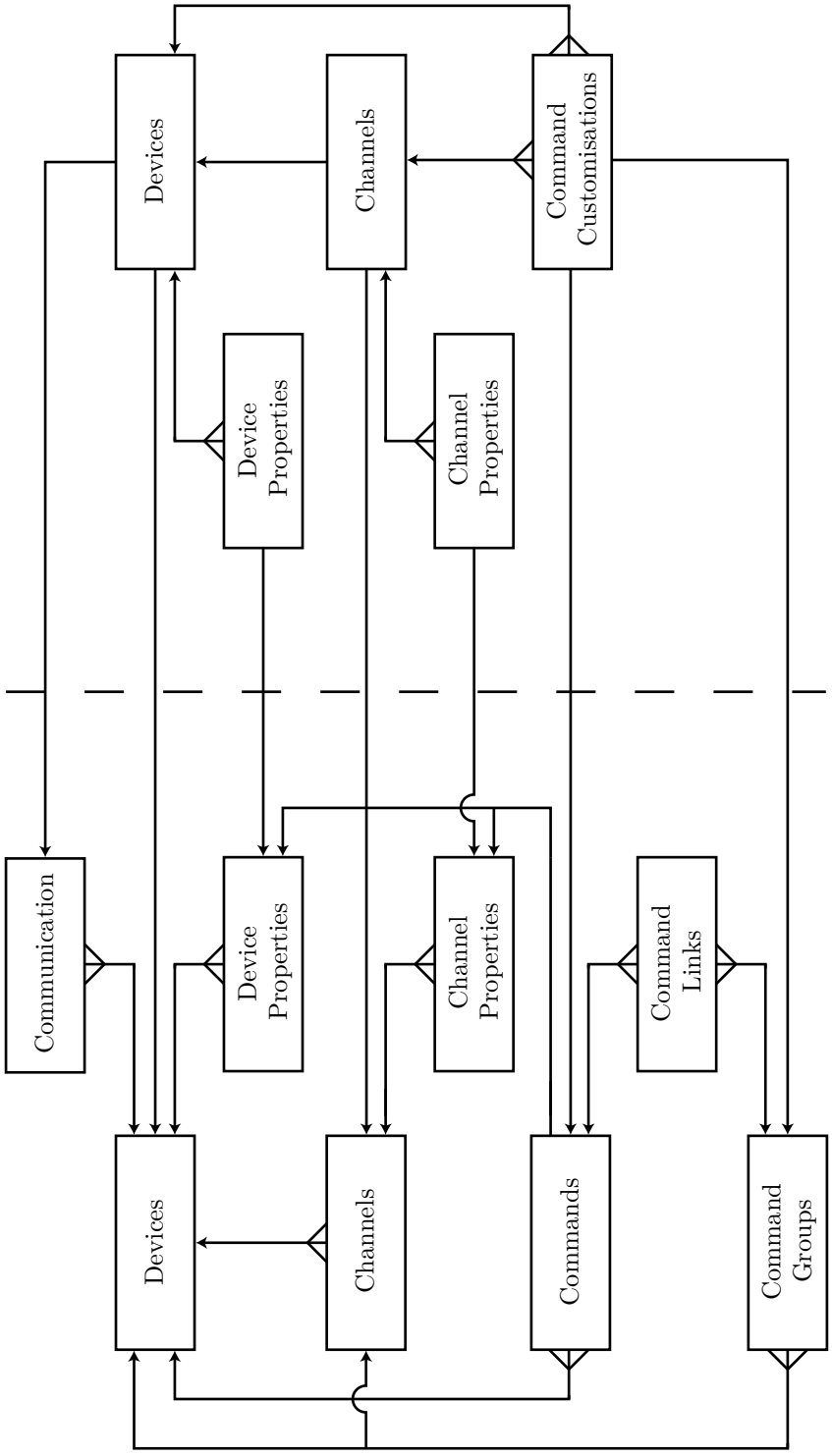

Figure 5.4: Database Table Relationships

and thermistors that can plug into any of the available channel sockets. As with the devices, the channel can have a multitude of properties defined. Over on the right of Figure 5.4 it can be seen that each channel can only be associated with one device and one channel template, whilst a channel may have any number of properties assigned to it, each property may only have one definition. For example, a tensiometer could be defined as a template with a property such as a 'model description'. Over in the data section, a channel could be created, of type tensiometer, and named tensiometer 1 with model 'mark 5'.

The final tier is for linking commands to a device. The left hand side of the figure displays one table for the commands associated with a device and another for the command groups. The commands have a direct many to one relationship with each device definition, as it is expected most devices have multiple input commands. The command groups definitions have a many to one relationship not just for the device but also for channel definitions. This means that where applicable the command group definitions will be applied to a device type, but if the channel type for a particular device type is also defined, the command group will only be tagged as belonging to a particular channel. If, as the case may be, the command groups need to be applied to specific channel types but not to all channel types, there exists an override tag so as to bypass the limitation. Linking the command definitions to the command group definitions is done by way of a third table with a many to many relationship between the two, so as each command group can have many commands and each command can be assigned to many command groups. The command link definitions also store the order of execution for each of the commands as part of the command group.

Over on the right of the figure is a table entitled command customisations, which contains all information as to how a user can alter the functionality of the command and command group definitions. Each customisation may be applied to any device, channel, command group definition or command definition, setting repeat counts, timers and whether to initialise with the command or command group before issuing any user or timed commands to the device. For example, if the customisation is applied to a command as part of a command group for a TDR probe on a TDR device, the repeat count would be the number of times to repeat the command e.g. read moisture content, as part of the group before moving on to the next command, the wait timer would tell the serial port to wait for a fixed period before sending next command and initialise would be ignored. If however the same customisation was applied to a command group, the repeat count would be the number of times to repeat the whole command group, the wait period would be the period utilised by the scheduler for when to send the command group and the initialise would tell the system to send this command group to the device when the serial port first opened.

As for communication to and from the database, the commands are compiled in standard MySQL syntax in their associated ViewModels. In the MySQL create ViewModel, holding all command compilers for the creation of new database content, a new device definition is compiled as per algorithm 5.2.

On line 1, the method takes a string argument for the new name of the device type. A MySQL query is then compiled on lines 4 to 10 using this name and the database name as passed down from the main MySQL ViewModel. This query is stored on a Model designed for keeping all relevant information on how to process this command in one place. Line 11 sets the mode, in this case with a keyword "create", and line 12 describes that the function will create a new device definition, both of which are interpreted in the main MySQL ViewModel before the final query is executed. Lines 13–14 define the success message for when the command is successfully executed, so as the correct and relevant information is recorded in the applications local log. Finally, lines 15–16 send a notification to any receivers on the internal messaging network tagged as QUEUE_MYSQL_MESSAGE. These receivers pick up the contents of the message, in

Algorithm 5.2 Algorithm to compile a new device type MySQL insert query

```
1  public void CreateDeviceDefinition(string DeviceType)
2  {
3      _mysqlMessageModel = new MysqlMessageModel();
4      _mysqlMessageModel.Query = "INSERT INTO `" + Database +
5                                 "`.`tbl_device_definitions`" +
6                                 "(`Device_type`) " +
7                                 "VALUES " +
8                                 "(`" +
9                                 DeviceType +
10                                "`);";
11     _mysqlMessageModel.Mode = "Create";
12     _mysqlMessageModel.Selection = "Device Definition";
13     _mysqlMessageModel.SuccessMessage =
14     "Mode: Create, Selection: Device definition.";
15     App.Messenger.NotifyColleagues("QUEUE_MYSQL_MESSAGE",
           _mysqlMessageModel);
16 }
```

this case the contents are the newly created and populated message Model, or more specifically, a pointer to this model. The main MySQL ViewModel listens in to the message and then has access to all the data pertaining to this particular query and how to execute it.

Similarly in the read ViewModel, a slightly different message is compiled. This one takes no arguments but fills out the same Model to send across the internal messaging system, this time using the key word "read".

Algorithm 5.3 Algorithm to compile a new device type MySQL read query

```
1  public void ReadDeviceDefinitions()
2  {
3      _mysqlMessageModel = new MysqlMessageModel();
4      _mysqlMessageModel.Query = "SELECT * FROM " + Database + ".
           tbl_device_definitions";
5      _mysqlMessageModel.Mode = "Read";
6      _mysqlMessageModel.Selection = "Device Definitions";
7      _mysqlMessageModel.SuccessMessage = "Mode: Read, +
8      Selection: Device definitions.";
9      App.Messenger.NotifyColleagues("QUEUE_MYSQL_MESSAGE",
10     _mysqlMessageModel);
11 }
```

The method takes no arguments as seen in algorithm 5.3. Instead a broad query is created on lines 4–5 to read off every item stored in the table containing device definitions. The remainder of the message is compiled in the same manner, with only some of the keywords changing such as the mode being set to "read" instead of "create". The Model is sent in the same way to the main MySQL ViewModel yet is interpreted slightly differently.

In the main MySQL ViewModel, any of the models sent from the child ViewModels via the internal messaging system, such as those created by algorithms 5.2 and 5.3, are queued for processing on the background worker thread. The method run on the thread is given in algorithm 5.4 and continues to run whilst queries are still available on the system. On line 3, the connection string is initialised with the

current information such as username and password. Following that, on line 4 the connection is opened and whilst messages are queued they continue to be processed. The types of command that can be sent are broken down into two subsets, that of query and non-query.

Lines 13–21+ deal with a variety of query commands, one for each table in the database, which all expect a return value and need to deal with each table in a unique manner. The switching statement, shortened for brevity here, chooses between which method to run based on the keywords used in the message, e.g. "Device Definitions", and reads the data into a suitable Model. This Model is a copy of that instantiated by the associated ViewModel that the data is destined for. Once read, this Model is sent on the internal messaging system and added to the local data Models for the user to interact with. Line 28 sends all other commands classed as non-queries. Non-queries include create, update and delete commands, which all expect zero return from the database.

Each execution of a command within algorithm 5.4 is wrapped in a try and catch statement for dealing with errors that occur and informing the user of the details. Normally, the success message contained within the Model being processed is posted to the log, yet if anything should go awry, a fail message composing of the exception details is instead sent; for example, suggesting that the table does not exist on the database.

Overall, this makes for a very flexible database design. A single set of definitions combined with data listings takes up a minimal number of database tables and properties and when read into the software package, these definitions are replicated and fill out with the desired properties forming fully functional objects. Creating a new device definition is a one-time task which can be reused across many devices, each of which can swap computers etc. and keep their settings intact. Within the application, the algorithms to create queries are robust yet allow room for expansion for additional features e.g. differentiating between different non-queries, and the processing of queries provides feedback via the internal log pertaining to both successes and failures, without crashing the application.

5.3.5 Scheduling System

Initially, a custom built timing system was implemented using dispatcher timers, a timer specifically built for WPF. However, the implementation included several large bugs including inaccurate timekeeping and it simply was not feasible to spend the quantity of time required build a fully functional scheduler. Instead a third party scheduler was employed. The scheduler of choice was Quartz, an advanced scheduling library rich in features and available for free inclusion and redistribution as is, according to the Apache Licence, Version 2.0 [94].

Quartz, or rather Quartz.NET, is an open source job scheduling system based off the open source java project, Quartz. It came as a library that was capable of being included directly with any C#.NET project. Once included, the library was fairly straight forward to use. Each schedule required two components, a job and a trigger, which once built allowed for the schedule to be added to the timer factory, the key component that manages all the distinct schedules. Although many complex timers can be implemented, such as running a job on certain days, not on certain days and a specific number of times etc., the simplest one was repeat indefinitely at a specified interval. The code for this is demonstrated in algorithm 5.5.

Firstly, the internal messenger system picks up on any new schedule requests sent to the job scheduler registry and using the contents of the message, referred to locally as *param*, creates a job of type MyJob-Class as given in Algorithm 5.6. Lines 9–11 create the job, which has an identity and type, however it is the identity that is of importance. The identity was one of the properties sent through the internal messaging system and is a unique identifier formed from multiple IDs, from the device ID through to the command group ID, and referred to here as the composite ID. With the properties assigned, the job is built followed by the trigger on lines 13–16. The trigger defaults to triggering as soon as the job is added

Algorithm 5.4 Algorithm to process MySQL queries

```
1  private void _worker_DoWork(object sender, DoWorkEventArgs e)
2  {
3      InitialiseConnectionString();
4      OpenConnection();
5      while (MysqlMessageQueue.Count > 0)
6      {
7          DequeuedMessageModel = MysqlMessageQueue.Dequeue();
8          try
9          {
10             MySqlCommand cmd = new MySqlCommand(DequeuedMessageModel.
                   Query, _connection);
11             if (DequeuedMessageModel.Mode == "Read")
12             {
13                 switch (DequeuedMessageModel.Selection)
14                 {
15                     case ("Device Definitions"): ReadDeviceDefinitions
                           (cmd);
16                         break;
17                     case ("Command Group Definitions"):
                           ReadCommandGroupDefinitions(cmd);
18                         break;
19                     case ("Command Definitions"):
                           ReadCommandDefinitions(cmd);
20                         break;
21                     // Shortened for brevity...
22                 }
23             }
24             else
25             {
26                 try
27                 {
28                     cmd.ExecuteNonQuery();
29                 }
30                 catch (Exception ex)
31                 {
32                     _logMessageViewModel.FailMessage("MySQL", ex, ex.
                           Message);
33                 }
34             }
35         }
36     catch (MySqlException ex) { _logMessageViewModel.FailMessage("
           MySQL", ex, DequeuedMessageModel.Query); }
37     }
38 }
```

Algorithm 5.5 Algorithm to add jobs to a scheduler

```
1  // Construction
2  _scheduleFactory = new StdSchedulerFactory();
3  _scheduler = _scheduleFactory.GetScheduler();
4  _scheduler.Start();
5
6  App.Messenger.Register("JOB_SCHEDULER_REGISTER",
7  (Action<JobScheduleModel>)(param =>
8  {
9      _job = JobBuilder.Create(typeof(MyJobClass))
10     .WithIdentity(param.CompositeID, "Schedule Group")
11     .Build();
12
13     _trigger = TriggerBuilder.Create()
14     .StartAt(DateTime.UtcNow)
15     .WithSimpleSchedule(x => x.RepeatForever().WithInterval(param.
           Interval))
16     .Build();
17
18     _scheduler.ScheduleJob(_job, _trigger);
19 }));
```

Algorithm 5.6 Algorithm to run when a schedule is triggered

```
1  class MyJobClass : IJob
2  {
3      public void Execute(IJobExecutionContext context)
4      {
5          App.Messenger.NotifyColleagues("JOB_SCHEDULER_NOTIFICATION",
               context.JobDetail.Key.Name);
6      }
7  }
```

to the schedule and issuing a trigger at repeated set intervals. With both these components present, the schedule is then ready to be added to the scheduler.

When the schedule triggers, the code in Algorithm 5.6 is run. This broadcasts a message on the internal messaging system back to any listeners. The content of the message is the unique composite key first entered into the scheduler under the job's identity. Each command group ViewModel can then check to see if its key matches and if so the command group is recompiled and sent to its associated serial port ViewModel for processing.

5.3.6 Serial Port

The serial port connection runs on a queue system off the back of a background worker thread. Firstly, each serial port ViewModel subscribes to all broadcast command messages on the internal messaging system as in algorithm 5.7.

Algorithm 5.7 Serial port listener

```
1 App.Messenger.Register("BROADCAST_COMMAND_MESSAGE", (Action<
      CommandMessageModel>)(param =>
2 {
3       if (this.DeviceID == param.DeviceID)
4       {
5           _commandMessageQueue.Enqueue(param);
6           EmptyCommandMessageQueue();
7       }
8 }));
```

The received device ID is then checked against the device ID stored locally on line 3 and if it matches, the command message Model is added to a queue of command message Models on line 5, and a function to start emptying the queue is called on line 6. This method can be seen in algorithm 5.8, which first checks to see if the ViewModel is busy or not on line 3. If it is not busy, the method checks that there is a message in the queue on line 5, and if so, sets the status to busy. The message containing the command group is finally dequeued and a second method called for processing the individual commands held in the group, entitled *EmptyCommandQueue*, on line 11.

The method for dequeuing the individual commands, given in Algorithm 5.9, first checks that commands are present on line 3, before dequeuing the individual properties one at a time and storing in a local set of properties for use through another method on line 5. These properties are the command itself, whether a return value is expected, a timeout, the character to read to, whether the result should be logged, any wait periods, the total number of repeats and the command definition unique ID. The function then attempts to run a background worker asynchronously for processing the command on a separate thread as per lines 6–16.

The background worker, as given in algorithm 5.10, first checks to see if the character to be read to is multiple characters long on line 3, if so the string is compared against common shorthand for some of the special characters without symbols. Following on line 4, a loop is initialized between 1 and the number of repeats required. For each loop, if the serial port is open, the command is sent and if a response is expected a function named *ReadSerialPort* has the job of picking up the response and checking when the message is complete, be that due to a time-out, or because the character to be read to has been detected. Finally, the result is logged if required and the received data reset back to an empty string before the process is repeated.

Should the command have a wait timer included, the process pauses before the next command is sent

Algorithm 5.8 Serial method for emptying a queue of command group messages

```
1  public void EmptyCommandMessageQueue()
2  {
3      if (IsBusy == false)
4      {
5          if (CommandMessageQueue.Count != 0)
6          {
7              IsBusy = true;
8              try
9              {
10                 CommandQueue = CommandMessageQueue.Dequeue();
11                 EmptyCommandQueue();
12             }
13             catch (Exception ex)
14             {
15                 // Skipped for brevity
16             }
17         }
18     }
19 }
```

Algorithm 5.9 Serial method for emptying the queue of command messages

```
1  public void EmptyCommandQueue()
2  {
3      if (_commandQueue.Commands.Count > 0)
4      {
5          DequeueCommandProperties();
6          try
7          {
8              if (_worker.IsBusy == false)
9              {
10                 _worker.RunWorkerAsync();
11             }
12         }
13         catch (Exception ex)
14         {
15             // Skipped for brevity
16         }
17     }
18     else
19     {
20         IsBusy = false;
21         EmptyCommandMessageQueue();
22     }
23 }
```

Algorithm 5.10 Serial method for emptying the queue of command messages

```
1  void _worker_DoWork(object sender, DoWorkEventArgs e)
2  {
3      ConvertToSpecialCharacter();
4      for (i = 1; i <= Convert.ToInt32(DequeuedCommandModel.RepeatCount)
           ; i++)
5      {
6          if (_serialPort.IsOpen == true)
7          {
8              WriteSerialPort();
9              ReadSerialPort();
10             LogResult();
11             ReceivedData = "";
12         }
13     }
14     if (DequeuedCommandModel.Wait != "" || DequeuedCommandModel.Wait
           != "0")
15     {
16         Thread.Sleep(Convert.ToInt32(DequeuedCommandModel.Wait));
17     }
18 }
19
20 void _worker_RunWorkerCompleted(object sender,
       RunWorkerCompletedEventArgs e)
21 {
22     EmptyCommandQueue();
23 }
```

by placing the whole thread to sleep as per lines 14–17. Once everything is complete, the worker triggers the worker completed event running lines 20–23, thereby triggering the *EmptyCommandQueue* process to check for more commands to dequeue from this command group. If more commands are found the process repeats until the command group is empty at which point the whole process is flagged as not busy and the next command message can be dequeued from the system.

In general this process works well, the UI never locks up due to heavy use of the serial port and the transitions between commands is particularly fluid with no downtime, increasing the potential timing resolution obtainable with reading serial port devices.

5.3.7 Analysis

Although simple analysis, by applying a regular expression followed by a calibration, could be done internally within the software relatively easily, one of the more interesting challenges was TDR waveform interpretation.

A TDR algorithm was in part required due to errors returned by the waveform analysis algorithm that came with the TDR100 device. At particularly low and high permittivities, when the waveform was relatively short or long respectively, the algorithm tended to misinterpret the start and end points. In turn, the distance between the start and end points would be transferred into an incorrect determination of volumetric water content.

For instance, with a probe in air or a similarly low relative permittivity material such as dry sand, the end point could be interpreted as occurring before the start point, resulting in a negative relative permittivity and meaningless volumetric water content. This is understandable to some extent due to the very close proximities of the start and end points and that they lie upon the same upward sweeping curve. At the other end of the spectrum, some of the wetter samples with high relative permittivities, similar errors were observed with up to 30% of readings across a very broad range of probes returning negative relative permittivities. This was on the other hand, somewhat surprising, particularly as 70% of the readings returning positive values were within given expectations of the estimated volumetric water content of the material. As to why the TDR100 algorithm determined that the start point, in a minority of cases, existed after the end point is unknown.

Although other algorithms are available to analyse TDR waveforms in stand-alone programs, inclusion of a waveform analysis algorithm allowed for a direct integration with the database, modification of the sensitivity of the algorithm and allowed for inclusion with the data acquisition software to give real time feedback. The implemented algorithm, in its own testing environment, is shown in Figure 5.5.

The program reads any number of waveforms from the database for analysis, based upon a series of property values in the settings menu. When run, the property values are compiled into a MySQL query that returns values tagged as waveforms from a database and optionally for a specific probe. The waveforms read are streamed live into the UI, which remains responsive as the analysis begins and continues to run. Down the left hand side of Figure 5.5, a list of the waveforms indexed by number is shown. On the remainder of the UI, different groups of properties and derived properties are displayed with their own heading, the contents being updated during analysis. At the top of the screenshot a context sensitive heading is displayed, in this case giving a preliminary suggestion that one thousand readings have been successfully analysed from this particular test case, and on the right of that are buttons for running and changing settings.

The summary for any particular waveform selected is displayed on this window. At the top is the analysis results returning a raw value for the root of apparent permittivity, indicated by L_a/L, a corrected value taking into account an offset and finally a conversion to volumetric water content. Below, a graphical representation of the waveform is shown plotting the reflection coefficient against the number of zero

Figure 5.5: Waveform Analysis Main Window Screenshot

indexed data points the waveform is composed of, in this case 251. Beneath, the upper and lower limits for each axis are displayed, the zero indexed start and end points and also the analysis parameters used in the calculations.

The algorithm produces results using the following steps:

1. A regular expression is applied to split a single string representing a waveform into indexed values representing reflection coefficients;
2. The reflection coefficient values are smoothed to minimise noise;
3. An algorithm is applied to the data series to find curves of significance categorising them as data, curve up or curve down; as shown in the waveform details views in Figure 5.6;
4. The correct curves are selected and tangents calculated - The first tangent is calculated based on the first 0.5 m of flat waveform tagged as data and the second from the point on the first curve upwards with the maximum gradient. The third tangent is to the smallest gradient at the start of the second rise and the fourth is to the maximum gradient of the second rise;
5. The intersections of the left most pair and right most pair of tangents are calculated;
6. The difference between the right and left intersects is calculated;
7. An offset is applied to calculate the permittivity of the medium;
8. A calibration is used to convert the permittivity to a volumetric water content.

Firstly, each waveform was composed of a series of comma delimited, alternating index and reflection coefficient values. From the series, all floating point numbers were extracted and stored as a series of objects. Smoothing was applied using Gaussian values as weightings on the five data points to the left and five data points to the right, so as not to shift the waveform features, and scaling was applied to shift the result back into proportion for consistent graphing with the raw waveform. After, waveform properties including minima and maxima for the index, reflection coefficient and derivatives were calculated and used in conjunction with a percentage significance to define what constituted as a significant feature on the waveform, such that it could be called a curve. A curve was required to have a certain significance in terms of length, represented by the number of data points, and also significant derivative, relative to the maximum derivative detected on the waveform. If either condition was not met, the potential curve was either too short or too shallow to be certain of its nature, and instead was tagged as data.

In addition to the length and maximum derivative, each curve detected on the waveform had to conform to a pattern. The pattern was based on a series absolute derivatives of increasing, decreasing and then increasing magnitude. The approach using absolute magnitudes simplified the algorithm from having to deal with curves going up and curves going down, so instead only one pattern matched all instances, which could later be tagged based on the true value of derivative at the absolute derivatives maxima. A requirement for each component part of a curve was it had to be composed of a significant number of data points to count as a positive match. In each case, this was half the total number of required data points to avoid picking up noise as a false positive.

Each waveforms details were shown in a view breaking the analysis down into its component parts, two of these views for the same waveform being shown in Figure 5.6. Each view, selectable on the left panel, is for a section of the waveform categorised as data, curve up or curve down. The waveform in this case was found to be composed of data initially, followed by a bump as described by a curve up followed

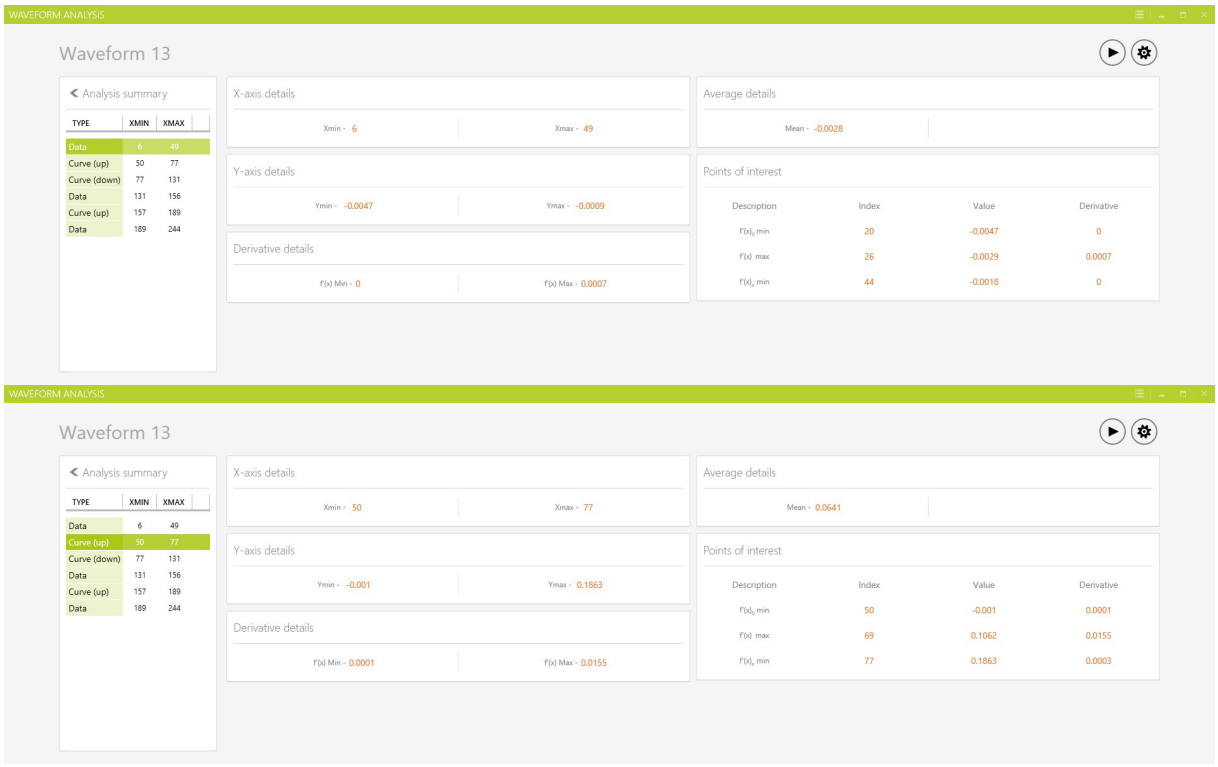

Figure 5.6: Waveform Analysis Details View Screenshots

by a curve down. The first tangents were drawn parallel to the data and the maximum derivative of the initial curve up, with the intersects defining the start point. The segments following, picked up a series of data, a curve up and more data, with it being this second curve up that was of interest for defining the end point. A tangent was drawn at the base of the curve at its lowest derivative before a maxima, where another tangent was drawn, the intersects of these two gave the end point. This particular approach, taking the lowest derivative before a maxima, was necessary for the correct analysis waveforms in air, where the base of the second rise did not necessarily have a gradient of zero.

The final steps were to take the difference between the start and end point indexes, relative to the number of points on the waveform. This fraction multiplied by the waveforms apparent length and an offset was used to determine the apparent permittivity, which in turn yielded a volumetric water content with an appropriate calibration, as shown on the main view in Figure 5.5.

This multi-staged approach to analysing waveforms is significantly different to the predominantly linear calibrations associated with the other instruments. This meant that the method could not easily be broken down into a more fundamental approach.

In conclusion, the unique characteristics of multiple data points in a single reading, the seven steps that had to be applied in the analysis and the program architecture that had to be built to deal with these issues, proved to be challenging. The result was most gratifying, the algorithm being able to cope with a varying number of data points and level of sensitivity for the desired features. In tests, the algorithm proved to be exceptional, exceeding expectations and providing reasonable results even on some of the more erroneous waveforms that resulted occasionally, those typically with a much flatter inexplicable profile.

5.3.8 The User Interface

The UI was constructed using a combination of WPF controls skinned using an open source toolkit entitled MahApps Metro [95]and some custom controls provided by the same kit. The MahApp Metro toolkit is designed for providing a modern and simple flat metro UI, which was deemed suitable for this application with a limited number of functions as compared to some heavier applications that require complex menu systems. Alternatives were to use the out-of-the-box WPF controls, reminiscent of Windows® in look and feel but somewhat uncharacteristic of tablet devices, or a ribbon UI which was suited to applications with more functions.

The UI was written in Extensible Application Markup Language (XAML), an extended version of Extensible Markup Language (XML) created by Microsoft®. The XAML language describes controls using a series of hierarchical opening and closing tags. Within these tags, properties for dimensions, behaviour, look and content are defined. To organise the structure of an interface more readily, controls and their properties are grouped together as user controls, as with Algorithm 5.11.

Algorithm 5.11 refers to part of the device view given in Figure 5.7 in reference to each devices details. Surrounding the details view is a ScrollViewer, opened on line 1 and closed on line 18, for automatic generation of scrollbars for smaller windows or for when large quantities of information are present. Inside, a StackPanel organises the views into a vertically aligned stack of user controls, the user controls being given on lines 5, 13, 14 and 16, with each referring to a specific layout of controls. As shown in Figure 5.7, the main device view is composed of four components namely About, Control, Communication and Properties, matching the four controls defined in the XAML. The middle two controls, Control and Communication, are arranged in a grid opened on lines 6–7 and defined on lines 8–12. Each of these user controls remains in the grid, the closing tag being later on line 15, and are given properties stating where on the grid the user controls should be placed, in this instance being column 0 and column 2 with column 1 being used as a spacer.

Algorithm 5.11 XAML defined user control

```
<ScrollViewer VerticalScrollBarVisibility="Auto"
                        HorizontalScrollBarVisibility="Auto"
                        MinWidth="400">
    <StackPanel Orientation="Vertical">
        <vw:DeviceDetailAboutControl />
        <Grid Margin="0,15,0,0"
              Width="Auto">
            <Grid.ColumnDefinitions>
                <ColumnDefinition Width="10*" />
                <ColumnDefinition Width="15" />
                <ColumnDefinition Width="10*" />
            </Grid.ColumnDefinitions>
            <vw:DeviceDetailControlControl Grid.Column="0" />
            <vw:DeviceDetailCommunicationControl Grid.Column="2" />
        </Grid>
        <vw:DeviceDetailPropertiesControl Margin="0,10,0,0"/>
    </StackPanel>
</ScrollViewer>
```

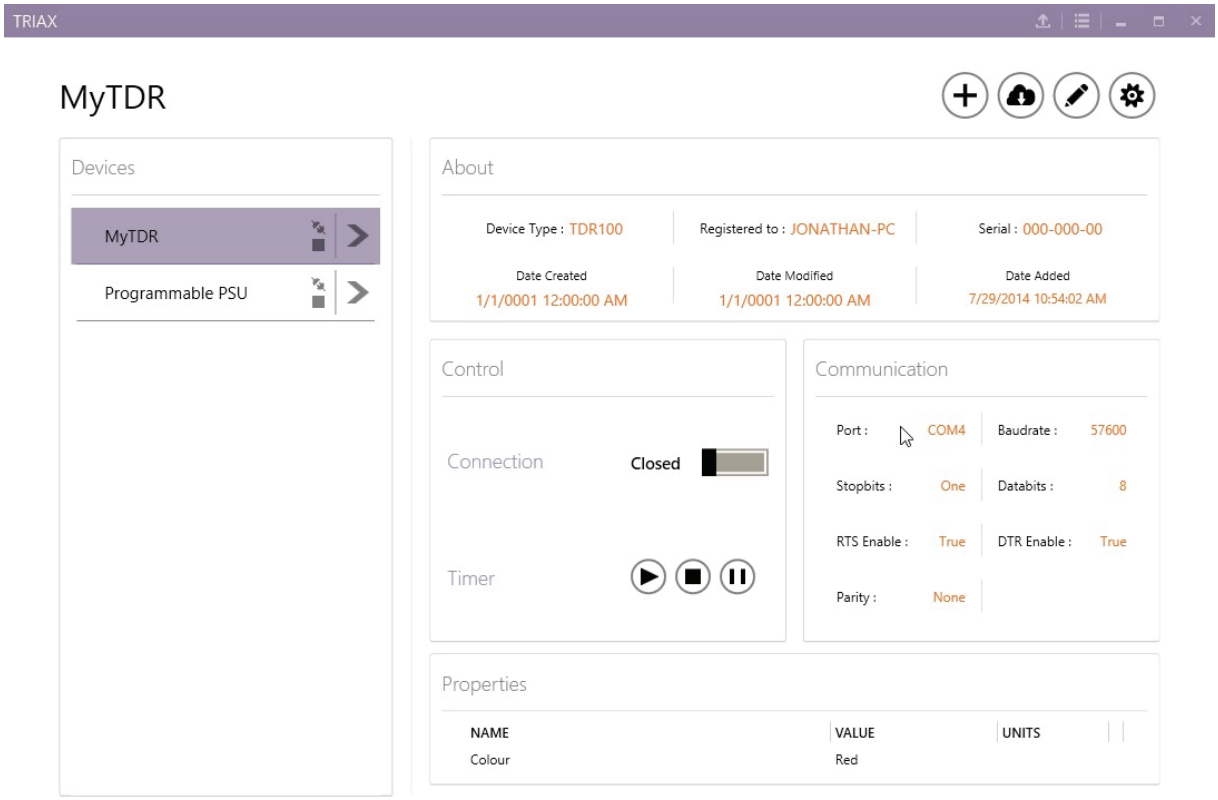

Figure 5.7: User interface screenshot

This method was used to describe all of the controls used in the application, breaking the requirements down into logical blocks and putting them together in a hierarchical fashion. The UI is currently a work in progress but provides the necessary information and controls for running the application as required on the project.

5.4 Conclusion

A piece of software has been developed and designed for interacting with serial port devices with cloud storage in the form of a MySQL database. Device definitions and customisations are both stored on the database, allowing for portability of entire devices and their channels between computers. The software has the potential for communicating with any serial port device, applying calibrations to responses for real time feedback and logging the results to a fully contextualised and queryable results table, meaning results from individual probes over given time periods can be queried. The interface is both modern and functional, readily able to change for future iterations thanks to the loose coupling provided by data binding, yet still requires some refinement for the more advanced or case specific features such as TDR waveform analysis. In general, the program is robust, highly responsive and fulfils the criteria required by the project.

Chapter 6

Materials and Methods

6.1 Introduction

Three soil mixes were chosen for filling the lysimeters. The first lysimeter being a control, had just the soil from the St Anthony's Lead-works site. The second was filled with soil from St Anthony's Lead-works amended with only Water Treatment Residual (WTR) and the third, a combination of WTR and compost. The materials that were used directly influenced the methods applied to fill each of the lysimeters. Particularly the properties of the soil in the field, as when it came to recreating the same conditions within the lab, getting the balance between high quality repeatable homogeneous samples, and recreating the more arbitrary random nature of the soils in the field, was critical. The ratios of amendment to soil, were based on a field trial that ran ahead of the lysimeters, in which both WTR and compost were applied to a lightly contaminated site. In the field trial, it was assumed that the amendments would treat the top half metre of soil in quantities measuring approximately 10% by mass of the treated soil layer. This chapter discusses these materials and their properties at source, the logic as to how the fill methods were designed, and the resultant non-time dependent properties of the soil columns produced.

6.2 Material Properties

Discussed here are the material properties of the soil, WTR and compost before preparation for compaction into the large lysimeters.

6.2.1 Soil

The soil was sourced from the St Anthony's Leadworks site in Newcastle Upon Tyne, as briefly discussed earlier in Chapter 2. During the remediative works being carried out by the local council over this project, approximately 10 m^3 of soil material, without turf, was taken from adjacent to a path passing under what used to be the rolling mill and red lead furnaces, on the lower middle tier terrace. Work was carried out by Newcastle City Council (Phil Hartley, personal correspondence), prior to the remediation of the site, to determine spot concentrations of lead in mg per kg. These were used in conjunction with feedback from the contractors remediating the site, so as to choose the optimal place to excavate soil from, and are given in figures 6.1 and 6.2. The figures show the concentrations of lead, both at surface and depth, with spot concentrations near the the excavation work varying considerably from $2,800$ to $100,000$ $mg\ kg^{-1}$. Indeed, the spot concentrations varied significantly across the entire site, suggesting the distribution of lead containing compounds was far from homogeneous and making the true average concentration in the excavated soil hard to predict.

The particular location for excavation was chosen primarily due to the depth of the surface soil before

reaching hard pan, approximately 0.5 m. On other terraces, the depth of soil was known to be as little as 0.15 m, including the turf, meaning large areas would have to be excavated and the quality of the material would be harder to guarantee. The other main criteria was the soil had to be contaminated, which was demonstrated by the data in figures 6.1 and 6.2 for this terrace. As for the position of the excavation on the terrace, this was chosen due to an alignment of interests, as much of the soil near the path had to be excavated during remediation works hence 10 m^3 of material was placed in dumpy bags and delivered to the Civil Engineering Laboratory at Durham University. On site, the soil had an average bulk density, taken from four 100 mm core samples, of 1743.5 $kg\ m^{-3}$, an average dry density of 1428.8 $kg\ m^{-3}$ and an average gravimetric water content of 22.0 %.

After the soils were delivered, each of the ten dumpy bags was assessed for gravimetric water content and grading, so as to assess the consistency of the material and how to proceed. The water content samples were taken well below the surface for each of the dumpy bags, to avoid skewing data, and two samples approximating 2.5 kg were taken for testing. The results are shown in Table 6.1 and give an average gravimetric water content of 22.1 % ±2.1 % *s.d.*, similar to the average water content found in the samples assessing field densities.

Table 6.1: Gravimetric Water Contents for St Anthony's Excavated Materials

Dumpy Bag	**Mass of Sample** (g)	**Gravimetric Water Content** (%)
1	2472.94	23.2
1	2158.80	22.9
2	2412.02	19.3
2	2648.19	19.7
3	2838.08	18.6
3	2736.29	25.6
4	2582.52	21.9
4	2617.59	21.6
5	2417.86	21.6
5	2572.56	19.8
6	2932.12	22.7
6	2155.26	27.6
7	2629.55	22.1
7	2680.04	22.5
8	2734.37	21.4
8	2238.75	20.7
9	2353.76	22.8
9	2489.81	23.8
10	2584.45	21.7
10	2460.14	22.9

Upon inspection of the materials, it was found that some of the bags contained significant quantities of coarse dolomite gravel and cobbles, associated with the foundations of the path to which the excavation was adjacent. Particularly dumpy bags 2 and 5, which showed overall lower water contents. Particle size distributions were taken of each individual bag according to BS1377-2 [96] using the wet sieving method and excluding sedimentation. A representative average mass of 5.1 kg, above the 2 kg recommended for this soil according to the standard, was taken from each dumpy bag for the particle size analysis, with the results being shown in Figure 6.3.

As Figure 6.3 displays, the bags varied considerably but particularly with the coarser material which was predominantly from the nearby path. Bags 2 and 5, comparatively had a higher quantity of larger particles, which is consistent with their lower water contents. Conversely, bag 6 had the lowest quantity

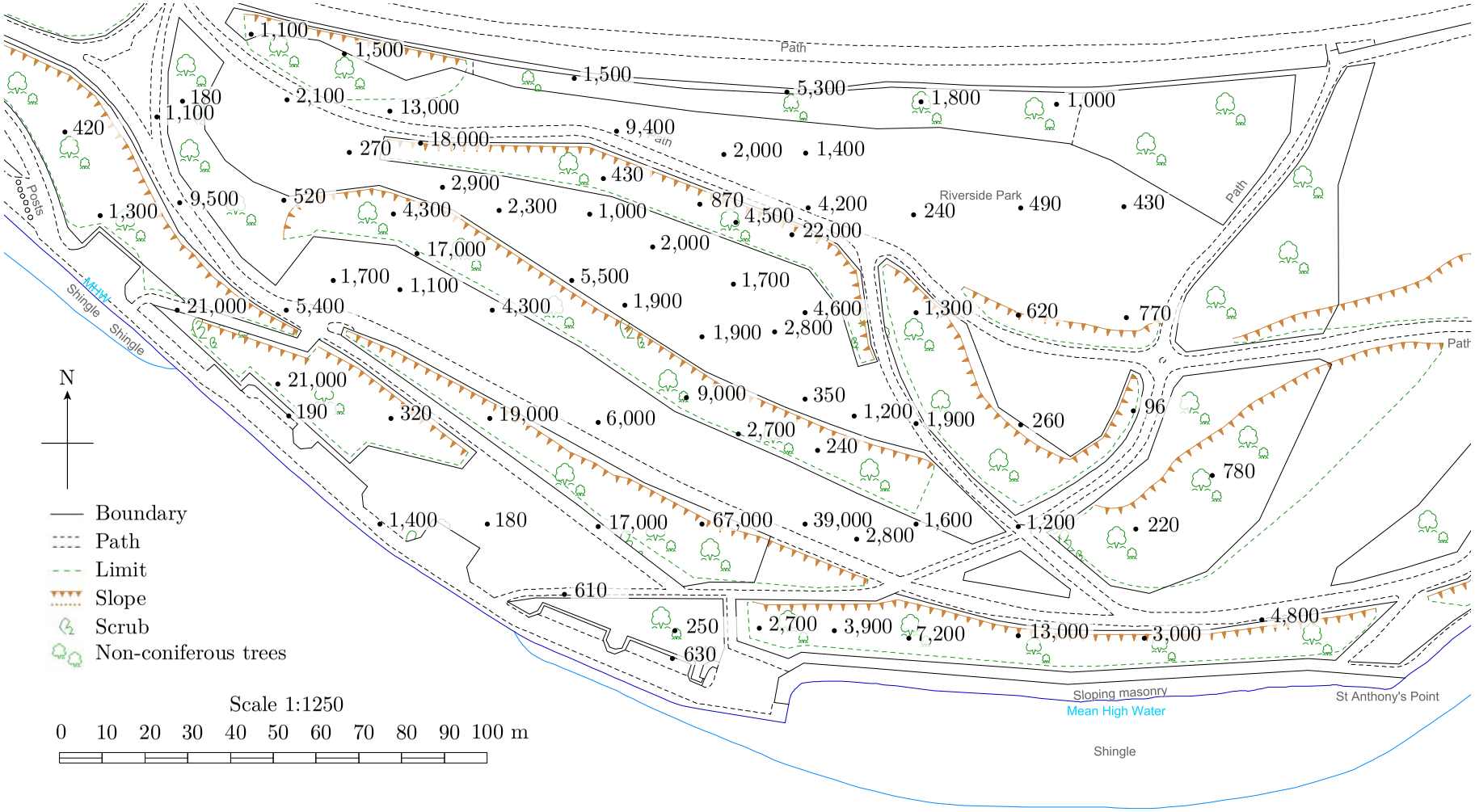

Figure 6.1: Map of St Anthony's 19th Century Lead Works with Surface Concentrations of Lead ($mgkg^{-1}$)

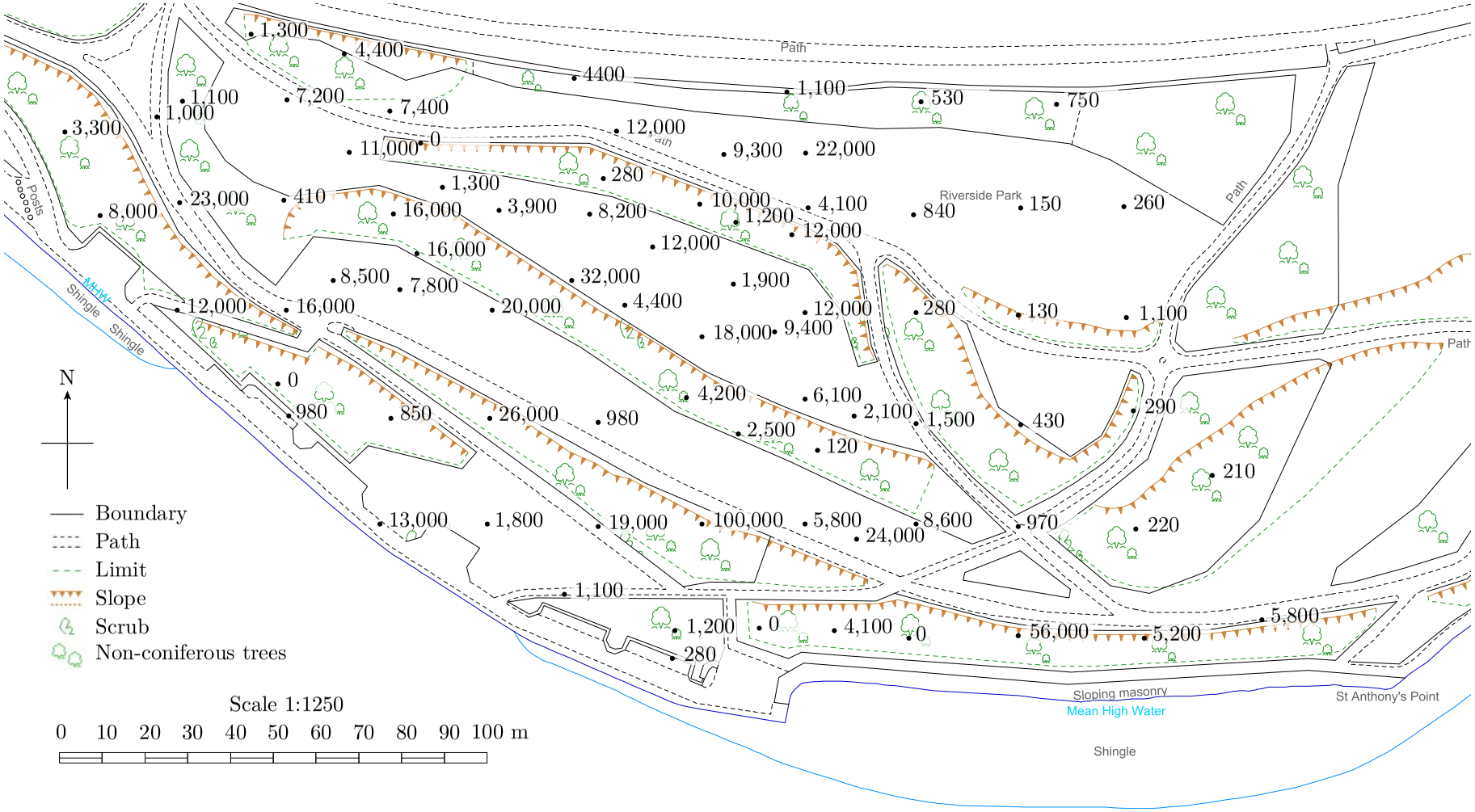

Figure 6.2: Map of St Anthony's 19th Century Lead Works with at Depth Concentrations of Lead ($mgkg^{-1}$)

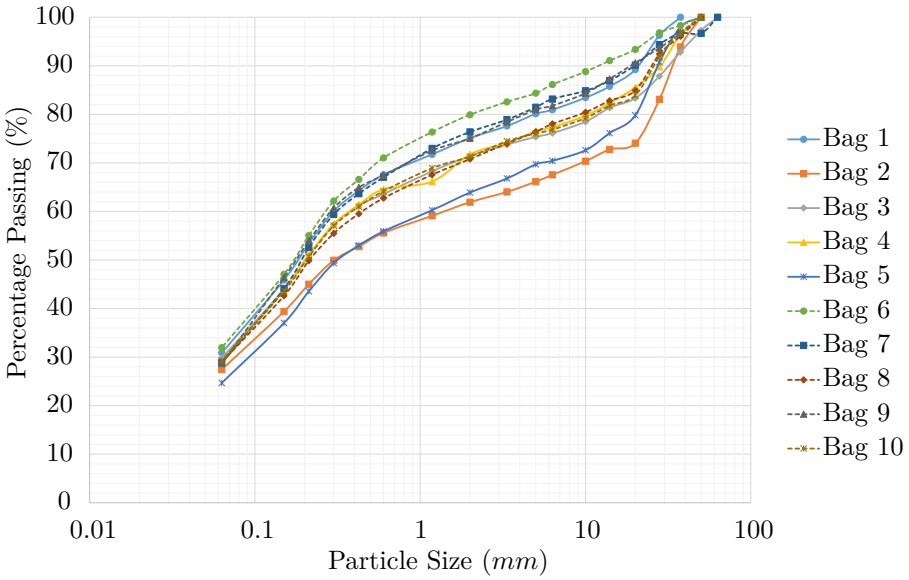

Figure 6.3: Particle Size Distributions for St Anthony's Soil

of the larger particles and the highest average water content. Removal of the path substrate material was necessary to address these discrepancies and for the soil to better represent the leadworks site. This was achieved by sieving out all particles greater than 10 mm. Applying this method to the same data set as before yielded Figure 6.4, demonstrating a much greater consistency between the different particle size distributions.

A particle size distribution of soil passing the 10 mm sieve size was then carried out for a representative sample of all ten bags. This time a full sedimentation was carried out for a complete grading, with the results displayed in Figure 6.5. The soil contained 10 % gravel, 48 % sand, 34 % silt and 7 % clay, with a uniformity coefficient (C_u) of 53 and coefficient of gradation (C_k) of 1.9.

Although the loss of larger particles was predominantly the dolomite substrate from the path, other genuine particulates were lost in the the process. Upon inspection these were found to consist of pottery, glass, brick shards, coarse gravels and other miscellaneous debris, reflecting the history of the site. It was deemed as no great loss and indeed acted as a compromise between reflecting site conditions and offering a degree of refinement within the laboratory environment. The inclusion of glass would have posed a small risk to health and safety, and the vast majority of particulates of this size would have potentially complicated the insertion of probes and ports, for which even particles up to 10 mm across were causing some concern. In total with this approach, it was estimated approximately 20 % of the total mass of soil available would be discarded in this manner, with a significant proportion coming from bags 2 and 5.

Unfortunately, with the degree of compaction sought combined with discarding such a high proportion of material and the looseness of soil in the dumpy bags, 10 m^3 of material was insufficient. To fill the final lysimeter, a second collection had to made at the leadworks site but at a different location due to remediation works having been completed. The excavation plot was chosen on one of the slopes between the upper middle and upper terrace, on a plot which was also previously used for red lead furnaces. The material was different as can be seen in the particle size distribution given in Figure 6.6. There is almost a plateau around the 50 % mark which remained after running multiple sedimentations and recalibrating the equipment. The main difference between the two samples were a significant drop in sand and silt, down to 36 % and 26 % respectively, and a significant increase in clay content, up from 7 % to 25 %.

As for other properties according to BS1377-2, the soil used in lysimeters 1 and 2 had a liquid limit of

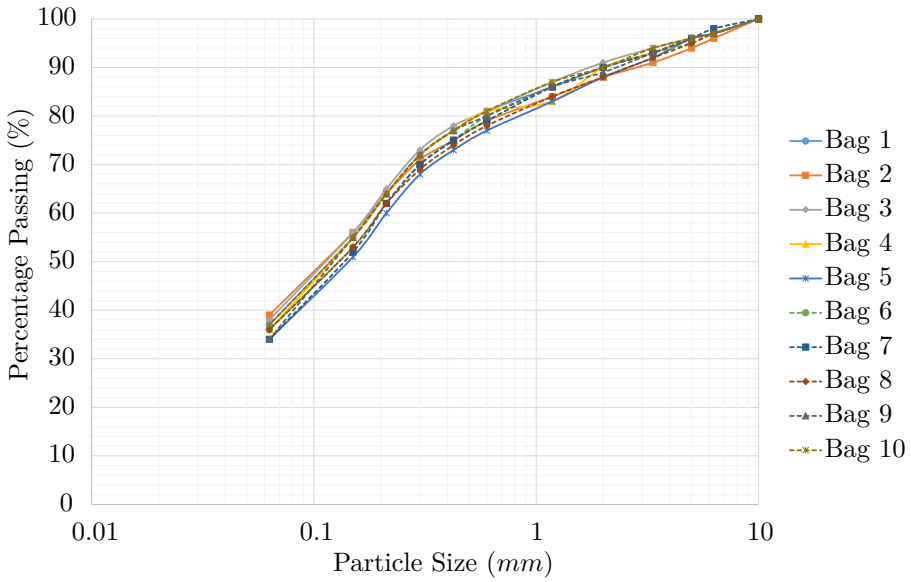

Figure 6.4: Modified Particle Size Distributions for St Anthony's Soil

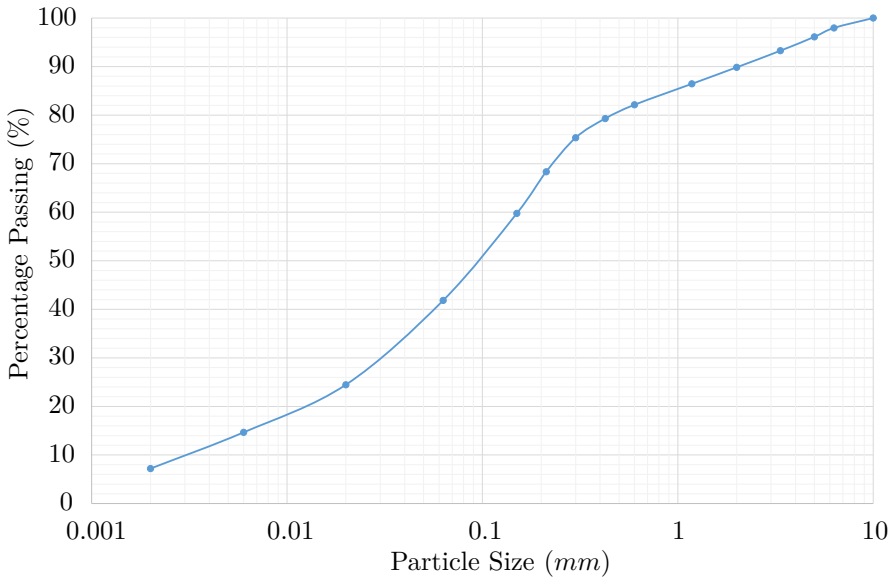

Figure 6.5: Final Particle Size Distribution for St Anthony's Soil - Lysimeters 1 and 2

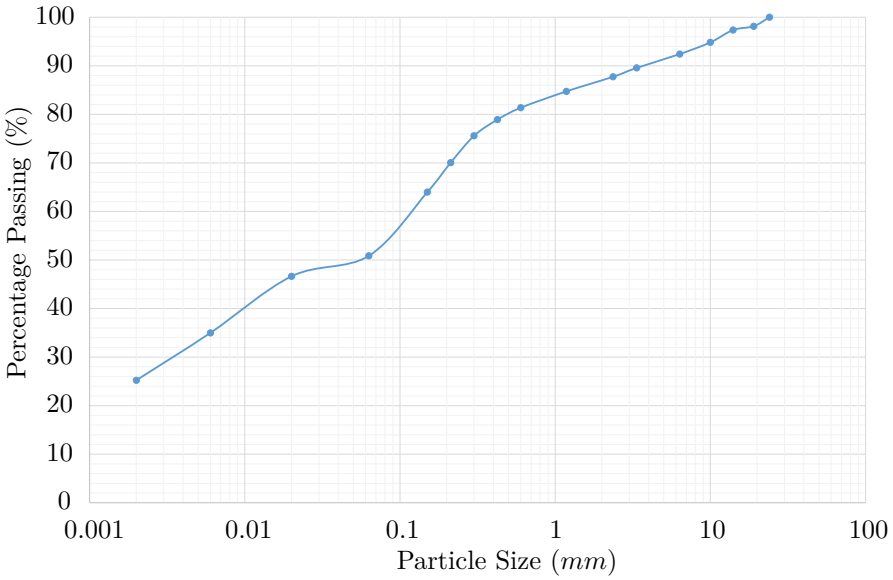

Figure 6.6: Final Particle Size Distribution for St Anthony's Soil - Lysimeter 3

42.4 % and a plastic limit of 24.2 %, yielding a plasticity index of 18.2 % and suggesting the soil material behaved as a silty clay of intermediate plasticity. The soil used in lysimeter 3 was similar, with a liquid limit of 39.5 % and a plastic limit of 21.7 %, yielding a plasticity index of 17.7 % and likewise was classified as a clay of intermediate plasticity. The particle density of the soil was found to be 2.579 $Mg\ m^{-3}$ as based off three samples with standard deviation of 0.004 $kg\ m^{-3}$, and linear shrinkage tests showed a percentage change in length was on average 8.7 % based on six samples with a standard deviation of 0.4 %. Loss on ignition found the organic content of the soil to be relatively high at approximately 9 % by dry mass.

A Proctor compaction test (BS light) was carried out on the soil used for lysimeters 1 and 2 according to BS1337-4 [97], the result of which can be seen in Figure 6.7. Each data point was prepared for with a different sample, the soil being that sieved past 10 mm, resulting in an approximate optimum water content of 20.5 % at a dry density of 1537 $kg\ m^{-3}$. Also plotted in Figure 6.7 is a bulk density curve, four data points showing the samples taken in the field and lines depicting the degree of saturation for the dry density samples. The optimum water content appears to align approximately with a degree of saturation of 0.82, whereas three of the samples from the field have a degree of saturation approximating 0.76, close to optimum but with a significantly decreased dry density over BS light Proctor samples.

In summary, well graded soils with average water content of 22 % were collected from St Anthony's Leadworks in Newcastle. The samples were sieved past 10 mm for use, and tests upon the processed soil suggested the material behaved as a silty clay of intermediate plasticity and low shrinkage. The optimum water content was approximately 20.5 % at a dry density of 1537 $kg\ m^{-3}$ and at a degree of saturation approximating 82 %.

6.2.2 Water Treatment Residual

Water Treatment Residual (WTR) was selected as a potential treatment for soil containing contaminants due to two criteria. The first was due to the current classification of WTR as a waste from industry. All WTR is produced in the process of creating clean drinkable water at treatment plants. The treatment plants take in water and remove unwanted particulates, such as organic or mineral matter, through a process called clarification. The removal of suspended matter is accomplished chemically through the

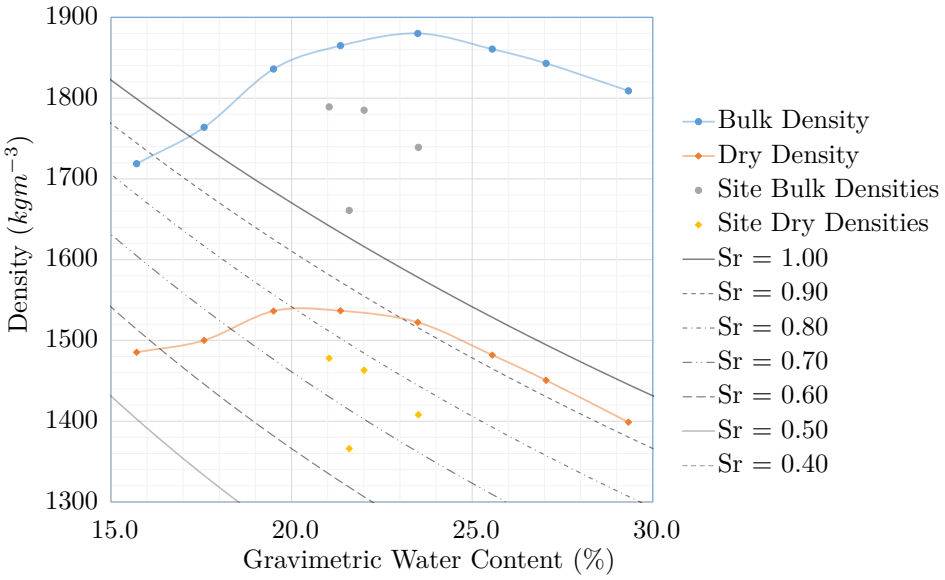

Figure 6.7: Light Proctor Compaction of Leadworks Soil

addition of compounds to aid in coagulation, followed by flocculation and dewatering. Once the coagulant has been mixed in a turbulent environment, the flocculant is added and gently stirred allowing the flocs to settle before dewatering occurs, typically in a centrifuge, to remove as much water as possible and limit the mass of material produced. The product is classed as a waste as it has no current beneficial use and is disposed of by spreading repeatedly on the same plots of land. As such, it was a material that was a prime contender for the ROBUST project as it fulfilled the sustainability goals.

The second criteria was a high content of metal oxides. Metal oxides, and more specifically Manganese, Aluminium and Iron Oxides, were of extreme interest due to their ability to adsorb Potentially Toxic Elements (PTEs) [98, 99]. The metal oxides are formed due to the addition of coagulants, which contain the associated metal and form the oxides during the coagulation and flocculation processes. Combining this with the nearly endless supply of WTR, provided a sustainable supply of a potential remediative material.

Sourcing WTR primarily focused upon local water treatment plants to fit in with the theme of sustainability. The local water company for the north east of England, Northumbrian Water, had a series of ten Water Treatment Works (WTW) spread across the region as shown in figure 6.8. Each treatment works was different, from the local water through to chemicals added during clarification and tonnage produced per year, some details being shown in Table 6.2.

The final form of the WTR varied between sludge and cake, where sludges were formed by centrifuging the flocc and cakes by pressing the flocc. The coagulants varied between iron based and aluminium based across the region whilst the flocculants, long chained organic polymers, were either cationic, anionic or neutral, with varying degrees of molecular weights and charge densities. The final column in Table 6.2 displays the quantity of WTR produced per year, totalling approximately seventy thousand tonnes.

The WTR chosen was that from the Mosswood WTW for two major reasons. Firstly, the site was one of two that were most local to Durham and a site being remediated in Easington, as a separate part of the ROBUST project. Secondly, the tonnage produced per year was the third highest, at a little under eight thousand tonnes, meaning it was sustainable in large quantities if necessary.

Collection of half a tonne of WTR was carried out from a large pile of the material at the Mosswood site, post centrifuging, and transported to Durham in a series of heavy duty rubble sacks. The appearance

Table 6.2: Water Treatment Residual - Water Treatment Works Details

Water Treatment Works	**State**	**Coagulant**	**Flocculant**	**Production** (T/yr)
Broken Scar	Sludge	Fe	Flopam AN913 SEP	17852
Lartington	Sludge	Fe	Flopam AN923 SEP	17216
Mosswood	Sludge	Fe	Flopam AN923 SEP	7957
Wear Valley	Cake	Fe	Flopam AN913 SEP	1989
Honeyhill	Sludge	Fe	Flopam AN910 SEP	5517
Fontburn	Sludge	Fe	Magnafloc LT25	5210
Gunnerton	Cake	Al	Flopam AN905 SEP	552
Whittle Dene	Cake	Al	Flopam AN905 SEP	6922
Horsley	Cake	Al/Fe	Flopam AH912 SEP	4557
Warkworth	Cake	Al	Flopam AN910 SEP	1894

of the Mosswood WTR on site was that of a moist dark brown soil that formed clumps or large clods, an image being shown in Figure 6.9.

The WTR had some interesting properties that made it unusual as a material. After collection, samples were taken from eight of the rubble sacks resulting in an average gravimetric water content of 424 %, with a sample standard deviation of 4 %. In storage, the WTR continued to de-water, first with a sheen over the surface as in Figure 6.10, and then slowly pooling the water in the rubble sacks. Upon mixing back into a homogeneous material, the reintroduction of pooled water caused all structure previously associated to disintegrate, forming a slurry. This made assessing some of the material's geotechnical properties somewhat difficult. The liquid limit was found to be 466 % gravimetric water content (GWC) for the new material taken from site, however with the maturation of the WTR, this had the potential to reduce significantly. As for the plastic limit, it was found to be non-plastic.

Drying the Mosswood WTR in an oven at 105 $^{\circ}C$ produced hard black crystals, that when broken open had shiny internal surfaces. A selection of WTRs was taken from the other sites across the region, which when oven dried produced similar results but at different resultant grain sizes and shades from dark brown through to light brown as seen in Figure 6.11. Reintroduction to water resulted in no absorption for any of the oven dried residuals, the crystals remaining the same volume. A couple however produced significant quantities of a colourless gas on introduction with water, resulting in the grains fracturing into smaller particles. A similar process was observed on introduction to air with the same two samples, the samples being nominally kept in sealed containers. In air, the fracturing was much slower but was highly energetic with small particles being fired off larger parent material for distances of up to two metres, resulting in the parent material scattering. Mosswood WTR however exhibited no fracturing or bubbling on contact with water.

In terms of composition, the WTRs were determined to be composed of significant quantities of organic material, metal oxides and minerals, Mosswood being composed of 37 % organic matter, 50 % iron oxyhydroxides and the remaining 13 % being trace elements and compounds. Assessment of the specific densities of the oven dried material were attempted. With such high organic matter contents, it was decided to leave the organic matter in the crystalline material.

The process of de-airing the water in the pycnometers, containing any of the WTR, was hindered by the production of gasses, even by those not producing visible bubbles. This resulted in carefully applying and maintaining vacuums for prolonged periods of time, in the case of Mosswood WTR a period of two months was taken, with the water turning a vibrant rust red as seen in Figure 6.12. Even after this period, the water was not perfectly de-aired but was considered to be as good as reasonably possible, resulting in a strong agreement across three samples of a specific density approximating 2.503 $Mg\ m^{-3}$.

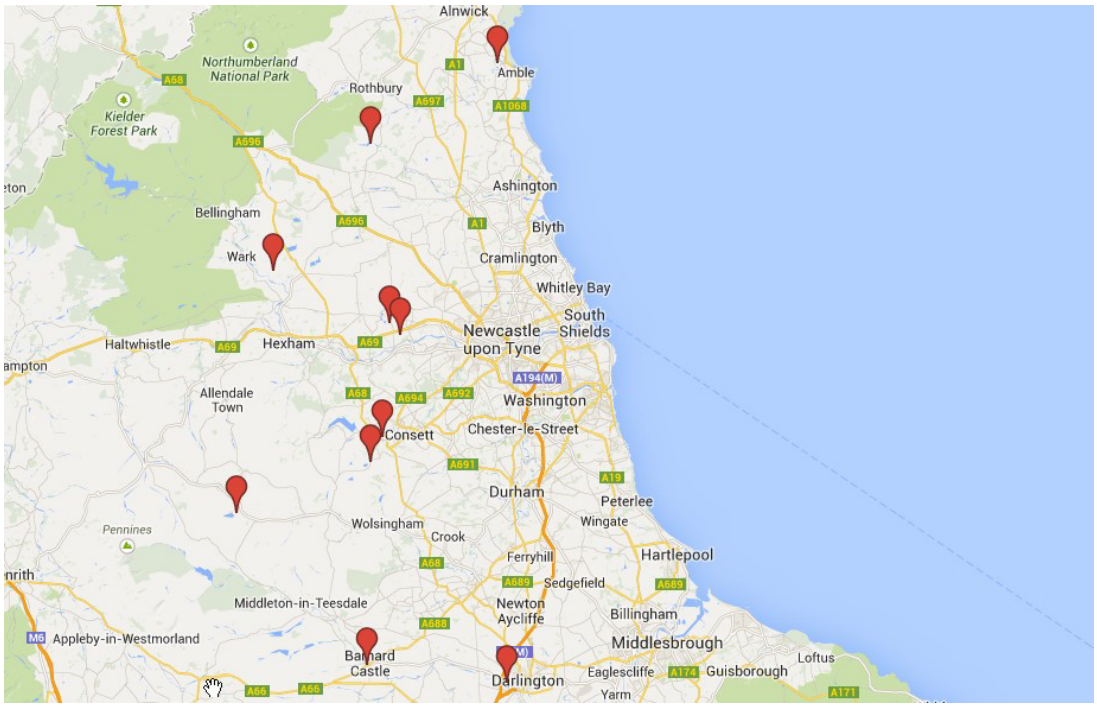

Figure 6.8: Locations of Water Treatment Works

Figure 6.9: Clod of WTR

Comparatively, Glassford (provided by Scottish Water) and Gunnerton, which were both aluminium based WTRs, had considerably lower specific densities at 1.907 $Mg\ m^{-3}$ and 2.025 $Mg\ m^{-3}$ respectively. This ties in with the literature where aluminium WTRs are quoted to have quite low specific densities as compared to iron based WTRs, as can be seen in Table 6.3.

Table 6.3: Water Treatment Residual - Specific Densities

Study	**Year**	**Coagulant**	**Specific Density** ($Mg\ m^{-3}$)
Babatunde et al. [100]	2009	Aluminium	1.95 to 2.35
Raghu et al. [101]	1997	Aluminium	2.02 and 2.33
O'Kelly [102]	2008	Aluminium	1.86
Wang et al. [103]	1992	Aluminium	2.26 and 2.33
Wang et al. [103]	1992	Iron	2.72
Willetts and Toll [104]	2011	Iron	2.38

As for the particle size distribution of Mosswood WTR, this remained unknown. The particles in wet WTR were clearly similar to silt or clay in size, but the determination through sedimentation proved difficult. Considering the WTR was formed from a coagulant and flocculant, addition of a deflocculant for sedimentation did not provide confidence in results during early work [104].

In summary, WTR as a material was not suited to BS1377 tests designed for soils, partially due to its evolving nature and partially due to its composition, particularly the high organic content and the inclusion of coagulants and flocculants. The high levels of iron oxyhydroxides suited the ROBUST project as a remediative material and its inclusion as a soil amendment proved to be interesting.

6.2.3 Compost

Compost was used as an additional amendment for the third lysimeter, along with the Mosswood WTR, to investigate if there was any beneficial influence to the remediation process. With composts varying significantly on locality, input organic matter and other potential inclusions, it was important to use a standard of compost that was recognised and useable for the foreseeable future. The compost included on the field site, associated with the ROBUST project, conformed to the BSI PAS 100 composting standard and was sourced from a local supplier (Comvert Ltd).

The standard was developed to aid in combatting the large quantities of biodegradable material that goes to landfill within the U.K., and to provide a minimum level of quality to composts produced. This in turn meant waste materials could be reclassified as a product, similar to how WTR was being treated within the ROBUST project. The standard defines maximum levels of certain pathogens; PTEs; respiration rates; weed seeds and propagules; physical contaminants such as metals and plastics; and stones, the stones greater than 4 mm accounting for a maximum of 8 % by mass of the air dried compost. As for the compost used in tthis project, it had an average gravimetric water content of 87 %.

6.3 Fill Method

The first lysimeter to be filled was the control, for which the fill method was based off having a high degree of confidence, both in replicating the bulk field conditions and conforming to a relatively high degree of homogeneity for the lysimeters size. The second and third lysimeters with their amended soils had two choices available, to either use the same compaction regime or to aim for maintaining a physical property of the control, such as dry or bulk density.

The field site took a real world approach, opting for adding amendments by spreading the WTR and compost over the surface, and mixing in using the backhoe of a JCB tractor. Although representative of

Figure 6.10: Clod of WTR dewatering

Figure 6.11: Oven dried WTR samples from different Water Treatment Works

a real world scenario, it was felt replicating the addition of the amendments through the same approach in the laboratory would produce incomparable results between lysimeters, given the rough nature of the mixing and compaction. The main influence from the site instead was the quantities of material used, where approximately 10 % by mass of wet soil, of each amendment was applied. The upper limit of 10 % by mass of WTR being matched approximately to current practice for the disposal of WTR by water companies on theirs and others land per year, whilst matching quantities of compost was deemed appropriate.

In the laboratory, using the same degree of compactive effort on each of the lysimeter soils was chosen rather than maintaining certain properties. The addition of compost and WTR in these quantities would have upset the process of finding compactive efforts to match dry or bulk densities, especially considering the high water contents associated with both materials and the strange behaviour of WTR. In terms of homogeneity, it was decided to mix in water and amendments thoroughly, so as point sensors would be monitoring the same bulk materials and not the occasional high concentration of WTR etc., making for more internally comparable results. In essence, the application of amendments in the lysimeters approximated an ideal mixing, followed by compaction with significant enough effort to represent a real sites soil.

6.3.1 Preparation

The initial preparation involved passing the soils through a 10 mm sieve and collecting the passed material in a separate series of dumpy bags. The soil, having dried out partially, was approximately slightly dry of optimum and passed the sieves with little problem, the work being conducted outside for ventilation considering the contaminated nature of the material. Soil was sampled from each of the original ten dumpy bags in turn to attain fairly representative dumpy bags of material, and once filled the bags were wrapped in clingfilm and left to equilibrate.

With all the bags being dry of the target 22 % GWC, water content samples were taken to calculate quantities of water to make up the deficit. The soil used for the control lysimeter was made up by adding water to the soil using a large paddle mixer, which took sub 100 kg batches. The soil amended with WTR was mixed up similarly, but instead of adding the WTR straight to the soil and adding the water separately, the two were mixed together in a planetary mixer before addition, likewise with the compost and WTR amendments for the third lysimeter. This aided in making a homogeneous mix, preventing clumps of dried material where the soil had absorbed water from the amendments.

Once the soil batches were mixed, they were stored in large dustbins, sealed and left to equilibrate once more before use.

6.3.2 Filling Process

The filling process involved weighing out the correct quantities of material, compacting and scarifying the surface ready for the next layer. The compactive effort employed was determined empirically on a smaller, but still representative, scale.

The control material was used initially to determine the compactive effort required to form a layer of approximately 20 mm thickness at a dry density of approximately 1429 $kg\ m^{-3}$ and at 22 % GWC. The 20 mm thickness was chosen as a sensible number yielding 50 layers in the lysimeter for a relatively homogeneous compactive effort. With a fixed 5 kg tamper of base plate dimensions 120 mm by 120 mm, the variables available to control were the height of the drop and the number of tamps. A rectangular test box was used, with base dimensions of 365 mm by 263 mm in which layers of material were placed before levelling off and tamping.

It was immediately found that the soil material had an affinity for sticking to the tamper, so a

preventative plastic sheet between the tamper and soil was used as a solution. Each test used multiple layers of five or more to minimise the effects of tamping straight onto the containers base when assessing the degree of compaction, the tamper being roughly expected to compact 60 mm deep, or three layers worth, of soil. Tests initially started at 100 tamps with a drop of 300 mm but the drop height was reduced to 150 mm for user comfort after tests showing over-compaction. The number of tamps was finally reduced to 75, which produced a degree of compaction similar to field conditions, and when scaled up to the cross-sectional area of the lysimeters, approximated to 884 tamps per layer for a full fifty layers. Each lysimeter was initially marked at for differing poisitions on the inside wall every 20 $mm$from the base to a height of 1 m using a paint pen. This helped to spread the soil evenly and prevent sloped surfaces from being tamped. The final method for a layer was as follows:

1. 39.433 kg of soil for a layer was weighed into four buckets;
2. The lysimeter was entered by the person compacting and the first three buckets of soil were distributed evenly into the first three quarters of the lysimeter using a coarse rake;
3. A plastic sheet was placed on one quarter and the person compacting stood on the sheeting whilst distributing the final bucket evenly in the last quarter;
4. The heights around the circumference were checked against each of four series of wall markings that indicated layer heights every vertical 20 mm;
5. Any anomalies were distributed whilst trying to minimise the amount of raking as this caused separation of the larger soil particles from the smaller;
6. For each quarter, 100 tamps were applied with 150 mm drops whilst the person compacting preferentially stood on compacted soil;
7. Using a trowel, the circumference of the lysimeter was navigated, sliding the trowel flat against the soil to remove any lip forming against the side wall;
8. Soil cuttings were distributed where appropriate, gauged using the markers on the side walls;
9. The process continued with covering with a plastic sheet once more and repeating 100 tamps per quarter of the lysimeter;
10. The plastic sheeting was removed and the final 84 tamps were applied over the entire surface of the lysimeter;
11. All but the last layer was scarified to aid in interlocking between layers;

After each layer, the level of the surface was assessed to check if more soil needed to be distributed into some sections over others to maintain a flat surface area during the filling process, whilst every few layers the water content of the fill material was checked for quality control. The final layer had more time allocated to flattening of the surface as to avoid pooling of water during irrigation, as this would cause discrepancies for water infiltration. As for filling the lysimeters with amended soils, the mass of soil required for a 20 mm layer was assessed using the same compactive method in a test box. This mass of soil was then scaled up for use in the lysimeters.

6.3.3 Probe Insertion

The Time Domain Reflectometry (TDR) probes were inserted at six layers with four at each layer. The cabling for the probes was inserted through the ports described in Chapter 2 before the soil was compacted over the port layer, the TDR probes hanging over the top of the lysimeter. When the soil was at a sufficient depth over where the probes were to be inserted, typically one layer, a rectangular cutting was taken out normal to the lysimeter wall, just over the length of one TDR probe which approximated to 170 mm. The cutting was taken down to a depth of one half the height of a TDR probe below the centre of each port whereby the probe could sit comfortably in the hole as shown in Figure 6.13.

Insertion of each probe into the soil mass was done slowly, keeping a watch for deviation of the wave guides and resistance due to stones. The ideal insertion would occur on the first attempt with no indication of the wave guides crossing, which could be monitored by checking for a short circuit, or splaying, which was harder to assess. The first insertion into the soil was important for good contact between the wave guides and the soil fabric and in the scenario where a probe met significant resistance or deviation, the probe would be reinserted within 2 mm above or below the original attempt.

Unfortunately, this was no guarantee that the probe was sitting well within the soil matrix and on one occasion, subsequent tamping of layers forced a short circuit on a probe but this was an isolated case. In general, approximately one in every four probes required re-insertion based on experience, with it being fortunate that the length of the TDR probes was so short, as with the more common longer probes this may have been a greater issue. At completion of the three lysimeters, only one of seventy two probes was short circuiting with the others behaving adequately.

6.3.4 Port Insertion

The insertion of the larger ports used by tensiometers was conducted after the completion of compaction and flattening of the surface. Each port hole was drilled out using a 30 mm diameter wood drill bit attached to a hand drill with brace. When nearing the end of the required hole length, approximately 180 mm into the soil core, a custom made reamer was used to flatten the end of the hole in preparation for the port insert. The port insert was then pushed down the length of the hole and tapped into place with the butt of a hammer before sealing by tightening the gland nut. Finally, a blank tensiometer was placed down each of the ports to prevent leakage and evaporation of water out of the ports.

6.3.5 Result

The bulk properties for each lysimeter are given in Table 6.4. Each soil column is practically identical in volume but differs in mass, density and water content. The amendments in lysimeters 2 and 3 approximate to 9.1 % and 16.7 % of the total mass respectively, each reducing the sum dry density of material present, regardless of the increases on bulk density primarily due to the high water contents present.

With regards to the water contents, the final estimates of average water content put both lysimeters 2 and 3 below expectations, potentially due to some water loss during mixing and equilibration. Original estimates had put the final water contents closer to 31 % for lysimeter 2 and 34 % for lysimeter 3. This was taken into account for calculating the components, such as dry mass, of each material added to the lysimeter by assuming all mass loss was due to a water deficit and splitting this across the materials as per the mixing ratios by mass. This allowed for a breakdown of the components and the estimation of void ratios and degrees of saturation.

Lysimeter 1 had the most accurate estimations of void ratio and degree of saturation, with both having a magnitude of 0.74. Lysimeters 2 and 3, with their amendments, showed both an increase in void ratio and degree of saturation. Interestingly, the degree of saturation for lysimeter 3 was estimated as 1.05,

Figure 6.12: Mosswood WTR in a pycnometer under vacuum

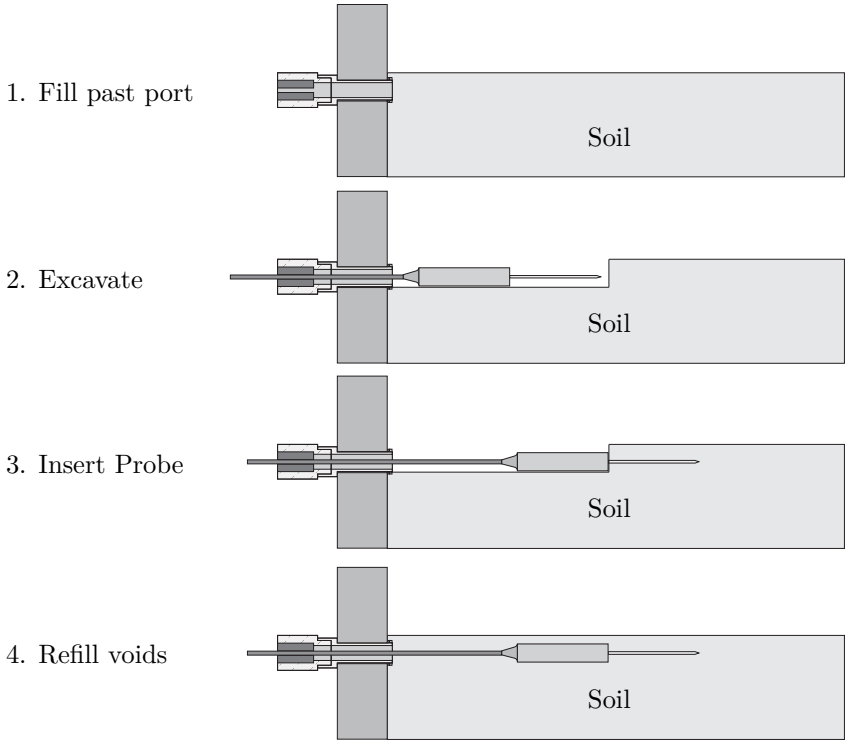

Figure 6.13: TDR Probe Insertion Steps

suggesting excessive quantities of water, although this may be an overestimation with the assumption that all water contributed by the organic matter filled voids, at the very least the degree of saturation was above 0.87. Indeed, the experience of filling lysimeter 3 was in contrast to the prior two, which both formed a firm surface during the tamping process. Tamping the soil amended with WTR and compost showed significant deviation in surface level around the area struck by the tamper. To corroborate, it was observed after filling lysimeter 3 was complete, very small amounts of leachate were being collected from beneath the lysimeter, hence it seemed likely that the degree of saturation was 1.00 and that some water was driven out.

Table 6.4: Lysimeter Soil Column Properties

Grouping	Property	Lysimeter 1	Lysimeter 2	Lysimeter 3
Bulk	Bulk Mass (kg)	2011	2086	2062
	Bulk Volume (m^3)	1.13	1.13	1.13
	Bulk Density ($kg\ m^{-3}$)	1778	1845	1823
	Dry Density ($kg\ m^{-3}$)	1462	1428	1381
	Bulk Water Content (%)	21.6	29.2	32.0
Soil	Total Mass (kg)	2011	1897	1718
	Dry Mass (kg)	1654	1577	1432
	Specific Density ($Mg\ m^{-3}$)	2.5434	2.5434	2.5434
	Solid Volume (m^3)	0.65	0.62	0.56
	Mass of Water (kg)	357	320	286
	Volume of Water (m^3)	0.36	0.32	0.29
WTR	Total Mass (kg)	0.0	189.7	171.8
	Dry Mass (kg)	0.0	38.4	35.2
	Specific Density ($Mg\ m^{-3}$)	2.5028	2.5028	2.5028
	Solid Volume (m^3)	0.000	0.015	0.014
	Mass of Water (kg)	0.0	151.2	136.6
	Volume of Water (m^3)	0.000	0.151	0.137
Compost	Total Mass (kg)	0.0	0.0	171.8
	Dry Mass (kg)	0.0	0.0	94.3
	Specific Density ($Mg\ m^{-3}$)	-	-	-
	Solid Volume (m^3)	-	-	-
	Mass of Water (kg)	0.00	0.00	77.52
	Volume of Water (m^3)	0.00	0.00	0.08
Void	Volume (m^3)	0.48	0.50	0.48
Derived Properties	Void Ratio	0.74	0.80	0.85
	Degree of Saturation	0.74	0.95	1.00

Table 6.5: Total Mass of Constituents in Each Lysimeter

Component	Lysimeter 1	Lysimeter 2	Lysimeter 3
Mineral (kg)	1505 (75%)	1439 (69%)	1311 (64%)
Organic (kg)	148.8 (7%)	156.1 (7%)	231.5 (11%)
Water (kg)	357.2 (18%)	470.9 (23%)	499.8 (24%)
Iron Oxyhydroxide (kg)	0.0	19.2 (1%)	17.6 (1%)
Misc (kg)	0.0	1.2 (≈0%)	1.5 (≈0%)

The mass of constituents in each of the lysimeters is given in Table 6.5. The mineral component decreased in quantity with the addition amendments as expected, whilst the water content only signifi-

cantly increased with the addition of WTR and likewise with the organic component with the addition of compost. It can be seen that the total mass of oxyhydroxide amendment applied to the second and third lysimeters was relatively small compared to the mineral and organic content of the soil. The miscellaneous category accounted for other materials present in both the WTR and compost amendments, such as other oxides, nitrogen compounds, plastics etc..

6.4 Small Scale Laboratory Testing

Two laboratory tests were carried out on the soil placed in lysimeter 1 to determine permeability and the soil water retention behaviour. Tis was to provide a comparison between small and large scale laboratory testing as given in Chapter 7.

6.4.1 Permeabilities in Triaxial Apparatus

A sample of the lysimeter 1 soil was prepared and tested in a triaxial cell to assess its permeability. The soil was prepared in the same manner as the soil in the lysimeter, at 22 % gravimetric water content and tamped in 20 mm thick layers using the 5 kg hand tamper, but into a split mould 100 mm in diameter by 200 mm tall. The resultant samples were checked for a bulk density approximating to 1778 kgm^{-3} before having 25 mm of material trimmed from the top and bottom to ensure the sample was representative of the bulk soil material in the lysimeter, removing any end effects.

The sample was placed in a triaxial cell where the cell pressure, top back pressure and bottom back pressure were controlled and two volume change gauges were used to monitor the inflow and out flow from the sample as per BS1377-6 [105]. The sample was not however saturated but was tested at very low confining pressures, around 10 kPa, and by applying a small head difference across the sample of 6 kPa yielding field saturated hydraulic conductivities. This was repeated until the volume change readings resulted in linear responses and the volume of water going into the sample approximately matched the volume of water leaving the sample, as with the difference between Figure 6.14 showing Run 1 and Figure 6.15 showing Run 6.

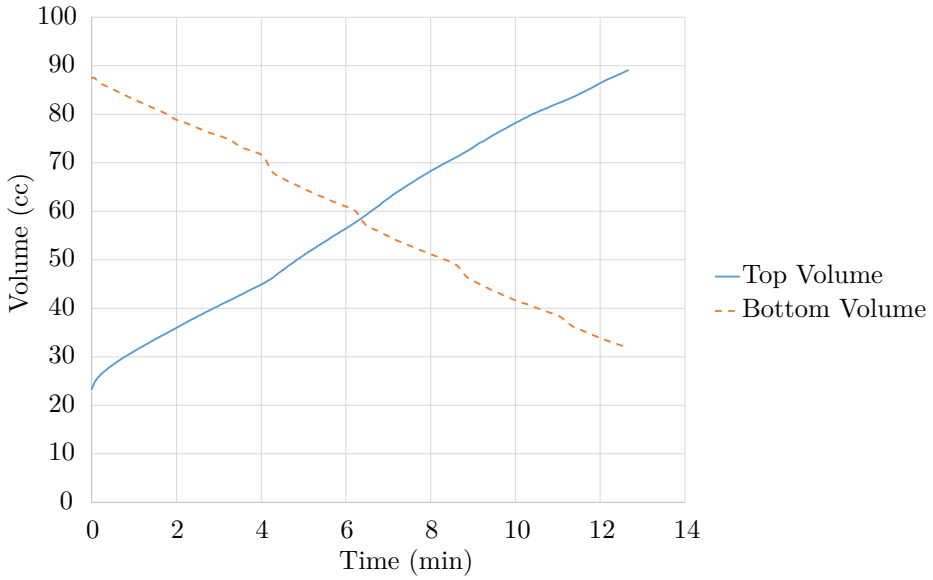

Figure 6.14: Graph of Volume Changes for Run 1

The results of six consecutive permeabilities are shown in Figure 6.16 and the data given in Table 6.6. It can be seen there was a downward trend, tending towards lower hydraulic conductivities. potentially

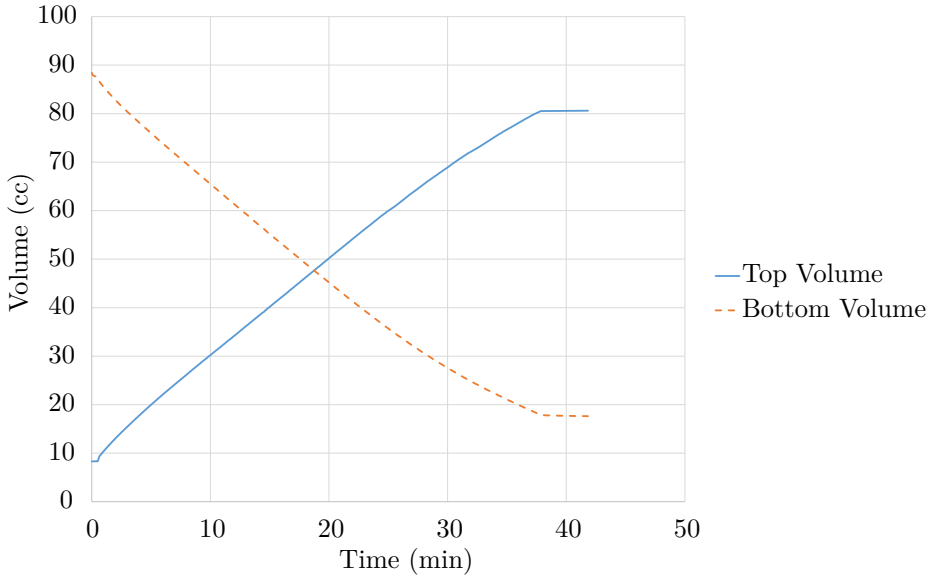

Figure 6.15: Graph of Volume Changes for Run 6

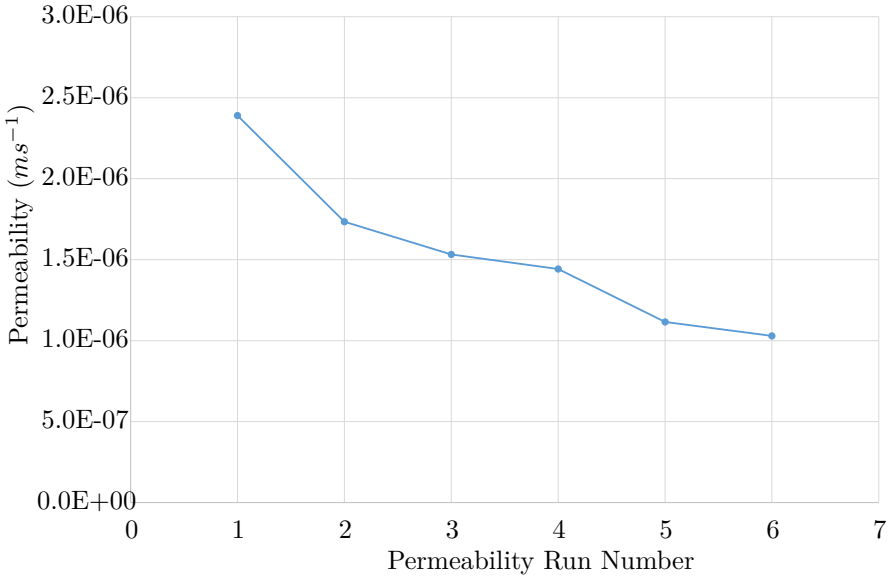

Figure 6.16: Graph of consecutive Permeabilities run on Lysimeter 1 Soil

Table 6.6: Lysimeter 1 Permeability Data determined in a Triaxial Cell

Run	Average Volume Change (ml)	Head Difference (kPa)	Permeability (ms^{-1})
1	4.87 ± 0.439	6.89	2.39×10^{-6}
2	3.04 ± 0.166	5.91	1.73×10^{-6}
3	2.90 ± 0.060	6.39	1.53×10^{-6}
4	2.84 ± 0.005	6.66	1.44×10^{-6}
5	2.24 ± 0.004	6.77	1.12×10^{-6}
6	2.03 ± 0.035	6.65	1.03×10^{-6}

due to the swelling of clays into the void spaces. The volume change given in Table 6.6 displays the standard deviation as an indicator for discrepancies between water entering and leaving the sample. Run 1 and Run 2 fair poorly by this metric, both having more water enter the sample than leave, indicating the soil was becoming more saturated. Runs 3 to 6 however, had stabilised significantly with the volume change readings agreeing more consistently. This put the field saturated hydraulic conductivity of the sample between $1.0 \times 10^{-6}\ ms^{-1}$ and $1.5 \times 10^{-6}\ ms^{-1}$.

6.4.2 Soil Water Retention Behaviour

The samples were cut from the saturated sample used in the permeability tests in the triaxial cell. The triaxial sample was cut into 30 mm thick sections before a cutting ring, 80 mm in diameter and 20 mm deep, was used to form uniform discs of soil which was studied using soil water retention behaviour testing equipment.

The testing equipment, pictured in Figure 6.17, used six Linear Variable Differential Transformers (LVDTs) held in a frame to monitor volume change in the samples. Two LVDTs were positioned on the top of a sample to measure vertical displacements and four LVDTs were placed horizontally in pairs, to measure lateral displacements. Beneath a sample, was a platform with a seal in the centre, allowing a tensiometer to be inserted and held firmly for monitoring matric potentials. The entire frame was placed on a mass balance, where the change in mass with time was attributed to evaporation of water off the sample. This allowed for calculation of volumetric water contents for plotting soil water retention curves.

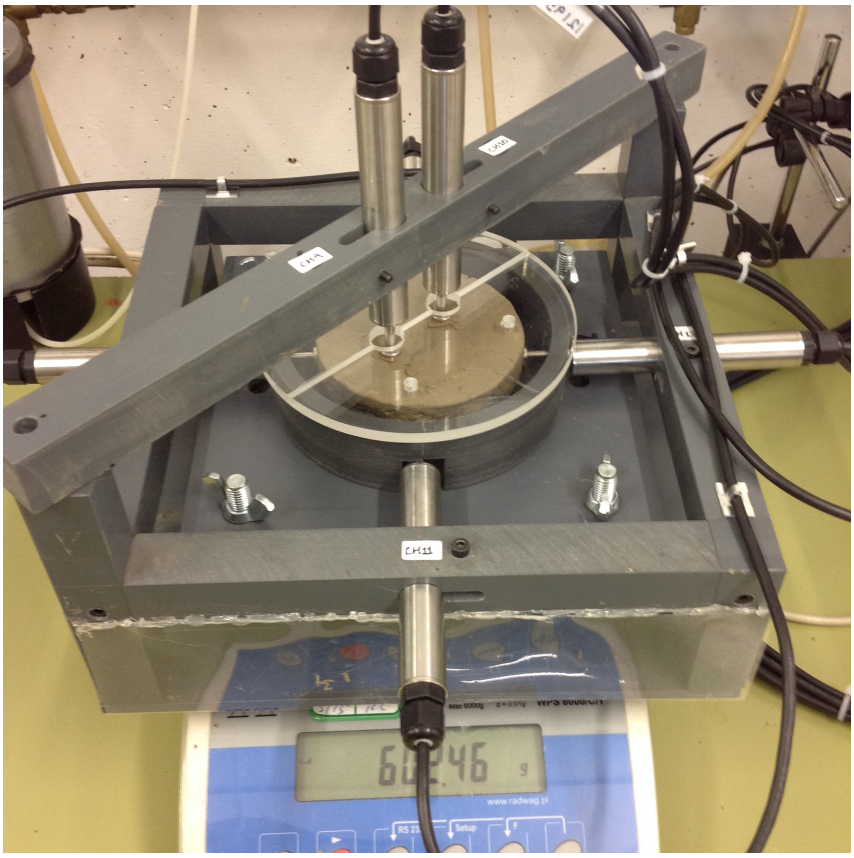

Figure 6.17: Picture of Soil Water Retention Behaviour Testing Equipment

Three samples were tested in the soil water retention behaviour testing equipment in a temperature controlled laboratory at 21 $°C$. For each, a drying curve was obtained. The results of the three curves are given in Figure 6.18.

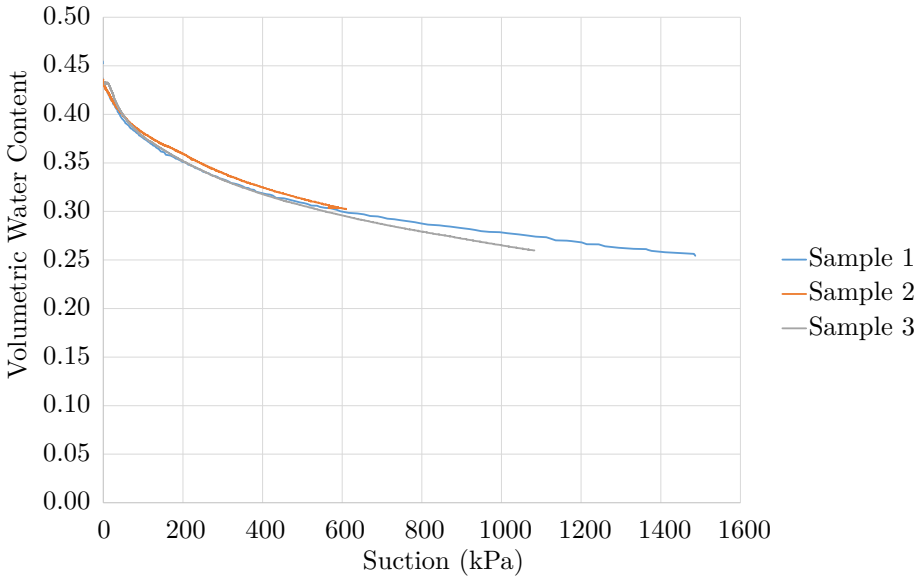

Figure 6.18: Drying Curves Obtained for Lysimeter 1's Soil
determined using the Soil Water Retention Behaviour Testing Equipment

Samples 1 and 2 started at a degree of saturation of 1.00, and sample 3 started at a degree of saturation of 0.97 corresponding to volumetric water contents around 0.43. All three samples followed the same approximate path, with the first sample reaching suctions nearing 1500 kPa, corresponding to a volumetric water content of approximately 0.25. Some error was expected in terms of suction, with the tensiometer being beneath the sample it was assumed the suction profile was quasi-constant throughout. Steps were taken to ensure this was reasonable by ensuring the sample was dried slowly by surrounding it in a small enclosure. A comparison of these curves to those obtained in the lysimeter, is given in Chapter 7.

6.5 Conclusion

Contaminated soil was sampled and analysed from the St Anthony's Leadworks in Newcastle, England. The material was a well graded silty clay which was passed through a 10 mm sieve to remove unwanted materials, providing consistent results across sub-samples. An amendment from a local WTW was sourced, that was high in iron oxyhydroxides, to remediate the contaminated soil. The WTR amendment had some odd properties preventing it from being analysed using standard geotechnical tests effectively. The second amendment sourced was a BSI PAS-100 compost, bought commercially from a local company.

Three lysimeters were filled; the first a control, the second amended with WTR and the third amended with WTR and compost. The amendments were applied in a by mass basis, 10 % by mass relative to the mass of the soil in field conditions assuming the top 0.50 m of soil was being treated. The fill method dictated consistent compactive efforts across lysimeters, with layers not exceeding 20 mm in depth. This resulted in relatively homogeneous soil columns being formed, with lower dry densities and higher void ratios and degrees of saturation upon addition of the amendments.

Small scale unit tests were performed on the soil mix used in Lysimeter 1 for comparison to the trends observed in the lysimeter itself. A permeability between 1.0×10^{-6} ms^{-1} and 1.5×10^{-6} ms^{-1} was determined alongside three drying curves.

Chapter 7

Results

7.1 Introduction

In this chapter, the results from fourteen months of testing the lysimeter containing the unamended control material are presented, alongside results from smaller laboratory samples for comparison. The two amended lysimeters are not included, as construction and filling was completed at the end of the project and have not yet undergone testing.

First, the water contents for the large control lysimeter during two wetting periods are given, alongside a discussion on the intermediary drying period. Trends in suction measurements are then presented for the wetting and drying cycles in the large lysimeter. Permeabilities determined from the two wetting periods are then shown and compared to the small scale laboratory tests in a triaxial cell. Finally, the soil water retention behaviour for the control lysimeter is presented. The data set is then compared to the soil water retention behaviour acquired using the smaller sccale laboratory testing apparatus to determine if there is a significant difference in results between normal laboratory scale samples and large lysimeter testing.

7.2 Water Contents

Water contents were determined for the lysimeter using the Time Domain Reflectometry (TDR) probes buried within the bulk volume and applying the custom calibration determined in Chapter 3.

7.2.1 The first Wetting Period

The quantity of water applied to the lysimeters during wetting was based on the average rainfall per year for the period 1961 to 1990 for the north east of England. The total rainfall for a year was 753.9 mm, which was on average 2.0 mm of rain per day. The irrigation system was set to provide an intensity of 1 mm of rain per minute for 2 minutes, meaning a total of 2 mm of rain was applied per day. With the rainfall periods being intensive, pooling of water was noticed to occur on the surface of the lysimeter after a period of approximately 1 minute. As the pooling water altered the distribution of water applied over the surface of the soil column, the irrigation period was broken into two separate periods of rain per day, each 1 minute in length set 12 hours apart.

Within the lysimeter, columns A, B, C and D refer to the four columns of instrumentation, labelled in ascending order anticlockwise around the circumference of the lysimeter as shown in Figure 7.2. The layers themselves were numbered 1 to 6, with layer 6 being closest to the surface and layer 1 closest to the lysimeter base as shown in Figure 7.1.

The initial distribution of water contents measured by the TDR probes can be seen in Figure 7.3.

The figure shows that there was broad agreement as the volumetric water contents lay between 30 % and 38 % for layers 1 to 5 at depths of 0.2 m and below, but there a much greater spread of volumetric water contents at the near surface on layer 6. The greater spread and low water contents for layer 6 was likely due to some evaporation of water whilst the lysimeter was covered over prior to starting the irrigation. The lysimeter had an estimated initial bulk volumetric water content of 31.6 % based on the estimated total mass of the constituents in the lysimeter calculated in Chapter 6, whilst the TDR probes here estimated the initial conditions were on average closer to 33.2 %, a difference of 1.6 % Volumetric Water Content (VWC).

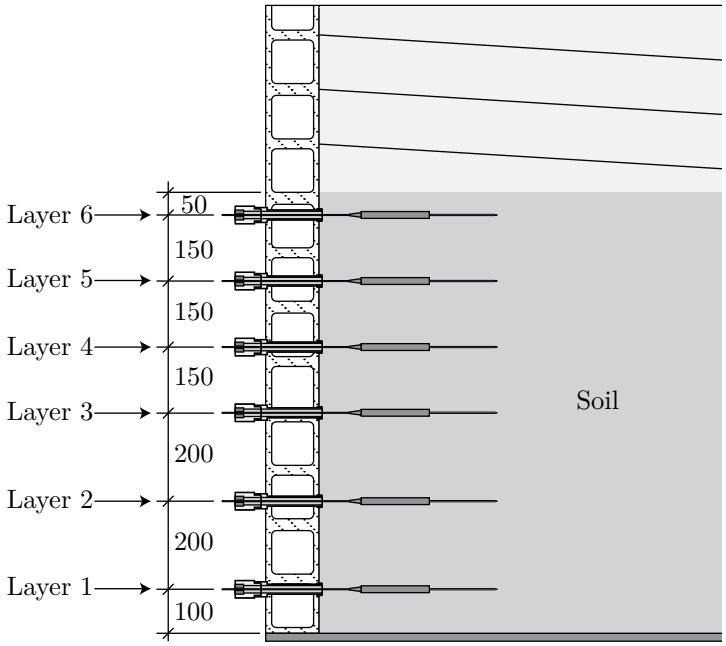

Figure 7.1: Diagram of Vertical Port Labelling

The TDR probe data for the first five month wetting period applied to lysimeter 1 can be seen in Figures 7.4, 7.5, 7.6 and 7.7. Each figure depicts six probes of data labelled layers 1 to 6, except column C, where the probe on layer 2 was not functioning. The data shows clearly the wetting front caused by the application of irrigation passing through the soil column. As the wetting front passed each probe, the response was a sharp upward sweeping curve, followed by a predominantly steady state condition.

In the layer 6 (near surface) probes, it can be seen that the daily variation was greater than for the other probes. This is particularly apparent for Figure 7.7, where the volumetric water contents cycle by approximately 2 %, as irrigation is applied and evaporation occurs on a twice daily cycle. A period of one week is shown in Figure 7.8 for the top layer probe, where fourteen individual steep increases in water content are to be seen followed by gradual declines over the following 12 hour periods. Another observation with layer 6 is the continued upward trend when compared to the steadier water contents deeper within the soil column. Columns C and D in Figures 7.6 and 7.6 shows this upward trend almost continuously, whereas columns A and B plateau after the wetting front passes before then showing an upward rise. This was explained by the tendency for water to pool above columns C and D in preference to A and B due to unevenness on the soil surface. The effect of this pooling became more apparent as the soil column became more heavily saturated.

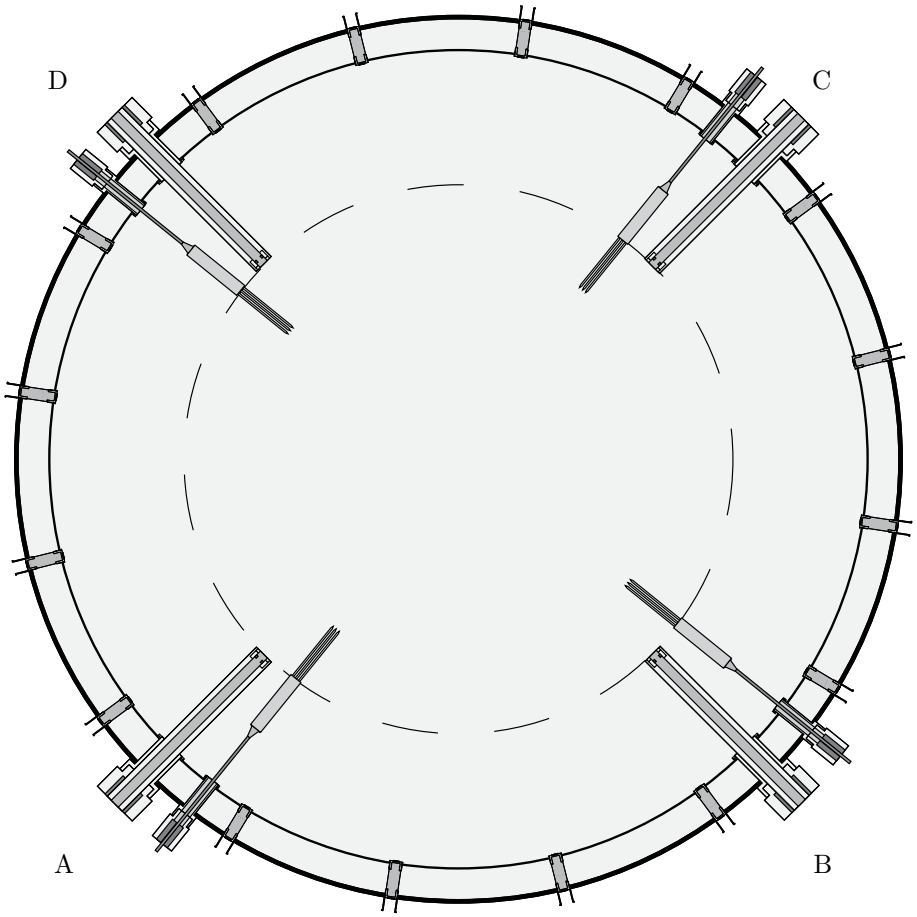

Figure 7.2: Diagram of Horizontal Port Labelling

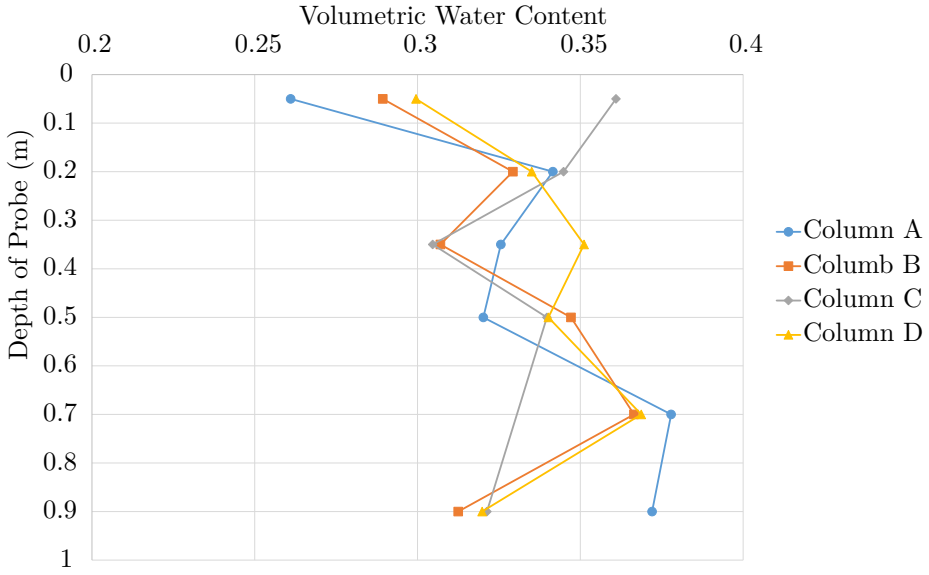

Figure 7.3: Initial Volumetric Water Content Distribution for Lysimeter 1 Using TDR Probes

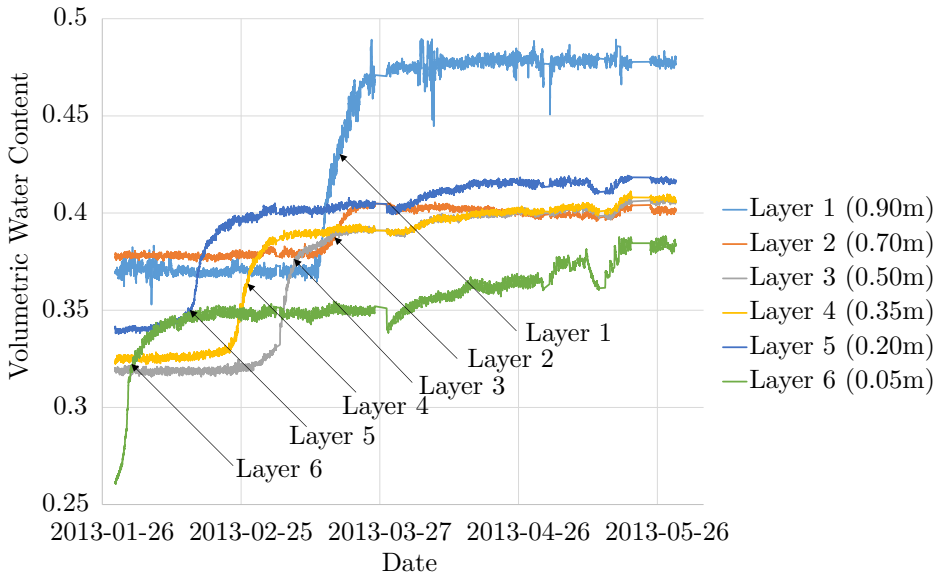

Figure 7.4: Lysimeter 1 Column A Wetting Profile for the First Wetting Period

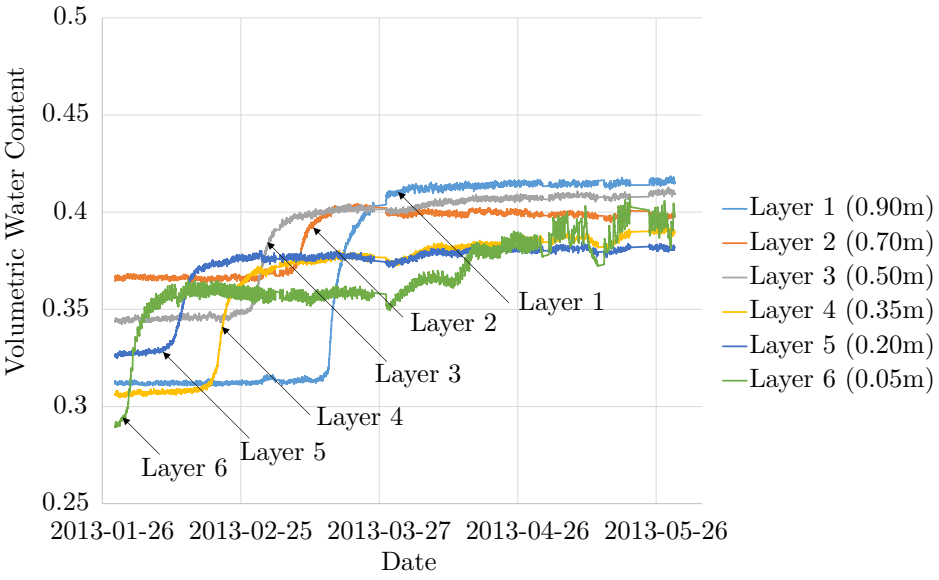

Figure 7.5: Lysimeter 1 Column B Wetting Profile for the First Wetting Period

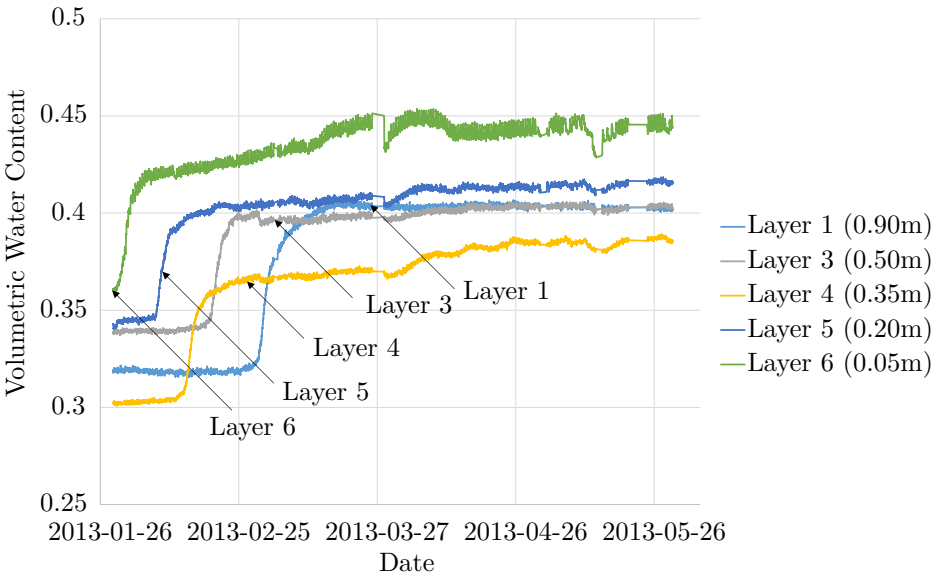

Figure 7.6: Lysimeter 1 Column C Wetting Profile for the First Wetting Period

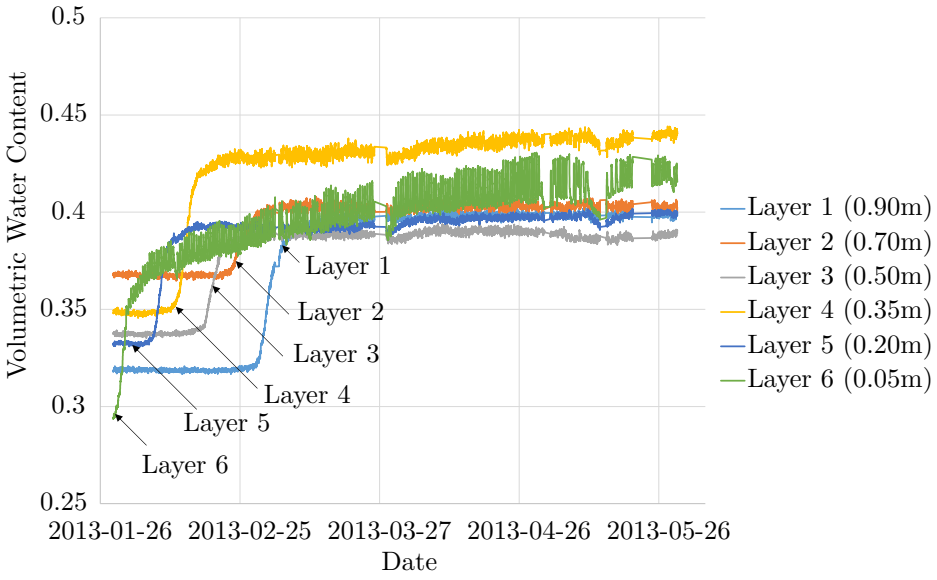

Figure 7.7: Lysimeter 1 Column D Wetting Profile for the First Wetting Period

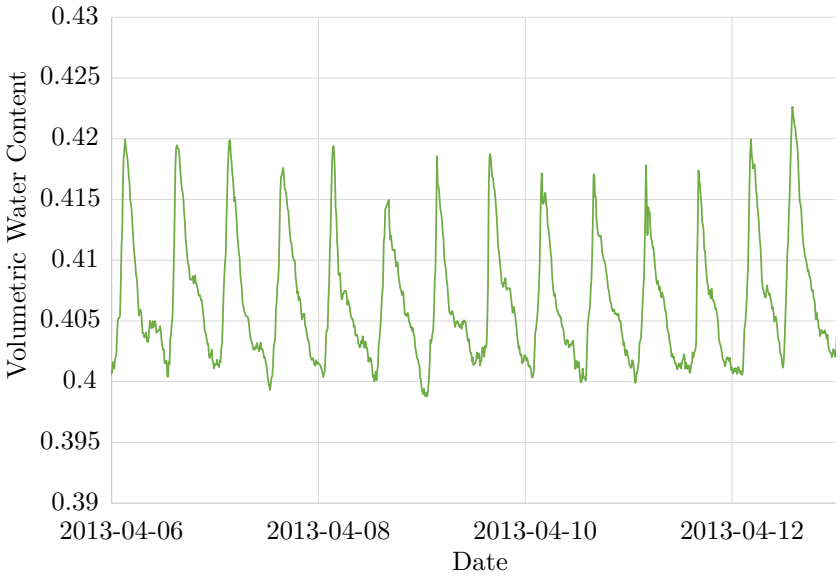

Figure 7.8: Lysimeter 1 Column D Layer 6 Daily Wetting and Drying Cycles for 1 Week

The upward trend seen for columns A and B only appeared after the layer 1 TDR probes above the lysimeter base registered the wetting front passing. Similarly, smaller upward trends were observed in layers 3, 4 and 5 around the same time, however not in the bottom two layers. This also coincided with larger quantities of water pooling on the surface of the lysimeter immediately after irrigation, all pointing towards the lysimeter reaching a high degree of saturation.

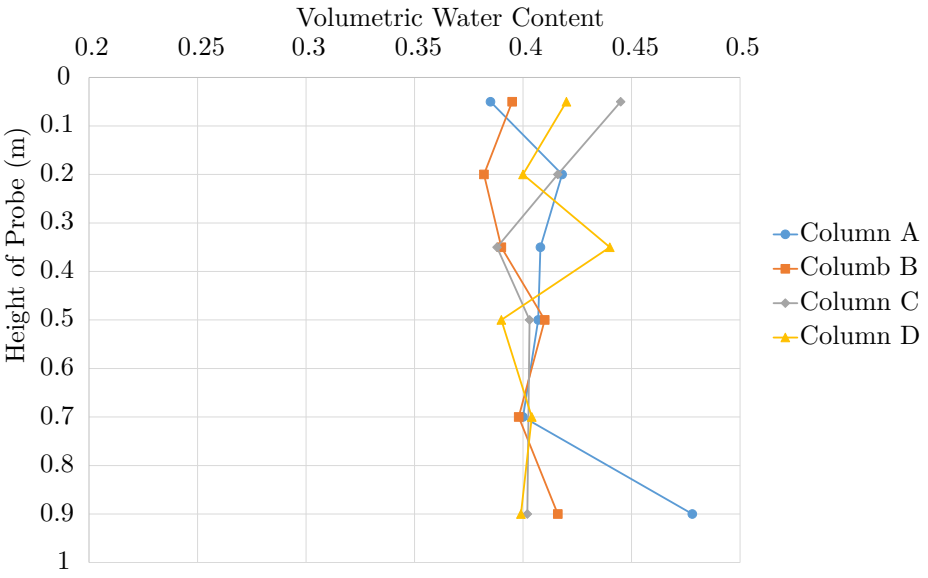

Figure 7.9: Final Volumetric Water Content Distribution for Lysimeter 1 Using TDR Probes

The final volumetric water contents for steady state conditions are displayed in Figure 7.9. It can be seen that there is good agreement with the majority of the probe readings, with all lying within a few percent of each other, apart from the lowest probe in column A which can be noted in Figure 7.3, was also reading relatively high compared to the other probes in the same layer.

In all, irrigation was applied for a period of six months for the first wetting of lysimeter 1. This

was well beyond the period of time observed that water took to permeate the length of the soil column, approximately 2 months. This was to ensure sufficient quantities of leachate could be collected for other members of the ROBUST project interested in the geochemistry and also to study the steady state conditions.

7.2.2 The First Drying Period

The lysimeter was left for a period of 5 months to dry after the first wetting period and before the second wetting period. The TDR probe readings for each column of probes are presented in Figures 7.10, 7.11, 7.12 and 7.13. The probe located in column C layer 2 is once again omitted as it was not functional. Also, there was concern over the reliability of the probe located in column A layer 1, which had significant scatter and an unusual increase in volumetric water content during a drying period.

Across the four figures, there was a general trend for the near surface probes in layer 6 to register the greatest decrease in volumetric water content, whilst the probes in layers 1 and 2 remain constant. The probes in layers 3, 4 and 5 all showed a similar response to the layer 6 probes; a general decrease in volumetric water content but to a much lesser extent. In particular, the water contents in layers 3, 4 and 5 were only observed reducing after a period of constant volumetric water content with the lower layers tending to display the greatest period of time between drying initiating and registering any decrease in water content.

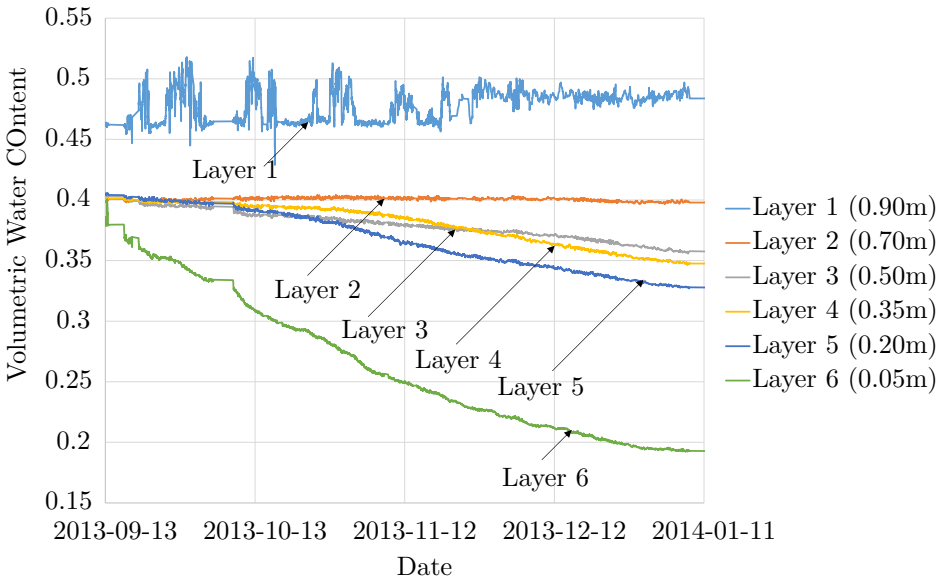

Figure 7.10: Lysimeter 1 Column A Drying Profile

The evolution of the water contents in column A over the drying period are plotted in Figure 7.14 and the final volumetric water contents for the drying period are plotted for each column of TDR probes in Figure 7.15. It can be seen that the probes near the surface in layer 6 registered the greatest decrease in water content, with subsequent layers responding with ever smaller changes as would be expected. In terms of depth, layers 1 and 2 were 0.90 m and 0.70 m from the surface respectively. With the layer 4 probes being situated 0.50 m below the surface, it was presumed that over the five month drying period, significant changes in water contents only occurred in the top 0.50 m to 0.70 m.

Over the course of drying, crack formations were observed using a web camera positioned above the soil surface. Select images from the web camera are given in Figure 7.16. In image 7.16a, the soil surface was unblemished apart from tiny mounds caused by worms during the previous wetting period. In image

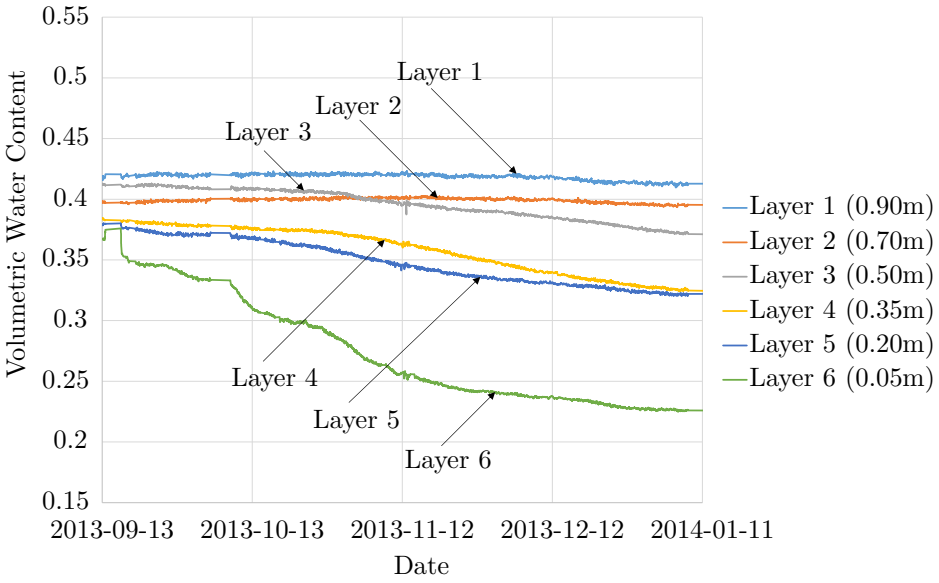

Figure 7.11: Lysimeter 1 Column B Drying Profile

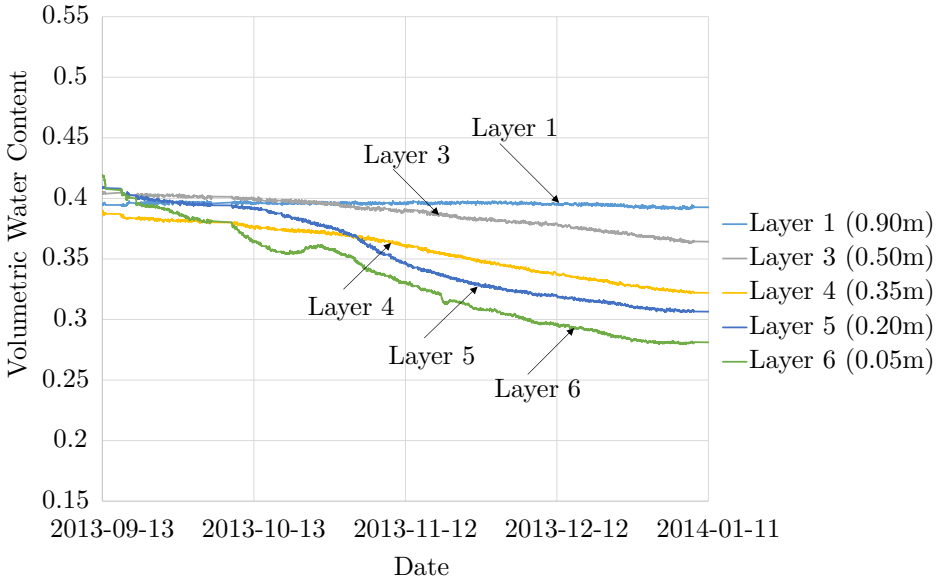

Figure 7.12: Lysimeter 1 Column C Drying Profile

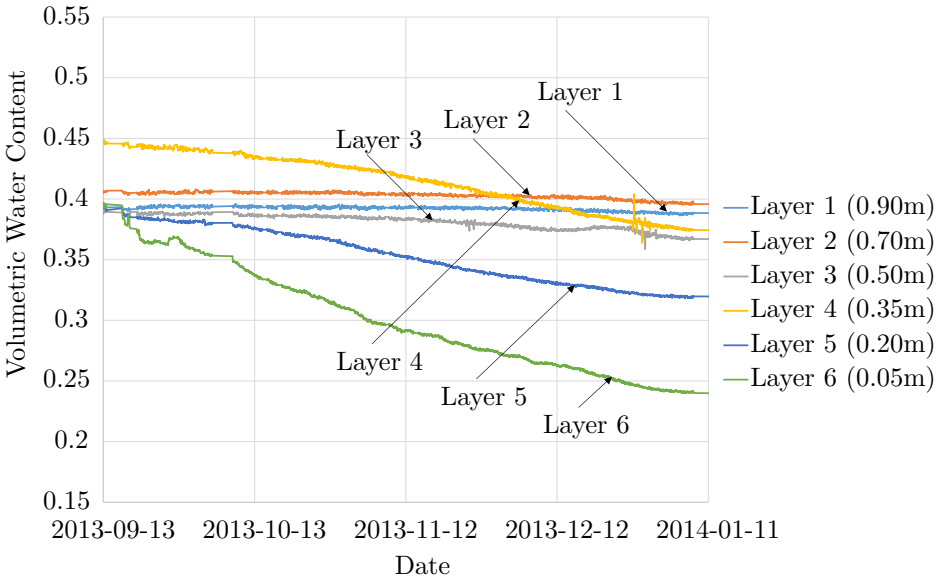

Figure 7.13: Lysimeter 1 Column D Drying Profile

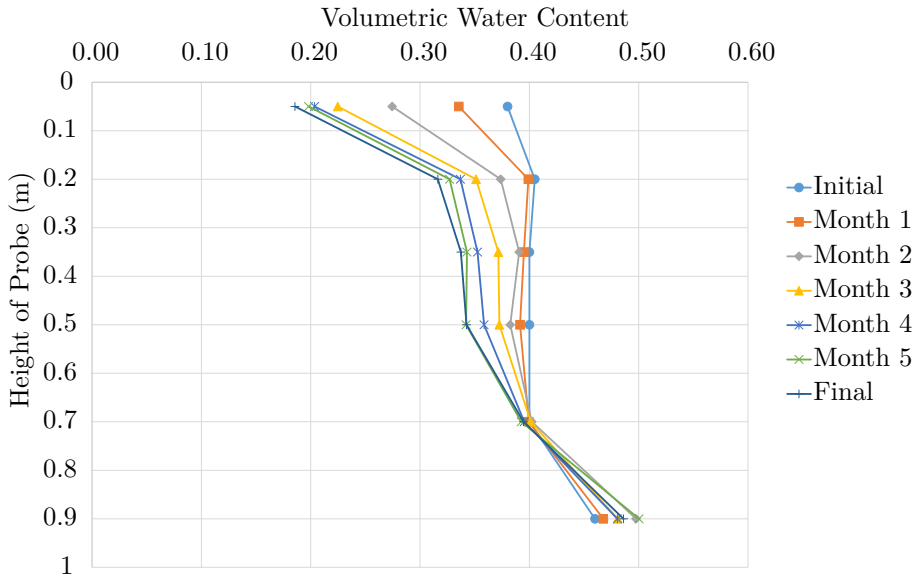

Figure 7.14: Evolution of Column A Water Contents over Drying Period

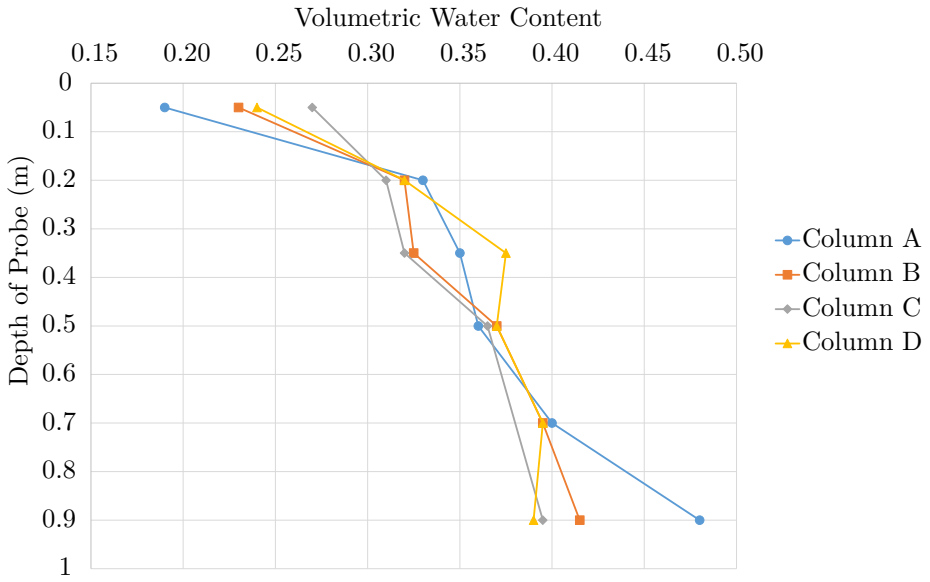

Figure 7.15: Final Volumetric Water Content Distribution for Lysimeter 1 after Drying

7.16b, cracks had begun to form, one series in the centre of the lysimeter and others further towards the outside. By image 7.16c, these cracks had widened and smaller cracks formed joining the cracking sites together. Later, these smaller cracks became more wider as seen in image 7.16d. By image 7.16e, a large crack has formed encircling the centre of the lysimeter, with some larger cracks running out to the soil columns circumference, where previously there had been none. In the final picture, image 7.16f, the soil has become a much lighter shade of brown when compared to the previous images. This indicated a higher state of desiccation with all the major cracks having continued to widen.

7.2.3 The Second Wetting Period

The second wetting period for lysimeter 1 began with the soil in a heavily cracked state, as seen in Figure 7.16. Water was applied as with the first wetting period, at 2 mm of rainfall per day (1 mm applied twice, 12 hours apart) to observe differences in permeability. Figures 7.17, 7.17, 7.17 and 7.17 display the point water contents of the four columns of probes over a 5 month drying period.

As before, the probe in column C layer 2 was not functioning and the probe in column A layer 1 was still behaving with significant scatter whilst the remainder of the probes were behaving within expectations. Unfortunately, an unforseen problem arose when there was an issue with the irrigation system during the wetting period. When this was resolved the effects were however noticeable in the figures, particularly by the probes in layer 6 for which there was period in the first month of no data.

Regardless of the pause in irrigation, it was still apparent that there was a well defined wetting front moving through the soil column. This time however, the wetting front approached both the probes in layers 5 and 6 almost simultaneously due to the high degree of cracking on the soil columns surface increasing infiltration. This can be seen in Figures 7.17, 7.17, 7.17 and 7.17 by the almost immediate, but less steep, increase in water contents measured by the layer 5 probes. This suggested that water was permeating 0.20 m below the surface of the soil column relatively easily.

The layer 4 and layer 3 probes responded similarly to the original wetting period, with relatively sharp increases in water contents being detected as the wetting front passed. The probes in the lowest two layers showed the smallest of variations. In column A, seen in Figure 7.17, the layer 2 probe only registered a decrease in volumetric water content of 0.005 over the drying period. As such, the wetting

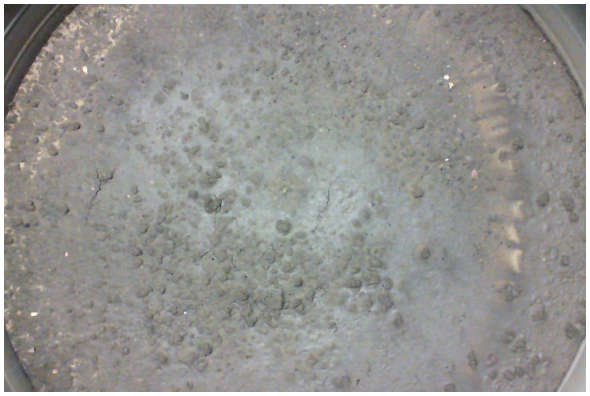

(a) 1 day

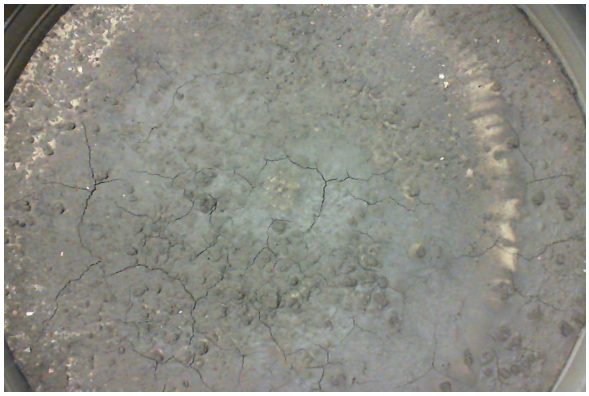

(b) 1 week

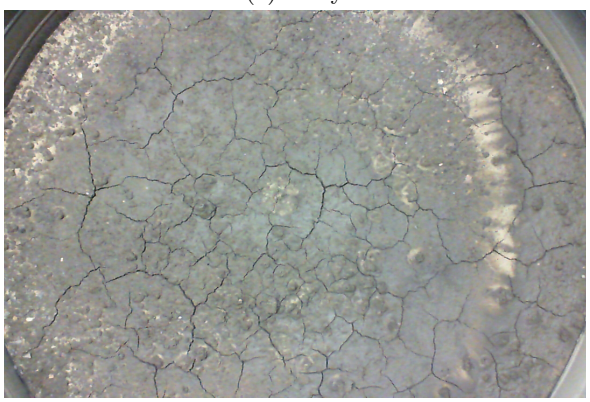

(c) 3 weeks

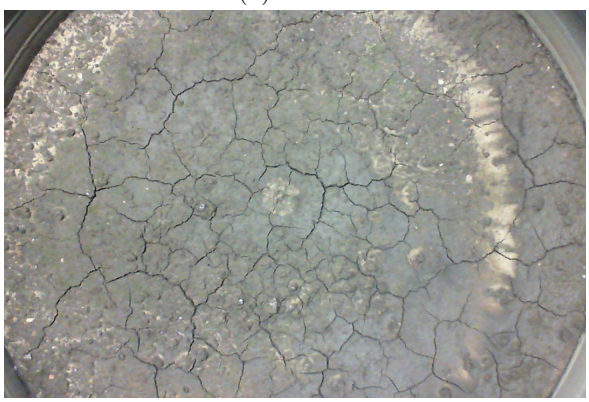

(d) 6 weeks

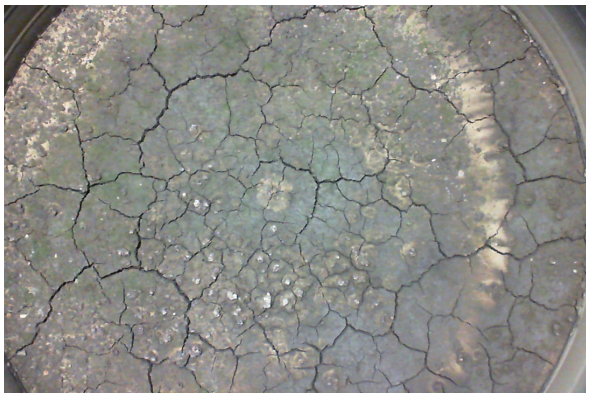

(e) 3 months

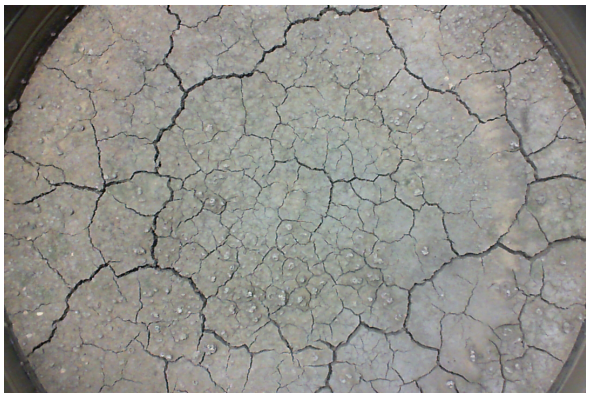

(f) 5 months

Figure 7.16: Successive Images of Crack formation during the first drying phase of Lysimeter 1

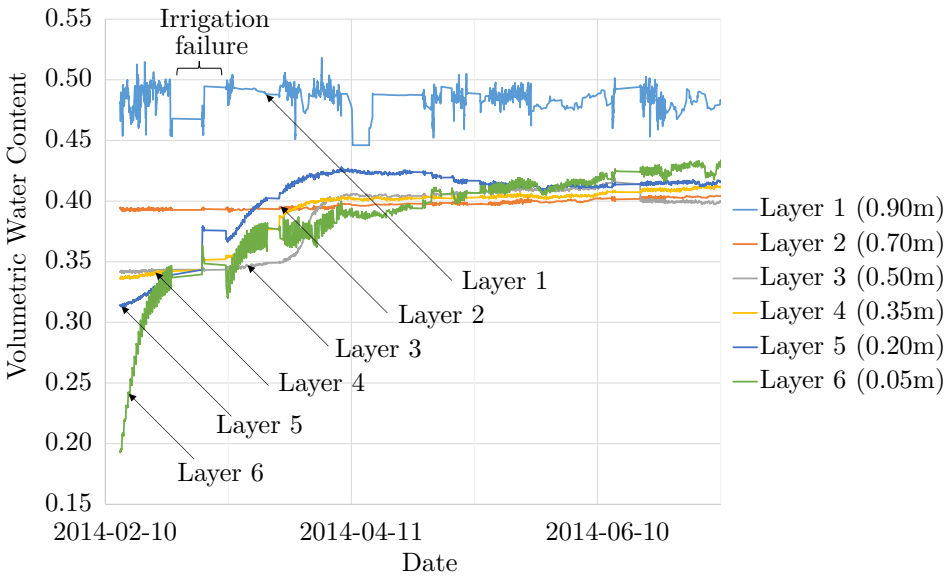

Figure 7.17: Lysimeter 1 Column A Wetting Profile for the Second Wetting Period

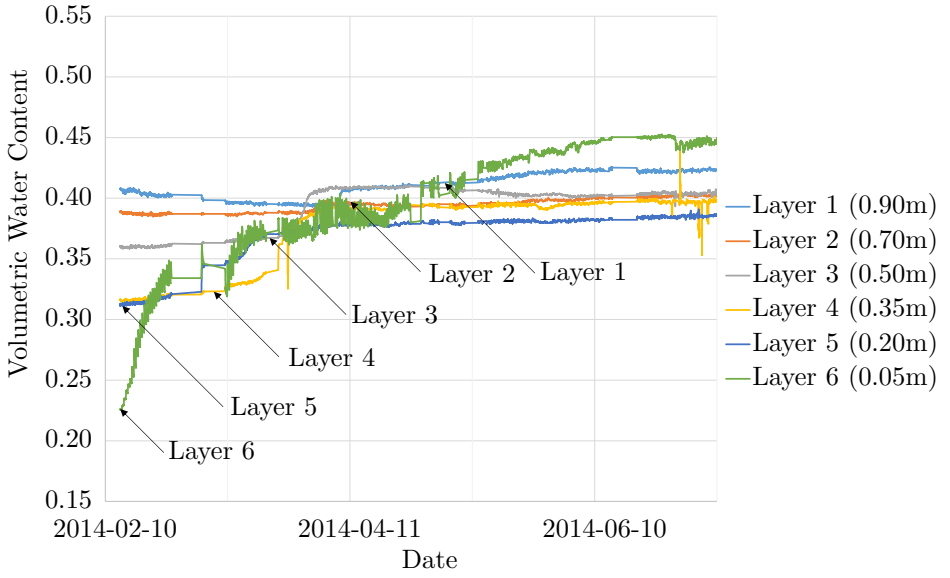

Figure 7.18: Lysimeter 1 Column B Wetting Profile for the Second Wetting Period

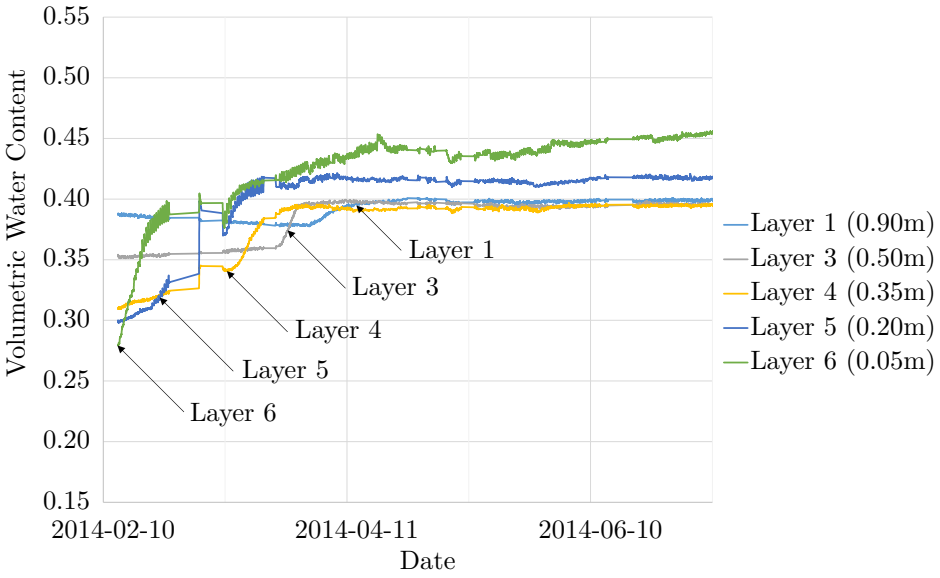

Figure 7.19: Lysimeter 1 Column C Wetting Profile for the Second Wetting Period

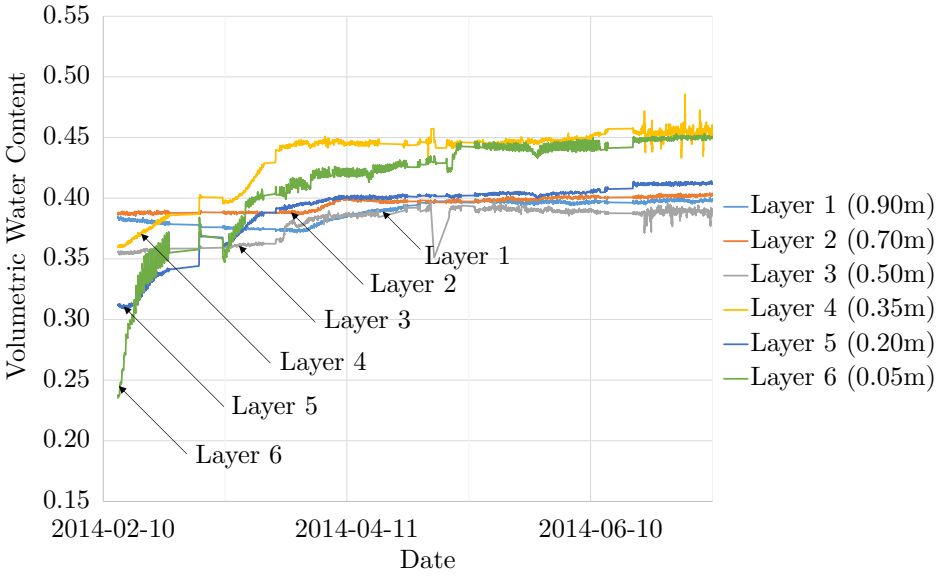

Figure 7.20: Lysimeter 1 Column D Wetting Profile for the Second Wetting Period

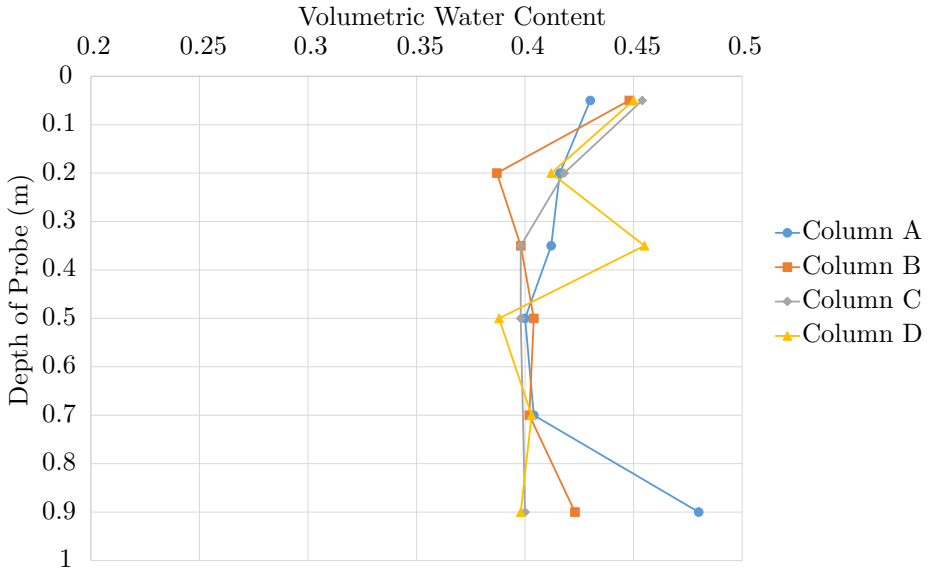

Figure 7.21: Final Volumetric Water Content Distribution for Lysimeter 1 after Second Wetting

front registered a similar increase in volumetric water content. The layer 3 and 4 probes in columns B, C and D all showed larger increases, corresponding to the larger decreases in volumetric water contents over the drying period.

The final water contents with depth are shown in Figure 7.21. The water contents below 0.20 m show no significant variation when compared to the final water contents from the first wetting phase. The water contents in the near surface layers however show more of a difference, with the probes in layer 5 (0.20 m) showing slightly higher water contents, particularly in column D. The probes buried just 0.05 m below the surface in layer 6 show significantly higher water contents across all four columns, potentially due to water filling cracks that have not fully closed.

7.3 Suctions

Suction measurement in the lysimeter was carried out using the tensiometers described in chapter 4. The improvements to the construction process of the tensiometers occurred simultaneously with the early monitoring of the control lysimeter and hence meant only a fraction of the final selection of reliable tensiometers were available. In particular, the first wetting period applied to the lysimeter used a number of tensiometers that were later found to be unreliable. Below, the behaviour of the reliable tensiometers is described over the first wetting period, the drying period and the second wetting period.

7.3.1 The First Wetting Period

The early data for the first wetting period was particularly unreliable, using many of the second generation tensiometers discussed in Chapter 4. The probes produced unexpected results, tending to wander and jump instantaneously to different values of suction. This meant that the initial wetting period for the lysimeter was not captured as intended.

A series of the first generation tensiometers was used to replace the broken tensiometers for the remainder of the wetting period and were placed in the top layer. The results from three tensiometers placed in the top layer of columns A, B and D (0.05 m depth) for a period of six days can be seen in Figure 7.22. The points at which irrigation was applied can be seen clearly as peaks in the pore water pressure, occurring twice a day at 12 hour intervals. The matric potentials were otherwise relatively

steady for the duration for the wetting period, whilst the figure shows a slight upwards trend.

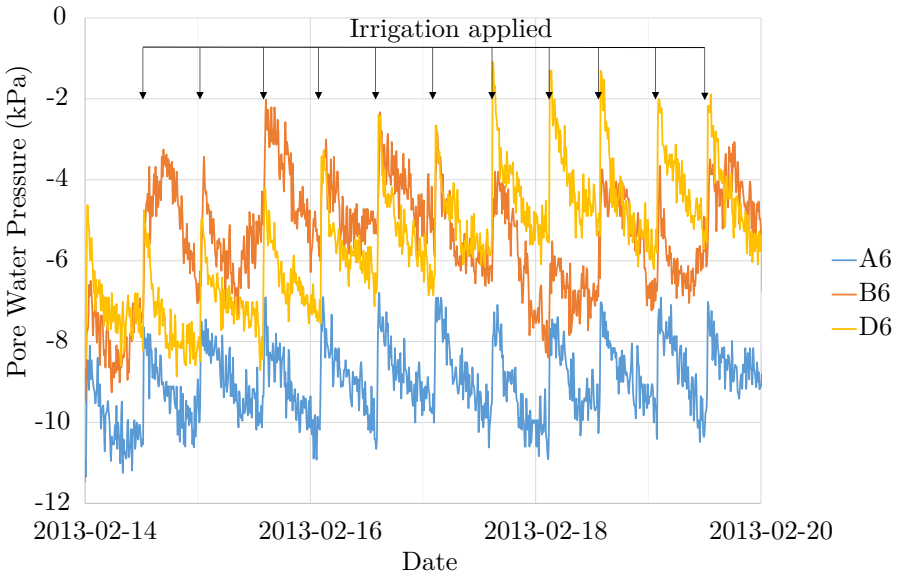

Figure 7.22: Suctions in Lysimeter 1 During First Wetting Period

7.3.2 The Drying Period

The drying period used a selection of seven tensiometers to monitor the suctions in the top two layers of the lysimeter, one of which provided erroneous readings due to unstable voltages. The other six tensiometers were placed in columns A, B and C on levels 5 and 6 near the surface.

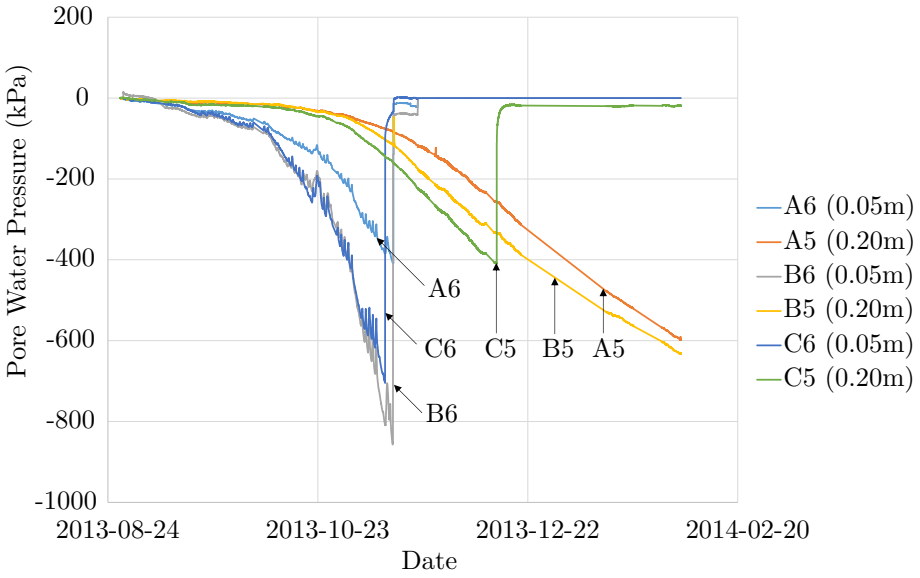

Figure 7.23: Suctions in Lysimeter 1 During First Drying Period

The results of the drying period are shown in Figure 7.23. It can be seen that the tensiometers in level 6 immediately showed a decrease in pore water pressure, reaching suctions as low as 900 kPa. The tensiometers in layer 5 instead remained steady for nearly 2 months before starting to show any significant suctions. Once below 100 kPa suction, the probes in layer 5 showed a relatively steady negative gradient

that was shallower than the near surface probes in layer 6.

The probes in layer 6 were seen to have a much higher variability than those in layer 5, and the variability followed a pattern. Figure 7.24 shows a three week period taken from Figure 7.23 to see the variability more clearly. It was apparent that over the three weeks, there were three periods of high variability and three periods of low variability. The periods of high variability were five days in length with five peaks and four troughs. In between each highly variable period, was a relatively smooth period.

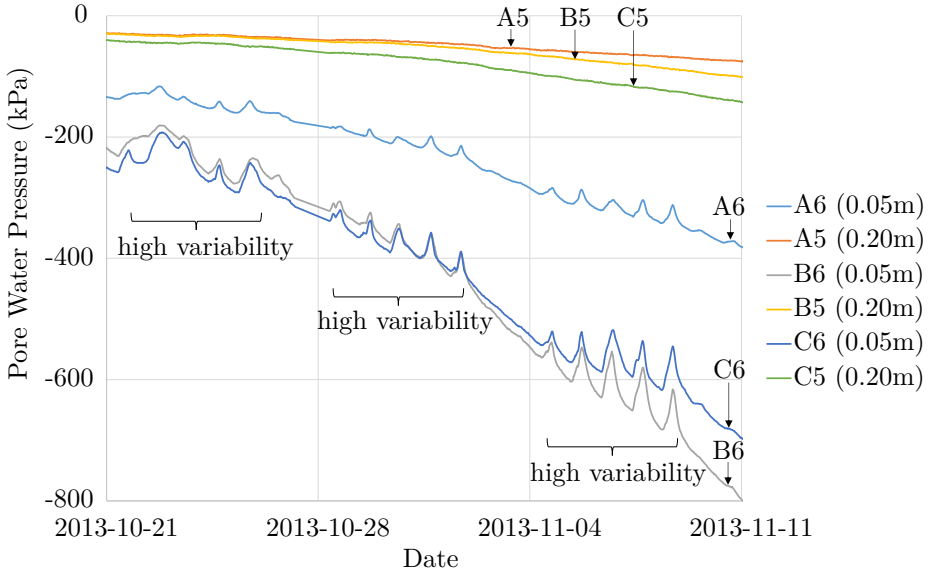

Figure 7.24: Variability in Suctions in Lysimeter 1 During First Drying Period

When the suctions were plotted alongside laboratory temperatures taken directly above the lysimeter surface, it was apparent the temperatures were having an effect on either the behaviour of the tensiometers, the suctions, or a combination of both. Figure 7.25 shows the effect quite clearly. The peaks in temperature corresponded with peaks in suction, and similarly the low points for temperature matched the low points for suction. It was discovered that the five day periods of high variability in Figure 7.23, were associated with more extreme cycling of temperatures in the laboratory during week days. Likewise, the calmer periods were associated with weekends. In the centre of Figure 7.25, the difference in temperature associated with a weekend can be seen to be around half that as compared to a weekday variation in temperature.

With regards to the magnitudes of the changes in suctions with temperature, there was a trend for the probes in layer 6 of Figure 7.23 to show increasing variability as suctions increased. The probes in layer 5 however, showed no such trend for the same given suctions. This suggested the temperature effect on layer 6, at 50 mm below the surface, was much greater than the layer 5 probes at 200 mm below the surface and approximately 180 mm in from the side wall of the lysimeter. This was assumed to be due the dampening of daily temperature variations deep inside the soil column.

In the laboratory, based on logged data a daily cycle in temperature was expected to be lower than 2 $°C$. As can be seen in Figure 7.25, the daily temperature change between peak and trough was approximately 1.5 $°C$. If the assumption was made that the lysimeters varied in temperature by a conservative 2 $°C$, the worst case scenario (based upon tensiometer VI1 in Figure 4.23) meant a corresponding change in pore water pressure in the order of -9 kPa. This in fact counteracts the trend observed for the tensiometer behaviour in the lysimeters, where an increase in temperature was associated with an increase in pore water pressure. This meant there was another temperature related cause of the variation.

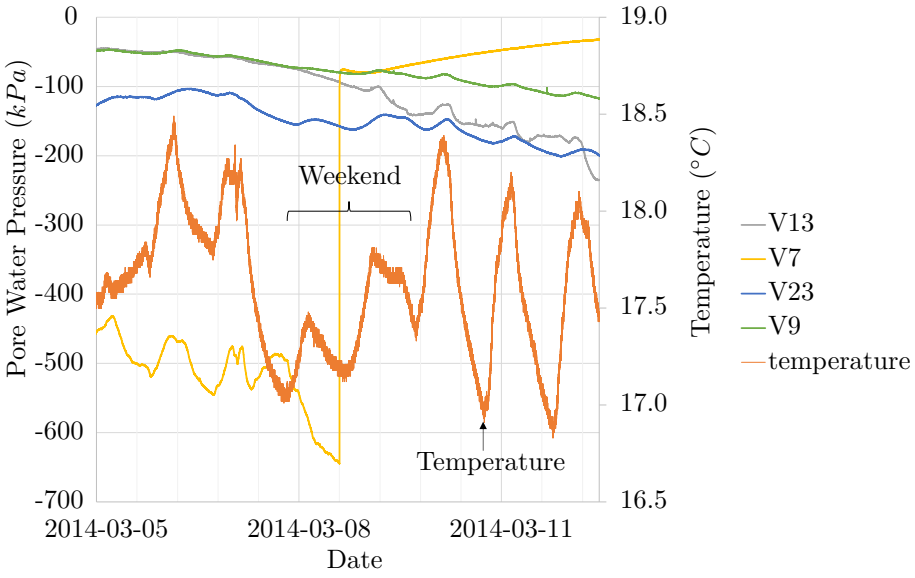

Figure 7.25: Variability in Suctions plotted with Temperature

An alternative theory was based around the expansion and contraction of the tensiometer materials as temperatures varied. As expansion occurred water would be pushed out from the tensiometer, and as contraction occurred water would be drawn in. As this cycle repeated for higher suctions, the availability of pore water would become more and more limited, and variability in measured potentials would be exaggerated. For this behaviour to be true however, a latency between temperatures and pore water pressures was expected. In Figure 7.25, the low suction measurements displayed a time lag between the temperature peaking and the suctions peaking. The time lag was associated with a damping effect of the lysimeter soil. The mass of soil insulating against significant changes in temperature. The higher suction measurements however, showed the peaks and dips aligning with the peaks and dips in temperatures concisely, effectively ruling the expansion/contraction theory out for these suctions.

Alternatively, the effect could have been caused by the expansion and contraction of water within the tensiometer itself, both the reservoir and porous stone. This would only be exacerbated in the presence of air, particularly in the case of poor saturation for which high temperature sensitivity was noted.

The final theory was based around changes in surface tension. With an increase in temperature, the surface tension of water decreases and similarly with a decrease in temperature, the surface tension of water increases. This trend appeared to match the data but not only that, it explained the increase in variability with higher suctions. With low suctions, only a limited number air-water interfaces could exist and changing the temperature had a limited effect. With higher suctions however, a far greater number of air-water interfaces formed, magnifying the effects of changing the temperature which were most apparent in the near surface probes.

7.3.3 The Second Wetting Period

The second wetting period started with the near surface soil in a heavily desiccated state. The tensiometers were therefore placed in layers 4 and 5 to prevent immediate cavitation. Figure 7.26 shows the results from six tensiometers, two placed in layer 5 and four placed in layer 4, over a period of two months.

The tensiometers showed good grouping for initial pore water pressures. The two tensiometers in layer 5 started with the lowest potentials, around 600 kPa suction and three of the probes in layer 4 initially read 280 kPa suction, with the tensiometer in port A4 starting between the two groupings.

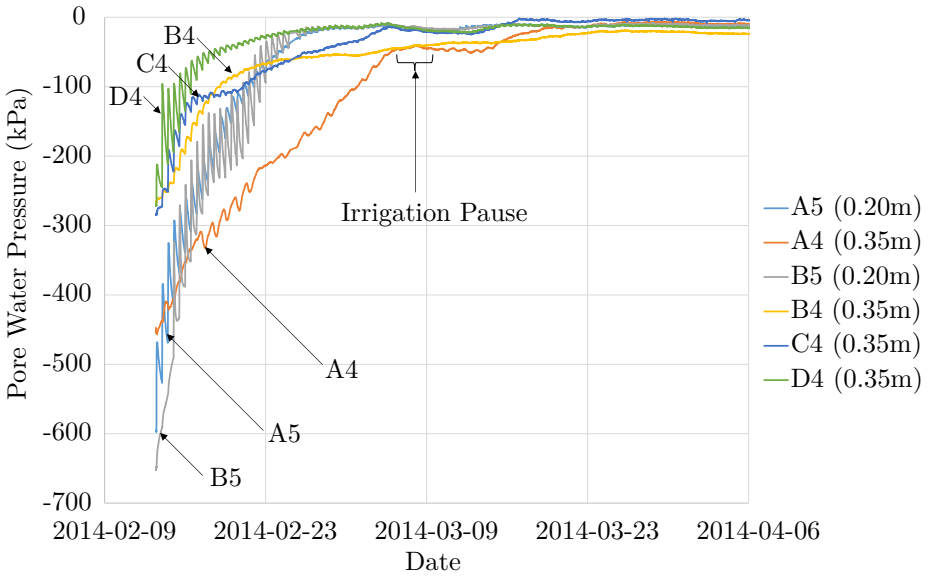

Figure 7.26: Pore Water Pressures in Lysimeter 1 over the Second Wetting Period

When irrigation was applied, there was an immediate response on both layers. The probes in the layer 5, being nearest to the surface, showed the sharpest and steepest response aided by the large degree of surface cracking. The irrigation cycles are clearly seen as sudden increase in matric potential, followed by a period of gradual decline, with an overall upward trend. The probes in layer 4 show the irrigation cycles in a similar manner, with the cycles in suction being clearly apparent yet more rounded in all but port D4 which presumable was located near a crack.

For all the tensiometers, low levels of suction were reached within 1 month of irrigation being applied. The potential exceptions, reaching suctions near 50 kPa after a month, were the tensiometers in ports B4 and A4. The tensiometers showed very different characteristics for the soil they were situated in. Port A4 had a relatively high initial suction and constant gradient. Had it not been for a two day pause in the irrigation from 2014-03-08 to 2014-03-09, it may have continued on its upwards trend and joined the other tensiometers earlier, sitting slightly below 0 kPa.

The readings from port B4 were more perplexing. The shape of the response was the same as the tensiometer in port D4, yet the response plateaued at 50 kPa suction whilst irrigation was still being applied. The response then tended to drift upwards through the period where irrigation had stopped for two days, eventually settling below the readings of the other probes. This whole process occurred over a six week period and for which no explanation could be given.

7.4 Permeabilities

The unsaturated permeabilities of the lysimeter were gauged using the point water content values provided by the installed TDR probes within the lysimeter's soil bulk volume. Wetting of the lysimeter samples was carried out by using the irrigation system to apply water to the surface of the lysimeter soil column. The propagation of the wetting front was then used to gauge unsaturated permeability indicators, which are proportional to the true unsaturated permeability of the soil but not within the scope of this work.

7.4.1 The first Wetting Period

Permeability indicators were estimated based on the rate of propagation of the wetting front by drawing tangents to the steady state conditions prior to irrigation, and tangents to the highest rate of change of

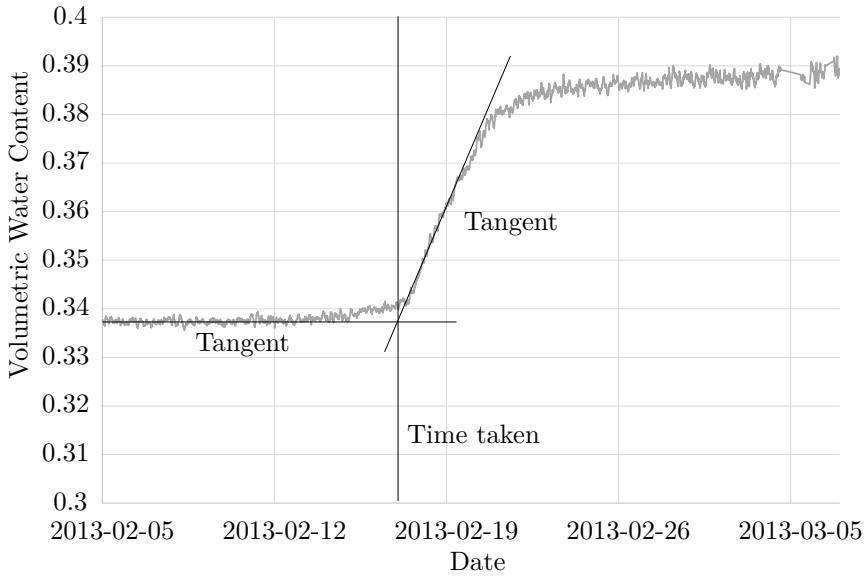

Figure 7.27: Volumetric Water Content Tangents

volumetric water content, as shown in Figure 7.27. The intersects were taken as an approximate date and time that the wetting front reached each level in the lysimeter. Using the distance between the probes, unsaturated permeability indcators based on the rate of propagation of the wetting front were calculated and are shown in Table 7.1. The data for layer transitions 3 to 2 and 2 to 1 for column C used the average arrival time of the wetting front for layers 3 and 1 due to the layer 2 probe not functioning correctly, yet being equidistant between the two.

Table 7.1: Calculated Permeability indicators from a Wetting Front passing through Lysimeter 1

Layer Transition	Column A (ms^{-1})	Column B (ms^{-1})	Column C (ms^{-1})	Column D (ms^{-1})
6 to 5	1.05×10^{-7}	1.40×10^{-7}	1.85×10^{-7}	1.99×10^{-7}
5 to 4	2.04×10^{-7}	1.95×10^{-7}	2.99×10^{-7}	3.51×10^{-7}
4 to 3	1.98×10^{-7}	2.06×10^{-7}	2.88×10^{-7}	3.13×10^{-7}
3 to 2	1.99×10^{-7}	2.56×10^{-7}	3.80×10^{-7}	3.63×10^{-7}
2 to 1	-2.26×10^{-6}	3.18×10^{-7}	5.36×10^{-7}	4.42×10^{-7}

The permeability indicators in lysimeter 1 varied between 1.05×10^{-7} ms^{-1} and 5.36×10^{-7} ms^{-1} with one anomaly from Column A in layer transition 2 to 1. This irregularity was caused by the wetting front apparently reaching both layer 1 and layer 2 almost simultaneously, as can be seen in Figure 7.4. This was likely caused by side wall flow saturating the base of the lysimeter, whilst the wetting front was gradually passing down the column. When the wetting front reached layer 2, it happened to coincide with a wetting front passing up the column and reaching layer 1. None of the other columns monitored displayed this behaviour, so significant side wall flow was likely occurring around column A.

As for the other permeability indicators, there was a trend for increased permeability towards the lower layer transitions. The five highest permeability indicators featured in the final two layer transitions. A graph displaying calculated permeability indicators against volumetric water contents is shown in Figure 7.28. There is a loose trend for increasing water contents leading to higher permeability indicators which was to be expected.

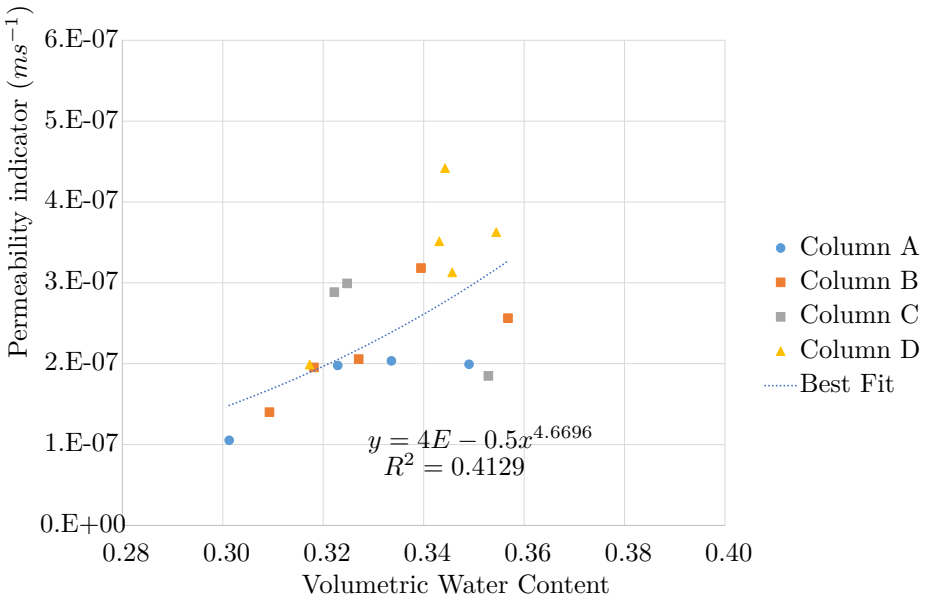

Figure 7.28: Permeability against Volumetric Water Content for the First Wetting Period

7.4.2 The Second Wetting Period

When the permeability indicators were calculated, there was less data due to both the wetting front effectively reaching the top two layers of probes simultaneously, and the lower layers in column A not registering distinct changes. The 13 permeability indicators that were calculated are presented in Table 7.2.

Table 7.2: Permeability indicators of Lysimeter 1 on the Second Wetting

Layer Transition	Column A	Column B	Column C	Column D
6 to 5	-	-	-	-
5 to 4	7.63×10^{-8}	4.99×10^{-8}	6.18×10^{-8}	5.94×10^{-8}
4 to 3	8.30×10^{-8}	2.08×10^{-7}	1.44×10^{-7}	1.59×10^{-7}
3 to 2	-	6.11×10^{-7}	6.01×10^{-7}	3.76×10^{-7}
2 to 1	-	3.80×10^{-7}	6.01×10^{-7}	-

The trend observed in Table 7.2 was for the lower water contents, found in the near surface layers, to lead to lower permeability indicators when compared to the more heavily saturated layers lower down the soil column. In magnitude, the permeability indicators calculated in layer transition 5 to 4 were a factor of ten smaller at 6.2×10^{-8} on average, than the permeability indicators in layer transitions 3 to 2 and 2 to 1, which on average were 5.3×10^{-7} and 4.9×10^{-7} respectively.

The permeability indicators are plotted against volumetric water contents in Figure 7.29. There is a much stronger trend here for the lower water contents to have lower permeabilities.

7.4.3 Permeability Discussion

The permeabilities measured in the triaxial sample (given in Chapter 6) were the greatest, between 1.0×10^{-6} ms^{-1} and 1.5×10^{-6} ms^{-1}. This was likely due to the higher degree of saturation that the permeabilities were measured over. Whilst comparatively, both the lysimeter permeability indicators were based on wetting fronts moving though soil of a much lower water content.

The permeability indicators during the lysimeter wetting periods were calculated based on the prop-

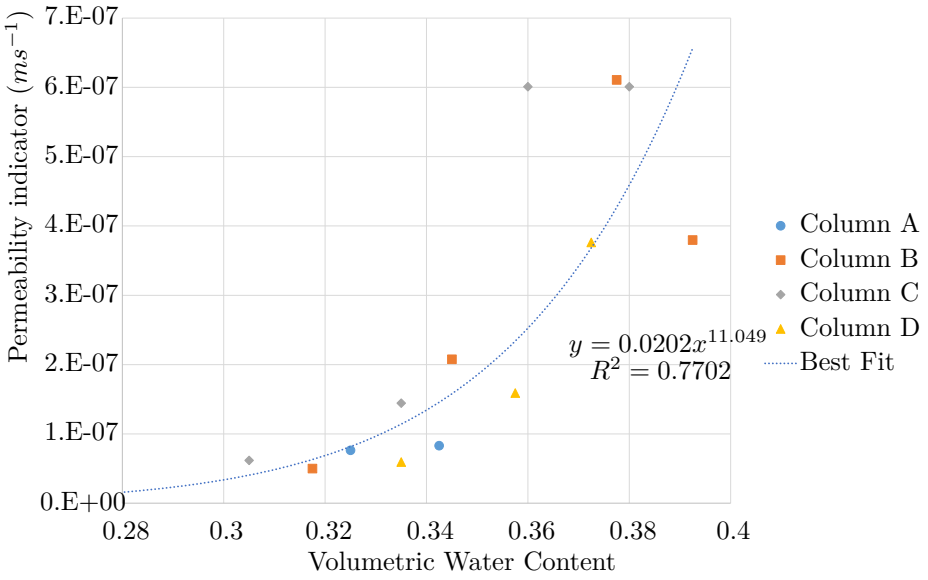

Figure 7.29: Permeability indicator against Volumetric Water Content for the Second Wetting Period

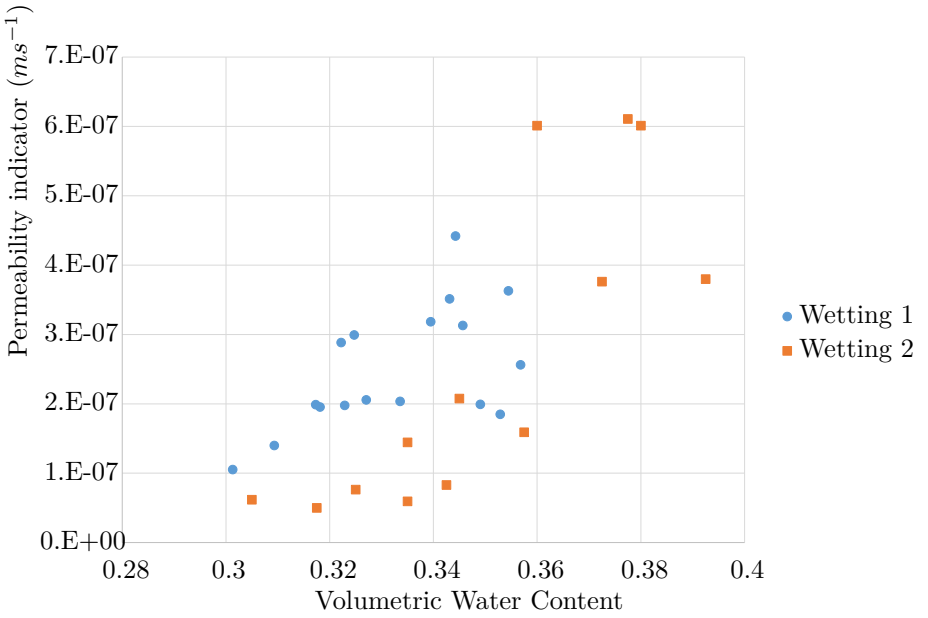

Figure 7.30: Graph depicting the Lysimeter 1 Wetting Front Permeabilities against Average Initial Volumetric Water Contents

agation of the wetting fronts. The results for the first wetting period were an order of magnitude smaller than the triaxial permeabilities, between $1.1\times10^{-7}\ ms^{-1}$ and $5.4\times10^{-7}\ ms^{-1}$. The second wetting period had similar results, with permeability indicators spread between $5.0\times10^{-8}\ ms^{-1}$ and $6.1\times10^{-7}\ ms^{-1}$.

Taking the lysimeter permeability indicators and plotting against the average initial volumetric water content for each layer transition and for each wetting period gave Figure 7.30. Based on the figure, there was a loose trend for layer transitions of lower water content to have lower permeability indicators. This was potentially due to the effect of soil shrinkage causing a change in void size distribution and a change in the degree of saturation.

The difference in the level of agreement the trends offer between the two different wetting periods is likely down to how the water contents were estimated. The initial water contents from when the lysimeter was first filled may have been more variable than the water content distribution for the second wetting phase. The level of scatter can be seen in Figure 7.3 and this likely continued in the 20 mm thick layers between the levels the probes were buried at regardless of quality control on the water contents during the filling process. The change in water contents down with depth after the drying phase would have been much more continuous and hence the average water content estimations between layers would have been much better.

7.5 Soil Water Retention Behaviour

The soil water retention behaviour of the lysimeter soil was assessed using two methods. The first method used a compilation of both the water content and suction data from the lysimeter, seen previously. The second method, discussed in Chapter 6, used smaller samples, prepared from the soils used in testing permeabilities in the triaxial cell.

7.5.1 Soil Water Retention Behaviour in the Lysimeter

The soil water retention behaviour of the lysimeter soil column was plotted using data from in-situ TDR probes and tensiometers over the course of a drying period. The results for six tensiometers and their corresponding TDR probes are plotted in Figure 7.31. Three tensiometers were placed in layer 6 and three tensiometers in layer 5.

All the soil water retention behaviours started at similar volumetric water contents, between 0.38 and 0.43, and similar suctions, between 0 kPa and 20 kPa. During the drying process, the suctions tended to decrease with volumetric water content however there was significant variability.

The retention behaviours determined using the layer 6 near surface probes were particularly varied. Both A6 and B6 initially displayed significantly steeper gradients than any of the other ports. Port C6 on the other hand, had a much shallower initial gradient and showed a slight increase in volumetric water content between 200 kPa and 300 kPa suction.

The results from the ports on layer 5 show stronger agreement. Readings from A5 and C5 were in very close agreement until 130 kPa suction, at which point they diverged; whilst the readings from port B5 started at a lower initial water content with a steep gradient before shallowing out and converging with the results from C5.

The discrepancies between the layer 6 and layer 5 readings were likely due to the influence of cracks forming throughout the drying process, reducing the bulk permittivity of the material around the TDR prongs and hence reducing the interpreted volumetric water content. This made sense for the readings in ports A6 and B6. For the same suctions, significantly lower water contents were observed when compared to the readings from layer 5. The 75 mm length of the TDR probes, and hence their relatively large sample volume when compared to tensiometers, was the likely cause for this. The probability of a TDR probe encountering one of the many cracks near the soil surface was considered relatively high when compared

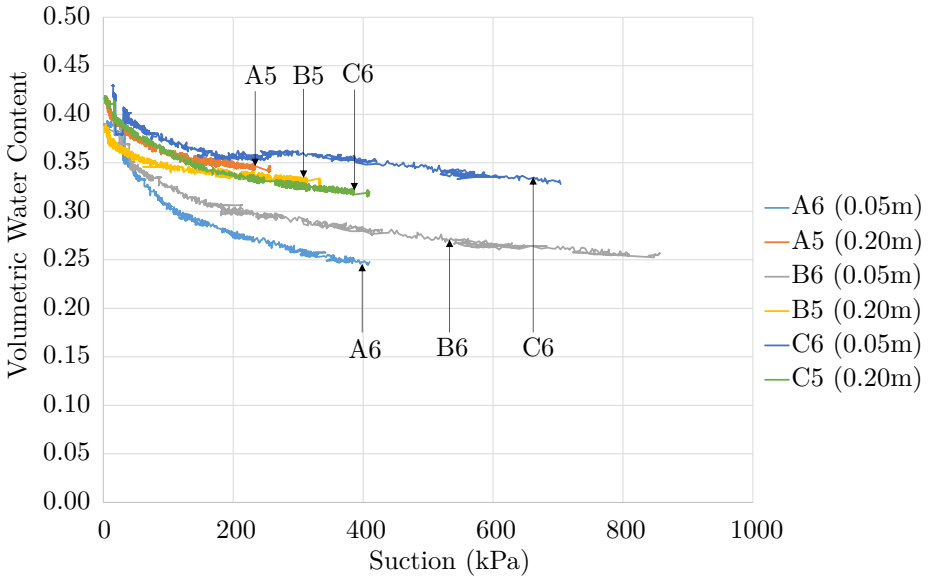

Figure 7.31: Drying Curves Obtained for Lysimeter 1's Soil determined using in-situ TDR Probes and Tensiometers

to the tensiometers 10 mm diameter front face.

As for the readings from port C6, there was one potential explanation for the odd behaviour between 200 kPa and 400 kPa suction. It relied upon the TDR probe having avoided all near surface cracks, meaning the probe remained buried in a shrinking soil mass at a relatively steady gravimetric water content. As the soil shrunk away from the surrounding cracks this may have resulted in an increase in volumetric water content locally, however this was unproven.

It was therefore concluded from the data, that the soil water retention behaviour determined in layer 5 was the most representative for the bulk soil.

7.5.2 Soil Water Retention Behaviour Comparison

For comparison, all three of the small samples tested and the three data series from ports A5, B5 and C5, being considered as representative, were plotted together. The results are shown in Figure 7.32.

It can be seen that there were differences between the data measured in the soil column and the small laboratory samples. The laboratory samples started at the highest volumetric water contents at around 0.43. Ports A5 and C5 started at suctions of 0.42 whilst port B5 started at the lowest water content of 0.39.

The soil water retention curves from the lysimeter had steep initial gradients before sweeping out to meet up with the three curves from the smaller samples, whilst they in turn had a much more gradual change in gradient. Unfortunately, the data for the ports in layer 5 did not measure higher suctions. It was therefore impossible to tell if the two data sets would align at higher suctions or not.

It was concluded that the results were promising. The soil water retention curves from the large lysimeter were believable. Furthermore, they aligned well with the data from smaller laboratory samples, unlike the water retention behaviour seen in layer 6. It was unknown if the disparity in soil water retention behaviours was due to difference in material or difference in method. The main explanation would be that the drying curves in the lysimeter represent scanning curves, with the small samples more closely representing a primary drying curve and the lysimeter results trending towards these values. It would be expected that when the lysimeter curves intersect the primary drying path, they would follow the trend

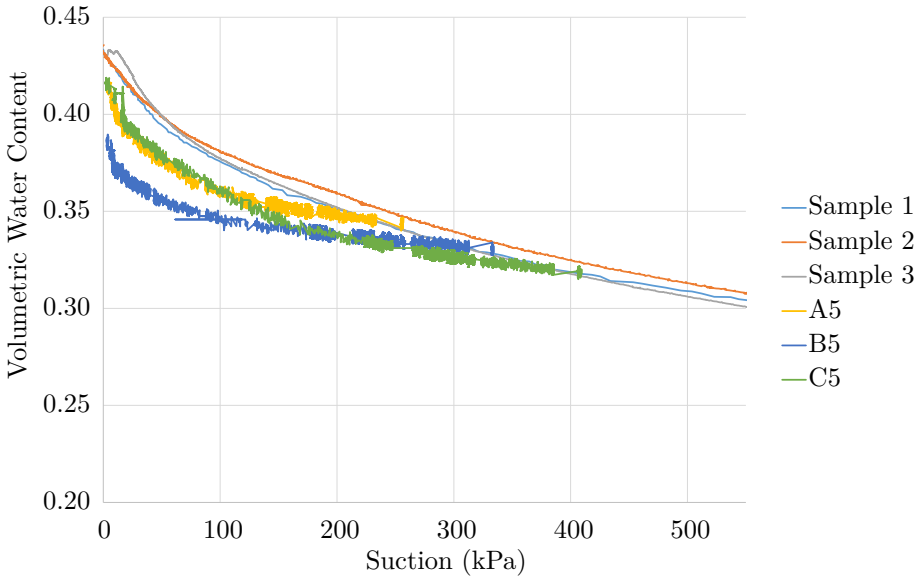

Figure 7.32: Soil Water Retention Behaviour Comparison

of the primary drying path. Further work using tensiometers capable of measuring higher suctions may help resolve this.

7.6 Conclusion

In conclusion, small laboratory samples of lysimeter soil were tested to determine permeability and soil water retention behaviour for comparison to a large lysimeter undergoing wetting and drying cycles. Permeabilities for the small samples were found to be an order of magnitude higher, at 10^{-6} on average, when compared to the velocity of the wetting front permeating the large lysimeter on both the first and second wetting period. When the first wetting period was compared to the second wetting period, it was found that the sites where lower volumetric water contents were reached during drying tended to have lower wetting front propagation velocities, as with an unsaturated permeability function.

Suctions measured in the lysimeters proved to be susceptible to temperature changes on a daily cycle. This was particularly significant at the higher suctions associated with low volumetric water contents. It was concluded that the two major factors for the variations were due to a change in suctions within the soil and expansion of reservoir pore water, as oppose to temperature effects on the tensiometers which were proven to be minimal.

Soil water retention behaviour, measured using two techniques, was compared. The data sets from the large lysimeter and soil water retention behaviour testing equipment proved to be similar yet there were clear differences. These differences were primarily due to cracking in the near surface zone yet in deeper layers the results may have been more representative of scanning curves. The data sets were comparable but it cannot currently be determined if the disparity between the data sets was due to experimental method or due to physical difference in the soils tested, hence further experimentation may be needed to clarify the results.

Chapter 8

Conclusions and Further Work

8.1 Summary

This thesis described the design, construction and instrumentation of large lysimeters for the measurement of soil water retention behaviour and permeabilities. The design elements of the large lysimeters allowed for integration with the aims and goals of other academics working on the ROBUST project, in the areas of computational modelling and geochemistry.

Three lysimeters were fully built, with the novel leachate drainage system allowing side wall flow to be differentiated from water passing directly through the soil bulk volume. This improved upon previous designs, where both were sidewall flow and leachate mixed, meaning results likely became irrelevant. The lysimeters implemented three different port systems for three different types of probes: glands for Time Domain Reflectometry (TDR) probes, which had the flexibility to be placed anywhere in a soil column; glands and port extensions, to deliver tensiometers up to 180 *mm* deep, straight into the soil column, avoiding the influence of boundary conditions; and self healing, hermetically sealing rubber septums allowing for future work with Electrical Resistivity Tomography (ERT).

The TDR point water content system was controlled by a new, custom built, data acquisitions program. This had many advantages over other software packages: it leveraged the power of The Cloud as an online unified data repository; provided an interface for connectivity to any serial port device; offered templating for simplified setup; and realtime feedback for the end user. All data was queryable from the repository, which maintained a backup of all raw data, so the data pertaining to any time period or probe could be requested if and when needed.

A commercial TDR100 device and multiplexers were used as the centre of the moisture content measurement system. Probes were custom built, which when combined with the logging software, made significant reductions to the set up costs. The probes were calibrated for offsets and probe constants rigorously, where it was found the recommended procedure left significant room for error. This was corrected by using the new software system to automate much of the calibration process, reducing the 95% confidence intervals for probe offsets down to $\pm 0.02\%$ and thereby increasing probe accuracy for determining permittivity significantly. This was combined with a linear custom calibration for the soil used in the control lysimeter, so as to correctly interpret the measured permittivities as the correct volumetric water contents.

Suctions were monitored using high capacity tensiometers developed at Durham University. The assembly of the tensiometer components was brought to Durham to reduce failure rates by ascertaining problems with earlier build practices and making improvements to the process. Initially, problems were encountered with materials but once the spacers were altered to stainless steel and the High Air Entry

Value (HAEV) stones were confirmed to have an air entry value of 1500 kPa, many improvements were made. The cabling on the back of the tensiometers was wired directly into the transducers, limiting the quantity of wire that had to fit in the tensiometer casing. The wires were coated in acrylic to prevent short circuiting and water ingress affecting the back of the transducer and two new bonding agents, M-bond 600 and M-bond 610, were tried to great success, with 1 MPa sensors reading suctions of up to 960 kPa.

Three large lysimeters were filled with contaminated soil from the St Anthony's Leadworks, located in Newcastle. The first lysimeter was a control, which was made to best represent field conditions, by hand tamping the soil in 20 mm thick layers to the correct density. The two other lysimeters were filled with the same soil but were amended with a novel remediatitive material called Water Treatment Residual (WTR), and a combination of WTR and compost. The second two lysimeters were hand tamped using the same method as the control, but resulted in significantly different properties.

Soil water retention behaviour and permeabilities were assessed in both small laboratory samples and in the large control lysimeter. The permeabilities in the 100 mm diameter sample tended to 2.0×10^{-6} ms^{-1} for samples near saturation under a confining pressure of 10 kPa and head difference of 6 kPa. The wetting fronts for both the wetting cycles were used to assess the unsaturated flow in the control lysimeter, resulting in permeabilities an order of magnitude smaller. In particular, the wetting front moving through the heavily desiccated layers near the soil surface, were found to have permeabilities in the order of magnitude of 6.0×10^{-8} ms^{-1}.

The soil water retention behaviour of three small 80 mm diameter samples, each 20 mm thick, were assessed using soil water retention behaviour testing equipment developed at Durham University. When compared to the drying cycle in the control lysimeter, the results for the bulk material were very similar. The drying curves for the lysimeters soil was found to sit beneath the results for the smaller test samples, with a steep initial gradient followed by a shallow gradient as the results for both converged. Near surface readings were however affected significantly by cracking, reducing the usefulness of the retention curves generated.

8.2 Future work

- Lysimeter testing: With both the amended lysimeters finished, future work should concentrate on fully instrumenting these with a suite of reliable tensiometers and applying wetting and drying cycles. The control lysimeter should continue as it was before but ideally with higher capacity tensiometers situated in the bulk material to fully capture the soil water retention behaviour.
- Software: the software is in a usable state although it lacks a comprehensive user interface to make it more accessible to a normal user. This should be the next thing to implement before any new features such as tagging probes with experiment names or location metadata.
- Tensiometers: Although much progress has been made with tensiometers, moving to a higher capacity transducer would be recommended based onf testing the 1 MPa sensors. This would allow for saturation at higher pressures and ultimately higher suctions could be measured to get a more complete picture of the soil water retention curve in the large lysimeter environment.
- TDR probes: The TDR probes functioned extremely well for monitoring point water contents. In the future it would be useful to implement calculations of real permittivity in with the waveform analysis by taking account of the losses due to conductivities although considerable work is required on finding the best implementation. In addition, two probes failed during testing and a method of allowing these to be replaced could be developed.

References

[1] H. L. Curtis and F. M. Defandorf, "Dielectric constant and dielectric strength of elementary substances, pure inorganic compounds, and air," *International Critical Tables of Numerical Data, Physics, Chemistry and Technology, McGraw-Hill, New York.*, pp. 73–81, 1929.

[2] D. A. Robinson, S. B. Jones, J. M. Wraith, D. Or, and S. P. Friedman, "A review of advances in dielectric and electrical conductivity measurement in soils using time domain reflectometry," *Vadose Zone J*, vol. 2, no. 4, pp. 444–475, 2003.

[3] D. G. Toll, S. D. N. Lourenço, and J. Mendes, "Advances in suction measurements using high suction tensiometers," *Engineering Geology*, vol. 165, no. 0, pp. 29–37, 2013.

[4] R. E. Hester, R. M. Harrison, J. E. Harries, P. K. Hopke, J. T. Houghton, N. J. King, S. Matsui, D. H. Slater, T. G. Spiro, D. Taylor, F. Warner, J. L. Schnoor, L. E. Erickson, G. M. Pierzynski, P. Doyle, J. N. Lester, J. Denner, P. Young, S. Pollard, P. Crowcroft, D. L. Rimmer, A. Younger, A. K. Barbour, G. Griffiths, S. Smith, A. J. Lennon, M. Lambert, M. Harris, M. E. Consultants, P. A. Wood, N. A. Burdett, J. J. Cairns, P. A. Chave, P. Crutzen, H. Fish, and M. J. Gittins, *Contaminated Land and its Reclamation*, vol. 7 of *Issues in Environmental Science and Technology*. London: The Royal Society of Chemistry, 1997.

[5] B. J. Alloway, *Zinc in Soils and Crop Nutrition*. International Zinc Association and International Fertilizer Industry Association Brussels, Belgium and Paris, France, 2008.

[6] M. Moats, V. Ramachandran, W. Robinson, and D. W. G., *Extractive Metallurgy of Nickel, Cobalt and Platinum Group Metals*. Elsevier, 2011.

[7] A. Gomez-Caminero, P. Howe, M. Hughes, E. Kenyon, D. Lewis, M. Moore, J. C. Ng, A. Aitio, and G. Becking, *Environmental Health Criteria 224 Arsenic and Arsenic Compounds*, vol. 13. Geneva: World Health Organization, 2 ed., 2001.

[8] R. A. Wuana and F. E. Okieimen, "Heavy metals in contaminated soils: A review of sources, chemistry, risks and best available strategies for remediation," *ISRN Ecology*, vol. 2011, p. 20, 2011.

[9] R. Naidu, E. Smith, G. Owens, and P. Bhattacharya, eds., *Managing Arsenic in the Environment: From Soil to Human Health*. CSIRO Publishing, 2006.

[10] Organisation for Economic Co-operation And Development, "Risk reduction monograph no. 5: Cadmium. OECD environment monograph no. 104," 1995.

[11] M. Cavendish, *Chromium*. New York: Juvenile Nonfiction, 2005.

[12] T. Swaddle, *Inorganic Chemistry: An Industrial and Environmental Perspective*. Science, 1997.

[13] Z. Goffer, *Archaeological Chemistry*. London: John Wiley & Sons, 2nd ed., 2006.

[14] B. J. Alloway, ed., *Heavy Metals in Soils - Trace Metals and Metalloids in Soils and their Bioavailability*. Dordrecht, Netherlands: Springer, 1995.

[15] Schwarzbauer, *Organic Contaminants in Riverine and Groundwater Systems: Aspects of the Anthropogenic Contribution*. Dordrecht, Netherlands: Springer, 2006.

[16] C. P. Nathanail and R. P. Bardos, "Chemistry for contaminated land," in *Reclamation of Contaminated Land*, pp. 16–33, Chichester, England: John Wiley & Sons, Ltd, 2005.

[17] E. V. Lau, S. Gan, H. K. Ng, and P. E. Poh, "Extraction agents for the removal of polycyclic aromatic hydrocarbons (pahs) from soil in soil washing technologies," *Environmental Pollution*, vol. 184, no. 0, pp. 640–649, 2014.

[18] Environment Agency, "Dealing with contaminated land in England and Wales," 2007. URL: http://publications.environment-agency.gov.uk/pdf/GEHO0109BPHA-e-e.pdf Accessed: 21-06-2010.

[19] P. Crowcroft, J. Denner, L. Erickson, G. Griffiths, M. Harris, M. Lambert, A. Lennon, G. Pierzynski, S. Pollard, D. Rimmer, J. Schnoor, S. Smith, P. Wood, P. Young, and A. Younger, *Contaminated Land and its Reclamation*. The Royal Society of Chemistry, 1997.

[20] S. Manning and A. Gittins, "Wiltshire Council contaminated land supplementary planning document," tech. rep., Wiltshire Council, UK, 2012.

[21] A. Otten, A. Alphenaar, C. Pijls, F. Spuij, and H. de Wit, *In Situ Soil Remediation*. Boston: Kluwer Academic Publishers, 1997.

[22] D. Corwin and R. LeMert, "Construction and evaluation of an inexpensive weighing lysimeter for studying contaminant transport," *Journal of Contaminant Hydrology*, vol. 15, no. 1-2, pp. 107 – 123, 1994.

[23] N. E. Derby, R. E. Knighton, and B. R. Montgomery, "Construction and performance of large soil core lysimeters," *Soil Sci Soc Am J*, vol. 66, no. 5, pp. 1446–1453, 2002.

[24] K. W. Brown, C. J. Gerard, B. W. Hipp, and J. T. Ritchie, "A procedure for placing large undisturbed monoliths in lysimeters," *Soil Sci Soc Am J*, vol. 38, no. 6, pp. 981–983, 1974.

[25] B. T. Bowman, R. R. Brunke, W. D. Reynolds, and G. J. Wall, "Rainfall simulator-grid lysimeter system for solute transport studies using large, intact soil blocks," *J Environ Qual*, vol. 23, no. 4, pp. 815–822, 1994.

[26] J. S. Strock and D. K. Cassel, "Developing and testing a system for studying unsaturated solute transport on undisturbed soil blocks," *Journal of Soil and Water Conservation*, vol. 56, no. 2, pp. 112–119, 2001.

[27] K. W. Brown, J. C. Thomas, and M. W. Aurelius, "Collecting and testing barrel sized undisturbed soil monoliths," *Soil Sci Soc Am J*, vol. 49, no. 4, pp. 1067–1069, 1985.

[28] J. P. M. Vink, B. Gottesbüren, B. DiekkrÃijger, and S. E. A. T. M. van der Zee, "Simulation and model comparison of unsaturated movement of pesticides from a large clay lysimeter," *Ecological Modelling*, vol. 105, pp. 113–127, Dec. 1997.

[29] J. L. Tackett, E. Burnett, and D. W. Fryrear, "A rapid procedure for securing large, undisturbed soil cores," *Soil Sci Soc Am J*, vol. 29, no. 2, pp. 218–220, 1965.

[30] J. W. Moyer, L. S. Saporito, and R. R. Janke, "Design, construction, and installation of an intact soil core lysimeter," *Agron J*, vol. 88, no. 2, pp. 253–256, 1996.

[31] A. D. Schneider, J. E. Ayars, and C. J. Phene, "Combining monolithic and repacked soil tanks for lysimeters from high water table sites," *Appl. Eng. Agric.*, vol. 12, no. 6, pp. 649–654, 1996.

[32] P. Debye, "Methods to determine the electrical and geometrical structure of molecules." Nobel Lecture, December 12th 1936. URL: http://www.nobelprize.org/nobel_prizes/chemistry/laureates/1936/debye-lecture.pdf Accessed: 19/5/2012.

[33] M. A. Malicki, R. Plagge, M. Renger, and R. T. Walczak, "Application of time-domain reflectometry (TDR) soil moisture miniprobe for the determination of unsaturated soil water characteristics from undisturbed soil cores," *Irrigation Science*, vol. 13, pp. 65–72, 1992. 10.1007/BF00193982.

[34] R. L. Smith-Rose, "The electrical properties of soil for alternating currents at radio frequencies," *Proceedings of the Royal Society of London. Series A, Containing Papers of a Mathematical and Physical Character*, vol. 140, pp. 359–377, May 1933.

[35] G. C. Topp and J. L. Davis, "Measurement of soil-water content using time-domain reflectrometry (tdr) - a field-evaluation," *Soil Science Society of America Journal*, vol. 49, no. 1, pp. 19–24, 1985.

[36] P. Brunet, R. Clament, and C. Bouvier, "Monitoring soil water content and deficit using electrical resistivity tomography (ERT) : A case study in the cevennes area, france," *Journal of Hydrology*, vol. 380, no. 12, pp. 146–153, 2010.

[37] L. Michalski, K. Eckersdorf, J. Kucharski, and J. McGhee, *Temperature Measurement*. John Wiley and Sons Ltd, 2001.

[38] M. Di Bonito, *Trace elements in soil pore water: a comparison of sampling methods*. PhD thesis, School of Biosciences, University of Nottingham, 2005.

[39] M. I. Litaor, "Review of soil solution samplers," *Water Resources Research*, vol. 24, pp. 727–733, May 1988.

[40] P. E. McGuire, B. Lowery, and P. A. Helmke, "Potential sampling error: Trace metal adsorption on vacuum porous cup samplers," *Soil Sci Soc Am J*, vol. 56, no. 1, pp. 74–82, 1992.

[41] J. Siemens and M. Kaupenjohann, "Dissolved organic carbon is released from sealings and glues of pore-water samplers," *Soil Science Society of America Journal*, vol. 67, pp. 795–797, 2003.

[42] A. B. Bryan, "The dielectric constants of argon and neon," *Phys. Rev.*, vol. 34, pp. 615–617, Aug. 1929.

[43] H. Fellner-Feldegg, "Measurement of dielectrics in the time domain," *The Journal of Physical Chemistry*, vol. 73, pp. 616–623, Mar. 1969.

[44] R. Černý, "Time-domain reflectometry method and its application for measuring moisture content in porous materials: a review," *Measurement*, vol. 42, no. 3, pp. 329 – 336, 2009.

[45] G. C. Topp, J. L. Davis, and A. P. Annan, "Electromagnetic determination of soil-water content - measurements in coaxial transmission-lines," *Water Resources Research*, vol. 16, no. 3, pp. 574–582, 1980.

[46] J. Ledieu, P. Deridder, P. Declerck, and S. Dautrebande, "A method of measuring soil-moisture by time-domain reflectometry," *Journal of Hydrology*, vol. 88, pp. 319–328, Nov. 1986.

[47] M. Malicki, R. Plagge, and C. Roth, "Improving the calibration of dielectric tdr soil moisture determination taking into account the solid soil," *European Journal of Soil Science*, vol. 47, no. 3, pp. 357–366, 1996.

[48] J. R. Birchak, C. G. Gardner, J. E. Hipp, and J. M. Victor, "High dielectric-constant microwave probes for sensing soil-moisture," *Proceedings of the Ieee*, vol. 62, no. 1, pp. 93–98, 1974.

[49] W. R. Whalley, "Considerations on the use of time-domain reflectometry (TDR) for measuring soil-water content," *Journal of Soil Science*, vol. 44, pp. 1–9, Mar. 1993.

[50] T. J. Heimovaara, W. Bouten, and J. M. Verstraten, "Frequency-domain analysis of time-domain reflectometry wave-forms. 2. a 4-component complex dielectric mixing model for soils," *Water Resources Research*, vol. 30, pp. 201–209, Feb. 1994.

[51] Y. Mualem and S. P. Friedman, "Theoretical prediction of electrical-conductivity in saturated and unsaturated soil," *Water Resources Research*, vol. 27, pp. 2771–2777, Oct. 1991.

[52] S. P. Friedman and N. A. Seaton, "Critical path analysis of the relationship between permeability and electrical conductivity of three-dimensional pore networks," *Water Resources Research*, vol. 34, pp. 1703–1710, July 1998.

[53] D. T. Purvance and R. Andricevic, "On the electrical-hydraulic conductivity correlation in aquifers," *Water Resources Research*, vol. 36, pp. 2905–2913, Oct. 2000.

[54] M. Bittelli, F. Salvatorelli, and P. R. Pisa, "Correction of TDR-based soil water content measurements in conductive soils," *Geoderma*, vol. 143, pp. 133–142, Jan. 2008.

[55] D. A. Robinson, M. G. Schaap, D. Or, and S. B. Jones, "On the effective measurement frequency of time domain reflectometry in dispersive and nonconductive dielectric materials," *Water Resources Research*, vol. 41, p. W02007, Feb. 2005.

[56] F. N. Dalton, W. N. Herkelrath, D. S. Rawlins, and J. D. Rhoades, "Time-domain reflectometry: simultaneous measurement of soil water content and electrical conductivity with a single probe," *Science*, vol. 224, pp. 989–990, June 1984.

[57] P. Castiglione and P. J. Shouse, "The effect of ohmic, cable losses on time-domain reflectometry measurements of electrical conductivity," *Soil Science Society of America Journal*, vol. 67, pp. 414–424, Mar. 2003.

[58] A. R. Von Hippel, *Dielectrics and Waves*. New York: John Wiley, 1954.

[59] G. C. Topp, S. Zegelin, and I. White, "Impacts of the real and imaginary components of relative permittivity on time domain reflectometry measurements in soils," *Soil Science Society of America Journal*, vol. 64, pp. 1244–1252, July 2000.

[60] D. Or and V. P. Rasmussen, "Effective frequency of TDR travel time based on measurement of bulk dielectric permittivity," in *Third Workshop on Electromagnetic Wave Interaction with Water and Moist Substances*, 1999.

[61] H. Johnson and M. Graham, *High Speed Digital Design.* Prentice Hall, Upper Saddle River, NJ 07458, 1993.

[62] T. J. Heimovaara and W. Bouten, "A computer-controlled 36-channel time domain reflectometry system for monitoring soil-water contents," *Water Resources Research*, vol. 26, pp. 2311–2316, Oct. 1990.

[63] J. H. Knight, "Sensitivity of time domain reflectometry measurements to lateral variations in soil-water content," *Water Resources Research*, vol. 28, pp. 2345–2352, Sept. 1992.

[64] S. J. Zegelin, I. White, and D. R. Jenkins, "Improved field probes for soil-water content and electrical-conductivity measurement using time domain reflectometry," *Water Resources Research*, vol. 25, pp. 2367–2376, Nov. 1989.

[65] Y. Gong, Q. Cao, and Z. Sun, "The effects of soil bulk density, clay content and temperature on soil water content measurement using time-domain reflectometry," *Hydrological Processes*, vol. 17, pp. 3601–3614, DEC 30 2003. Annual Meeting of the Canadian-Geophysical-Union, Banff, Canada, May, 2002.

[66] G. Blight, "Effective stress evaluation for unsaturated soils," *J. Soil Mechanics and Foundations Division, ASCE*, vol. 93, no. 2, pp. 125–148, 1967.

[67] R. Baker and S. Frydman, "Unsaturated soil mechanics: Critical review of physical foundations," *Engineering Geology*, vol. 106, no. 1-2, pp. 26–39, 2009.

[68] A. M. Ridley and J. B. Burland, "A new instrument for the measurement of soil-moisture suction," *Geotechnique*, vol. 43, no. 2, pp. 321–324, 1993.

[69] S. D. N. Lourenço, D. Gallipoli, D. G. Toll, C. E. Augarde, F. D. Evans, and G. M. Medero, "Calibrations of a high-suction tensiometer," *Geotechnique*, vol. 58, no. 8, pp. 659–668, 2008.

[70] Y. Guan and D. G. Fredlund, "Use of the tensile strength of water for the direct measurement of high soil suction," *Canadian Geotechnical Journal*, vol. 34, no. 4, pp. 604–614, 1997.

[71] K. Sjoblom, *The mechanisms involved during the desaturation process of a porous matrix.* PhD thesis, Massachusetts Institute of Technology, 2000.

[72] A. Tarantino and L. Mongiovi, "Calibration of tensiometer for direct measurement of matric suction," *Geotechnique*, vol. 53, no. 1, pp. 137–141, 2003.

[73] A. Mantho, *Soil atmosphere transfers - application to drought.* PhD thesis, École National des Ponts et Chaussées, Paris, 2005.

[74] S. Lourenço, D. Gallipoli, D. Toll, and F. Evans, "Development of a commercial tensiometer for triaxial testing of unsaturated soils," in *Proc. of the 4th International Conference on Unsaturated Soils, Phoenix, USA*, vol. 2 of *Geotechnical Special Publication No. 14*, pp. 1875–1886, ASCE, 2006.

[75] I. Meilani, H. Rahardjo, E. C. Leong, and D. G. Fredlund, "Mini suction probe for matric suction measurements," *Canadian Geotechnical Journal*, vol. 39, pp. 1427–1432, Dec. 2002.

[76] A. M. Ridley, K. Dineen, J. B. Burland, and P. R. Vaughan, "Soil matrix suction: some examples of its measurement and application in geotechnical engineering," *Geotechnique*, vol. 53, pp. 241–253, Mar. 2003.

[77] W. A. Take and M. D. Bolton, "Tensiometer saturation and the reliable measurement of soil suction," *Geotechnique*, vol. 53, no. 2, pp. 159–172, 2003.

[78] S. E. Poirier, D. J. Degroot, and T. C. Sheahan, "Measurement of suction in a marine clay as an indicator of sample disturbance.," in *Proc. Geo-Frontiers 2005 Congress Earth and Space*, vol. 164, pp. 1–10, 2005.

[79] C. F. Mahler and A. A. Diene, "Tensiometer development for high suction analysis in laboratory lysimeters," *Experimental Unsaturated Soil Mechanics*, vol. 112, pp. 103–115, 2007.

[80] A. Jotisankasa, W. Porlila, S. Soralump, and W. Mairiang, "Development of a low cost miniature tensiometer and its applications," in *Proc. 3rd Asian Conference on Unsaturated Soils (UNSAT-ASIA 2007), Nanjing, China*, pp. 21–23, 2007.

[81] L. Tarantino, A. & Mongiovi, "Experimental procedures and cavitation mechanisms in tensiometer measurements," *Geotechnical and Geological Engineering*, vol. 19, pp. 189–210, 2001.

[82] O. Mendes, J. & Buzzi, "New insight into cavitation mechanisms in high capacity tensiometers based on high-speed photography," *Canadian Geotechnical Journal*, vol. 50(5), pp. 550–556, 2013.

[83] J. Mendes, *Assessment Of The Impact Of Climate Change On An Instrumented Embankment An Unsaturated Soil Mechanics Approach*. PhD thesis, School of Engineering and Computing Sciences, Durham University, 2011.

[84] S. D. N. Lourenço, *Suction Measurements And Water Retention in Unsaturated Soils*. PhD thesis, School of Engineering and Computing Sciences, Durham University, 2008.

[85] J. Asquith, D. G. Toll, and K. J. Johnson, "Design and construction of large lysimeters for monitoring unsaturated transport of contaminants," in *Proceedings of the 2nd European Conference on Unsaturated Soils 2012, Naples, Italy*, vol. 2, pp. 447–452, Springer, 2012.

[86] Microsoft, "Differences between Visual Basic .NET and Visual c# .NET," August 2012. URL: http://support.microsoft.com/kb/308470 Accessed: 09/06/2014.

[87] M. Clifton, "What is a framework?," November 2003. URL: http://www.codeproject.com/Articles/5381/What-Is-A-Framework Accessed: 09/06/2014.

[88] J. Likness, "Model-view-viewmodel (mvvm) explained," August 2010. URL: http://www.codeproject.com/Articles/100175/Model-View-ViewModel-MVVM-Explained Accessed: 09/06/2014.

[89] J. Joel, "MVVM vs MVP vs MVC: The differences explained," May 2011. URL: http://joel.inpointform.net/software-development/mvvm-vs-mvp-vs-mvc-the-differences-explained/ Accessed: 09/06/2014.

[90] J. Smith, "MVVM foundation," February 2010. URL: https://mvvmfoundation.codeplex.com/ Accessed: 09/06/2014.

[91] L. Bugnion, "MVVM lite," February 2013. URL: https://mvvmlight.codeplex.com/ Accessed: 09/06/2014.

[92] Microsoft, "Windows presentation foundation," 09 2014. URL : http://msdn.microsoft.com/en-us/library/ms754130(v=vs.110).aspx Accessed: 20/09/2014.

[93] J. Smith, "Using a ViewModel to provide meaningful validation error messages," November 2008. URL: http://joshsmithonwpf.wordpress.com/2008/11/14/using-a-viewmodel-to-provide-meaningful-validation-error-messages/ Accessed: 09/06/2014.

[94] J. House, Z. Deng, A. Craven, J. Rosenberg, H. Yandell, W. M. Price, B. Kratzer, B. Topping, B. Hedrick, C. Bonham, C. Cavaness, F. Ribeiro, D. James, J. Wescott, M. Payne, D. White, M. Curwen, M. Rezaei, S. Venkatarangaiah, and P. Inc., "Quartz: Job scheduling library," September 2013. URL: http://www.quartz-scheduler.net/ Accessed: 09/06/2014.

[95] P. Jenkins, B. Forster, D. Daume, A. Mitchell, and J. Karger, "Mahapps metro," July 2014. URL: http://mahapps.com/ Accessed: 29/7/2014.

[96] British Standards Institution, "BS1377 - 2: Classification tests," 1990. London.

[97] British Standards Institution, "BS1377 - 4: Compaction related tests," 1990. London.

[98] H. Potter and R. Yong, "Influence of iron-aluminium ratio on the retention of lead and copper by amorphous iron-aluminium oxides," *Applied Clay Science*, vol. 14, pp. 1–26, Feb. 1999.

[99] R. R. Gadde and H. A. Laitinen, "Heavy metal adsorption by hydrous iron and manganese oxides," *Analytical Chemistry*, vol. 46, pp. 2022–2026, Nov. 1974.

[100] A. Babatunde, Y. Zhao, A. Burke, M. Morris, and J. Hanrahan, "Characterization of aluminium-based water treatment residual for potential phosphorus removal in engineered wetlands," *Environmental Pollution*, vol. 157, no. 10, pp. 2830 – 2836, 2009.

[101] D. Raghu, H.-N. Hsieh, S. C. Basim, and M. Morgan, "Physical characterization of water treatment plant residual and top soil mixtures," in *Testing soil mixed with waste or recycled materials*, vol. 1275, pp. 3–15, ASTM, 1997.

[102] B. C. O'Kelly, "Geotechnical properties of a municipal water treatment sludge incorporating a coagulant," *Canadian Geotechnical Journal*, vol. 45, no. 5, pp. 715–725, 2008.

[103] M. C. Wang, J. Q. Hull, M. Jao, B. A. Dempsey, and D. A. Cornwell, "Engineering behavior of water-treatment sludge," *Journal of Environmental Engineering (ASCE)*, vol. 118, no. 6, pp. 848–864, 1992.

[104] C. Willetts and D. Toll, "The geomechanical properties of soil cemented with iron and manganese oxides." Unpublished MEng undergraduate report, Durham University, 2011.

[105] British Standards Institution, "BS1377 - 6: Consolidation and permeability tests," 1990. London.